CHARACTERISATION AND DIFFERENTIATION OF DENTINE CARIES USING OPTICAL COHERENCE TOMOGRAPHY

SAAD AHMED KHAN

FACULTY OF DENTISTRY
UNIVERSITY OF MALAYA
KUALA LUMPUR
2016

CHARACTERISATION AND DIFFERENTIATION OF DENTINE CARIES USING OPTICAL COHERENCE TOMOGRAPHY

SAAD AHMED KHAN

THESIS SUBMITTED IN FULFILMENT OF THE REQUIREMENTS FOR THE DEGREE OF DOCTOR OF PHILOSOPHY

FACULTY OF DENTISTRY
UNIVERSITY OF MALAYA
KUALA LUMPUR

2016

UNIVERSITY OF MALAYA

ORIGINAL LITERARY WORK DECLARATION

Name of Candidate: **SAAD AHMED KHAN**

Registration/Matric No: **DHA 120018**

Name of Degree: **DOCTOR OF PHILOSOPHY**

Title of Thesis: **CHARACTERISATION AND DIFFERENTIAION OF DENTINE CARIES USING OPTICAL COHERENCE TOMOGRAPHY**

Field of Study: **Restorative Dentistry**

I do solemnly and sincerely declare that:

(1) I am the sole author/writer of this Work;
(2) This Work is original;
(3) Any use of any work in which copyright exists was done by way of fair dealing and for permitted purposes and any excerpt or extract from, or reference to or reproduction of any copyright work has been disclosed expressly and sufficiently and the title of the Work and its authorship have been acknowledged in this Work;
(4) I do not have any actual knowledge nor do I ought reasonably to know that the making of this work constitutes an infringement of any copyright work;
(5) I hereby assign all and every rights in the copyright to this Work to the University of Malaya ("UM"), who henceforth shall be owner of the copyright in this Work and that any reproduction or use in any form or by any means whatsoever is prohibited without the written consent of UM having been first had and obtained;
(6) I am fully aware that if in the course of making this Work I have infringed any copyright whether intentionally or otherwise, I may be subject to legal action or any other action as may be determined by UM.

Candidate's Signature Date:

Subscribed and solemnly declared before,

Witness's Signature Date:

Name:

Designation

ABSTRACT

Introduction: It is clinically challenging to differentiate caries-infected dentine (ID), caries-affected dentine (AD) and healthy dentine (HD), especially during caries removal. The main aim of this study is to explore the potential of an optical method, Optical Coherence Tomography (OCT), in assisting caries removal decision making in a clinical setting. The initial step towards this aim is to characterise OCT signals in the carious dentine and identify OCT outcome measures that can discriminate these layers with high accuracy. **Objectives:** Firstly, to optically characterise these layers based on their microstructure, to develop and determine the OCT outcome measures that can differentiate the dentine layers and assess their accuracy of prediction. Secondly, to determine the relationship of OCT outcome measures with the quantity of major elements in carious and healthy dentine. Finally, to compare and explore the relationship of the mineral density (MD) and OCT outcome measures. **Methods:** Swept Source OCT (SS-OCT) was used to scan cross-sectioned natural dentine caries surfaces and validated against other reference methods. The microstructure, composition and MD characterisation were performed using field emission scanning electron microscopy (FESEM), energy dispersive X-ray spectroscopy (EDX) and micro computed tomography (micro-CT). A bespoke software developed with MATLAB (Mathworks Inc) was used for OCT data extraction and processing. **Results:** Characterisation of OCT signals based on the microstructure of the carious and healthy dentine showed that the OCT backscattered intensity, *I*, attenuated in two phases where it attenuated faster in the first phase relative to the second. When *I* of the top 100 µm physical depth was considered as a whole, it was observed to attenuate following a polynomial pattern in ID (R^2 = 0.794), while it assumed an exponential attenuation in AD and HD (R^2 = 0.783 and 0.998) respectively. Maximum Intensity (*Imax)*, and area under the curve (*AUC*), AUC_T were the

two OCT outcome measures that was able to differentiate the three dentine layers. Artificial neural network (ANN) showed higher accuracy for classifying dentine caries when using I_{max} and *AUC* combined, ID and AD, AD and HD and ID and HD were correctly classified with 84%, 88% and 94% accuracy respectively. Ca and P wt% were significantly different between all three dentine layers (p<0.05), except the Ca:P ratio between the AD and HD (p= 0.460). I_{max} demonstrated moderate positive relationship with Ca (r= 0.448) and P (r= 0.479), and moderate negative relationship with Ca:P ratio (r= -0.431). Mean MD of ID, AD and HD in this study was found to be 0.87 (± 0.10), 1.16 (± 0.82) and 1.52 (± 0.13) gm/cm^3 respectively. As a whole, there was a moderate but significant inverse correlation between MD and ΔI (r=-0.531). The mean ΔI for ID, AD and HD were significantly different between ID and AD, and ID and HD (p< 0.05), except AD and HD (p=0.851). ΔI discriminated ID and AD with 90.5% sensitivity and 81.0% specificity. **Conclusions:** The attenuation characteristics of OCT backscattered intensity characterisation and the derived outcome measure can significantly differentiate and be used for predicting dentine layers with high accuracy.

ABSTRAK

Pengenalan: Adalah amat mencabar untuk membezakan dentin terinfeksi(ID), dentin terpengaruh (AD) dan dentin sihat (HD) secara klinikal, terutamanya semasa pembuangan karies. Tujuan utama kajian ini adalah untuk mengkaji potensi kaedah optik klinikal, Optical Coherence Tomorgraphy (OCT), sebagai kaedah bantuan bagi membuat keputusan semasa pembuangan karies dalam situasi klinikal. Oleh itu langkah awal ke arah matlamat ini adalah pencirian isyarat OCT di lapisan karies dentin dan mengenal pasti OCT (*outcome measures)* yang boleh mendiskriminasi lapisan ini dengan ketepatan yang tinggi. **Objektif:** Pertama, untuk mencirikan lapisan dentin secara optic, berdasarkan mikrostrukturnya, membangunkan dan menentukan OCT *outcome measures* dapat membezakan antara lapisan dentin dan menilai ketepatan ramalannya. Kedua, untuk menentukan hubungan OCT *outcome measures* dengan kuantiti unsur-unsur utama dalam dentin yang berkaries dan sihat. Akhir sekali, untuk membuat perbandingan dan mengkaji hubungan antara ketumpatan mineral (MD) dan OCT *outcome measures*. **Kaedah:** *Swept Source* OCT (SS-OCT) telah digunakan untuk mengimbas permukaan karies dentin yang berlaku semula jadi dalam keratan rentang dan disahkan dengan merujuk pada kaedah-kaedah lain. Pencirian mikrostruktur, komposisi dan MD dibuat menggunakan mikroskop pengimbasan elektron *field-emission* (FESEM), *energy dispersive X-ray spectroscopy (EDX)* dan *micro computed tomography (micro-CT).* Perisian yang dibangunkan secara persendirian menggunakan MATLAB (Mathworks Inc) telah digunakan untuk pengekstrakan dan pemprosesan data OCT. **Keputusan**: Pencirian isyarat OCT berdasarkan mikrostruktur dentin yang berkaries dan sihat menunjukan bahawa keamatan isyarat *backscattered* OCT, *I,* dilemahkan dalam dua fasa di mana kelemahan adalah lebih cepat di fasa pertama berbanding fasa kedua. Apabila *I,* daripada 100 mikron kedalaman fizikal dianggap secara menyeluruh, pemerhatian menunjukkan

kelemahan yang bercorak polinomial bagi ID (R2 = 0.794) manakala ia menunjukkan kelemahan eksponen bagi AD dan HD (R2 masing-masing = 0.783 dan 0.998). Intensiti maksimum, I_{max}, dan kawasan di bawah keluk, *AUCr* adalah dua hasil OCT *outcome measures* yang didapati mampu untuk membezakan ke tiga-tiga lapisan dentin. ANN menunjukkan ketepatan yang lebih tinggi untuk mengklasifikasikan karies dentin apabila I_{max} dan *AUCr* digabungkan, ID dan AD, AD dan HD dan ID dan HD telah dikelaskan dengan betul dan ketepatan masing-masing ialah 84%, 88% dan 94%. Perbezaan berat peratusan Ca dan P adalah signifikan antara ketiga-tiga lapisan dentin ($p<0.05$) kecuali nisbah Ca:P antara AD dan HD ($p = 0,460$). I_{max} menunjukkan hubungan positif yang sederhana bagi Ca ($r = 0,448$) dan P ($r = 0,479$), dan hubungan negatif sederhana bagi nisbah Ca: P ($r = -0.431$). Min MD bagi ID, AD dan HD dalam kajian ini masing-masing ialah 0.87 (± 0.10), 1.16 (± 0.82) dan 1.52 (± 0.13) gm/cm-^{3}. Secara keseluruhannya, terdapat hubungan yang sederhana tetapi terdapat korelasi songsang yang signifikan antara MD dan ΔI ($r = -0,531$). Min ΔI bagi ID, AD dan HD adalah berbeza dan signifikan antara ID dan AD, dan ID dan HD ($p<0.05$), kecuali AD dan HD ($p=0.851$). ΔI mendiskriminasi ID dan AD dengan kepekaan 90.5% dan kekhususan 81.0%. **Kesimpulan:** Ciri pengecilan *backscattered* intensiti OCT dan *outcome measures* yang diperolehi dapat membezakan dan meramalkan lapisan dentin dengan ketepatan yang tinggi.

ACKNOWLEDGEMENTS

In the name of God, the Gracious, the merciful. All praise and thanks is due to Allah (SWT), the lord of mankind.

Many people have helped me to bring this thesis to completion. First, I thank my main supervisor Dr Chew Hooi Pin for believing in me and giving me an opportunity to work with her at the Faculty of Dentistry, University Malaya. Her dedication and pursuit to achieve quality research has immensely helped me personally and professionally. Her integrity and systematic approach in conducting research has been truly inspirational for me. Beyond what this thesis may reflect, good research practice is what I shall carry with me as I move forward in life. I especially thank her for allowing me to express my ideas and supporting me in various ways and advising me patiently during my ambitious journey.

A special thanks to Prof Dr Noor Hayaty, who provided me with significant guidance and support throughout my PhD. Her encouraging and positive attitude helped me collaborate with the genetics and biological science research group has helped me tremendously to learn methods in science which I wasn't earlier familiar with. I also, would like to acknowledge her undivided attention in helping me write manuscripts and this thesis.

I greatly appreciate Prof Dr Angus Walls' input in designing this research and for his valuable comments at several stages of research project.

I never would have completed this doctorate, without extensive support from Dr Christian Zakian. He has been instrumental throughout my candidature, especially in my learning about research using optics. I sincerely, thank him for his dedication and efforts; spending long hours discussing, designing and refining the methods involved in

this research project. He has also played a key role as a mentor and advisor at both the personal and professional levels.

I would like to thank Prof Dr Alex Fok for his scientific guidance and provision of facilities to use micro-CT at The Minnesota Dental Research Centre for Biomaterials and Biomechanics (MDRCBB). Thanks to the support team at MDRCBB who have all been extremely kind and helpful. I am very grateful to Prof. Williams Wade, Dr Chan Kok Gan, Dr Mahmoud Danae and Dr Tariq ur Rahman whose worthwhile input at different stages of my research has helped me strategize my work in a more efficient way.

Thanks to my wonderful colleagues, the OCT research team, scientific officers and amazing friends who have made my journey worthwhile and fun. I would like to express sincere gratitude to the University Malaya for offering the Bright Sparks scholarship and High Impact research grants from the Ministry of Education to conduct this research.

Most importantly my deepest appreciation and love towards my family who supported me unconditionally throughout this journey. Ala, Auj, Aisha and both my parents, thank you for believing in me, supporting me and allowing me to pursue my studies. Arianna has been a special motivation for me to learn, expand and become a better person and I dedicate this thesis to her.

TABLE OF CONTENTS

LIST OF FIGURES

LIST OF TABLES

LIST OF ABBREVIATIONS

ID	:	Infected dentine
AD	:	Affected dentine
HD	:	Healthy dentine
µm	:	Micrometre
I	:	OCT backscattered intensity
R	:	Ratio
$Imax$	:	Maximum intensity
AUC_T	:	Area under the curve Total
AUC_I	:	Area under the curve Phase I
AUC_{II}	:	Area under the curve Phase II
µ	:	Attenuation coefficient
ΔI	:	Maximum I – Minimum I

CHAPTER 1: INTRODUCTION

Dental caries is an adverse oral disease with multifactorial aetiology involving behavioural, environmental and genetic factors (Featherstone, 2004; Fejerskov, 2004). The caries process is initiated when the microbes within the dental biofilm respond to the increase in dietary fermentable carbohydrate intake by producing lactic acid. This leads to net loss of the minerals in the tooth structure that slowly progresses to form the carious lesion(E. A. Kidd & Fejerskov, 2004). According to global burden of disease, dental caries is ranked as the eighth most widely spread disease affecting more than 10% of the global population (Marcenes et al., 2013).

Effective treatment of deep dentine caries in teeth with vital pulp is a challenge to dental practitioners (Thompson, Craig, Curro, Green, & Ship, 2008). This is primarily due to the lack of methods to accurately identify the carious dentine layers, which leads to ill-defined caries removal (D. Ricketts, 2001), resulting in higher chance of pulpal trauma and complications (D. Ricketts, 2001; Schwendicke, Dorfer, & Paris, 2013). It has been reported that dentists showed variations in decision-making when managing deep caries lesions, frequently restoring them at varying depth points (Rindal et al., 2014). The outcomes of such variations in treatments could have a negative impact on the patients' wellbeing. While receiving treatment, 55% of patients with deep caries have had increased physical pain in comparison to patients with shallow caries (28%) and endodontic treatment (17%) (Botello-Harbaum et al., 2012).

While it is essential to remove carious tissues when treating deep dentine caries lesions, dentists should also aim to preserve remineralisable tissues and to protect and maintain pulpal health (F. Schwendicke, 2016). Traditionally, dentine caries excavation was based on the principle of *"extension for prevention"*. Black asserted that, " It is better to expose the pulp of a tooth than to leave it covered with soft dentine" (Black, 1908).

Fifty years later, this technique was challenged after Shovelton (1968), Silverstone (1981), and Murray (2003) reported that severe hyperaemia and pulpal inflammation was observed when excavation reached 0.25-0.50 mm away from the pulp (Murray, Smith, Windsor, & Mjor, 2003; Shovelton, 1968; Silverstone, Johnson, Hardie, & Williams, 1981).

In 1991, Handelman and Mertz-Fairhurst proposed another technique, which was a direct contradiction to that of Black (1908). They recommended not removing dentine caries at all but to instead seal the carious tooth with restorative material (Handelman, 1991; Mertz-Fairhurst, Curtis, Ergle, Rueggeberg, & Adair, 1998). Later Ribeiro et al (1999) introduced the concept of partial caries removal. In this technique, they proposed the removal of the infected tissue, leaving some infected dentine and sealing the cavity, without indirect pulp capping, with permanent restorative material (Ribeiro, Baratieri, Perdigao, Baratieri, & Ritter, 1999). Both of these techniques confirmed reduction in bacterial counts because of sealed caries lesion (Bönecker, Toi, & Cleaton-Jones, 2003; M. Maltz, de Oliveira, Fontanella, & Bianchi, 2002) and radiographic changes indicated mineral deposition (Alves, Fontanella, Damo, Ferreira de Oliveira, & Maltz, 2010). However, not removing dentine caries at all or partial removal of dentine caries in permanent teeth compromises the foundation for restoration and has consequences on its longevity (Hevinga, Opdam, Frencken, Truin, & Huysmans, 2010; D. Ricketts, Lamont, Innes, Kidd, & Clarkson, 2013).

In, 1977 step wise excavation was experimented to treat deep carious lesion in primary molars (Magnusson & Sundell, 1977). This technique was further developed and tested by partial removal of infected dentine and placing temporary restoration. A few weeks after the excavation, during a follow-up visit, the temporary restoration is removed along with any remaining soft dentine and is followed by permanent restoration

(Bjorndal, Larsen, & Thylstrup, 1997). This technique was later criticized, although there was a decrease in microbial count and cessation in caries progression, re-entering may risk pulpal trauma (E. A. Kidd, 2004).

The Cochrane review assessed the effectiveness of stepwise and partial caries removal in comparison to complete caries removal; the findings demonstrated 56% and 77% reduction in pulpal exposure respectively (D. Ricketts et al., 2013). Reduction in pulp exposure is a common outcome used to benchmark the effectiveness of such techniques (Opal, Garg, Dhindsa, & Taluja, 2014; D. Ricketts et al., 2013; D. N. Ricketts, Kidd, Innes, & Clarkson, 2006a; Thompson et al., 2008). However, pulp exposure as an outcome only highlights the comparative advantage of one technique over another; it does not provide the optimum clinical parameters for deep dentine caries management.

Fusayama and Terrashima (1972) characterised dentine caries histologically into two different layers: the outer demineralised infected dentine and the inner affected dentine (T. Fusayama & Terashima, 1972). These layers were further classified based on ultrastructural properties, crystal deposition, changes observed in inter and peritubular aiding in differentiation between outer soft demineralized layer and inner affected dentine (Ogawa, Yamashita, Ichijo, & Fusayama, 1983). Later, Kidd et al provided evidence for the clinical relevance of the histological layers; the outer demineralised infected dentine as the soft and wet layer which must be removed and the inner affected dentine with intact collagen as the hard and leathery layer which can be preserved (E.A. Kidd, Smith, & Pickard, 1998) thus recognizing that caries-affected dentine can be used as a benchmark for the optimum caries removal endpoint. However, the subjective and challenging nature of assessing changes in the texture of carious dentine makes it challenging for the dentists to differentiate them (A. Banerjee, T. F. Watson, & E. A. Kidd, 2000a). The perception of colour and texture using conventional visual and tactile

techniques currently employed have resulted in poor outcome (E. Kidd, 2004) and inconsistencies in the determination of the endpoint of caries removal (de Almeida Neves, Coutinho, Cardoso, Lambrechts, & Van Meerbeek, 2011). Chemomechanical method requires dentists to use 1% acid red solution in propylene glycol to stain the outer demineralised layer, leaving the collagen of the inner intact dentine unstained (Kuboki, Liu, & Fusayama, 1983). This technique enhances the visual assessment of the carious layer during the excavation process. However, staining of the inner affected and healthy dentine (Boston & Liao, 2004) can result in over prepared cavities (Banerjee, Kidd, & Watson, 2003).

Detection tools using the fluorescence phenomenon utilise the change of fluorescence to distinguish the healthy from the carious layers. This change of fluorescence occurs due to the presence of porphyrins, metalloporphyrins and various kinds of chromophores (Banerjee, Gilmour, Kidd, & Watson, 2004; Konig, Flemming, & Hibst, 1998). Red auto fluorescence is a characteristic associated with carious dentine as porphyrins synthesise during bacterial activity (Koenig & Schneckenburger, 1994). The Fluorescence Aided Caries Excavation (FACES) uses an orange red fluorescence configuration to distinguish between demineralised and healthy dentine. Although this technique is capable of producing smaller and conservatively sized cavities, small amounts of fluorescence may not be detected by the practitioner, resulting in caries being left behind (A.M. Lennon, Buchalla, Switalski, & Stookey, 2002). Similarly, the Light Induced Fluorescence Evaluator for Diagnosis & Treatment (LIFEDT) produces bright red fluorescence when viewing carious dentine. This phenomenon is attributed to the Millard Reaction (Panayotov et al., 2013) that magnifies and records the images for dentists to identify the red fluorescent area, thus aiding excavation while leaving out the healthy dentine that appears as green-blue florescence. The detection of infected dentine is dependent on the dentist's interpretation of the variations in brightness and

florescence observed on the images (Terrer et al., 2010). Laser Induced Fluorescence (LIFE), available commercially as DIAGNOdent®, objectively measures and produces numerical cut off values for sound and caries affected dentine tissues (Kinoshita, Shinomiya, Itoh, & Matsumoto, 2007; A.M. Lennon et al., 2002). However, higher values of fluorescence for healthy dentine near the pulpal floor leads to over excavation and ultimately unnecessary pulpal exposure (Krause, Braun, Eberhard, & Jepsen, 2007). All these techniques may aid in the removal of diseased tissues with different levels of efficiency, but they are not able to accurately identify and differentiate between caries-infected dentine and caries-affected dentine (A. Banerjee, T. F. Watson, et al., 2000a).

Optical Coherence Tomography (OCT) is a non-ionising imaging technique using a broadband light source to produce cross-sectional images by measuring the interference between the backscattered light from a sample and a reference beam. OCT is a highly sensitive tool to discriminate between sound and carious enamel surfaces of tooth tissues, as mineral loss as little as 10-15% can increase the light scatter by 50 times (Louie et al., 2010). Healthy dentine, when compared with enamel, shows lower birefringence, yet higher scattering anisotropy (Fried, Glena, Featherstone, & Seka, 1995). This occurs due to hollow dentinal tubules and their orientation being surrounded by highly mineralised structures (I. Hariri, A. Sadr, Y. Shimada, J. Tagami, & Y. Sumi, 2012). A lower scatter anisotropy is observed in the presence of collagen based organic matrix (X. J. Wang et al., 1999).

Several studies using Polarisation Sensitive (PS) and Swept Source (SS)-OCT systems have established change in backscattered intensity profile when caries was artificially induced on a human coronal teeth (Azevedo, Trung, Simionato, Freitas, & Matos, 2011) and root dentine surfaces (Amaechi, Podoleanu, Komarov, Higham, & Jackson, 2004; Freitas et al., 2009; Lee, Darling, & Fried, 2009; Manesh, Darling, & Fried, 2009a).

Strong correlation was found between the change of backscattered signals and mineral loss caused by demineralisation when PS-OCT (Amaechi et al., 2004; Lee, Hsu, Le, Darling, & Fried, 2009; Manesh et al., 2009a) and SS-OCT (Natsume et al., 2011) systems were used. However, considering the limitation of artificial induced caries model, the OCT backscattered intensity values reaches to a plateau with an increase in the decaying rates (Freitas et al., 2009). A natural caries lesion has a complex histological micro-structure due to the patho-morphological reaction of dentine caries, which *in vitro* caries models are unable to simulate (Marquezan et al., 2009; Shellis, 1994). Therefore it would not be appropriate to extrapolate the findings of artificially induced dentine lesions with that of naturally occurring ones.

There are a few studies that have explored the behaviour of OCT signals on natural occurring lesions. Chen et al. (2005) reported that qualitatively, the OCT scans show high contrast areas and rich texture information due to strong local light scattering for carious lesions when compared with non-carious sites (Chen, Otis, Piao, & Zhu, 2005). Whereas the inner translucent zone creates low intensity OCT signals due to lower backscattering of light (de Oliveira Mota et al., 2013). To date, no study has quantitatively identified and differentiated infected, affected and healthy dentine using natural occurring caries lesions.

To date, there is also no definite diagnostic tool available that could identify the carious layers and define caries-removal endpoints accurately (Neves, Coutinho, Cardoso, Lambrechts, & Van Meerbeek, 2011). There is therefore, a pressing need for a method that allows optical characterisation of caries-infected, caries-affected and healthy dentine layers with an aim to differentiate them from each other on the basis of structural and biological characterisation so as to assist cavity preparation. This thesis focuses on optical characterisation of naturally occurring dentine caries layers, and on

determining the potential for discriminating these layers from each other using their optical characteristics.

It is hypothesised that, if histological changes can be observed in dentine caries layers, each layer would show change in intensity of backscattering and change in light attenuation, providing discriminatory markers between demineralised carious layers and healthy dentine. In this study, natural dentine caries lesions were used to consider near to biological and pathophysiological stages occurring in dentine caries.

1.1 Research Motivation

The key impetus for conducting this research is to characterise naturally occurring dentine caries layers using the OCT as index test. These characteristics can then be used to quantitatively identify and differentiate between caries-infected dentine (ID), caries-affected dentine (AD) and healthy dentine (HD). The findings of this research could potentially be used to detect and differentiate each layer clinically and provide more accurate excavation end points, reduce pulp exposure and enhance the integrity of tooth structure.

1.2 Research Significance and Scope

Currently available technologies have limited capabilities to objectively and clinically identify the different layers in dentine caries lesions, which is an essential step in defining caries-removal endpoints. The currently available detection tools are dependent on fluorescence emitted by porphyrins (microbial by-product), which are used to differentiate between infected and non-infected layers (A. M. Lennon, 2003; Lussi, Hibst, & Paulus, 2004; Terrer et al., 2010). However, in addition to changes in microbial presence, the carious process involves changes in dentine structure and mineral composition (Marshall Jr, Marshall, Kinney, & Balooch, 1997), which were not

taken into account in these technologies. Although using these existing detection methods together with conventional tools increases the accumulative information to the dentists, they are unable to discriminate the junction between ID and AD layers that hypothetically should be the caries-removal endpoint. The overall purpose is to take initial steps in developing a diagnostic tool to assist dentists with decision-making in caries removal.

1.3 Aim

The aim of this study was to optically characterise dentine layers and identify OCT outcome measures which can discriminate dentine layers with high accuracy.

Based on the main aim stated above, the objectives of this study are:

Research Objective 1: To determine the microstructural classification of carious and healthy dentine layers and its corresponding quantitative OCT analysis.

Specifically this objective seeks to:

i) identify quantitatively the optical characteristics of ID, AD and HD layers from natural dentine caries specimens using OCT,

ii) determine the OCT outcome measures which can aid in differentiating ID, AD and HD layers in natural dentine caries using OCT and scanning electron microscopy (SEM),

iii) assess the accuracy of prediction to classify ID, AD and HD layers using the OCT outcome measures.

The Null Hypotheses are:

i) Optical characteristics of ID, AD and HD layers are not different from each other

ii) OCT outcome measures cannot be used to differentiate ID, AD and HD layers

iii) OCT outcome measures cannot classify or predict ID, AD and HD layers with high accuracy

Research Objective 2: To determine the major elements of dentine layers and its corresponding quantitative OCT analysis

Specifically this objective seeks to:

i) determine the calcium (Ca), phosphorus (P) wt% and Ca:P ratios of ID, AD and HD layers

ii) determine the nature of relationship between calcium (Ca), phosphorus (P) wt% and Ca:P ratio of ID, AD and HD and OCT outcome measures

The Null Hypotheses are:

iii) Ca and P wt% and Ca:P ratio are not significantly different between ID, AD and HD layers

iv) Ca and P wt% and Ca:P ratio have no correlation to their corresponding OCT outcome measures when comparing ID, AD and HD layers

Research Objective 3: To determine the mineral densities of dentine layers and their corresponding quantitative OCT analysis

This objective seeks specifically to:

i) quantify and compare the mineral density (MD) and OCT outcome measures of ID, AD and HD layers

ii) explore the relationship between MD and OCT outcome measures

iii) determine OCT outcome measures threshold values between ID and AD layer

The Null Hypotheses are:

1) There is no difference in the MD and OCT outcome measures between of ID, AD and HD layers

2) MD has no correlation to its corresponding OCT outcome measures

3) Threshold values of OCT outcome measures cannot be used to differentiate ID and AD layers

1.4 Research framework

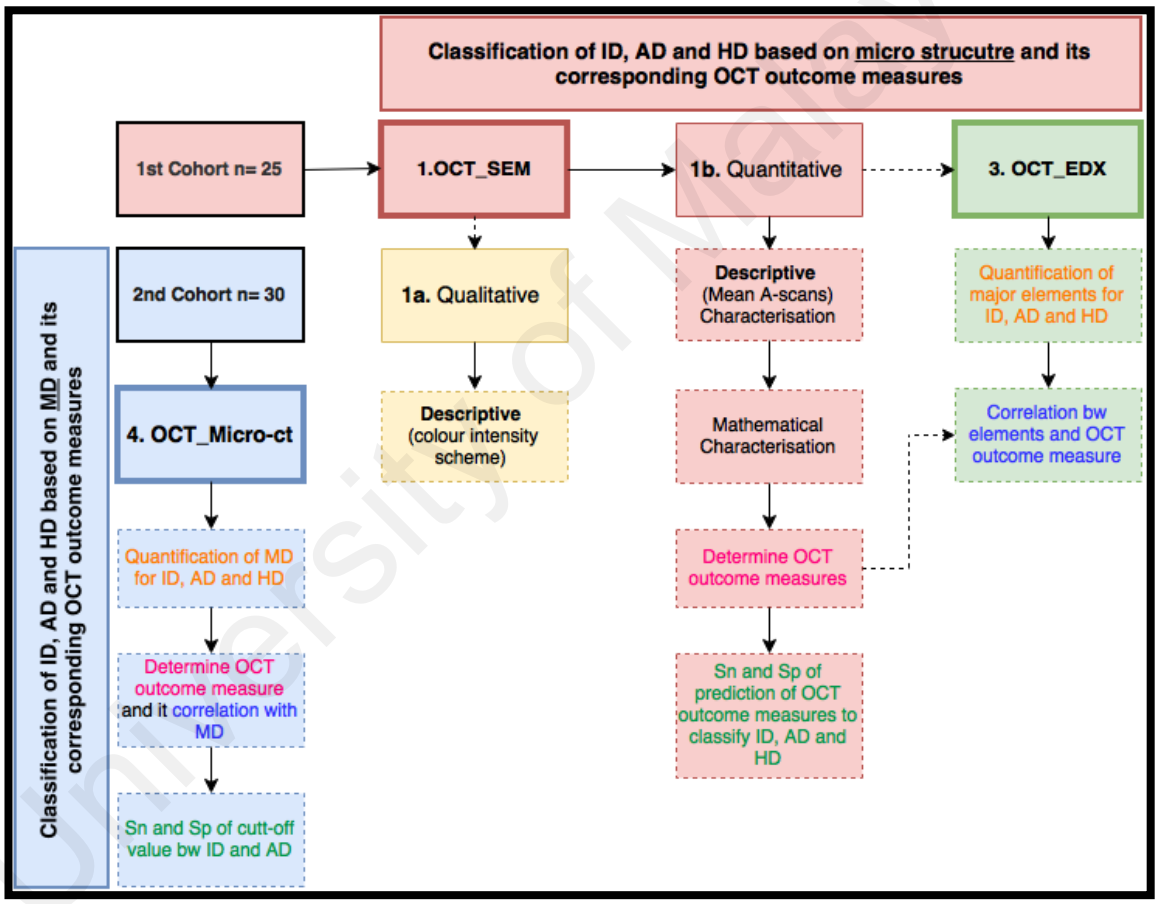

Figure 1.1: OCT characterization and its comparative methods used in this study

CHAPTER 2: LITERATURE REVIEW

2.1 Dental caries

The term dental caries can be used to represent both the caries process and the carious lesion (E. Kidd, 2005; N. B. Pitts, 2004). Caries lesion, depending on its location, can be further termed as enamel, dentine or root caries. In clinical management, cavitated or non-cavitated and active or arrested caries are commonly used to describe the state of the caries (Fejerskov & Kidd, 2008). The caries process, is often described as the outcome, the signs and symptoms of a localized chemical dissolution of the tooth structure caused by metabolic events occurring in the dental biofilm covering the affected region (Fejerskov & Kidd, 2008). Dental caries is not a singular event, but an accumulation of stages and events, a continuum of increasing severity of tooth disease and destruction (Featherstone, 2004).

Dental caries remains as a major dental public health problem, with the highest increase in prevalence among diseases worldwide (Marthaler, 2004). According to the 2010 global burden of disease (GBD) report, 3.9 billion people are affected by oral disease, of which untreated caries in permanent teeth is the highest, reaching up to 35% combined for all age groups (Marcenes et al., 2013). Meanwhile, the untreated caries in deciduous teeth affects 11% of the global population (Marcenes et al., 2013). The GBD refers to untreated dentine caries that is soft or leathery in consistency when probed (WHO, 2008). Subsequently, in 2013 the GBD report highlighted that caries in permanent teeth has increased and now ranked eighth worldwide affecting more than 10% of the world population. The overall caries estimates have reached over 41% for permanent dentition and 42% for deciduous teeth (Vos, 2015). Mild or severe untreated dentine caries exhibits symptoms such as pain, unlike the initial stage of enamel caries which is asymptomatic (Selwitz, Ismail, & Pitts, 2007). The pain can last between 1 hour to

several hours in a day with sudden shifts in hot or cold temperature, and when consuming drinks or sugary products, thus causing significant distress to patients (Fejerskov & Kidd, 2008). This can cause disability adjusted life-years (DALYS) up to 38% for permanent teeth (Marcenes et al., 2013). It is considered vital to manage dentine caries as the disease progression is faster in dentine when compared to enamel (Mejare, Stenlund, & Zelezny-Holmlund, 2004). It is particularly vital to manage the disease at this stage before it invades into the pulp and causes permanent damage to the pulpal tissues (E.A. Kidd et al., 1998).

2.2 Dental caries process

Dental caries is often referred as a multifactorial disease, factors such as consumption of dietary sugars, salivary composition and its flow, exposure to fluoride and surrounding dental biofilm (Selwitz et al., 2007). The caries process begins with an alteration in the microbial ecology when fermentable carbohydrates are metabolized and the pH falls below critical levels (Fejerskov & Kidd, 2008; Fejerskov & Nyvad, 2003). The endogenous bacterial ecology within the plaque biofilm produces acids as a by-product of the metabolism of fermentable carbohydrates (Aamdal-Scheie, Luan, Dahlen, & Fejerskov, 1996). These acids cause the pH levels to fall below a critical value causing demineralization of tooth structures (Featherstone, 2004; Fejerskov, Scheie, & Manji, 1992). The leaching out of calcium, phosphate and other minerals continues during the demineralization process and cavitation will ultimately occur (Featherstone, 2004).

The lesion progression from enamel to dentine begins when dental plaque is left undisturbed on the tooth surface for one week. At this stage, histologically macroscopic inter-crystalline spaces are seen, which suggest partial dissolution of enamel (Fejerskov & Kidd, 2008). After 14 days, the minerals from the surface have leached out and sub-surface mineral loss from deeper tissues begins, causing increased pore volume. After

air-drying clinically, a white opaque area is visible with mineral loss up to 20-100μm deep. After three to four weeks, marked irregularities and focal holes appear with an overall increase in porosity and white opaque areas could be seen without air drying (Holmen, Thylstrup, Ogaard, & Kragh, 1985). After week 4 the white spot lesion exhibits a chalky surface due to an increase in internal enamel porosity, causing loss of translucency and the enamel appears opaque (Fejerskov & Kidd, 2008). At this stage, depending on the size and number of porosities the dentine and the dentine pulp-complex will begin to respond to stimuli (Bjørndal & Thylstrup, 1995). The reaction from the dentine occurs even before the bacterial invasion, as acids continue to dissolve the apatite crystals and eventually reach the amelo-dentinal junction (Arends, Ruben, & Jongebloed, 1989). The minerals continue to dissolve and diffuse into the lumens of the dentine tubules causing new whitlockite to be formed (Pashley, 1996). Subsequently, the appetite crystals of the intertubular dentine and later the peritubular dentine begin to decrease in size, leading to softening and demineralization of the dentine (T. Fusayama, 1991).

At the enamel surface, the tooth becomes fragile and a cavity with a narrow surface opening and broader base is formed, favouring the undisturbed growth of bacteria to penetrate into the dentine (Arends et al., 1989). The proteolytic enzymes continue to destroy the non-collagenous and collagenous parts of the organic matrix (Larmas, 1972) The continuous process of destruction creates an aggregation of bacteria and necrotic coalesces of softened infected dentine (Frank, 1990). The mushy clump of bacterial aggregation and outer demineralized dentine zone increases with the ongoing progression of a lesion. The schematic diagram of Figure 2.1a shows the progression of enamel caries reaching to the sclerotic part of the dentine, Figure 2.1b shows a stereomicroscope image of sectioned carious tooth showing layers of dentine caries formed as a response to the carious process. As caries progresses within the dentine and

reaches towards the pulp, deposition of mineral in the dentinal lumens becomes restricted (Arnold, Konopka, Kriwalsky, & Gaengler, 2003). Ultimately, with further progression of carious attack, the bacterial penetration reaches the pulp, causing inflammation (Trowbridge, 1981).

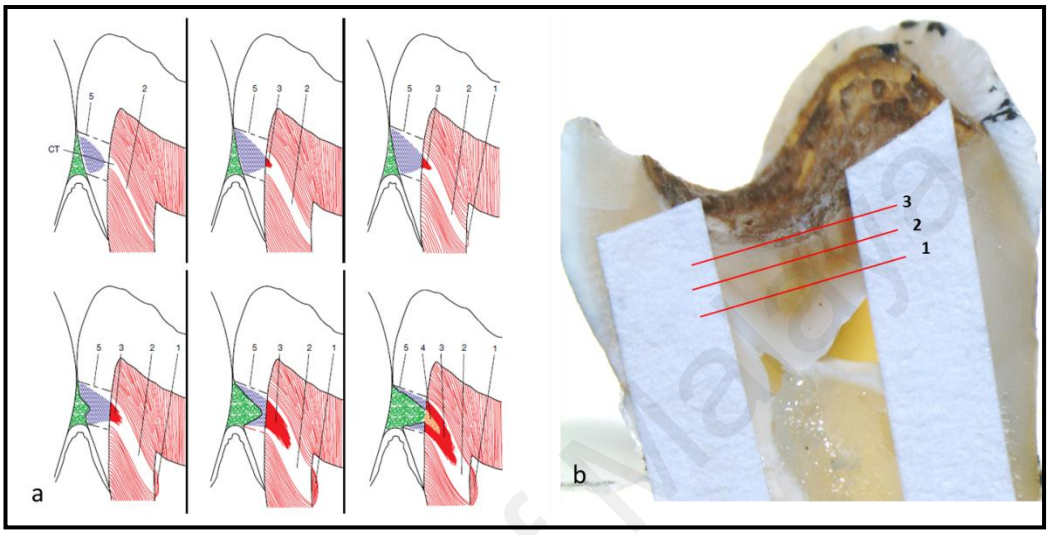

Figure 2.1 Schematic and stereomicroscope image of caries progression

a) Diagrammatic representation of the various stages of caries lesion: 1. Reactionary dentine, 2. Transparent zone, 3. Zone of demineralization, 4. Zone of bacterial invasion, 5. Enamel caries (Modified from Fejerskov and Kidd, 2008). b) Longitudinal section of dentine caries: 1. Reactionary dentine, 2. Transparent dentine, and 3. Zone of demineralization and bacterial invasion.

2.3 Zones of dental caries

The dissolution of minerals begins at the enamel rod boundary and widens the inter-crystalline spaces giving an appearance of needle-like appetite crystals (Palamara, Phakey, Rachinger, & Orams, 1986) resulting in nano-porous ultrastructure of crystallites (T. T. Huang, He, Darendeliler, & Swain, 2010). Early enamel caries or white spot lesions consists of two zones, surface layer and sub-surface zone, that are

often referred to as the body of lesion. The surface layers exhibit lesser mineral dissolution when compared to the body of lesion (Haikel, Frank, & Voegel, 1983)

Dentine is more complex, hydrated and structurally different compared to enamel. Dentine is comprised of: i) dentinal tubules surrounded by ii) highly mineralized peritubular dentine, with iii) intertubular dentine consisting of type I collagen and hydroxyapatite crystals and iv) dentinal fluid (Marshall Jr et al., 1997). Dentine is susceptible to caries attack as the apatite crystals are calcium deficient and carbonate-rich in content, and dentinal fluid fills the gaps between the collagen fibrils, leading to higher acidic solubility of the crystals (G. W. Marshall Jr, 1993). The other differentiating factor is the potential of dentine to remineralize, lay down reparative dentine and protect the pulp due to the presence of fibril cross-banding collagen (Marshall Jr et al., 1997) and the presence of vital odontoblast supplying calcium and phosphate that facilitate the remineralization process (T. Fusayama, 1991; Perdigao, 2010).

2.3.1 Zones of dentine caries

The demineralization process of dentine results in the formation of two structurally and chemically altered layers: the infected dentine (an outer carious layer) and the affected dentine (an inner carious layer) (T. Fusayama & Kurosaki, 1972; T. Fusayama, Okuse, & Hosoda, 1966). This classification is widely used and has been adopted and cited in the literature for the identification of carious dentine layers (Marshall Jr et al., 1997; Y. Wang, Spencer, & Walker, 2007). Arnold et al (2000) defined the carious layers into six: i) softened dentine, ii) demineralized dentine, iii) bacterial invaded dentine, iv) translucent zone, v) hypermineralized translucent zone and vi) secondary dentine (Arnold, Gaengler, & Saeuberlich, 2000). Besides classifying dentine caries into zones, Fusayama (1991) described the aspects of the carious process involved in dentine

demineralization: i) demineralization by dissolution of inorganic minerals, ii) destruction of organic structures and iii) bacterial invasion. In an earlier publication, Ohgushi and Fusayama (1975) described the key difference between caries-infected dentine and caries-affected dentine as the presence of the cross banded structure of collagen fibres that remained intact in the caries-affected dentine (Ogushi & Fusayama, 1975). Section 2.4.1 provides a detailed description of these zones.

2.4 Aetiological factors of dental caries

The understanding of the aetiology of dental caries has been evolving for many decades. It is now established that dental caries, being a multifactorial disease, is also regarded as a disease that is caused by an 'imbalance' between pathological factors and protective factors (Featherstone, 2006). The pathological factors are the cariogenic bacteria, which produces high levels of acids by metabolizing the carbohydrates and altering the pH within the dental plaque. The protective factors are the calcium and phosphate in saliva and the quantity of saliva, levels of extrinsic fluoride and other antibacterial agents (E. Kidd, 2005). When these factors shift and create an 'imbalance', the mineral maintenance of the teeth is disturbed, resulting in the initiation of the demineralization process (Kaidonis & Townsend, 2015). Some of the biological and external factors will be discussed in the following section.

2.4.1 The host - "Tooth Susceptibility"

As the literature suggests, the concepts of caries-resistant teeth hypothesized that individuals differed in their susceptibility towards dental caries. Factors such as nutrition and genetics could be the possible reason for the change in the structural layout of the organic or inorganic components in the teeth matrix (Cevc, Schara, & Skaleric, 1980), local factors and the physio-chemical behaviour of the tooth structure towards the changing environmental condition have been extensively studied. The enamel

surface is essentially a nano porous structure made up of hydroxyapatite layer, which allows the influx and outflux of calcium, phosphate, carbonate and other ions, depending on the presence of acid and the buffering mechanism of the saliva (E. Kidd, 2005). The ionic substitutions influence the physical strength of the apatite crystals making the enamel more or less more susceptible to demineralization (Nelson, 1981). However, in the presence of fluoride in the oral environment, the hydroxyapatite crystals transform to fluorapatite crystals making enamel more resistant to acid attack (Moreno, Kresak, & Zahradnik, 1974). When fluoride was applied on dentine surfaces in-vitro, a similar reduction in demineralization was observed, however higher levels of fluoride are required to create a resistant fluoride surface layer (ten Cate, Damen, & Buijs, 1998). On the other hand, if fluoride intake is increased during the teeth development phase, the mineralisation phase can be affected resulting in fluorosis. Teeth could be permanently hypomineralised, clinically white spots and pitted enamel surface can be observed in mild and severe fluorosis respectively (Robinson et al., 2004). These developmental structural alterations in enamel and dentine predisposes the teeth to caries (Slootweg, 2007).

2.4.2 The agent - "microbiome within dental plaque"

Dental caries is known as a bacterial disease, although not all microbes residing in the oral cavity induce or contribute to the caries process. This led researchers in the earlier half of last century to search for major pathogens which were cariogenic in nature (van Houte, 1994). The hypothesis supporting the search for predominant or major microbes involved in the caries process was elucidated by Marsh (1989), who stated that the shift towards specific and dominating cariogenic organisms by stable microbial plaque community will happen when environmental factors such as excessive quantity and frequency of carbohydrates are made available in the plaque and oral environment.

In the dentine caries lesion, the resident microflora is a mixed microbial community, predominant microbes in enamel caries shift from *Streptoccocus* mutans and *actinomyces* to *lactobacilli*, *prevotella* and *propionibacterium*, suggesting the role of these bacteria as more active in the progressive stages of caries (Chhour et al., 2005; Munson, Banerjee, Watson, & Wade, 2004; Takahashi & Nyvad, 2011). This shift of the selective microbial colonization at the advancing front of progression of caries is primarily due to the change of microbial acid-induced adaptation and acid induced selection of the non-mutans bacteria, which thrive better in a low-pH environment (Takahashi & Nyvad, 2011). The relationship between *Streptococcus* mutans and the aetiology of dental caries may be too simplistic and does not highlight the cause and effect relationship (Beighton, 2005). The use of next-generation-sequencing and metagenomics techniques has revealed that streptococcus mutans account for only 0.1% in dental biofilm and 0.7- 1.6% in carious lesions (Gross et al., 2012; Simon-Soro, Belda-Ferre, Cabrera-Rubio, Alcaraz, & Mira, 2013). In recent years, new molecular methods genus such as Veillonella has been found to be the dominant microbes within dentine caries (Belda-Ferre et al., 2012).

In conclusion, the polymicrobial occurrence in dental caries still does not explain the true aetiological picture of caries. Metatranscriptomics, metabolomics and proteomics are possible approaches which may explain the mechanism of pathogensis at the molecular level that initiates and progresses dental caries (Nyvad, Crielaard, Mira, Takahashi, & Beighton, 2013).

2.4.3 The environment - "Dietary sugars"

The Hopewood and Vipeholm studies which were carried out in 1942 and 1945 respectively are two human studies which established the cause effect relationship between fermentable sugars and dental caries. Both the studies were later terminated

due to ethical reasons. In the Hopewood study, no dental caries was observed when the children were given raw vegetables and soya bean; whilst in the Vipeholm study, mentally disabled patients were served with sugary and sticky candies between meals which resulted in cavitation in the teeth (Gustafsson et al., 1954). The Turku study which was carried out much later in the 1970s in Finland, revealed that not all types of sugar will cause dental caries. Sugars such as sucrose when replaced by xylitol can decrease incidence of caries activity (Moynihan & Petersen, 2004). Other cross sectional studies summed up by Rugg-Gunn and Hackett (1993) (Rugg-Gunn & Hackett, 1993) and longitudinal studies (Grindefjord, Dahllof, Nilsson, & Modeer, 1996; Lachapelle-Harvey & Sevigny, 1985) established the evidence linking sugars as an important aetiological factor for dental caries. However, one must be watchful that caries is not linked to a single causative factor.

There are various types of sugars. The fermentable carbohydrates are often referred to as free sugars, glucose polymers, fermentable oligosaccharides and refined starches. Free sugars are commonly used in reference to mono and disaccharides which are used by food manufacturers in the form of corn syrups, honey, fruit juices and other concentrates (WHO, 2015). Within these dietary sugars, sucrose in the form of processed food or in its monosaccharide form is considered as the most cariogenic sugar as it is readily fermented by the oral bacteria and serves as a substrate for the synthesis of extracellular polysaccharides in dental plaque (Ccahuana-Vasquez et al., 2007; Zero, van Houte, & Russo, 1986). Recently, similar sugars consumed in the form of carbonated soft drinks, juices and milk have revealed alarming association between children who consumed these fluids and incidence of dental caries (Sohn, Burt, & Sowers, 2006).

In the current era where exposure to fluoride is more common, the cause-effect relationship between amount of sugar consumption and incidence of dental caries is not as high as it was previously reported (Burt & Pai, 2001). An analysis of 90 countries by Woodward and Walker suggested that if individuals maintain good oral hygiene and are exposed to fluoride, higher levels of sugars may be endured before caries could occur (Woodward & Walker, 1994). Yet there is still significant emphasis on sugar being the key factor which sets up the causal chain of dental caries and there is a log-linear dose response between the amount of sucrose consumed and the progressive lifelong development of caries (Sheiham & James, 2015).

2.4.4 Other aetiological factors

There has been a significant amount of studies in the literature that had investigated the aetiology of caries and the probable role of genetics as a risk predictor. A study has provided evidence for protective and risk factors of dental caries having a strong genetic aspect (Bretz et al., 2005). There are several other traits such as tooth morphology, immune response, saliva and preference to diets that support the genetic determination of dental caries (Wright, 2010). Slayton et al (2005) reported that a few specific genes such as amelogin and tuffelin may indicate association with caries risk (Slayton, Cooper, & Marazita, 2005) However, Wendell et al. in 2010, investigated selected genes related to taste preferences that are linked to the taste pathways gene for a more direct association with dental caries. They found a significant association between the taste pathways and individuals with higher decayed missing filled teeth (DMFT) scores (Wendell et al., 2010).

2.5 Types of dentine lesion: detection and management

The superficial dental biofilm in contact with intact enamel continues to demineralize dentine within the same confined region in its depth. At this stage, the enamel-dentine lesion complex could be arrested by using a non-surgical intervention approach (Bjorndal, 2002). When demineralization progresses towards the enamel-dentine junction (EDJ), the reparative process of dentine initiates however the bacterial invasion has not occurred (Shovelton, 1968). The zone of dentine demineralization continues to be sub adjacent to the non-cavitated enamel as it narrows its progression towards the pulp, following the dentine tubules (Pashley, 1985). Clinically, dentine caries manifests as 'close dentine lesions' and 'open dentine lesions'; each requiring different methods of detection and treatment modality.

2.5.1 Closed dentine lesion

Closed dentine lesions develop as occlusal or approximal caries when microbial irritants and acids reach the EDJ and initiate dentinal demineralization. The enamel stays intact while common homogenous microflora such as lactobacilli dominate the bacterial community (Bjorndal & Larsen, 2000). At this stage, clinicians' are challenged to assess the extent of the spread of caries into dentine and to decide whether an interventive approach is required (E. A. Kidd, Ricketts, & Pitts, 1993). This dilemma arises because the dentine lesion at this stage is below the intact enamel and may not be visible on radiographs (Lehmann et al., 2012). Clinically, this stage is a non-cavitated stage. The International Caries Detection and Assessment System (ICDAS II) establishes that Code 2 is when distinct white colour is observed wider than the fissure, the lesion has progressed 50% into the outer third of dentine. In Code 3, there is minimal localized enamel breakdown (micro-cavitation), but dentine is not visible, and histological

assessment shows that the lesion is 77% in the dentine. Code 4 is when dark underlined shadows start appearing with or without enamel breakdown with the lesion having penetrated 88% into the dentine (K. Ekstrand, Kuzmina, Bjorndal, & Thylstrup, 1995; Ismail et al., 2007). Low quality bitewing radiographs have shown poor correlation with accurate detection of occlusal dentine lesions when using ICDAS. (Jablonski-Momeni, Stucke, Steinberg, & Heinzel-Gutenbrunner, 2012). Radiographically, dentine demineralization is only visible when the caries have extended into the middle third of the dentine and radio opacity is significantly associated with infected dentine (D. N. Ricketts, Kidd, & Beighton, 1995).

Monitoring lesion activity at this stage is critical, as rapidly progressing lesions lead to laying down of tertiary dentine and as it progresses dentine will show absence of a tubular dentine (Bjorndal, 2002). However, for a clinician to detect lesion activity and progression, they are restricted to using visual-tactile and even supplemental diagnostic information using laser fluorescence, light emitting diode fluorescence, spectral differences and alternative current impedance spectroscopy which provide no valid indication (Lehmann et al., 2012). Evidence has confirmed that due to these reasons, half of the suspicious or closed contact lesions are often later identified as being advance dentine caries (Bader & Shugars, 2006). It is without such concrete evidence that a dentist must decide whether to remineralise the lesion, seal the tooth with caries present or excavate and restore the tooth (Mount & Ngo, 2000). According to the National dental practice-based research network (National dental PBRN), to arrive at a diagnosis and treatment decision for suspicious or questionable occlusal dentine caries is one of the most challenging tasks a dentist faces (Makhija et al., 2014).

Abundant literature has shown that remineralization of dentine caries is possible (Alves et al., 2010; Bjorndal et al., 1997; Massara, Alves, & Brandao, 2002). The literature

supports the view that when the bacterial environment is changed, there is a difference in dentine consistency and radiolucency (Alves et al., 2010; Mertz-Fairhurst et al., 1998). Nonetheless, evidence has also shown that pulpal inflammation is linked to the level of bacterial microleakage, thus dentine which is heavily infected could lead to severe pulpitis (Grieve, Alani, & Saunders, 1991). A systematic review has shown little evidence that non-surgical treatments such as fluoride, sealant, resin infiltration, xylitol, chlorohexidine and CPP-ACP could arrest or slow down the progression of active dentine caries in young patients (Duangthip, Jiang, Chu, & Lo, 2015).

2.5.2 Open dentine lesion

If the dentine caries remains untreated in a closed environment, eventually the demineralized and undermined enamel breaks due to mechanical stress, changing the environment into an open ecosystem. This stage is known as 'cavitation' with exposure of dentine and invasion of microbes thus creating mixed lesion activity (Bjorndal, 2002). During the dentine exposure stage, heavy bacterial invasion takes place; clinically the dentine becomes soft, moist, disintegrated, demineralized and necrotic. Extensive mineral is lost at this stage and as the moisture decreases the dentine shrinks and a clinical visible gap develops between the enamel and the dentine (Bjorndal, 2008). Consequently, with the speed of the advancing front of the dentine lesion there is a fine balance with the rate at which the pulp-dentine defence can be laid down, which determines the thickness of the reactionary affected dentine (D. Ricketts, 2001). During deposition of reactionary dentine, there is amplification of collagen synthesis and alkaline phosphate, allowing the pulpal cells to deposit a cartilage-like layer appearing to be an abnormal tubular dentine (Massler, 1967).

In an open dentine lesion, discoloration of demineralized dentine is typical. According to Bjorndal and Larsen (2000), the Millard reaction occurs in the organic component of

the dentine, where dentine proteins interact with aldehydes produced by the bacteria, causing discolouration. On the other hand, others have attributed the dentine caries discoloration to the influx of external stains and the overall results of precipitation of dissolved minerals from the environment (Kleter, 1998). The colour of a demineralizing dentine lesion is yellowish to light brown and decreased in hardness compared to the unaffected dentine, whereas open lesions often appear darker and more pronounced with a softened consistency when compared to healthy dentine (A. Banerjee, T. F. Watson, & E. A. Kidd, 2000b). Minimal invasive dentistry (MID) emphasizes the protection and remineralization of dentine caries whenever possible. In an open lesion, the common practice is to remove only the soft wet necrotic caries-infected dentine and leave the remineralizable caries-affected dentine. This practice has shown adequate adhesive bonding potential (Banerjee, Kellow, Mannocci, Cook, & Watson, 2010) when restoring the cavity with material that has optimum biological and physical properties (Frencken et al., 2012). Considering affected dentine has the ability to remineralize, MID focuses on maximum tissue preservation and only on removing layers with high bacterial load (Hayashi, Fujitani, Yamaki, & Momoi, 2011; Orhan, Oz, Ozcelik, & Orhan, 2008). However, using change in colour and consistency of dentine caries layers are not reliable parameters for the identification of layers and they do not explain the correlation of the demineralization process with the level of infection (A. Banerjee, T. Watson, & E. Kidd, 2000). Nonetheless, the same parameters are used routinely as identification parameters for excavation of infected dentine (Bjorndal et al., 1997; M. Maltz et al., 2002).

2.6 Ultrastructure of dentine layers

In the following section detailed ultra-structure of dentine layers will be discussed.

2.6.1 Infected dentine

Caries-infected dentine in established cavities is located in the superficial region directly in contact with cariogenic pathogens and oral environment. However, prior to cavitation, demineralization of dentine has already begun caused by bacterial by-products and acid. Histologically, the demineralized dentine exhibits large tubular spaces due to demineralization of PTD compared with ITD. (Kinney, Balooch, Haupt, Marshall, & Marshall, 1995). At this juncture the collagen meshwork remains intact; it will only collapse when bacterial invasion occurs (G. W. Marshall Jr, 1993). Once there is a break in the enamel surface, the environment favours more towards a polymicrobial niche. These microbes directly come into contact with the dentine and the zone of advanced destruction establishes. The peripheral dentine tubules resorb and large caverns are dominated with bacteria (Frank, 1990). The odontoblastic process and peritubular dentine are completely absent with a few loosely scattered collagen like fibres with indistinct or no interbands; this zone is often referred to as the zone of destruction (Ogushi & Fusayama, 1975). Below this zone, tubular invasion of bacteria is often seen. The odontoblastic processes are completely destroyed without any sclerosis forming dead tracts and the tubules may coalesce to form liquefaction foci. This region is referred to as the zone of bacterial penetration (E. A. Kidd & Fejerskov, 2004).

2.6.2 Affected dentine

Beneath the ID layer lies the affected dentine (AD) layer as classified by Fusayama (1993). The AD layer has three zones: the turbid, transparent and sub-transparent zones (T. Fusayama, 1993). The essential defence reaction i.e. deposition of mineral within

the dentinal tubules occurs within this layer. The formation of sclerotic dentine process essentially requires vital odontoblast (Johnson, Taylor, & Berman, 1969). Massler (1967) suggested that superficial sclerosis in a reaction to saliva is an occurrence that is linked to re-precipitation of mineral from the carious lesion and saliva, while sclerosis occurring near to the pulp is from precipitation of calcium which is sourced from pulp.

The turbid zone is completely absent of the PTD cuffs, which is usually present surrounding the dentine tubules and varies in size and shape. In this zone, few needle like crystals of apatite can be observed within the ITD, although they are significantly smaller than those observed in the transparent zone (Zavgorodniy, Rohanizadeh, & Swain, 2008). The transparent zone is a bacteria free region with both PTD and ITD with less distortion in structures when compared to healthy dentine (Sarnat, 1965b). The classical feature of this layer is the mineral deposition of Beta-octatricalcium phosphate (β-TCP) within the tubules in an unstructured format (Daculsi, LeGeros, Jean, & Kerebel, 1987). These highly calcified rhomboid shape crystals completely occlude the lumen and are often referred to as whitelockite crystals (Frank, 1990). The sub transparent dentine is closest to the normal or secondary dentine, occluded with whitelockite crystals (Ogawa et al., 1983).

2.6.3 Healthy Dentine

The prominent features observed in healthy dentine when viewed in cross-section under scanning electron microscopes are dentine tubules, surrounded by PTD and the remaining tissues around this is referred to as ITD. The PTD is seen as ring-shaped structures cuffed around the dentine lumens (Frank, 1959; Takuma, 1960). PTD contains hyper-mineralized ground substance which makes it appear as an extremely smooth area when compared with that of the ITD (Frank, 1959).

2.7 Composition of dentine is a hard, elastic and avascular tissue, it is 70% inorganic, 20% organic matrix and 10% water by weight%, and 45%, 33% and 22% by volume, respectively(Nanci, 2008). . The inorganic phase is mainly formed by the hydroxyapatite crystals, which are of similar size. However, these crystals are approximately ten times larger in the enamel (Kirkham et al., 1998). The orientation of the dentine tubules, which is the hollow part of the dentine matrix, is believed to be straight or slightly curved (S-shape) throughout the dentine (Zaslansky, Zabler, & Fratzl, 2010). However, with recent 3-D microtomography imaging it was revealed that at approximately 300 and 800 µm below the DEJ, 75% of the tubules showed ≥ 90˚ and 20-30˚ tilts respectively (Zaslansky et al., 2010). There are numerous micro branches and ramifications seen branching out of the main tubules, especially at sites where the dentinal tubules are in low density (Kagayama et al., 1999).

Mineralized dentine is divided into intertubular (ITD) and peritubular dentine (PTD). Dentine is composed of mainly ITD, which is formed by odontoblast during dentinogenesis, and through pre-dentin mineralization. The volume (%) of ITD decreases from DEJ to the pulpo-dentinal junction, while PTD increases (Pashley, 1996). PTD is free of collagen matrix, and is formed by highly dense minerals inside the walls of the dentine tubules; its mineral content is 40% higher compared to ITD, and is spatially more homogenous (Tjäderhane, Carrilho, Breschi, Tay, & Pashley, 2009).

The dentine matrix is mainly (90%) composed of Type I collagen, with trace amounts of Types III and V collagen (Gage, 1984). Each collagen is made of a triple helix of three polypeptide chains, 300 nm long and has a diameter of about 1.5 nm. Other non-collagenous structures in the matrix are phosphoproteins, phospholipids and proteoglycans, which also play an important role in depositing minerals during dentinogenesis. During the carious process, demineralization affects the inorganic

portion of the dentine, while the collagen matrix stays unaffected as its extrafibrillar minerals protect its surface (Fejerskov & Kidd, 2008). As the caries process continues to advance, the extrafibrillar minerals begin to dissolve. The intrafibrillar minerals which is most resistant to demineralization remain intact, and act as the nucleus for remineralization when the environment becomes favourable (Bertassoni, Habelitz, Marshall, & Marshall, 2011). At this stage, due to enzymatic disturbance, Type III collagen is laid concurrent with the formation of sclerotic dentine (Karjalainen, Soderling, Pelliniemi, & Foidart, 1986).

2.8 Caries detection

Caries diagnosis provides the foundation to reach an appropriate treatment decision. To achieve good treatment outcomes, dentists requires a judicious approach aided by robust diagnostics techniques (Nyvad, 2004). The term "caries detection" implied that there are two objectives to be achieved: firstly, as an impartial method that could reliably determine the presence of caries, and secondly to ensure that the procedures or aids used in gathering the necessary information in the detection of dental caries enable dentists to arrive at the correct diagnosis (Baelum, Heidmann, & Nyvad, 2006). This repetitious search process using signs and symptoms during clinical examination to ascertain caries status is also commonly referred as "caries diagnosis" (Nyvad, 2004; N. B. Pitts, 2004; Ten Bosch & Angmar-Mansson, 2000). Similarly, when referring to the detection of caries in dentine, it infers towards sensitivity and specificity of radiographic techniques (Schwendicke, Tzschoppe, & Paris, 2015), visual inspection (Heinrich-Weltzien, Weerheijm, Kuhnisch, Oehme, & Stosser, 2002), laser-induced fluorescence (Lussi, Megert, Longbottom, Reich, & Francescut, 2001) or other fiber-optic and electrical resistance measurement methods (Ie & Verdonschot, 1994). However, the term caries detection during dentine caries management may refer to searching for those parameters

that could help in differentiating the caries infected dentine and its differentiation from remineralisable affected dentine (Banerjee, Yasseri, & Munson, 2002). Histologically, it is possible to differentiate between an outer unremineralisable and an inner remineralisable layer of carious tissue (Kuboki et al., 1983). However, to identify and differentiate the carious layers in a clinical setting is a challenging task, and to date no diagnostic tool is available to aid the accurate determination of the caries-removal endpoint (Neves, Coutinho, Cardoso, et al., 2011).

2.9 Clinical significance of identification of dentine layers

Clinical decision making is often considered as a multidimensional and complex task (Higgs, 2008). A common situation requiring health professionals to make clinical decisions encompasses an evaluation towards the performance of diagnostic tests and the administration of treatment accordingly. The accuracy of diagnostic tests aids results with favourable health outcomes that are beneficial to patients and induces fewer risks (Kassirer, 1976). In the discipline of restorative dentistry, extensive research has been undertaken towards the diagnosis, treatment planning (Bader, Shugars, & Bonito, 2002; Baelum et al., 2006; Maupome, Schrader, Mannan, Garetto, & Eggertsson, 2010) and outcomes related to caries management (Bader & Shugars, 1997; Bader, Shugars, & Bonito, 2001; Baelum, 2008). The treatment decision-making by dentists is often varied and there is evidence to show poor correlation with the number of positive treatment decisions made. Kay et al., (1992) reported that only 16% of dentists showed good agreement towards treatment for approximal caries lesions in relation to depth (Kay, Nuttall, & Knill-Jones, 1992). Reasons linked to such compromised decision-making in caries management are often due to lack of discrete analytical diagnostic steps in caries examination. Visual scripts and use of visual-tactile techniques both in caries examination lead to diagnosis based on a non hypothetical-deductive process (Bader &

Shugars, 1997). These caries diagnostic scripts are executed routinely without formal reasoning, drawing on pattern recognition and experiences from cases presenting similar features (Crespo, Torres, & Recio, 2004).

A similar practice of clinical pattern recognition script by dentists is the colour and consistency of dentine caries during deep caries management, which is commonly used by dentists for differentiating demineralized or infected dentine from remineralizable affected or healthy dentine (Fejerskov & Kidd, 2008; E. A. Kidd, Joyston-Bechal, & Beighton, 1993). However, change in colour and consistency of dentine caries layers do not correlate to the demineralization process and the level of infection (A Banerjee et al., 2000). Using these parameters for visual and tactile examination aid in differentiation and later in excavation; together they help clinicians to determine the caries-removal endpoint (Bjorndal et al., 1997; M. Maltz et al., 2002). Conversely, these parameters have shown lack of objectivity and to date no definite diagnostic tool is available to clinically define the carries-removal endpoint (A Banerjee et al., 2000; Neves, Coutinho, Cardoso, et al., 2011). To this end, the extent to which the carious dentine layer must be removed to achieve mechanical and biologically successful restoration is yet to be ascertained, and often results in overextended cavity preparations (Neves, Coutinho, Cardoso, et al., 2011) or incomplete removal of diseased tissues, leading to poor prognosis and durability of restorations (Bergenholtz & Spangberg, 2004; Weerheijm, Kreulen, de Soet, Groen, & van Amerongen, 1999).

Failure to differentiate infected, affected and healthy dentine layers leading to over or under extended preparation results in several complications during deep caries management. Systematic reviews have established that using manual methods to decide caries-removal endpoint and performing complete excavation or step-wise excavation or partial excavation have some advantage over each other, yet all techniques have resulted

in a certain amount of risk towards pulpal exposure (D. Ricketts et al., 2013; D. N. Ricketts, Kidd, Innes, & Clarkson, 2006b). When there is uncertainty in identifying the infected layer and excavation end point, the remaining dentine thickness (RDT) between the floor of the cavity and the roof of the pulp chamber is often too thin, thus compromising the pulpal health (Murray et al., 2003). This also suggests that removal of healthy dentine directly impairs the vitality of the tooth (Wisithphrom, Murray, About, & Windsor, 2006) and weakens the tooth structure, causing failure of future restorations (D. Ricketts et al., 2013). Without objective identification of dentine caries layers, the excavation process is difficult to execute.

Minimal intervention dentistry (MID) is the complete patient care perspective which encompasses a patient-dentist team-care approach to manage dental disease through identification and diagnosis, including caries risk assessment, preventive therapies, restoration and recall, and educating and empowering the patient to take responsibility for their personal oral health (Banerjee, 2013). MID also includes critical thinking during clinical caries diagnosis and when deciding on methods to be used in cavity preparation (Ericson, Kidd, McComb, Mjor, & Noack, 2003). During caries removal, the identification of dentine caries layers using MID strategies is limited to visual inspection upon using caries detector dye (Kuboki et al., 1983), light emitting diode fluorescence technique (Panayotov et al., 2013) and laser fluorescence (Neves, Coutinho, De Munck, Lambrechts, & Van Meerbeek, 2011).

Despite the advancement in caries diagnosis and management techniques over the last two decades, significant challenges and opportunities remain (Walsh & Brostek, 2013). Several diagnostic aids such as radiographic assessment, fibre optic transillumination (FOTI), laser-induced fluorescence (LIF), electrical conductance (EC), near-infrared light, and qualitative light-induced fluorescence (QLF) aid in the detection of hidden

dentine lesions (Pretty, 2006). However, during caries removal in a clinical setting, identifying the dentine layer with the aim to find the caries-removal endpoint is still unresolved. Dentists currently rely on the visual-tactile aspects of excavation methods, while the detection aids available can only provide feedback on the remaining amount of caries-infected dentine after excavation is done (Walsh & Brostek, 2013).

This limitation to accurately identify dentine layers substantiates a need for characterisation of dentine layers with respect to its properties. The soft necrotic nature of caries-infected dentine is inferior in chemical and physical properties for adhesion to dental materials, whereas caries-affected dentine exhibits adequate adhesive bonding potential, especially when the peripheral areas are surrounded by healthy dentine (Banerjee et al., 2010).

We propose that an ideal approach in the management of deep caries in a clinical setting would be to split it into two steps. Firstly, detection of dentine caries layers through structural and biochemical characterisation of soft decomposed caries-infected dentine, potentially remineralizable caries-affected dentine and healthy dentine. Secondly, using these characterised parameters to differentiate dentine layers and determine the end point for excavation.

2.10 Identification of dentine layers

In this section various instruments used as an aid to identify and differentiate dentine layers will be discussed.

2.10.1 Visual tactile methods

Black (1908) proposed the first operative concept to treat all layers of dentine caries, and to completely remove the infected and affected caries layers. Removal of soft dentine until hard dentine is reached was procedurally done using visual-tactile

assistance (Mount, 2007). Fusayama, (1972) later introduced a system based on the identification of two distinct dentine layers: an outer 'caries infected layer' and an inner 'caries affected layer' by means of fuschin-dye (T. Fusayama & Terashima, 1972). This led to a more conservative approach for caries management, that is removal of the outermost infected dentine layer with disrupted collagen structure and is incapable of remineralization. By doing so, the inner less demineralized affected layer retains its original collagen framework and could be remineralized. Kidd et al (1993), proposed clinical criteria to differentiate infected from affected dentine based on colour, consistency and humidity. These criteria are still commonly used today to determine excavation endpoints and to assess the amount of demineralized dentine that needs to be removed (A Banerjee et al., 2000). However the brown colour of dentine caries is attributed to several factors: exogenous stains from food over time, pigment-releasing bacteria or due to protein breakdown in the presence of sugar known as the "Maillard reaction" (E. Kidd, 2005). Due to these reasons, the identification of dentine caries layers based on colour is now considered as a weak parameter, whilst consistency and texture of tissue is comparatively more reliable (Massara et al., 2002). Dentine texture is further classified and often termed in the literature as soft, leathery or hard and is often used to classify the activity of caries lesion (Fejerskov & Kidd, 2008).

The relationship between dentine hardness and the presence of microorganisms is often debated. Some researchers reported no association between dentine consistency and bacterial colonization (Bönecker et al., 2003; M Maltz, Oliveira, Fontanella, & Carminatti, 2007), whereas there is a consensus that soft and wet dentine has a higher number of Streptococcus spp and Lactobacillus ssp (Ayna, Celenk, Atakul, Sezgin, & Ozekinci, 2003; Orhan et al., 2008). However, variations in dentine colour are not an absolute indicator of the presence of microorganisms during caries removal (M Maltz et al., 2007; Orhan et al., 2008). Nonetheless, microbiological analysis at the end of cavity

preparation showed that darker cavities contained a larger number of Streptoccpus spp and Lactobacillus ssp (Ayna et al., 2003; Bjorndal et al., 1997). The association between humidity and dentine colonization by microorganisms before and after the sealing of cavities following minimally invasive preparation, is unknown, although studies have shown that dentine becomes drier after a period of cavity sealing (Bjorndal et al., 1997; Orhan et al., 2008). Thus, based on the current literature, hardness and colour cannot be used as parameters for the identification of dentine layers. Furthermore, interpretation of these parameters through visual and tactile examination is too subjective.

2.10.2 Chemo-mechanical methods

Caries detector dyes are used for chemo-mechanical removal of caries infected dentine. The dye aids in the visual enhancement of the outer infected layer, followed by the mechanical removal of the infected layer using hand or rotary instruments until the stained outer dentine is completely removed (McComb, 2000). The first caries detection detector dye used was 1% acid red in propylene glycol solution (T. Fusayama & Terashima, 1972). It was based on a solution of 0.5% basic fuchsin in propylene glycol and is claimed to stain only the outer decomposed carious layer, leaving the affected dentine unstained. The selective staining of irreversible denatured collagen of infected dentine was due to the breakdown of the intermolecular crosslinks through bacterial lactic acid (Kuboki et al., 1983). Later, it was suggested that the staining was due to the difference in the degree of mineralization in dentine layers rather than the denatured collagen fibrils (Yip, Stevenson, & Beeley, 1994).

Histological sections of carious teeth excavated using fuchsin-guided techniques were used to assess the reliability of this caries-disclosing dye. Results showed that the tissue removal was much greater than the extent of the demineralized dentine when compared to using pre and post dental radiographs (Sato & Fusayama, 1976). The staining

specificity of caries detector dyes for infected dentine also resulted in the staining of healthy circumpulpal dentine and the DEJ due to a slight difference in mineralization levels when compared with the middle bulk of healthy dentine (Yip et al., 1994). Some concerns were also raised regarding the possible carcinogenic effects of fuchsin in intraoral use (Yip et al., 1994), thus the need for alternative caries-disclosing dyes.

Although a 1% acid-red solution (Caries Detector, Kuraray; Tokyo, Japan) was launched as an alternative to fuchsin, (Kuboki et al., 1983) clinical inconsistencies have been reported, showing the presence of stained tissue at non-carious DEJ sites (EA Kidd et al., 1989; E. A. Kidd, Joyston-Bechal, et al., 1993). Colour and microbiological assessment of the caries-stained and stain-free dentine failed to disclose the differences in the level of bacterial infection (Iwami et al., 2007; E. A. Kidd, Joyston-Bechal, et al., 1993). Using 1% acid-red solution can lead to staining of dentine clinically judged as "sound"; out of 10 non-carious teeth 30% had shown false positive diagnosis of residual caries (Boston & Liao, 2004). In another *in-vitro* study 100 cavities were prepared, out of which 57 cavities were considered caries-free and "hard and sound" while, the pulpal floors took up some stain from the disclosing dye (EA Kidd et al., 1989). In fact, it has been reported that it is with doubt that sound circumpulpal dentine will take up stain, because of its lower degree of mineralization (Boston & Liao, 2004; Yip et al., 1994).

Light pink staining from acid red at the inner layer of carious dentine is recommended to be left undisturbed as it shows that this layer has a lower degree of bacterial infection (Iwami, Shimizu, Narimatsu, Kinomoto, & Ebisu, 2005) and decreased demineralization of peritubular dentine (Zheng, Hilton, Habelitz, Marshall, & Marshall, 2003). The propylene glycol in both staining agents can easily infiltrate into normal dentine due its low molecular weight (76 MW), which explains the staining of healthy dentine

(Hosoya, Taguchi, & Tay, 2007). This finding has recently led to the introduction of a 1% acid-red dye in higher molecular weight polypropylene glycol (300 MW), making it caries specific (Boston & Liao, 2004). Although patients experienced less pain when chemo-mechanical methods are used during caries removal (Soni, Sharma, & Sood, 2015), sodium hypochlorite-based (Carisolv, Orasolv, Stockholm), enzyme based (papacarie, PAPACÁRIE , Brazil) and the conventional caries-detection dye have limitations and are considered to be time consuming (Hamama, Yiu, Burrow, & King, 2015).

2.10.3 Fibre optic transillumination

Fiber optic transillumination (FOTI) and Digital Imaging Fiber-Optic Trans-Illumination (DIFOTI), utilise light transmission through the tooth for caries detection (Cortes, Ellwood, & Ekstrand, 2003; Rechmann, Charland, Rechmann, & Featherstone, 2012). Fibre optic transillumination with a camera, the DIAGNOcam® (KaVo Dental, Lake Zurich, IL, USA), is based on simple transillumination and an excitation wavelength of 780 nm. The light that passes through the tooth is interpreted by a digital device positioned on the other side of the tooth. DIFOTI seems to perform well for early carious lesions and proximal lesions (Astvaldsdottir, Ahlund, Holbrook, de Verdier, & Tranaeus, 2012; Young & Featherstone, 2005), however, it has low specificity (Astvaldsdottir et al., 2012) and limitations in determining lesion depth and is considered exhausting and time consuming (Bin-Shuwaish, Yaman, Dennison, & Neiva, 2008). Evidence in the literature is still lacking with regards to the utilisation of the transillumination technique for identification of dentine caries layers.

2.10.4 Laser induced fluorescence (LIF)

Light fluorescence method used by Diagnodent® (Kavo, Biberach, Germany) utilises laser with wavelengths of 655 nm. Detection tools using the fluorescence phenomenon help to differentiate healthy from carious tissues via the presence of porphyrins, metalloporphyrins and various types of chromophores (Banerjee et al., 2004; Konig et al., 1998). For dentine, red autofluorescence is characteristic due to porphyrin synthesized bacterial activity in infected dentine (Koenig & Schneckenburger, 1994).The autofluorescence intensity of the emitted fluorescent light is captured and quantified (Hamilton, Gregory, & Valentine, 2006; Lussi et al., 2004). Few studies have shown the effective use of Diagnodent® for the detection of occlusal dentine caries underneath suspicious enamel and caries in residual dentine (Iwami, Shimizu, Hayashi, Takeshige, & Ebisu, 2006; Kinoshita et al., 2007; A.M. Lennon et al., 2002). Diagnodent® has also been tested as an objective tool to aid excavation for dentine caries (Eberhard, Bode, Hedderich, & Jepsen, 2008; Matsumoto, Wang, Zhang, & Kinoshita, 2007; Yonemoto, Eguro, Maeda, & Tanaka, 2006). For early caries diagnosis, LIF technology has been shown to be effective, however for caries excavation purposes, inconsistencies were observed (Neves, Coutinho, De Munck, et al., 2011); considerable variation in dentine caries removal has been reported (Eberhard et al., 2008). The Diagnodent® values tend to show higher values when the lesion is near circumpulpal dentine. This is attributed to the thickness of the remaining dentine, which influences the penetration depth of the incident laser and the excitation fluorescent properties of the tooth substance. Other limitation are staining which confounds the Diagnodent® readings, inability of the diagnodent tips to reach carious dentine due to the shape of the carious lesion and difficulty in determining the numerical value at which surgical intervention is indicated (Braun, Graefen, Nolden, & Frentzen, 2000; Chong, Seow, Purdie, Cheng, & Wan, 2003; Neves, Coutinho, De

Munck, et al., 2011; Yonemoto et al., 2006). In addition, dehydration or excessive moisture could also affect the readings (Al-Khateeb, Exterkate, De Josselin de Jong, Angmar-Månsson, & Ten Cate, 2002) and requires calibration (Krause et al., 2007).

2.10.5 Light induced fluorescence evaluator for diagnosis and treatment (LIFEDT)

Various kinds of LED are currently being used in intraoral cameras, to illuminate the tooth surfaces into the visible domain, either in the white light region or in a narrow band where the wavelength is 450 nm with a bandwidth of 20 nm. The Soprolife® camera (Acteon, La Ciotat, France)(Gugnani, Pandit, Srivastava, Gupta, & Gugnani, 2011; Panayotov et al., 2013) provides an anatomical image superimposed on an auto-fluorescence image. The device locates differences in the structure of the biological tissue by continuously illuminating with one frequency band while it generates a fluorescence phenomenon in a second frequency band. The brown colour of caries in daylight is perfectly superimposable over the dark red fluorescence detected with the Soprolife®. Sound dentine fluoresces green, and enamel has no fluorescence, although a bluish colour is often observed from the diffusion of the green light emitted by the dentine. The camera operates in three modes: the daylight mode utilises four white light LEDs; the diagnostic and treatment modes are provided by four blue LEDs (450 nm). A new camera, the Soprocare® , also provides three clinical modes: daylight, caries and periodontal. The caries mode focuses on enamel and dentine caries, and the periodontal mode on periodontal inflammation.

The images captured by Soprolife show a wide range of colours, healthy dentine appears green in fluorescence and the infected layer looks green black. In active caries, the infected/affected dentine interface appears bright red fluorescence and yellow brown in daylight. Abnormal dentine at the end of excavation appears grey-green, and

sometimes with a slight pink transparency (Terrer et al., 2010). The caries colour seems to describe the lesion well, yet it is not always an objective and reliable measure (Kuboki et al., 1983; Ogawa et al., 1983). In arrested lesions, the infected/affected interface appears dark red and dark brown in daylight mode. This tissue is difficult to excavate manually. Diseased dentine at the end of the excavation appeared light grey-green with systematically persisting shady pink fluorescence at the bottom of the preparation and opposite the pulpal wall. It has been recommended that the dentine need not be removed and it should not be considered as a false-positive signal (Panayotov et al., 2013). However, the authors stated that the deep red colour is observed in the deepest part of dentine caries along with some variation towards orange red colour which cannot be confirmed as to what this variation may indicate. The suggested idea for the colour to change in dental caries is linked to sugar protein reaction, and amino acid degradation in the presence of natural intermediate products - glycation or non-enzymatic browning (Maillard reaction) (Kleter, 1998). However, this may not be the only key factor for the colour to change and require further investigation. The current evidence provided from Soprolife is still in its infancy and lacks strong evidence to support the difference between the colours and its association with different layers of dentine caries.

2.10.6 Fluorescence-aided caries excavation (FACE)

Fluorescence Aided for Caries Excavation (FACE, SIROInspect® , Sirona Dental Systems GmbH, Germany) employs specific glasses to detect the fluorescence in dentine. This technique was developed as a direct method to clinically differentiate between infected and affected carious dentine. Several oral microorganisms produce orange-red fluorophores as the by-products of their metabolism (porphyrins), infected carious tissue will fluoresce red in a fraction of the visible spectrum (Alfano & Yao,

1981). These prophyrins were further categorized as proto- and meso-porphyrins (Lussi et al., 2004). FACE provides continuous visual detection of orange-red fluorescence during caries excavation and has higher sensitivity and specificity in differentiating infected from healthy dentine when compared to visual-tactile or the fuchsin dye-method (A.M. Lennon et al., 2002). FACE has also been shown to restrict over preparation of a cavity (A. M. Lennon, Attin, & Buchalla, 2007) and is less time consuming (A. M. Lennon, Buchalla, Rassner, Becker, & Attin, 2006). A study using a histological approach to evaluate fluorescence technology confirmed that dentine harvested at the end of cavity preparation contained fewer bacteria when compared to those from the visual-tactile method (A. M. Lennon, 2003). Software driven FACE equipped with a camera had also been tested and showed cavities, even under prepared cavities, were bacterial free compared to cavities excavated using manual methods (Ganter, Al-Ahmad, Wrbas, Hellwig, & Altenburger, 2014). However, the measure of these studies is the absence of bacterial load as an identification of affected dentine, (Ganter et al., 2014; A. M. Lennon et al., 2006) which may not be the true picture as it is the structural and biochemical composition of affected dentine that is critical in the remineralization process (Marshall Jr et al., 1997).

2.11 Optical coherence tomography

Optical coherence tomography (OCT) is an optical imaging tool which produces high resolution, cross-sectional topographic images of the microstructure of substance and biological tissues by computing backscattered light. OCT is also often referred to as an optical analog of ultrasound. It has an imaging range of 1-15mm and an axial resolution better than 5μm. It is capable of constructing cross-sectional and 3D tomographic images for oral screening and diagnosis. OCT is considered to fill a niche between ultrasound and confocal microscopy (Figure 2.2). The imaging can be achieved in a non-destructive optical approach in situ or in real time mode (D. Huang et al., 1991).

OCT is a non-destructive imaging modality that can produce cross-sectional images of internal biological structures, including ocular, intravascular, gastrointestinal, skin, and oral soft and hard tissue. In OCT, the tomographic image construction is done by measuring the echo time delay and intensity of backscattered light, with axial information as the first step from the tissue that is being scanned. Besides, the two dimensional images three dimensional data set can be extracted when scanning the cross-sectional plane or volume.

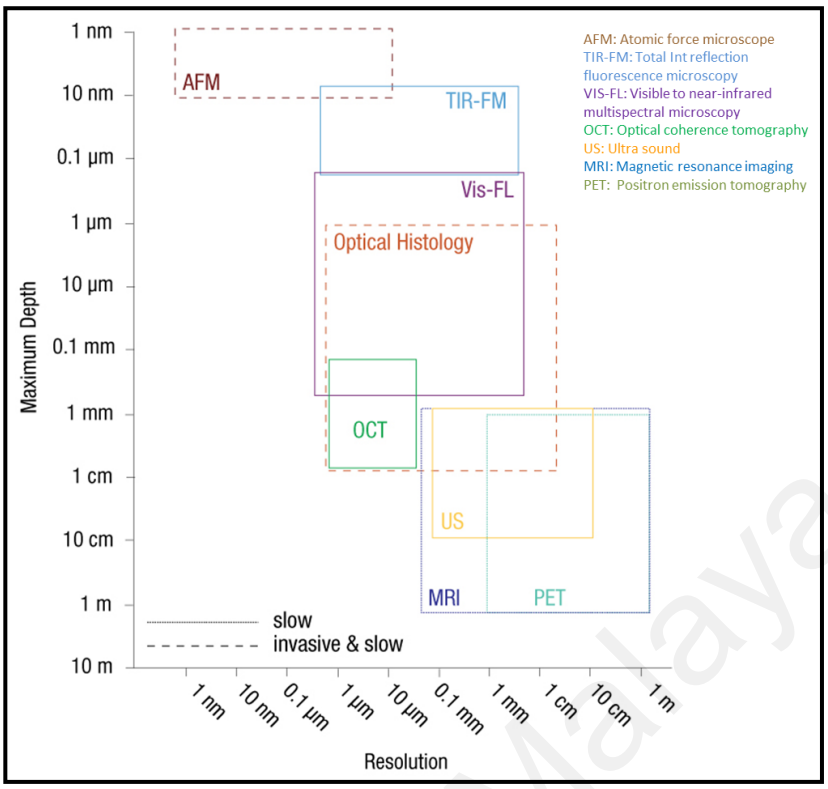

Figure 2.2: Comparison of OCT with other imaging systems

OCT being an optical analog of ultrasound, shows lowering imaging depth as a trade-off with significant higher resolution. OCT fills the imaging gap between confocal microscopy and ultrasound (Modified from Thorlab, Inc 1999-2016).

2.11.1 OCT background

OCT is considered similar to ultrasound imaging, except that it utilizes light instead of sound. However, the imaging resolution of 3-16µm can be attained using OCT, which is twice the higher magnitude than conventional ultrasound. Ultrasound imaging is a simpler version of reflection based imaging and can be used to understand OCT imaging. Unlike light in OCT, the acoustic pulses are generated by an ultrasound transducer which can penetrate and travel through human tissues. These sound waves are scattered and reflected depending on the tissues structures and its density. There are a series of reflections from the surface and the deep part of the tissues with variation in

intensities values. The transducers detect and emit acoustic pulses, depending on the time impediment between the pulses. The difference in intensity and distance between the natural structures provides information. The change in size of transducers can help capture depth resolved echo signals producing A-scan for an axial measurement of distance for thin tissue dimension and B-scans for tissues with larger sized areas. Ultrasound waves travel at 1500m/sec in water whereas the velocity of light is $3X10^8$m/sec. The spatial information can be determined using these measurements as there is a delay of reflected echoes according to the formula:

$$\Delta t = z/v$$

Where Δt is the echo delay, z is the distance the echo travels, and v is the velocity of sound or light.

However, for OCT, the speed of light is too high and echo time delays are extremely short for current detectors to capture this information. The measurement of a structure with 10μm resolution corresponds to a time resolution of 30fs. It is therefore not possible to detect the signal on this time scale. The echo pulse train of OCT can be indirectly measured by using interferometry. The interferometer technology, uses the spectral bandwidth of the light source which is equal to that of the pulsed light source,. Another advantage of OCT is that the light source may not need to be in contact with the material for an immersion light to transmit waves; this being an essential step in ultrasound.

2.11.2 Development of OCT

The first backscattered intensity interference for imaging was demonstrated by Huang et al (1991), who recorded the ex vivo images of retina using OCT. The images produced were 10 times the resolving power of ultrasound (depth resolution of 15 mm) and with 6

times deeper penetration depth (2mm). Later, the first *in vivo* imaging of retina was produced by Swanson et al. (1993).

One of the key developments in using high speed optical gating to achieve imaging in scattering biological tissues was the introduction of the Michelson-Morley interferometer (Figure 2.3). Interferometric detection is able to measure the backscattered light with high dynamic range and high sensitivity. The low coherence interferometry as proposed by Sir Issac Newton is now commonly used to characterise optical echoes and backscattering in optical fibres (Youngquist, Carr, & Davies, 1987).

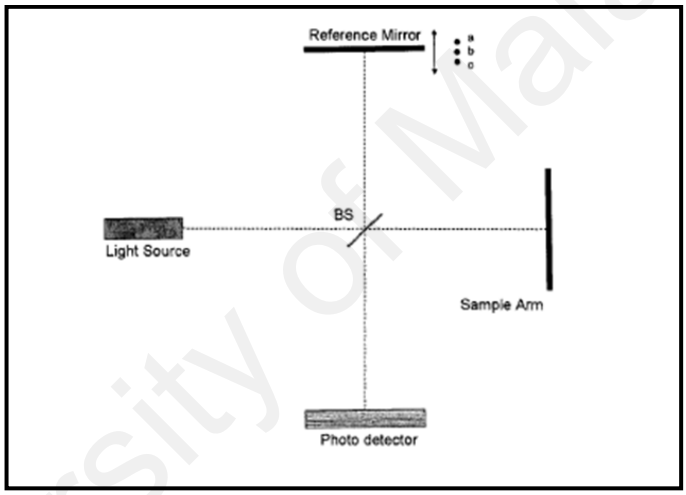

Figure 2.3: Low coherence Michelson interferometer

The Michelson interferometer enables scattering arising from the depths of tissues, also defining the axial resolution of the OCT system. It is designed to split the emitted light using a beam splitter (BS). The light being reflected from the sample and a mirror on the reference arm is recombined via the BS, which is then detected by the photodetector (Modified from (Feuchter., 2015).

In a generic OCT system (Figure 2.4), the light is sourced in a low-coherence format and directed into a 2x2 fiber-optic coupler Michelson interferometer. The optical light is split by a beam splitter with half of the light travelling towards the sample arm and the

other half towards the reference arm. The light being backscattered from the sample is interfered with the light travelling from the reference arm. When two path lengths rising from sample and reference arms are of the same length, then the relative phase difference of the light is zero and constructive interference occurs. While when two beams have a relative phase difference, the backscattered light emerges with the highest signal intensities and is marked easily against the darker background. Since the sample may have multiple scattering sights, the reference arm shortens and lengthens with respect to the sample arm, creating maximum signal where the path lengths are similar. The frequency of the interferogram measured by the Charged-coupled device (CCD) transformation is linked to depth location of the internal structure of the samples. As a result, depth resolved images or depth reflective profile (A-scan) is produced by taking the Fourier transform of the detected interferogram. As the raster scanning continues along the sample, a series of 2D cross-sectional (B-scans) are produced. Similarly, as the beam is scanned in a second direction, a series of 2D images are collected to produce an entire 3D (C-scans) volume data set.

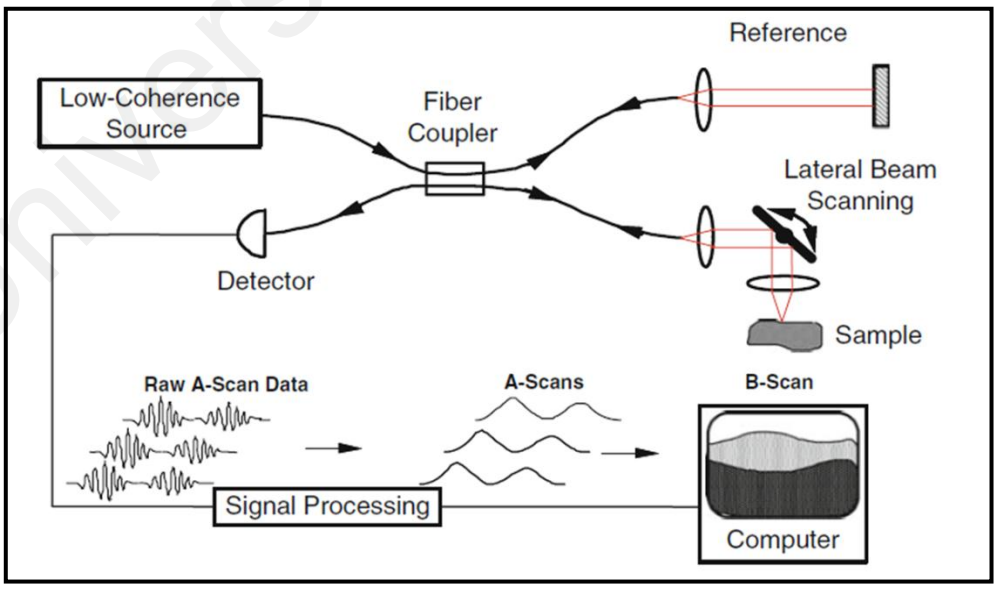

Figure 2.4: Illustration of generic OCT system

The fibre-optic paths are seen between the lower coherence sources and the reference arm and samples, passing through the fiber coupler or beam splitter. Meanwhile signal processing is taking place between the detector and projecting screen (from Thorlab, Inc 1999-2016).

When OCT was first developed, it was modelled using the Time domain (TDOCT) setup. It used a low-coherence light source, a moveable reference arm and repetitive scans in length. The signals were processed in correspondence to the interference between the reference arm light and the successive scattering site of the sample. The Fourier Domain optical coherence tomography (FDOCT) is based on earlier mentioned low-coherence interferometry, which uses the coherent properties of a light source to quantify the optical path distance delays in a sample. The interferometer is setup to monitor the optical path length difference between the light reflected from the samples and the reference arm. With FDOCT, B-scans are scanned on a time scale of milliseconds, and 3D images can be collected at a rate of below 1second.

There are two kinds of Fourier domains: spectral (SDOCT) and swept-source (SSOCT), each characterised by its light source and direction schemes. Back-scattered light, attributed to the differences in the index of refraction within a sample, is regrouped into the sample arm and combined with the light that has travelled a fixed optical path length along the reference arm. The resultant interferogram is measured through the detection arm of the interferometer. SDOCT is also known as spectral radar that uses low-loss spectrometer and broadband light usually a super luminescent diode (SLD) or mode-locked laser. The reference arm of the SDOCT is immovable and fixed at one point, corresponding to the position of the sample being scanned. This creates high mechanical stability and low phase noise. The spectrometer disperses and collects the light simultaneously coming from the sample and the reference arm on a CCD.

In the case of SSOCT, frequency sweeping is a technique for progressively choosing solo frequencies from a spectrum in specified time. The reference arm is fixed in one position, however the light is a tunable coherent narrowband width and rapidly sweeps in wavelengths, the spectral interference is sensed on photo receivers as a function of time. As the light source is swept, the interference signal is measured at respective optical frequencies. Various laser designs in 1300nm band have been used in SSOCT, which are tunable and based on a galvanometer scanning mirror, rotating mirrors and tunable Fabry-perot mirrors. Wider optical wavelength sweep range produces greater depth resolution and faster wavelength tuning acquires faster acquisition speed. Rapid sweeping of the laser source with intense peak powers at each discrete wavelength illuminates the sample and produces greater sensitivity. The spectral interference encodes the whole depth resolved structure of the sample at the site of focal point (Izatt & Choma, 2008). A common OCT setup uses a 120 nm tunable bandwidth centred at 1310 nm, and is capable of delivering 45 mW optical power output at a 20 kHz sweep rate (Huber, Wojtkowski, Taira, Fujimoto, & Hsu, 2005).

There are four fundamental design parameters for OCT which are considered for optimum functioning: optical power, acquisition speed, signal-to-noise ratio (SNR), and its axial resolution. These parameters are interdependent of each other and there is a linear relationship between SNR, source power incidence on the sample (P_s) and noise equivalent bandwidth (NEB).

$$\frac{SNR \times NEB}{P_s} = constant$$

However, to understand the relationship of all four parameters, we may include Δf, which is sequentially equal to the bandwidth of NEB and the electric bandwidth is the linear reference mirror scanning velocity *vs.* While the wavelength bandwidth is $\Delta\lambda$ of

the light source, it is inversely proportional to axial resolution Δl. Therefore the fundamental relationship between the four parameters with each other is:

$$\frac{SNR\ \ vs}{P_s\ \ \Delta l} = constant$$

In conclusion, the sensitivity of the OCT system can be increased by increasing the number of incident photons, the size of the resolution, or the time spent scanning each element.

In the SSOCT system, the output of the source can be written as S[k(t)]. Frequently k(t) is swept linearly and is stated as $k(t) = k0 + \delta k \times t$, where $\delta k = \Delta k / \Delta t$, such that Δk is the total optical bandwidth through which the narrowband source is swept, and Δt is the total sweep time. A SSOCT system ideally obtains signal at M equally spaced wavenumbers, such that $M \times \delta k = \Delta k$. In this context, the SSOCT system produces depth scan range.

$$X_{depth} = \frac{M\pi}{2\Delta k} = \frac{\pi}{2\delta k} = \frac{M}{2} l_c$$

The interference signal D[km] can be sensed by dual balanced detectors to compensate for intensity fluctuations. As the signal is attained at evenly spread out wavenumbers, D[km] can be discrete Fourier transformed (DFT) directly to derive the depth-resolved OCT line scan of the biological tissue.

In addition to comparable imaging performance, swept source systems feature reduced excess noise. This is because at each wavenumber *k*, the output of the swept source is a narrowband laser with much smaller noise than that of the broadband source. Furthermore, due to the nature of detection in swept source SDOCT, the SNR drop-off that usually occurs in spectrometer-based systems is not seen.

Refractive index mismatch is an important element in understanding the light behaviour when OCT is scanning biological tissues. This phenomena is mainly due to the reflection and scattering of the beam. In interferometric detection of low coherence, the light source continuously illuminates the sample, causing the superimposition of reflection signals to the sample arm. The sample arm detects the overlapping signals but is independent of the refelection signals. The difference in the index of refraction (n) is caused as the light travelling in the tissue is at a lower speed than in air. The change in path length between the sample and the reference arms is adjusted for this difference by:

$$Optical\ depth\ = real\ depth \times n$$

The interference between the sample and the reference arm signals will only occur when the relative path lengths coincide. Therefore it is dependent on the movement of the reference mirror which corresponds to a certain optical depth within the tissues in the sample arm. It is only the reflection signals from the sample arm, which coincides or matches the path length of the beam from the reference arm that will interfere, the remaining scattering of light, which is superimposition, is left un-interfered. If the two path lengths are within the coherence length (Figure 2.5), and the movement of the reference mirror can capture other scattering signals through the depth of the tissues, then the coherence length can determine the axial resolution of different reflection signals with the depth of the tissues. The recombined signals from the reference arm and sample are mixed or combined with lower carrier frequencies. The known frequency of the lower carrier beam is then easily demodulated using the power of the interference beam by the photodiode. This technique of shifting one frequency to another frequency increases the sensitivity of signals against background noise to detect minor variations in the interference signals. Consequently, the SSOCT setup using interferometric detection is able to produce higher axial resolution images of the tissues being scanned.

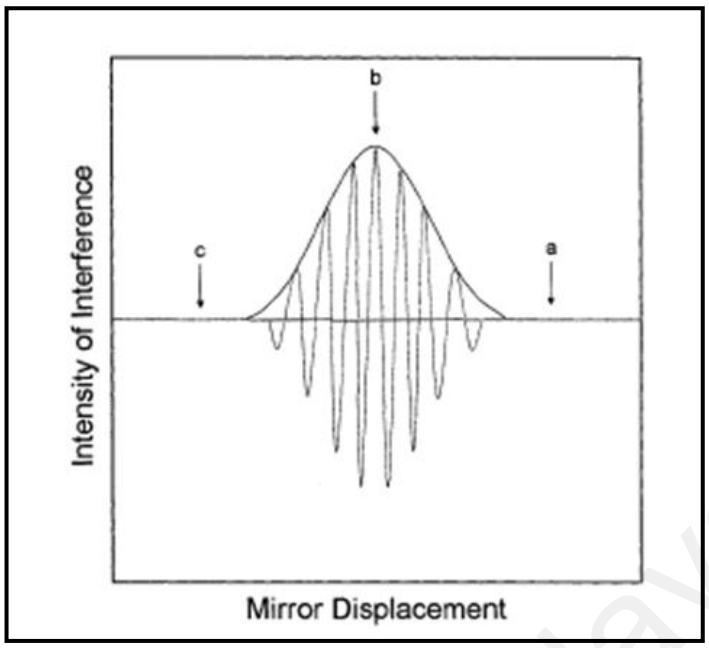

Figure 2.5 Schematic diagram of interference between sample and reference arm

The highest position of the wavelength (Point b) in Figure 2.5 shows that the relative path length is within the coherence length, between the light emitted from the source than the sample arm and the reflected beam from the reference arm, increasing signal sensitivity and producing higher axial resolution. Whereas the lowest position shown as Points a and c, both show that when the interference beam increases (a) or decreases (c) beyond the coherence length and are not related, it will exhaust towards zero (Modified from (Feuchter., 2015).

2.11.3 Axial and lateral resolution

Axial and lateral resolutions are essential properties for imaging the internal structures of biological tissues. The axial resolution is based on the bandwidth characteristics of the light source whereas the lateral resolution of the OCT setup is based on the system optics. A common kind of light source used is the super luminescent diode (SLD). The SLD is similar to a diode laser, except that the mirrors within the diode cavity are attuned to avoid the output of coherent high energy light. Thus, the SLD releases low

coherence light with a centre wavelength and a distribution or range of wavelengths above and below the canter wavelength. An example of the interference signal from a single reflective point and a movable mirror within the interferometer is the autocorrelation function (Figure 2.5).

The phenomenon showing bandwidth or distribution of frequencies of the source spectrum around the centre wavelength (autocorrelation) is referred to as Gaussian and defines the resolution of the system (Figure 2.4). There is a general inverse relationship between time domain signals, i.e. a beam of light, and the frequency components within that signal, i.e. the spectrum of the light. The coherence time, T_c, is related to the frequency bandwidth, $\Delta\lambda$, as in:

$$T_c = \frac{1}{\P \times \Delta\lambda}$$

If the bandwidth of the light source is a smooth broad Gaussian phenomenon, then the frequency around the centre wavelength will be a smooth narrow Gaussian phenomenon. This inverse relationship between the time and the frequency bandwidth can be converted using the time domain signal into frequency domain called Fourier transformation. Subsequently, it is the spectrum of the light source which plays the significant role in determining the axial resolution. The axial resolution Δl is commonly referred to as the full width at half Max (FWHM) of the Gaussian phenomenon in the time domain as the FWHM of two equal intensity reflections separated by the coherence length can be resolved visually. The FWHM of Δl at a single depth point is related to the FWHM of the bandwidth $\Delta\lambda$ of the Gaussian source as in:

$$\Delta l = \frac{2\, In\, 2}{\P} \times {\lambda^2}/{\Delta\lambda}$$

The autocorrelation of the centre wavelength of light λ within this equation signifies two important properties: as λ increases, the bandwidth of the light needs to be amplified to maintain the resolution and the greater the refractive index tissues, the greater will be the resolution attained. Within this thesis, the parameters and functioning of OCT have been considered, in using the refractive index of dentine (n= 1.55) (Meng et al., 2009) and the optical bandwidth which can provide smooth optical spectra. Throughout all, the research objectives related to this work has used en-face imaging, which only requires superficial optical depth, thus the axial resolution of OCT imaging may not matter much.

As for lateral resolution, the lenses with certain focal points can be achieved using plano-convex lenses. In addition, the spot size on the objective lens determines the lateral resolution. In achieving a good lateral resolution, there is loss of depth of field, which is represented by the confocal parameter. Linear reduction in the lateral resolution creates a rapid decrease in the confocal parameter. To achieve high resolution by the lens, the beam will diverge rapidly from the focal point. If the beam is focused at the surface, the lateral resolution decreases as the illuminating beam penetrates deeper inside the tissue. Wavelengths with longer λ have greater beam divergence thus lowering the focal parameter. The focal parameter directly influences the axial imaging depth, and the intensity of the beam attenuates by scattering and absorption as it travels in depth. The OCT set up considers an acceptable lateral resolution so that the illuminating beam has the greatest focal parameter of the optical imaging depth.

The changes between the hard tissues, such as the enamel and the dentine, and between healthy and demineralized or carious states can then be interpreted to create 2D and 3D images of the hard tissues. As such, various optical properties are under investigation as potential quantifiers of the mineralization changes to detect dental caries (Li, Bowman,

Fazel-Rezai, & Hewko, 2009) The polarized sensitive OCT (PS-OCT) can be correlated with the degree of demineralization and severity of the lesion. Monitoring *in vivo* carious lesion changes could be helpful with this device (Daniel Fried et al., 2002; R. Jones, C. Darling, J. Featherstone, & D. Fried, 2006; Robert S Jones, Cynthia L Darling, John DB Featherstone, & Daniel Fried, 2006). Optical coherence tomography (OCT) is a nonionizing imaging technique that can produce cross-sectional images of biological tissues using an infrared light at 1310 nm. Light, when passed through different structures, moves faster in material with a low refractive index and slower in media with a high refractive index. Additionally, when the light hits a sharp change in refraction, the wave is reflected either externally or internally. The amount of reflection depends on the amount of change in refraction, the angle the light is traveling at and the polarization of the light. If the change of refraction between the media is gradual, the reflection will be minimal (Brezinski, 2006; Otis, Everett, Sathyam, & Colston, 2000).

2.12 Optical light: Dental tissues and caries

The difference in light propagation when passed through various biological tissues is used in the detection of tissue alteration and diagnostic research (Mourant et al., 2002; Perelman et al., 1998). A significant anisotropic effect is created when light is transmitted through these biological tissues, due to its microstructural properties (Heino, Arridge, Sikora, & Somersalo, 2003; Alwin Kienle, Forster, Diebolder, & Hibst, 2003) and its chemical composition (Darling, Huynh, & Fried, 2006).

The anatomical crowns of teeth are covered by dental enamel, which is composed of 92-96% inorganic, 1-2% organic and 3-4% water by weight, while the inner core is made up of dentine that is composed of 70% inorganic, 18% organic and 12% (wt%)(Nanci, 2008). The highly inorganic material is structurally laid down in a complex manner and is considered as high scattering media, slight structural and biochemical changes in

tissues directly affects the optical backscatter properties that can provide vital information in caries diagnosis (Chen et al., 2005; D. Fried et al., 2002; X. J. Wang et al., 1999). Hydroxy-apatite crystals in enamel are sized up to 50 nm x 25 nm up to 1mm long nano rods. Approximately, hundreds of such crystals are bundled together into a larger scale prismatic structure with up to 5 micro metres in diameter. These prisms are arranged parallel to one another at an acute angle to the DEJ (Macho, Jiang, & Spears, 2003). Whereas, in dentine, the HA crystals are calcium deficient and carbonate rich, closely packed and incorporated within the gaps between the collagen fibrils. They are sized up to 5nm x 30nm x 100nm and have less calcium than stoichiometric HA and contain 4-5% carbonate (Grayson W Marshall Jr, 1993) and the mineralized collagen fibrils are arranged orthogonal to tubules forming the matrix, which is completely random (Marshall Jr et al., 1997).

Dentinal tubules are surrounded by a highly mineralized peritubular zone with a mineral content 40% higher than Intertubular dentine and are spatially more homogeneous than intertubular dentine (Tjäderhane et al., 2009). The wavy structure of the tubule vary in diameter from the pulp to dentine enamel junction (DEJ), from 22% and 2.5mm to 1% and 0.8mm respectively, while the intertubular matrix and peritublar dentine varies from pre dentine to the DEJ, 12% to 96% and 60% to 2.9% respectively (Marshall Jr et al., 1997). Intense optical scattering observed from healthy dentine is due to these variations in the structural orientation and arrangement of dentinal tubules (Ilnaz Hariri, Alireza Sadr, Yasushi Shimada, Junji Tagami, & Yasunori Sumi, 2012). It was reported that the cylindrical shaped dentinal tubules are the main reason for the highest anisotropic light scattering (Alwin Kienle et al., 2003), while the total reflection, which is necessary for optical fiber effects, takes place in peritubular dentine due to a high refractive index, compared to the intratubular dentine and tubules, which are the neighbouring media (A Kienle, Michels, & Hibst, 2006). In addition to the tubular structure of dentine, the

organic matrix is made of the non-centrosymetric collagen structure, which fluoresces to indicate the condition of dentinal caries when using optical property of light (Terrer et al., 2010). It is due to these variations that sound dentine strongly scatters light in the near-infrared region and is highly birefringent when compared to sound enamel (Darling et al., 2006; Fried et al., 1995).

Alteration in mineral content due to the carious process within the enamel and the dentine affects the optical transmission such as reflection, colour absorption and scattering of light (Ko, Tantbirojn, Wang, & Douglas, 2000). Enamel caries under a light microscope shows an opaque appearance due to the sub-surface enamel dissolution, creating porosity and affecting the scattering of light (KR Ekstrand, 2004). The light behaviour of healthy enamel differs from demineralized enamel as the refractive index changes when light travels from the enamel (n=1.7) to air (n=1.0) and water (n=1.3) (Brodbelt, O'brien, Fan, Frazer-Dib, & Yu, 1981). Similarly, carious dentine has a lower concentration of calcium and phosphates than sound dentine (Magnus, Maltz, Bavaresco, Bastos, & Hashizume, 2013) with increased porosity and change in mean crystallite size (Angker, Nockolds, Swain, & Kilpatrick, 2004). The HA crystal arrangement after natural caries destruction in dentine is significant as the crystalline length deceases by 53% and width by 12% for translucent dentine and 65% and 32% in demineralized intertubular dentine (Porter et al., 2005; Zavgorodniy et al., 2008). A few studies that have explored the behaviour of optical signals on natural occurring causes lesions have qualitatively identified a strong contrast due to an increase in light scattering (Chen et al., 2005; de Oliveira Mota et al., 2013; Manesh, Darling, & Fried, 2008). Optical broadband light has shown a difference in the light propagation and scattering behaviour of demineralized dentine when compared to sound dentine. Results have shown that there is a significant change in the integrated

reflectivity of light between demineralized and sound dentine (Freitas et al., 2009; Manesh et al., 2008, 2009a).

CHAPTER 3: MATERIALS AND METHODS

3.1 Introduction

Human extracted teeth with coronal dentine caries were used for specimen preparation. They were sectioned to produce flat dentine slabs with carious and healthy dentine layers exposed on the surfaces. Several pilot studies were attempted prior to deciding on the final design of this research to ensure that the natural lesion was preserved to its maximum. Special emphasis was given on techniques of samples storage, specimen preparation and preservation of lesion pre and post duration of imaging.

3.2 Microstructure of Dentine layers, as characterised by OCT

3.2.1 Pilot studies

The pilot studies mentioned in this section are applicable to all research objectives, except the removal of smear layer, which was not used in Objective 3.

3.2.1.1 Selection of caries lesion and sectioning planes

The aim of this pilot study was to determine the optimum sectioning plane of the caries lesions that would exhibit the full spread of dentine caries layers along with healthy dentine over a maximum bulk of tissue, and is within the physical scanning limits of OCT. Another objective was to determine the arrangement of dentinal tubules with different planes of sectioning and how that would affect the backscattered intensity of OCT. Eleven extracted human molars with ICDAS Code 5 and 6 occlusal, proximal or proximo-occlusal caries were used. These teeth were longitudinally (n=5) and transversely (n=6) sectioned using a low speed cutter machine (Metkon 125, Instrument ltd, Bursa, Turkey) with a 5-inch diamond wafer blade under copious water flow. All of the sections showed a wide spread of soft light-dark brown outer infected dentine

followed by hard and yellow brown inner affected dentine surrounded with yellow healthy dentine (Figure 3.1).

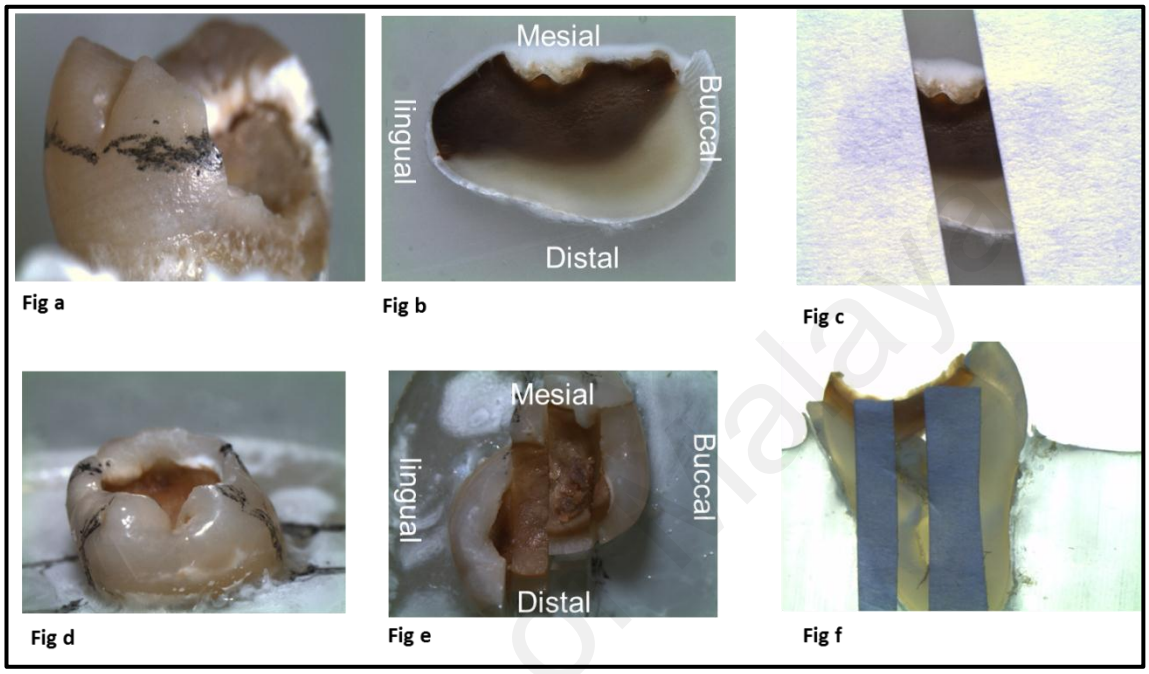

Figure 3.1: Stereomicroscope image comparisons of dentine caries with two different planes of sectioning

Figure 3.1 shows six stereomicroscope images of carious teeth, sectioning plane and dentine slabs. Figure 3.1a shows an extracted human molar with a mesio-occlusal caries; Figure 3.1b shows a dentine slab of 2 mm thickness after the tooth had been cross-sectioned following the direction of progression of caries showing spread from outer ID, AD and inner HD layer (Figures 3.1c & f). An adhesive tape was placed on either side of the region of interest for demarcation. This area was then imaged with SEM and OCT. Figure 3.1d shows an extracted human molar with occlusal caries and Figure 3.1e are dentine slabs, each with 2 mm thickness after the tooth was longitudinally-sectioned.

The sections were viewed with a stereomicroscope under 1.8 x magnification, and then scanned with OCT and SEM. It was found that lesions of proximal origin, when sectioned cross-sectioned, i.e. following the plane of caries progression, showed the best spread of dentine layers. OCT B-scans did show a difference in the shape of the boundaries between the tooth-air interface however no differences in backscattered intensity was observed between the longitudinal and cross-sectional views (Figure 3.2a & 3.2b).

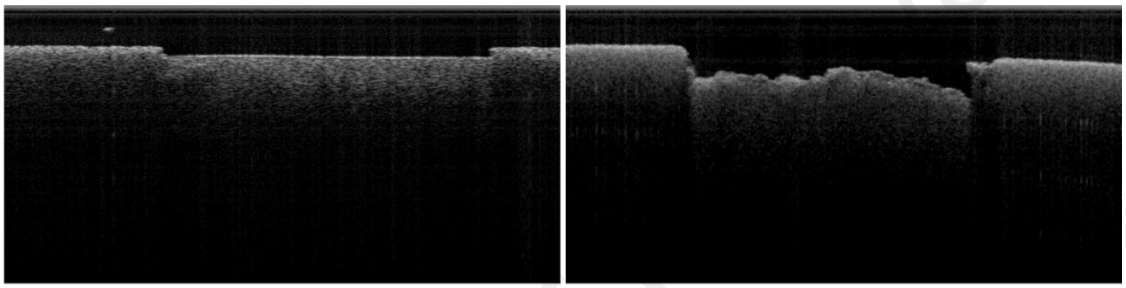

Figure 3.2: OCT B-scan comparison of backscattered intensity from infected dentine

Previous reported studies which attempted to differentiate infected, affected and healthy dentine layers have preferred to use the cross-sectional planes across dentine tubules than the longitudinal section parallel to dentine tubules (Marshall Jr et al., 1997; Ogawa et al., 1983; Pugach et al., 2009; Zavgorodniy et al., 2008). SEM images of the cross-sectional planes presented clear micro-structural anatomy of the intertubular dentine and the peritubular of healthy dentine (Figure 3.3). Hence, it was decided that teeth with proximal and proximo-occlusal caries were to be used, and they were cut in cross section along the progression of caries (Figure 3.1).

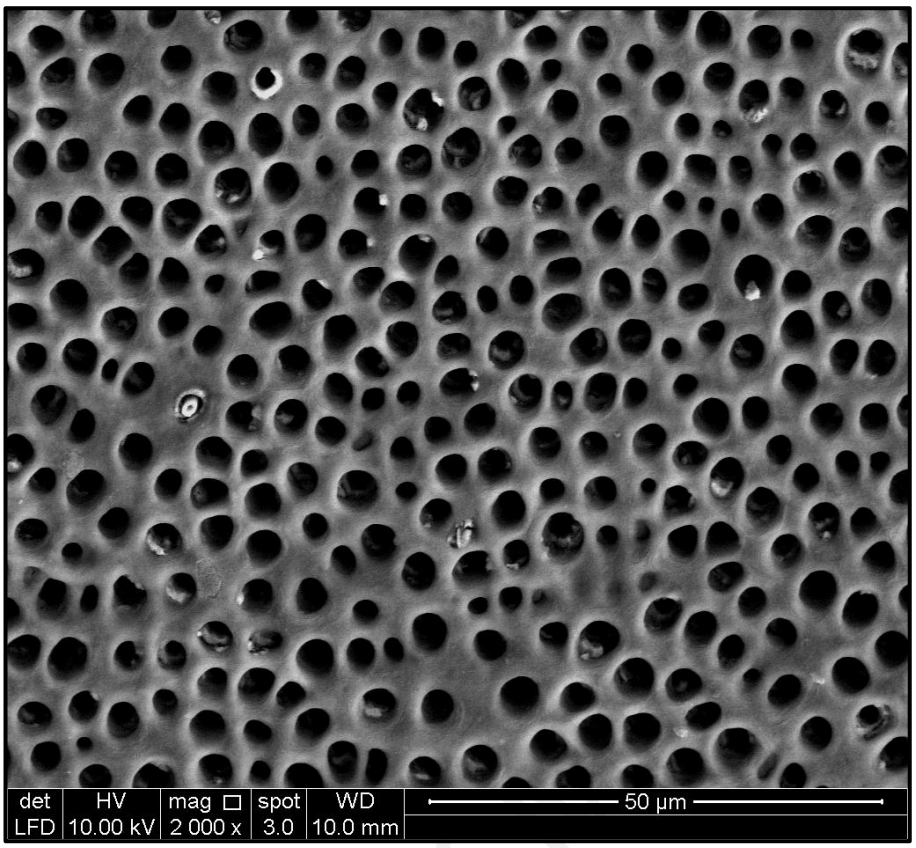

Figure 3.3: Intertubular and peritubular dentine structures in cross-sectional healthy dentine

3.2.1.2 Storage of carious tooth / lesion

One of the challenges of studying natural occurring dentine caries is the preservation of structural, biochemical and mechanical characteristics of the dentine tissues. Storage media has long been studied to assess the effectiveness in preserving tooth structure and their possible deleterious effects on the teeth tissues (Secilmis, Dilber, Ozturk, & Yilmaz, 2013; Sultana, Toru, Asafujjoha, & Junji, 2006). The common storage media such as saline solution (NaCl), Hanks balanced salt solution (HBSS), deionized water and phosphate buffered saline (PBS) solution have shown to affect the mechanical properties of dentine if stored for more than 30 days (Sultana et al., 2006). Similarly, in this pilot study, when the carious teeth were stored in PBS and deionized water, the friable outer infected dentine, which is soft and loose erode off into the storage media

after a period of 30 days. Extracted teeth stored at -20°C, compared to chloramine, formalin and thymol solution, showed preservation in laser fluorescence properties (Francescut, Zimmerli, & Lussi, 2006). This method had later been adopted by other studies which required prevention of deterioration of caries lesion at various severities (Diniz, Rodrigues, Hug, Cordeiro Rde, & Lussi, 2009; Rodrigues, Hug, Diniz, & Lussi, 2008). A pilot was undertaken using extracted permanent carious molars that were kept frozen at –20 °C from the time of extraction up to 20 days. At the beginning of the defrosting process, the teeth were positioned in individual plastic dishes and defrosted at room temperature (about 24°C) for 14 hours. In order to ensure 100% humidity, a moist paper towel was placed at the bottom of each container. Care was taken to avoid contact between the tooth and the paper towel. All teeth were then cleaned with a toothbrush and water for 15 seconds. At the end of the defrosting process, the carious part of the tooth was completely intact and undisturbed, although the outer layer was observed to be not as soft and mushy as it was prior to freezing. The non-carious part of the teeth was identical before and after freezing. Observation of teeth surfaces post freezing at –20°C confirmed this to be the best approach to store the teeth for this study.

3.2.1.3 Sectioning protocol

The aim of this pilot study was to identify a minimally traumatic cutting method that would not leave severe defect marks on the cut surface of the caries lesion. Since the loose and friable infected dentine is loosely held against the resin (Quick Mount 2 Epoxy resin, Ace technologies), the sectioning method should ideally yield a surface which is relatively defect free and does not require polishing. Six carious molars were completely embedded in resin and cured for 1-2 hours. A slow speed cutting machine (Metkon, Bursa, Turkey), a high speed cutting machine (Metkon, Bursa, Turkey) and the Exakt 300CP Band system (Exakt, Germany) systems were tested. Four teeth were

sectioned into 0.5mm thick slabs with the high speed cutting machine using 150 grit grain size diamond cutting blade with medium concentration. Sectioning settings were set at 800 RPM and 350 mm/rev feed-rate, 1200 RPM and 250 mm/rev feed-rate, 1500 RPM and 250 mm/rev feed-rate and 1800 RPM and 150 mm/rev feed-rate respectively. While the remaining two teeth were sectioned with the same high speed cutting machine using a high concentration diamond grit cutting blade, at 1200 RPM and 250 mm/rev feed-rate and 1500RPM and 350 mm/rev feed-rate. Two teeth with each cutting system were sectioned using slow speed cutting machine and Exakt 300CP band system. The Exakt 300CP band system and the slow speed cutting machine were set at 2N cutting force on the sample and 9000 RPM respectively with a constant feed-rate. The cross-sectional specimen was prepared according to the details stated in Section 3.2.1.1. The Scanning Electron Microscope (FEI Quanta 250 FEG, UK) was used to observe the sectioned surfaces and they were viewed at 1000x magnification for all groups to assess for defect marks. It was noted that the slow speed cutting machine and the Exakt 300CP band methods produced sections with longitudinal cutting marks similar to that seen in (Figure 3.4a) and (Figure 3.4b). The high speed cutting machine with 150 medium grit diamond concentration at 1500 RPM and the 250 mm/rev feed-rate yielded the best results (Figure 3.4c).

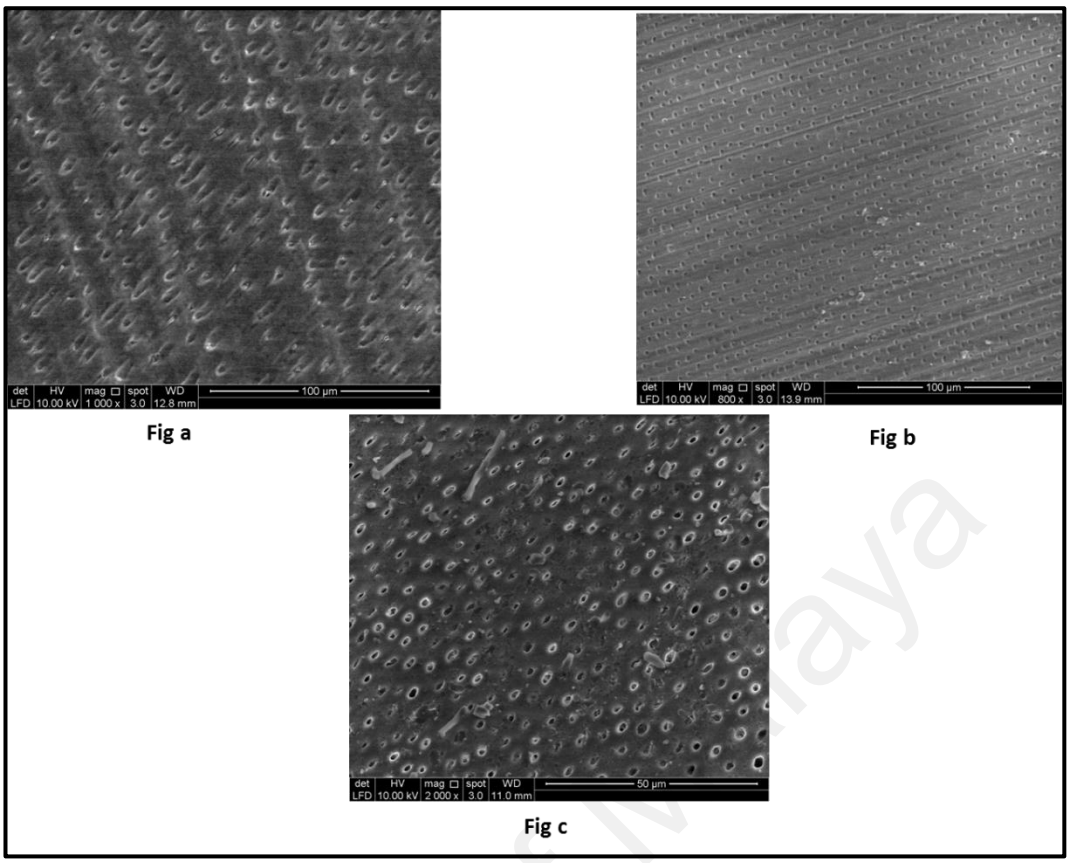

Figure 3.4: Defects marks results from sectioning

Figure 3.4a shows longitudinal scratch (top to bottom direction) marks on the healthy dentine surfaces in the cross-section view with the slow-speed cutting machine with 150 medium grit diamond blade. Figure 3.1b shows an increased number of longitudinal defects (left to right direction) marks produced by the Exakt band system. Figure 3.4c shows the cross-section of a healthy dentine with minimal sectioning scratches through the use of a high speed cutting machine, a 150 medium grit diamond disk with copious water at 1500RPM / 250 mm/rev feed-rate.

3.2.1.4 Localisation of regions of interest

The aim of this pilot study was to explore the use of grids that were able to divide the identified area of carious and sound dentine into standardised quanta of tenths of micrometres. This is necessary to facilitate the precision needed in the localization of

the three layers of interest, i.e. infected dentine (ID), affected dentine (AD) and healthy dentine (HD) between the gold standard, in this case SEM and OCT.

The following methods were explored:

i) dimensional calibration ruler, micro ruler-1 (MR-1) (Figure 3.5e)

ii) copper mesh, (Figure 3.5a)

iii) paper based stamp for micro-printing, on adhesive tape (Figure 3.5b)

iv) microscopic calibration rulers, (Figure 3.5c)

v) gilder grid with known distance (Figure 3.5d)

The limitation of some of the micro-rulers was that it could only be used under SEM but were too fine to be used with OCT. The micro prints on the adhesive tape on the other hand could not offer the precision needed in micrometres.

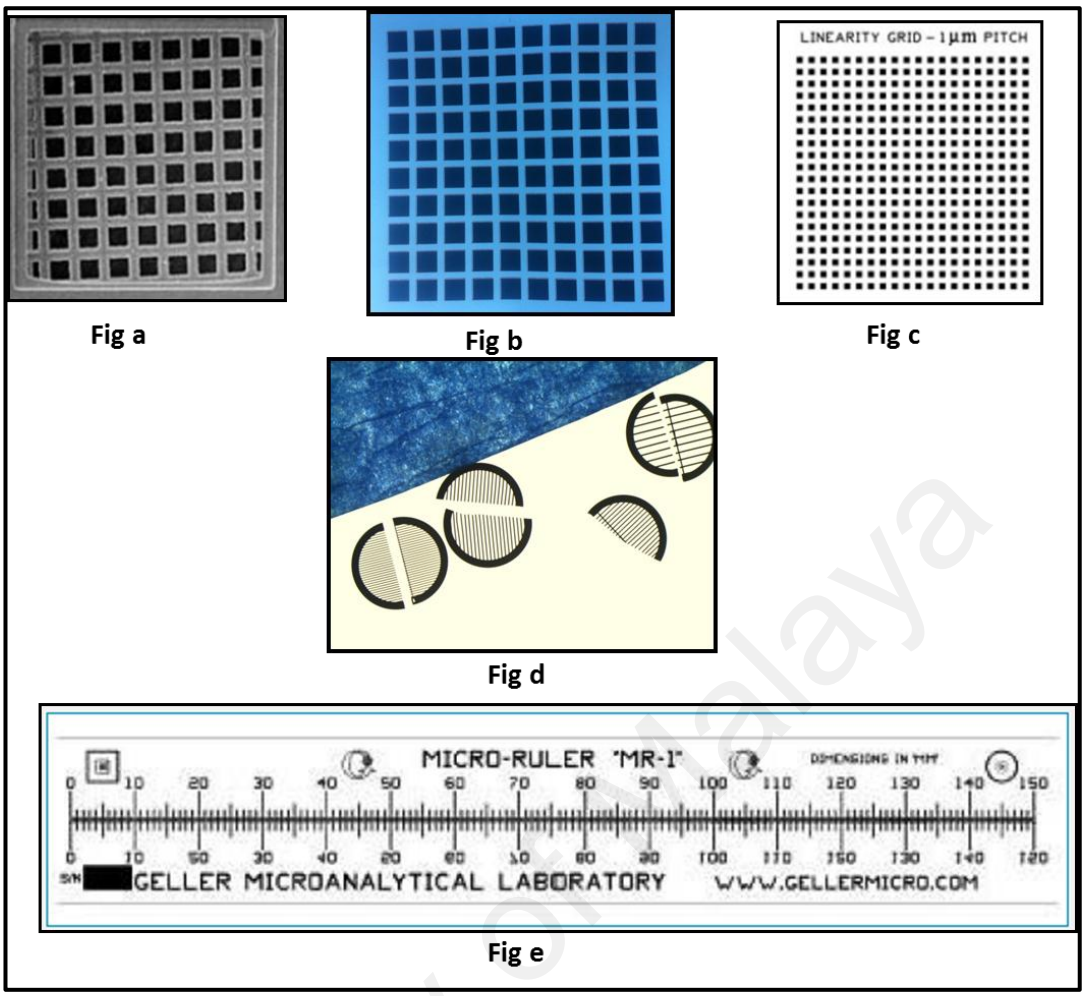

Figure 3.5: A selection of grids

Figure 3.5a is a copper mesh measuring 3.05mm. Figure 3.5b is a paper based stamp for micro-printing with a 2mm square print and spacing of 10X across horizontally and 10 across vertically on a single-sided adhesive tape. Figure 3.5c is an approximately 2 x 2 x 0.5 mm Geller Magnification calibration standard (MRS-5) wafer with a silicon oxide layer to enhance imaging under SEM. Figure 3.5d shows three 3.05 mm diameter, half cut copper gilder grids with 10, 20 and 30 bars with 30 µm, 80 µm and 125 µm inter-bar distance respectively. Figure 3.5e is a micro ruler MR1.

Copper gilder grids are commonly used as specimen trays to be imaged under Transmission electron microscope (TEM) and were found to be the most suitable for the purpose of this study due to its quantum of inter-bar distance, toughness and clarity when scanned under SEM and OCT. Among the several options of inter-bar distances and designs, the 3.05 mm diameter, 0.7 mg weight, 10 µm thick grid with 20 parallel lines, 45 µm bar width and 80 µm inter-bar distance was chosen for the study. Pilot OCT scans were taken with the grid placed over the area of an identified area of carious and sound dentine. The copper bars produced high specular reflection that confounded the backscattered intensity of the adjacent dentine. Hence the copper grid was halved (Figure 3.5c), and placed this time not over the identified area of carious and sound dentine but next to it. Another pilot OCT scan was then done and the image was compared to a prior scan done without the presence of the copper grid. It was found that the high specular reflection from the copper grid did not affect the backscattered intensity from the area of interest.

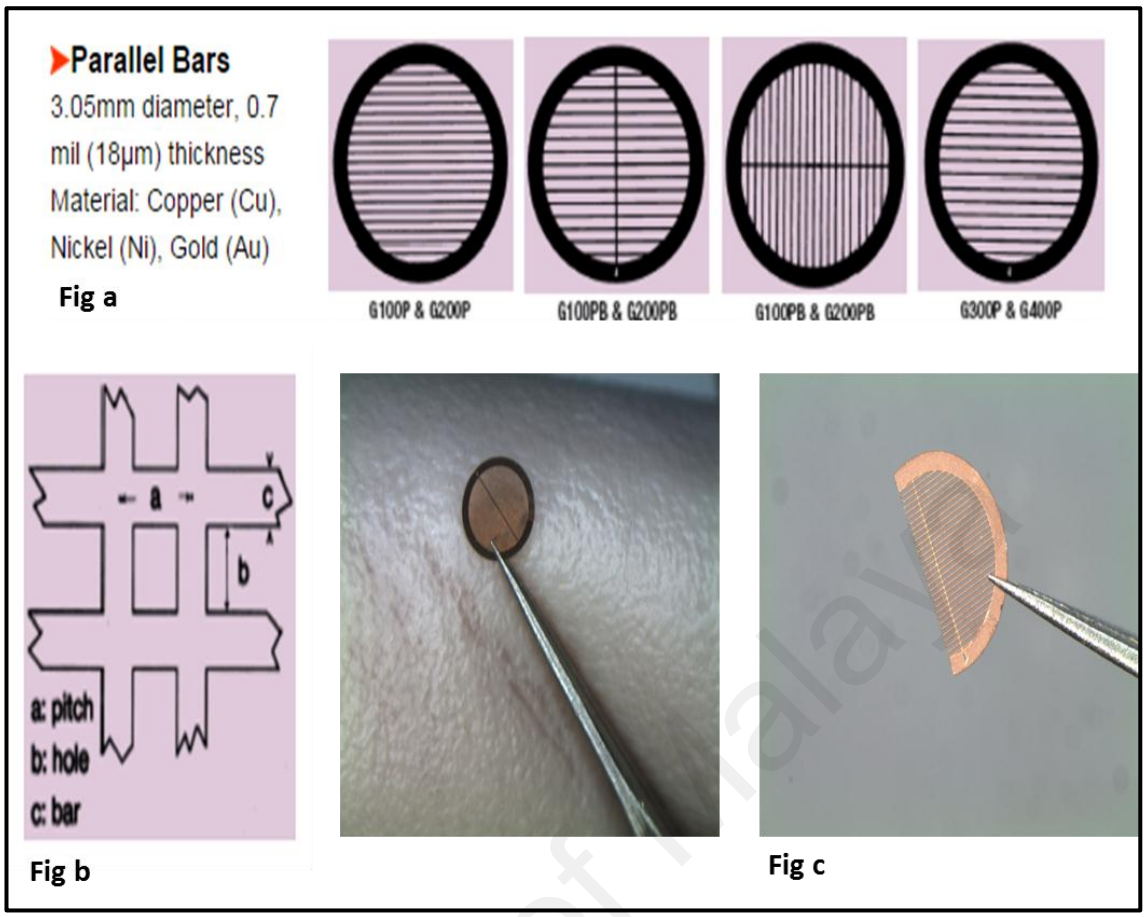

Figure 3.6: Copper grids

Figure 3.6a presents four kinds of designs and the inter-bar distance of the copper grid. Figure 3.6b is the selected copper grid (G200PB) with a= 125 µm , b= 80µm and c= 45µm. Figure 3.6c shows the copper grid held with a pair of handling tweezers (Dumont N-5 tweezer, 72845) and split into two halves using a pair of sharp scissors.

3.2.1.5 Removal of smear layer

The aim of this pilot was to assess the effectiveness of various agents in removing the smear layer resulting from the sectioning of the caries lesion without damaging the topographical micro-structures of the carious dentine. One of the most common agents used to remove smear layer is 35% phosphoric acid applied for 10 seconds. This however is known to also etch the intertubular and peritubular dentine, often removing Ca and P completely from the dentine surface (Ayo-Yusuf, Driessen, & Botha, 2005).

Even 10% phosphoric acid has been shown to cause more intense demineralisation on the peritubular dentine when compared to 7% maleic acid (Nor, Feigal, Dennison, & Edwards, 1997). It has been proposed that for removing thick smear layers, it is ideal to use milder acid conditions such as 10% citric acid (Tay, Carvalho, Sano, & Pashley, 2000) or 40% polyacrylic acid (Raggio, Sonego, Camargo, Marquezan, & Imparato, 2010). Another popular agent used for removal of the smear layer is Ethylenediaminetetraacetic acid (EDTA). Its chelating action is used to disintegrate the smear layer and open up the dentine tubules, and its effectiveness depends on the concentration, pH and time of exposure (Serper & Calt, 2002). Other than chemical removal of the smear layer, sonication has also been shown to remove the smear layer and smear plugs from dentinal tubules (Koutsi et al., 1994). As it is established that strong acids such as phosphoric acids do not only remove smear but also demineralises the dentine. It was therefore not included in this pilot whilst mechanical disintegration using sonication was tested along with mild agents.

Twelve sectioned molar teeth were divided into three different testing groups: detergents (n=2), chelators (n=8), and mild acids (n=12). The pH was kept constant while the duration of exposure, strength of reagents and sonication were varied (Table 3.1). Five types of agents were explored in this pilot study: Trypsin (Trypsin EDTA, Sigma-Aldrich) and a commercially available soap ($C_{17}H_{35}COONa$, or sodium stearate) in the detergent category, EDTA in the chelator category and maleic acid and polyacrylic acid (GC Dentin Conditioner – GC Corporation, Tokyo, Japan) in the mild acid (Scotchbond Multi-PurposeTM, 3M Co, St Paul, MN) category. Dentine slabs measuring between (2.0 to 2.5 mm), which were exposed to detergents, were kept up to 24 hours at room temperature. Two organic acids: 10% poly-acrylic, 10% maleic acid with exposure time of 30 and 50 seconds for each sample plus pre and post 50 seconds sonication were tested. While 0.5M EDTA (Sigma-Aldrich, St. Louis, Mo.)

with 3%, 10% and 17% with exposure time of 1 and 3 minutes and 50 seconds pre-and post-sonication was submerged in distilled water using an ultrasonic bath (UC1-230, Biosonic Ultrasonic Bath, Whaledent, USA) (Figure 3.7).

Table 3.1: Smear layer removal parameters

	Detergents		**Chelators**			**Mild acids**			
	Trypsin	**sodium stearate**	**0.5M EDTA**			**maleic acid**		**polyacrylic acid**	
Strength (%)	-	-	3%	10%	17%	10%		10%	
Exposure time (secs)	1440	1440	60		180	30	50	30	50
Sonication time (secs)	50	50	50			50		50	

Figure 3.7: Ultrasonic bath

Figure 3.7 shows the Ultrasonic bath (UC1-230, Biosonic Ultrasonic Bath, Whaledent, USA).

The pH values of sound dentine and carious dentinal lesion is reported to be 7.0 and 6.6 respectively (Hiraishi et al., 2003). The earliest changes observed on cut dentine surfaces are preferential etchings of the peritubular dentine with the narrow portion of the funnel pointing inwards (Marshall et al., 1997). Since the samples in this study contained natural carious lesions and sound dentine, the pH of the EDTA was kept above pH 6.6 and checked using a pH meter (pH 700, Benchtop pH mete, Oakton, USA). The criteria for selecting the reagent was to assess complete absence of smear layers from the dentine surfaces and dentine tubules and the presence of undistorted and round to elliptical shaped PTD. Images showing dentine tubules that were partially blocked with smear layer were inferred as reagent being ineffective. During post treatment all teeth were examined under 2000 x magnifications using SEM. Images with 10% EDTA for 3 minutes exposure time and 50 seconds sonication time showed complete absence of smear layer and no signs of demineralisation of PTD (Figure 3.12b).

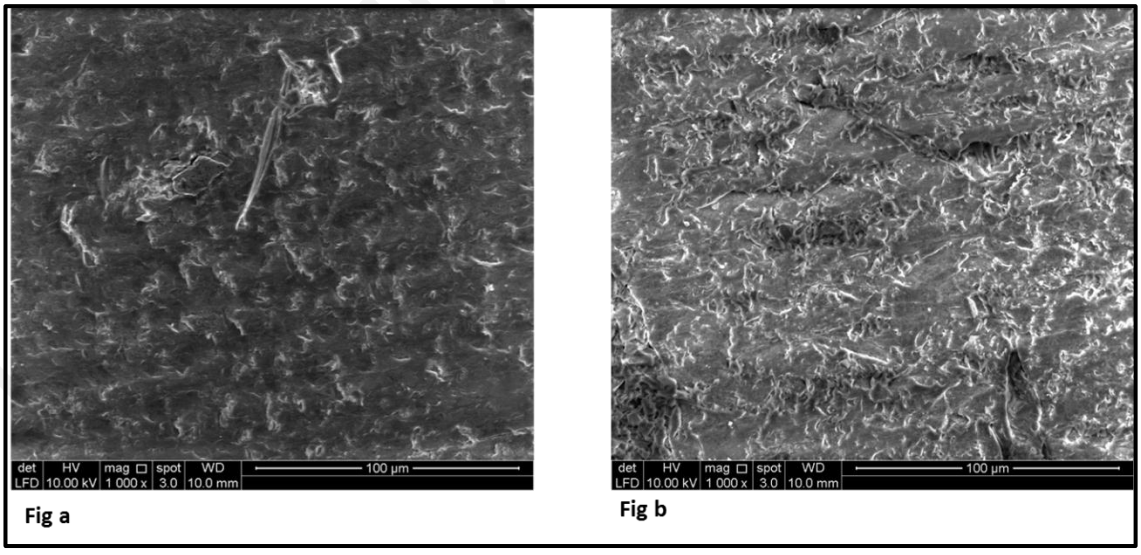

Figure 3.8: Trypsin exposure

Figure 3.8 are SEM images of the sectioned dentine surface at 1000x magnification, in trypsin (Figure 3.8a) and sodium stearate (Figure 3.6b) post trypsin treatment, plus 50

seconds sonication pre- and post- exposure. The dentine surface is completely covered by a smear layer and no ultrastructure of dentine was visible. However, there was a significant increase in precipitation observed at exposure time with sodium stearate compared to trypsin on the surface of the dentine slab.

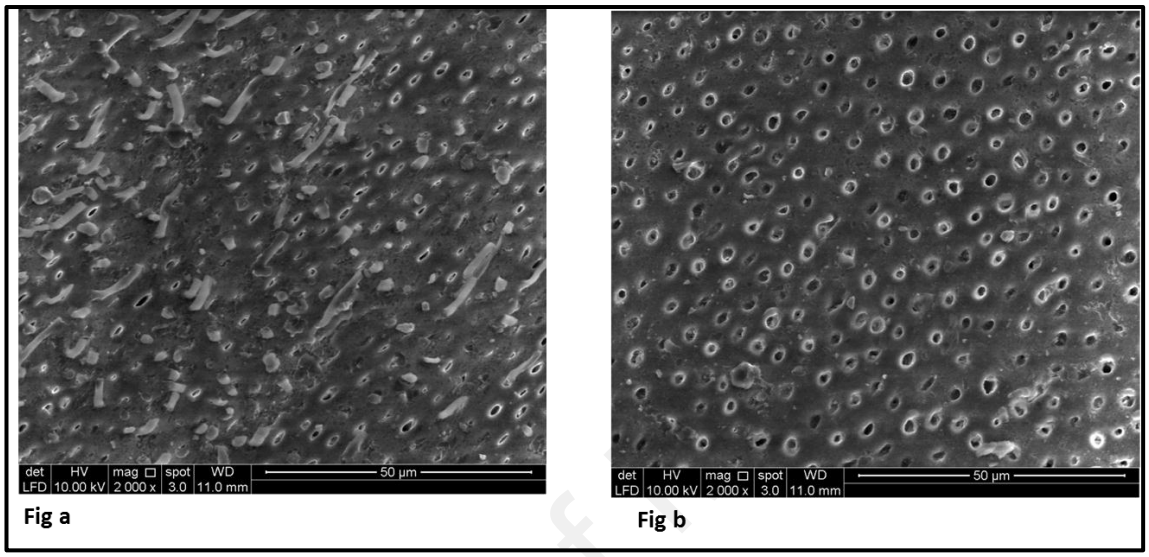

Figure 3.9: 10% polyacrylic acid exposure

SEM images of a dentine surface at 2000x magnification after exposure to 30 seconds (Figure 3.9a) and 50 seconds (Figure 3.9b) of 10% polyacrylic acid plus 50 seconds of sonication pre- and post- exposure. Exposure of 1 minute showed that the intertubular dentin was partially covered by a smear layer with a distorted shape of peritubular dentine. The peritubular dentine of the dentine slab treated with 50 seconds exposure shows a more visible shape and cleaner inter-tubular dentine area.

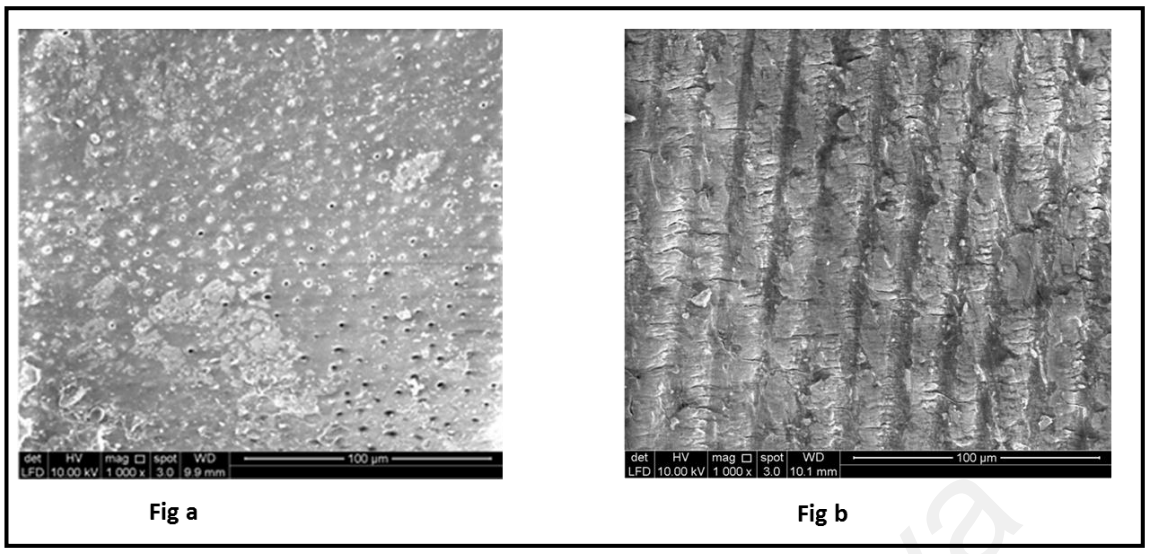

Figure 3.10: 10% maleic acid exposure

Figure 3.10 shows SEM images of dentine surface at 1000x magnification after exposure to 30 seconds (Figure 3.10a) and 50 seconds (Figure 3.10b) of 10% maleic acid for plus 50 seconds of sonication pre- and post- exposure. The intertubular dentin is completely covered by a smear layer.

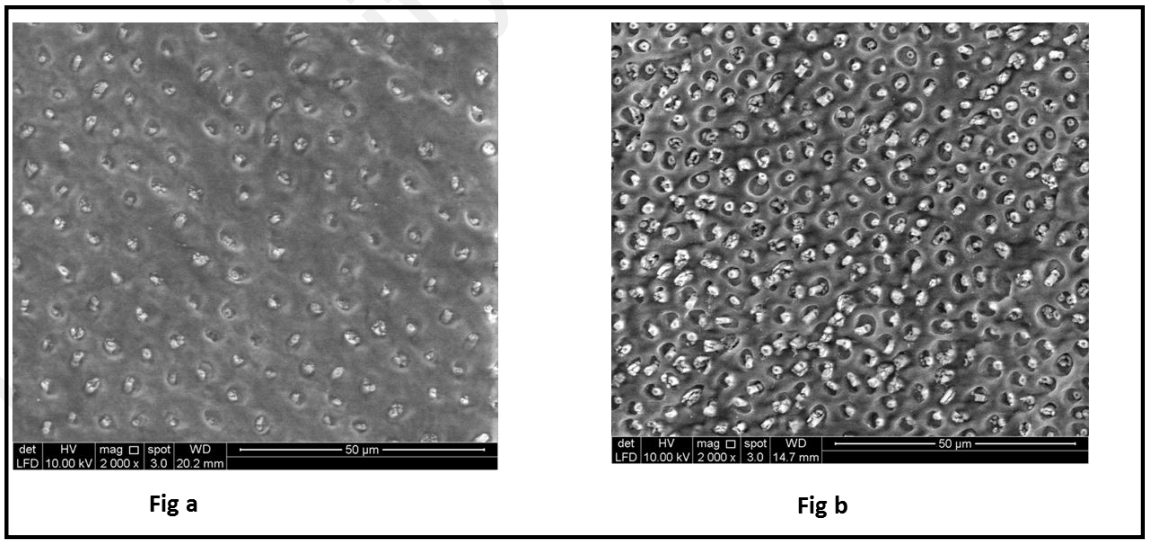

Figure 3.11: 3% EDTA exposure

Figure 3.11 are SEM images of the sectioned dentine surface at 2000x magnification, 1-minute (Figure 3.11a) and 3-minute (Figure 3.11b) post 3% EDTA treatment, plus 50

seconds of sonication pre- and post- exposure. The smear layer is absent at the intertubular dentine area in both images, however the dentine tubules are blocked and both exposure shows a distorted slightly round to elliptical shaped peritubular dentine.

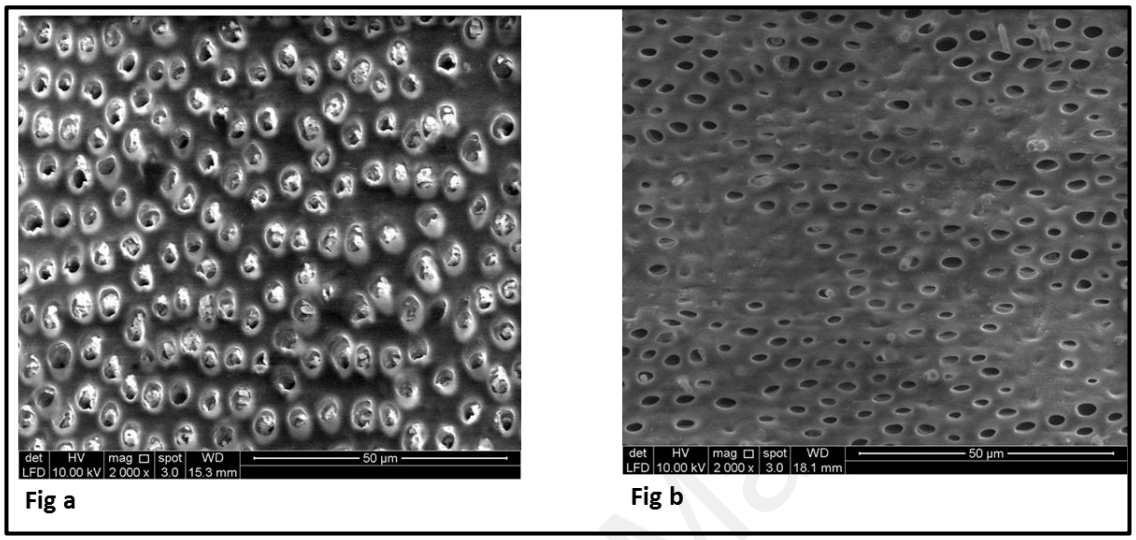

Figure 3.12: 10% EDTA exposure

Figure 3.12 are SEM images of the sectioned dentine surface at 2000x magnification, 1-minute (Figure 3.12a) and 3-minute (Figure 3.12b) post 10% EDTA treatment, plus 50 seconds of sonication pre- and post- exposure. Smear layer is not present at the intertubular dentin region, but smear plugs are observed within dentinal tubules when treated for 1 minute. Dentine surface treated with 10% EDTA for 3 minutes showed an absence of smear layer at the intertubular dentine region, complete absence of smear plugs within distinct dentinal tubules. Non-distorted and elliptical shaped peritubular dentine was observed.

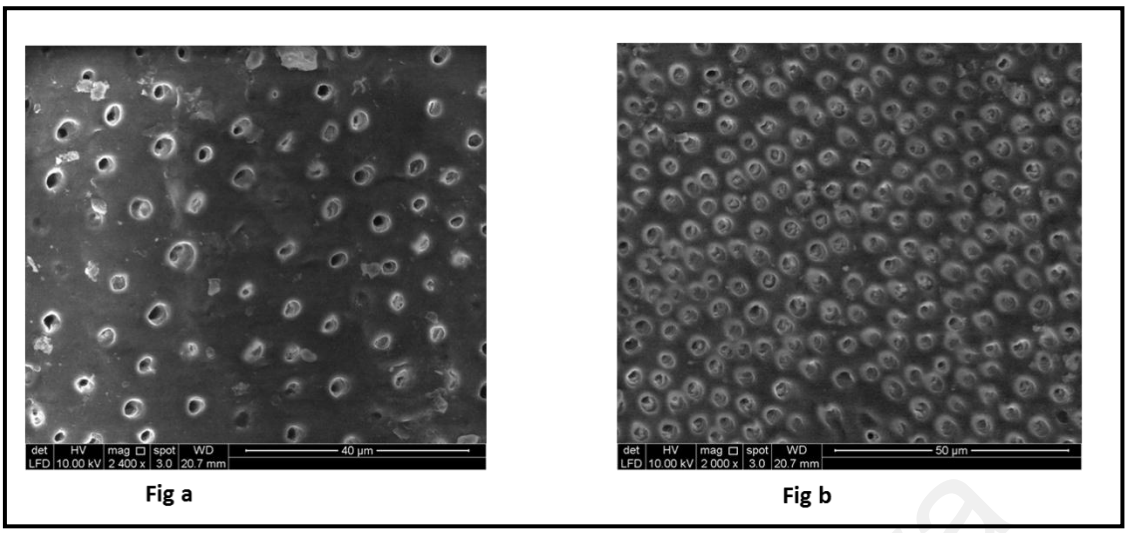

Figure 3.13: 17% EDTA exposure

Figure 3.13 are SEM images of the sectioned dentine surface at 2000x magnification, 1-minute (Figure 3.13a) and 3-minutes (Figure 3.13b) post 17% EDTA treatment, plus 50 seconds of sonication pre- and post- exposure. The smear layer was absent in the intertubular dentine area, however the dentine surface treated for 1 minute showed some debris in the inter-tubular dentine region. Dentine slabs treated for 3 minutes showed a distorted non-elliptical shaped peritubular dentine, suggesting occurrence of demineralization and a change in the peritubular dentine structure.

3.2.2 Sampling of specimens

Thirty-two extracted human molars with proximal caries were collected for this study. The teeth were collected after expressed consent was obtained from patients under a protocol reviewed and accepted by the Dental Faculty University of Malaya Ethics and Research Committee (DFRD-1302/0033-L).

The inclusion criteria of the carious teeth used in this study were:

i) Presented with International Caries Detection and Assessment System (ICDAS) Codes 5 and 6 (N.B. Pitts, 2004) (Figure 3.14), i.e. teeth that presented with a

cavitated dentine lesion, with cavitation involving half or more than half of the dentine surface but not involving the pulp

ii) Lesion that had initiated either from the mesial or distal surface and had progressed towards either one or more of the occlusal/lingual/buccal/ surfaces.

iii) Presented as soft when inspected with a ball-ended probe and appeared yellow to light brown in colour.

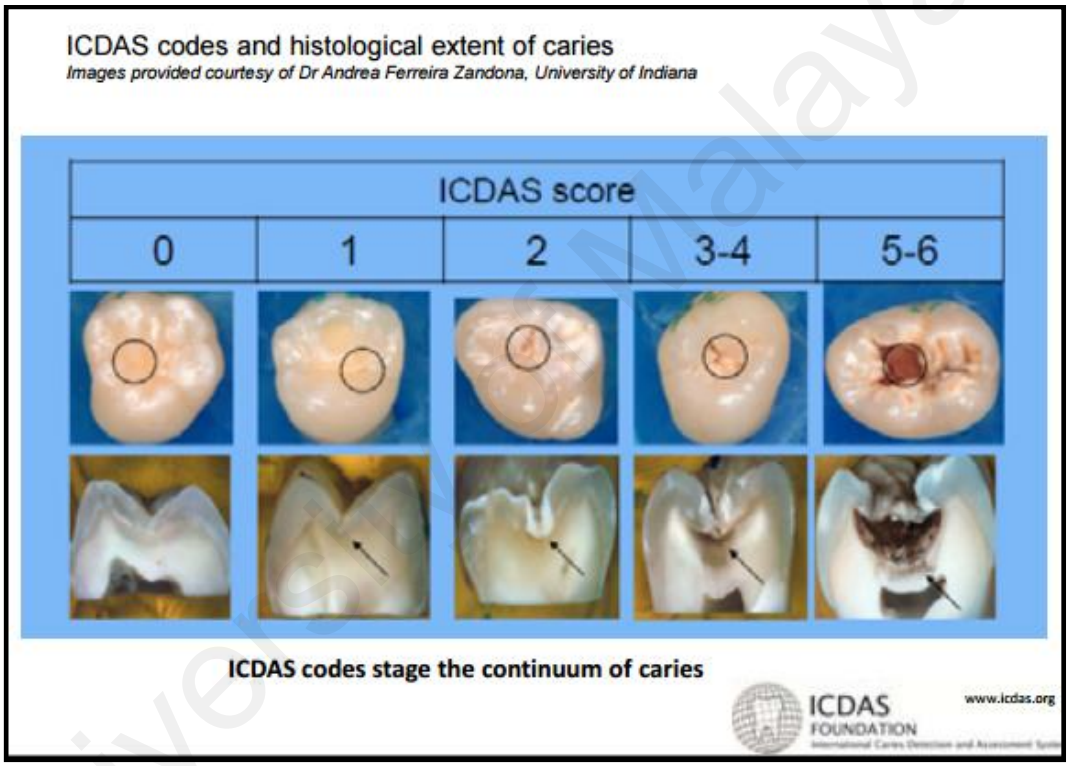

Figure 3.14: ICDAS

The Figure 3.14 shows the ICDAS coding of healthy and carious teeth, based on the severity of the lesion. Although, ICDAS Code 4 is considered as established dentine caries, there is an absence of frank cavitation. Lesions with ICDAS Codes 5 and 6 were best suited for this study (N.B. Pitts, 2004).

The extracted teeth were transferred on the same day of extraction to the laboratory and placed in phosphate buffered saline (PBS) solution as the transport medium. To ensure

that the outer-infected dentine remained intact during storage, the teeth were removed from the PBS solution, washed and wrapped in aluminium foil (Diamond Aluminium foil) and frozen at -20°C as recommended by Francecut et al (2006). The teeth were stored for a period of one to three months.

3.2.3 Specimen preparation

Prior to imaging, the teeth were transferred to single dry containers and defrosted at room temperature (approximately 24° C) for 14 hours. A wet paper towel was placed at the bottom of each container to keep samples moist and prevent dehydration. Careful attention was paid to avoid contact between the paper towel and the carious surface.

Soft tissue and extrinsic deposits were carefully removed when needed without altering the carious site using an ultrasonic scaler (Cavitron; Dentsply Professional, York, PA, USA). For orientation purposes, the carious surfaces were photographed at 1X magnification using a 2048 x 1536 resolution stereomicroscope (Nikon Eclipse 55i, Nikon, Japan) with an integrated digital camera (Nikon DSFI2, Nikon, Japan). After imaging with the stereomicroscope, moistened cotton pellets were placed loosely over the carious surface to protect it from dehydration. The roots were sectioned 1.5 mm below the cemento-enamel junction (CEJ) and each crown was then glued upright inside separate plastic moulds (5x5x2 mm) using fixation adhesive (Technovit 7230 VLC, Exact) at room temperature. Epoxy resin (Quick Mount 2 Epoxy resin, Ace technologies) was then poured into the mould until the crown was fully submerged and was left to set for 24 hours.

The set resin blocks with the carious crown completely embedded were subsequently sectioned using a high speed microtome cutting machine (Micracut 176, Metkon Ins., Ltd., Bursa, Turkey) with a 150 diamond grit blade and medium concentration under

copious water lubrication as selected in Section 3.2.1.3. They were cross sectioned transversely along the plane of caries progression, as described in Section 3.2.1.1. The transition of the dentine caries layers could be observed on the cut surface, from the outer light-dark brown layer of carious dentine to the inner yellow-white sound dentine (Figure 3.1b). The thickness of the dentine slabs was measured between 2.0 to 2.5mm. Since the OCT and SEM measurements were taken from the superficial depths of the lesions (100µm), the standardization of the thickness of slabs does not affect the experiment. To avoid affecting the friable ID layer, polishing and finishing was not performed after sectioning.

Areas on the cut surface with maximum variations of colours of diseased and healthy dentine, over a relatively large area were identified for investigation. The variances of colours observed ranged from light and / or dark brown at the area of carious dentine to light yellow and / or white at areas for sound dentine. A 3.05 mm-diameter copper grid (G200PB, Durasin Inc, PA) with 85 µm inter-bar distance and 45 µm-bar width were halved and placed next to the identified investigation areas in order to divide the area into 20 quanta of 85 µm (Figure 3.5d). These quanta were used to facilitate localisation of the layers of ID, AD and HD (as identified by SEM) in OCT scans. An adhesive tape was used to maintain the position of the copper grids over the carious surfaces (Figure 3.1c). Another adhesive tape was placed 2 mm away from the outer edge of the cut copper grid to demarcate the area of interest for OCT and SEM scanning.

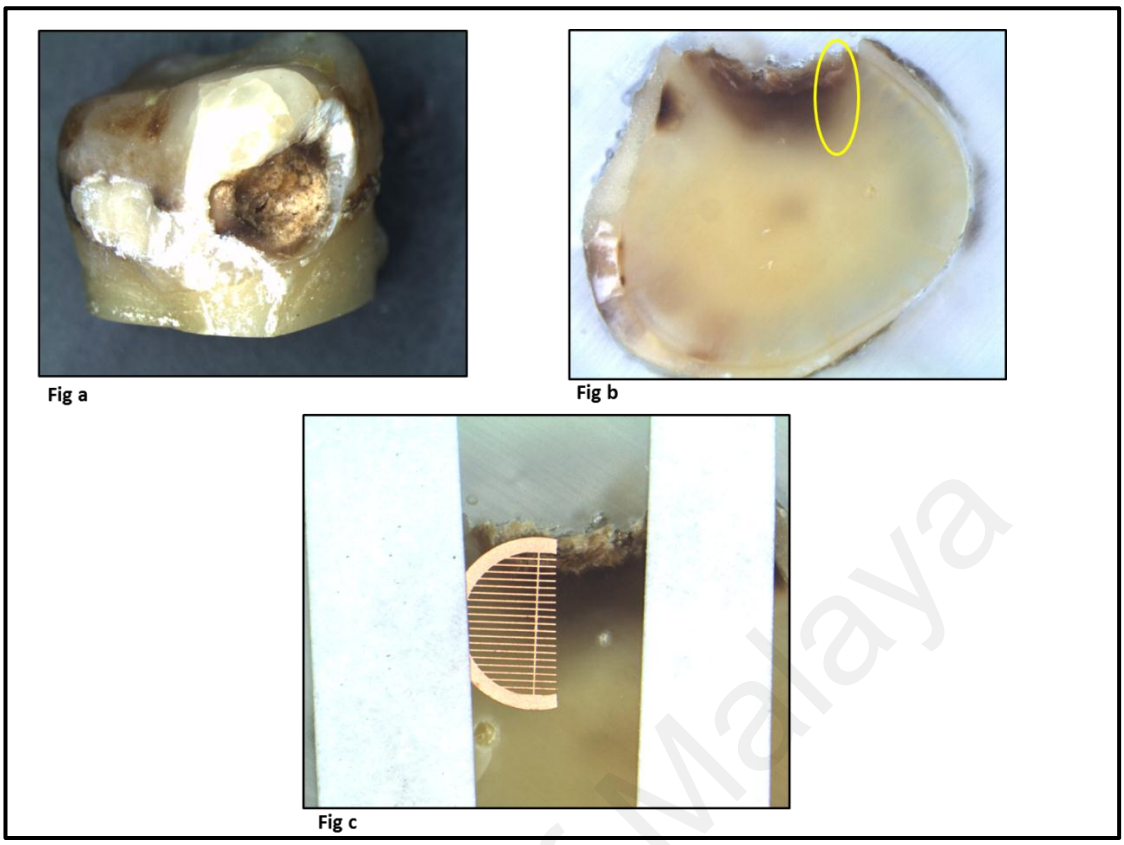

Figure 3.14: Steps of sample preparation

Figure 3.14a shows a stereomicroscope image of a carious tooth with ICDAS Code 5. Figure 3.14b shows a transversely sectioned tooth embedded in resin with carious and healthy dentine layers. The top/outermost carious layers appear dark to light brown protected by the surrounding resin, followed by a continuum of inner healthy yellow-white dentine layer. The chosen area of investigation is circled in yellow (Figure 3.14c) A half cut copper grid was placed adjacent to chosen region of interest on the prepared dentine specimen. White adhesive tapes show the demarcation area which will be area of investigation.

3.2.4 OCT scanning

A Swept Source OCT imaging system (SS-OCT 1300SS Thorlab Ltd., USA) with an emission wavelength centred at 1325 nm, lateral resolution of 11 µm and axial resolution of 9 µm in air was used in this study. The Thorlab OCT software was used to

configure the scan settings, view real-time B-scans and capture the scans. Three-dimensional (3D) scans of 1024 x 1024 x 512 pixels in the x-y-z directions were obtained from each sample. This corresponded to a scanned surface of 3.0 mm x 3.5 mm (x-y direction), which fully encompassed the investigation area, and an optical depth of 3 mm in air or physical depth of 1.90 mm in the dentine when the refractive index of the dentine ($\eta = 1.54$) in the near-infrared spectrum was used (Meng et al., 2009). The dentine slabs were placed horizontally on a translation stage, perpendicular to the OCT laser probe. The translation stage was adjusted on the x – z axes between 10 - 20 degrees to reduce specular reflection. The distance of the sectioned surface to the top border of the displayed B-scan window on the Thorlab OCT software was set at 0.3 mm and the laser was positioned at the centre of the investigation area. Three hundred and one B-scans were generated with an approximately 3.41µm distance between each scan. The B-scans were captured in a logarithmic scale with a brightness and contrast configured to cover an intensity signal level range of -40 dB to -10 dB.

3.2.5 Scanning electron microscope imaging

After being scanned with OCT, the samples were prepared for SEM imaging. In order to elucidate the minute ultrastructural details of the various layers of carious dentine, the smear layer and smear plugs in the dentinal tubules have to be removed without inadvertently affecting the underlying tissue. After conducting the pilot studies described in Section 3.2.1.5, the following protocol was adopted where the dentine slabs were subjected to 50 seconds of sonication in a stainless steel basket (UC1-230, Biosonic Ultrasonic Bath, Whaledent, USA) filled with distilled water at a frequency of 20 kHz without heat prior to and after etching. Then 0.5 Mol 10% EDTA (Sigma-Aldrich, St. Louis, Mo.) was prepared and placed on the investigation area for 3 minutes. The dentine slabs were stored in a humidifier for 24-hour.. The samples were

sputtered-coated with gold before the imaging.An initial 50X-magnification image encompassing the entire area of investigation was captured of each sample for orientation, using a SEM (FEI Quanta 250 FEG, UK). Thereafter, one 2000X magnification SEM image was captured of the area immediately adjacent to every inter-bar space of the copper grid, resulting in 20 SEM scans for each sample.

3.2.6 Criteria for identification of infected, affected and healthy dentine

Infected (ID), affected (AD) and healthy (HD) dentine were identified on the SEM images from each sample, based upon Pugach et.al.'s histological classification (Pugach et al., 2009). The three micro-structural criteria explored by Pugach et al were Intertubular roughness, peritubular dentine and tubule occlusion. Out of the three criteria, the loss and distortion (not rounded or elliptical) of the peritubular dentine (PTD) were established as the main feature to distinguish infected from affected dentine. Pugach et al's AD rating of 4 and 3, which depicts dentinal tubule lumen that are completely or partially surrounded by PTD was used as the criteria of identification of AD for this study. Pugach et al's AD rating of 2 and 1, which depicts undistorted or distorted shape of dentinal tubules with no peritubular dentine, were considered as regions with advanced demineralization and were not included as AD in this study (Figure 3.15). HD visibly showed the tubule lumens were lined with a highly mineralized cuff of PTD, distinctly separated by the Intertubular dentine (ITD).

The SEM orientation image (60x magnification) and of the dentine layers (250x magnification) were used to assess the location, thickness and selection of the region of interest (ROI) to capture images of the microstructures of ITD and PTD for each dentine layer. Twenty SEM images (2000x magnification) of the ROI were captured adjacent to the interbar space of the copper grid from each specimen, repeated images of healthy dentine were excluded. The images were placed in Microsoft Office PowerPoint®. As

per Pugachs criteria; complete loss and distortion of PTD was used to discriminate between the ID and AD layers. Multiple images from top order (line one to four) often fulfilled the criteria as ID layers, therefore one particular image was selected and its adjacent line number was noted. Observation of the images following the selected image as ID was continued, and gradually PTD started to appear in the images but often exhibited distortion of shape and was considered as part of the ID layer. The first emergence of partial or complete PTD with no distortion was considered as AD and its corresponding line number was noted. Following the images after the established AD layer, the parameter to ascertain the HD layer was observation of thick PTD forming the dentine tubule walls. The ROIs and the corresponding line number was used to draw the ROI at enface images of OCT using bespoke software.

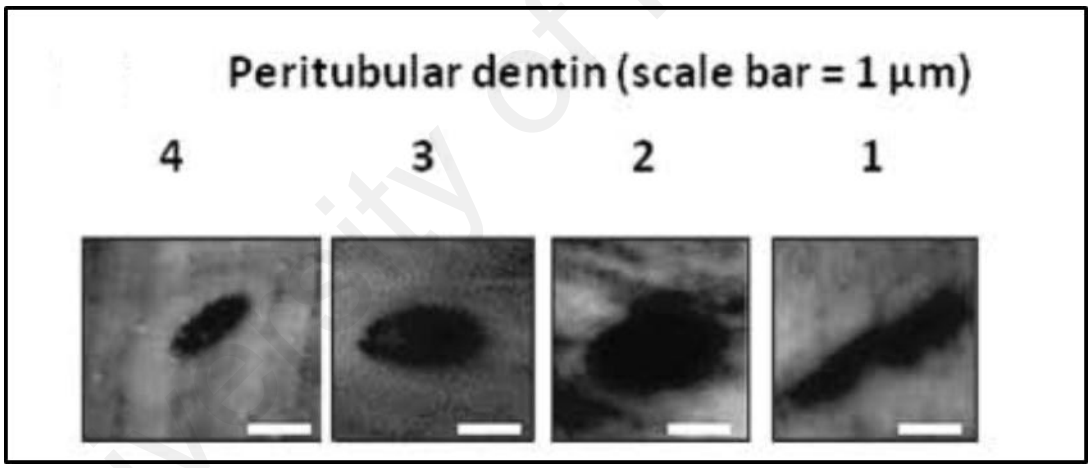

Figure 3.15: Pugach's histological classification using PTD as a parameter

Figure 3.15 shows peritubular dentine (PTD) (scale bar = 1 μm), 4 = complete, 3 = partial, 2 = none, 1 = distorted (images 30 x 30 μm). Illustration taken from Pugach (2009)

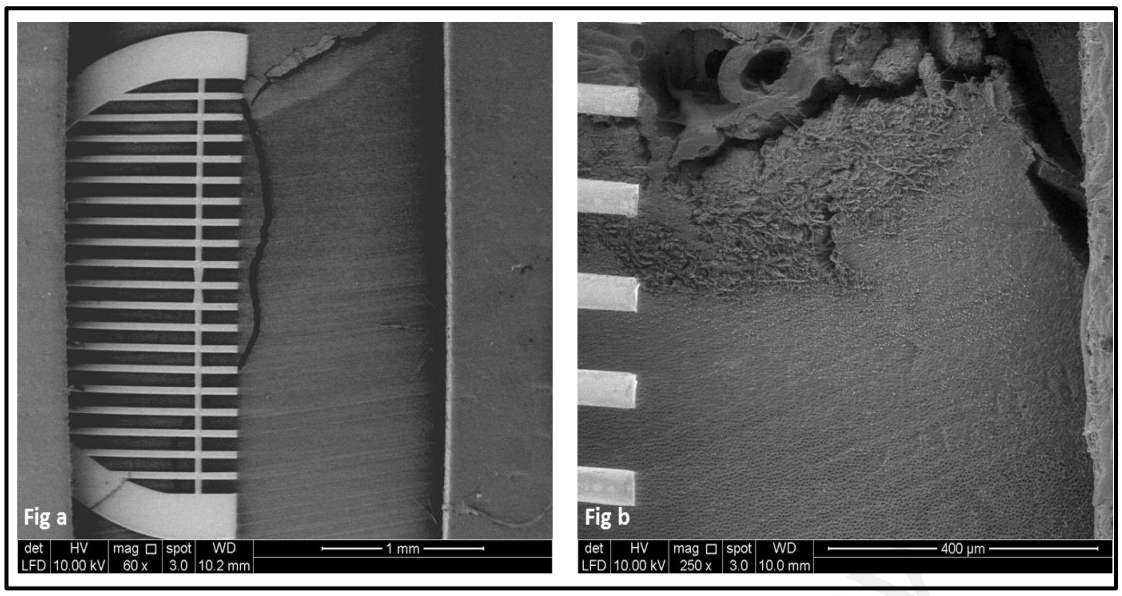

Figure 3.16: Orientation images for location of dentine layers

Figure 3.16 are SEM images of the sectioned dentine surface, Figure 3.16a shows the orientation image (60 x) and Figure 3.16b shows all three dentine layers (250x).

3.2.7 OCT data processing

3.2.7.1 Using Thorlab OCT software

The Large DR1 colour scheme of the Thorlab OCT software was chosen to generate en-face (x-y plane) images of the 3D scans, as it rendered the best backscattered intensity distribution and contrast of the investigation sites (Figure 3.17). As the dentine slabs were not polished after sectioning, the surfaces were not absolutely flat and hence there were large pockets of air on the surface of a few x-y planes. The first x-y plane that was observed to be free of air pockets was identified and generated. These en-face images were then used to make comparisons with the corresponding stereomicroscope images.

3.2.7.2 With a bespoke software

A bespoke OCT data processing software with a Graphic Unit Interface (GUI) was developed in MATLAB (The Mathworks, USA) for the processing of OCT data. The 3D OCT scans were loaded with B-scans as the default view. Surface determination was automated and fine-tuned manually. The final surface determination settings were then applied on the entire volume data to align the surface of the 3D scan of each sample. An en-face view of the surface-aligned 3D scans (Figure 3.17b) was then generated to enable the selection of regions of interest. The locations of the three regions of interests (ROIs) representing ID, AD and HD identified with SEM for each sample were ascertained on the aligned enface OCT scans described above (Figure 3.17b) and an area measuring approximately 150µm x 120µm were drawn at each ROIs. The depth-resolved backscattered intensity for each of the ROI area drawn was generated for each of the 25 samples. The depth-resolved intensity (I) were generated in both the logarithmic scale for each of the 25 samples and exported into Microsoft Office Excel® 2010 for further analysis.

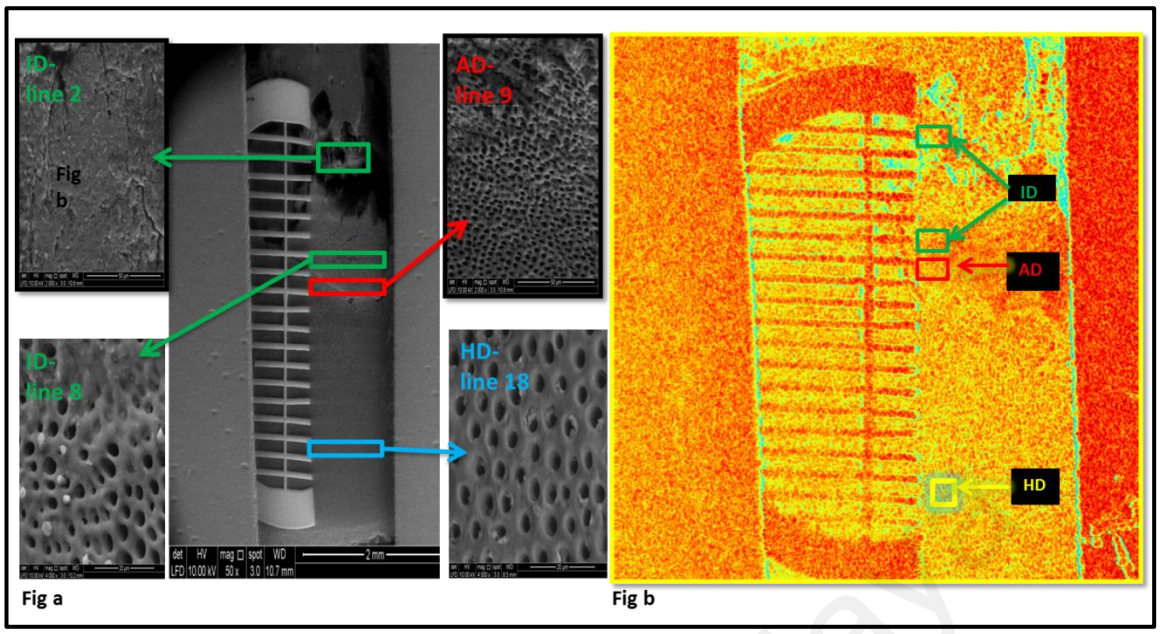

Figure 3.17: ROIs on OCT enface representing ID, AD and HD identified with SEM

Figure 3.17a shows a SEM scan and Figure 3.17b is the corresponding OCT en-face view of the surface aligned with the bespoke software. The identified regions of interest (ROI) of ID, AD and HD on SEM images were ascertained on the OCT en-face scan. Areas measuring approximately 150 µm x 120µm were drawn at these ascertained ROIs on the OCT en-face view in order to generate a MEAN depth-resolved intensity profile for each region.

3.2.8 OCT data analysis

An assumption was made where a physical depth of 100 µm was considered to consist of 'similar tissue' and there was very little risk of the presence of more than one type of carious dentine layer at that depth to confound the analysis. Therefore the intensity profile of ID, AD and HD beyond the physical depth of 100 µm depth were not explored and analysed.

3.2.8.1 Attenuation characteristics and mathematical characterization of OCT backscattered intensity through ID, AD and HD

In order to study the attenuation characteristics of the near-infra red light passing through ID, AD and HD, the depth-resolved intensity (*I*) from each of the 25 samples for each of these ROIs, were collated to produce a mean depth-resolved intensity (*I*) profile, or the A-scan of the first 100 μm from the surface (Figure 4.4). With the scanning resolution of 512 pixels in 1.90 mm in the z-axis, there were 25 depth points in 100 μm.

Characteristics of the A-scans such as the maximum intensity (I_{max}), the rate and pattern of attenuation of *I* through the first 100 μm were observed and compared between ID, AD and HD. In an attempt to further characterise the observed patterns of attenuation for each dentine layers, mathematical curve fitting was used to identify the best line fit line. The R^2 value signified the most suitable equation for each layer and it was performed with Microsoft Office Excel® 2010.

3.2.8.2 Differentiation of ID, AD and HD with outcome measure derived from the depth-resolved intensity (I) profile / A-scan.

Three outcome measures derived from the depth-resolved intensity (*I*) profile / A-scan were explored and used to differentiate ID, AD and HD. They are listed in Table 3.2

Table 3.2: OCT outcome measures for differentiating carious and healthy dentine layers

Outcome measures	***Description***
Maximum intensity, I_{max}	The highest intensity measured, often a couple of pixels from the tooth-air interface.
Ratio, R	$$R = \frac{I_z}{I_{max}}$$ With I_z being the intensity at the physical depth point of z.
Area under the curve, AUC	$$AUC = \left(\frac{I_{z1} + I_{z2}}{2}\right)(z2 - z1)$$ With I_{z1} and I_{z2} being the intensity at the physical depth point of z1 and z2

Statistical software v2.0 (SPSS; Chicago, IL, USA) was used for analysis. The Shapiro-Wilk test for testing normality, One-way ANOVA and Post hoc Tukeys HSD were used to compare the I_{max} between ID, AD and HD. Two-way repeated measures ANOVA was used to R at 17 depth points and, AUC_T, AUC_I, and AUC_{II} between ID, AD and HD. Mauchly's Test was used to evaluate the sphericity assumption. If sphericity was not met, the adjusted F-value of the Greenhouse-Geisser correction was considered. Post hoc test (Bonferroni) was applied to compare the mean scores R, AUC_T, AUC_I, and AUC_{II}.

3.2.8.3 Performance of OCT Intensity derived outcome measures in identifying ID, AD and HD

Linear discriminant analysis (LDA) and Artificial Neural Network (ANN) were used for assessing the accuracy of the OCT outcome measures ($I_{max,}$ *R* and *AUC)* in identifying ID, AD and HD. Microsoft Office Excel® 2010, Statistical software® v2.0 (SPSS; Chicago, IL, USA) and MATLAB® (Mathworks. Inc, USA) were used for data analysis.

ANNs can simulate the behaviour of biological neural nets, and have effectively predicted, through generalization of a limited quantity of training data, overall trends in functional relationships. A well trained ANN can be used to simulate and predict the output response for various control factor-level settings. (Tu, 1996). To train the network, input data are inserted into the network, which splits the data into training, validation and testing samples. Training samples are used to train the network, and adapt to its error and retraining produces better prediction results. Validation samples recognize the generalization and suspend the training when improvement occurs. Testing samples provide an autonomous measure of the network performance. If errors remain high, the network is retrained to acquire more accurate results. In this study, 25 ROIs representing each dentine layer yielded multiple data points from three outcome measures which were used for ANN analysis. For training, 70% of data were utilized, 15 % for validation, and 15 % of the data for testing.

All OCT outcome measures were tested for their accuracy in the prediction of dentine caries layers using the neural network pattern recognition tool (npr tool) in MATLAB (Mathwork Inc.). *R* was analysed separately from I_{max} and AUC. *R* was used as a single input layer and AUC and I_{max} as grouped input layers with ID, AD and HD as three

output layers. One or more hidden layers were extracted for essential information during learning.

The overall classification accuracy is represented in the confusion matrix, which represents true positive (Sn), true negative (Sp), false positive (1-Sp), false negative (1-Sn), and overall accuracy of the network. In addition, the receiver operator characteristic curve (ROC) is presented to show the performance of ANN. ANN Confusion Matrix represents horizontal cells displaying the number of classes that were correctly classified for each dentine layer and the vertical cells show the misclassified cases. In addition, best performance is taken from epoch which has a minimum validation error. Figure 3.18 shows the study analysis work flow.

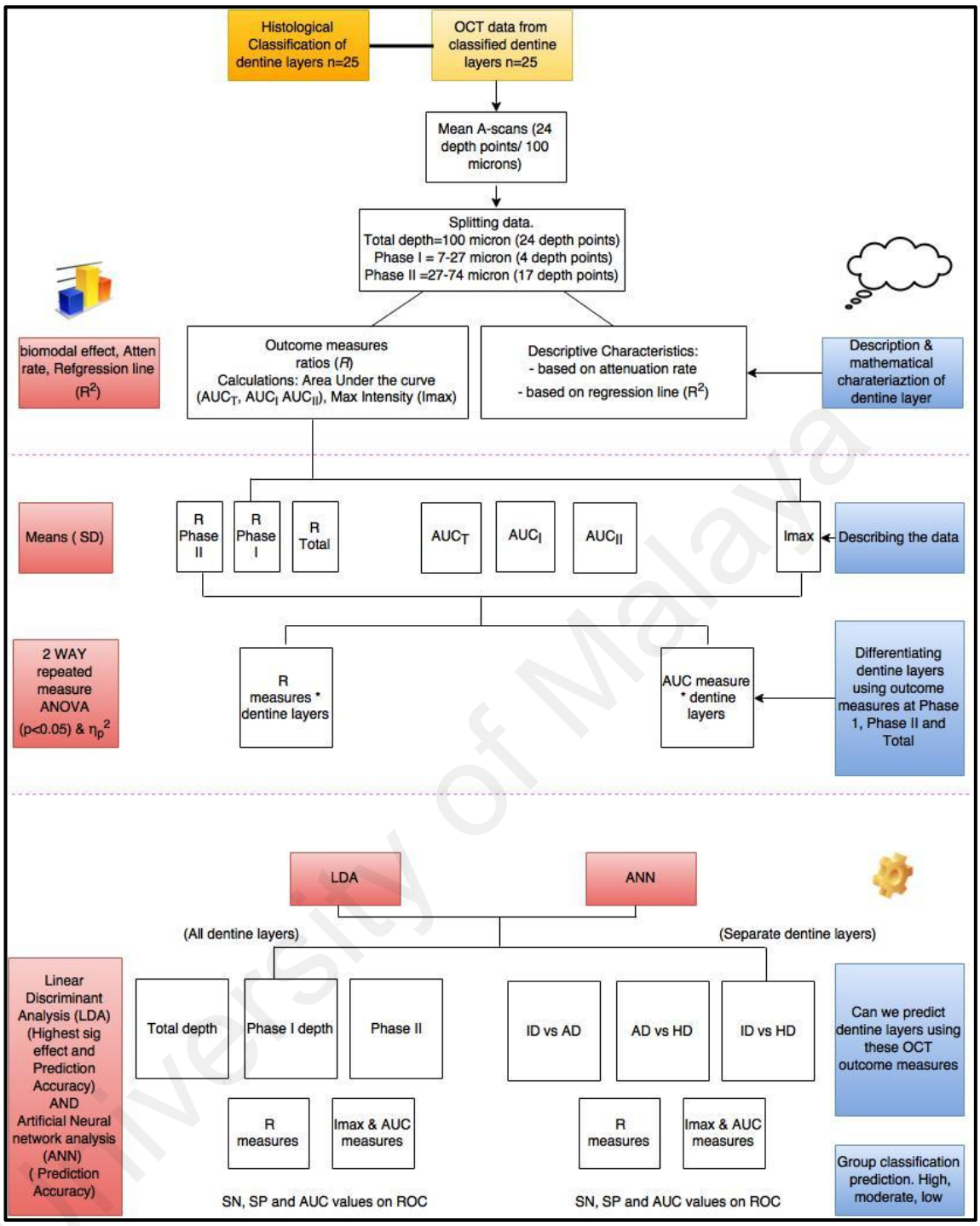

Figure 3.18 study analysis work flow

.

3.3 Dentine caries chemical composition and OCT methods

3.3.1 Selection of teeth and sample preparation

The dentine slabs used for this section were the same cohort as those used in Section 3.2.3 up to 3.2.5.

3.3.2 Energy dispersive X-ray system (EDX) analysis

The regions of interest as selected in OCT where matched and selected for EDX analysis. Elemental analysis was achieved under high-vacuum at 50X magnification using energy dispersive X-ray system (EDX) (Microanalysis suites, Quanta V4.11, Oxford Instrumental Analytical Ltd, UK), attached to field emission scanning electron-microscopy (FESEM) (FEI Quanta 250 FEG, UK). To enhance the accuracy of chemical analysis the full frame scan mode was selected instead of the spot scan mode. The frame was selected using the region of interest adjacent to the respective interbar space and around the ROI selected in Graphic User Interface (GUI) software for OCT covering an average area of 500μm. The x-ray beam excitation voltage was adjusted at 20 kv, and the beam current at 5 nA with spot size of 4μ for 50 secs of acquisition time. To further standardize, all the operating settings of the beam power and scanning parameters were standardized to collate the average mineral content from the samples of each layer and compare between ID, AD and HD.

The output data were saved in word doc format, which included the full scale spectrum showing the peaks of the elements analysed. Quantitative weight% and atomic% of the major elements along with the bar-graph expressed in weight% were included for the respective layers from each sample. An illustration representing the frame scan mode drawn at the respective ROI was also attached (Figure 3.19).

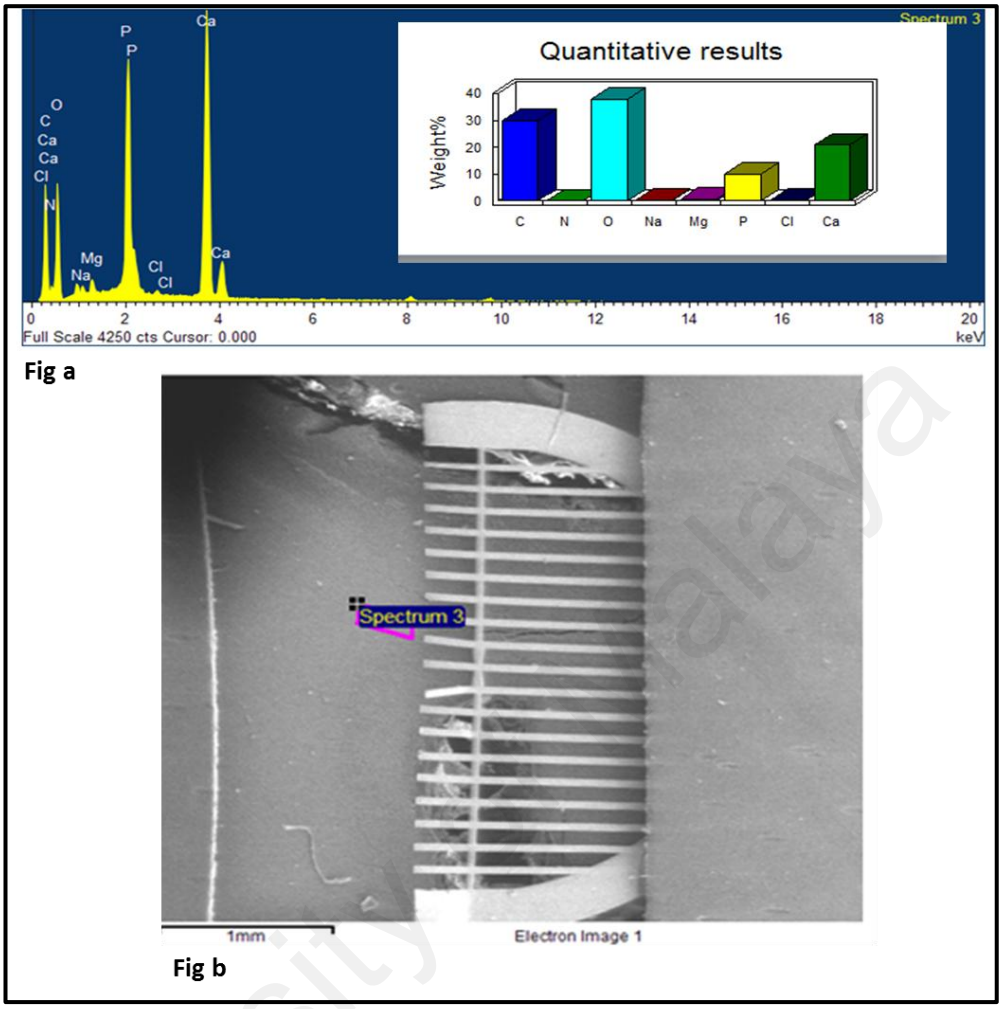

Figure 3.19: Quantitative mineral analysis and selection of ROI

Figure 3.19a is a wide scale graph showing the spectra and the quantitative (wt%) of the elements detected. Figure 3.19b shows how the ROI was drawn using the full frame mode on the specimen surface adjacent to the copper grid.

3.3.3 OCT scanning and data processing

Same methods of OCT scanning were used for Research Objective 1.

3.3.4 Statistical Analysis

Statistical software v2.0 (SPSS; Chicago, IL, USA) was used for analysis. One-way ANOVA was performed, considering that the Leven test of homogeneity of variance was not violated and the Bonferroni test was attempted, to evaluate the statistical difference between the major elements and the Ca:P ratios between the three dentine layers. When the Leven test was violated, the Welch's ANOVA and the Brown-Forsythe followed by the Games-Howell tests were applied due to their robustness towards homogeneity of variance. The Pearson correlation test was used to determine the statistical significance and the level of relationship between the major elements and the OCT outcome measures of the three dentine layers.

3.4 Mineral density of Dentine layers, as characterised by OCT

3.4.1 Sample collection and storage

Thirty extracted human molars with proximal caries were used in this study. Molar teeth were chosen as they provided a bigger bulk and spread of caries when compared to premolar and anterior teeth. The teeth were stored for a period of one to seven months. The teeth were collected between January-August 2015. The inclusion criteria, transfer of extracted teeth and storage technique remained the same as discussed in Sections 3.2.2 and 3.2.3. The extracted teeth were transferred on the same day of extraction to the laboratory and phosphate buffered saline (PBS) solution was used as the transport medium. The teeth were removed from the PBS solution and all the soft tissue and extrinsic deposits were cleaned using a hand scaler (Cavitron; Dentsply Professional, York, PA, USA), with care taken during the procedure to protect the caries from being

disturbed. To ensure that the outer infected dentine remains intact during storage, the teeth were removed from the PBS solution, washed and wrapped in aluminium foil (Diamond Aluminum foil) and kept frozen at -20°C as reported by (Francescut et al., 2006). The carious surfaces were photographed at 1X magnification using a stereomicroscope. The teeth were labelled and wrapped in foil and frozen at -20° C.

3.4.2 Radiographic imaging (micro-CT)

The micro-CT imaging of carious teeth was scheduled to take place in Minnesota Dental Research for Biomaterials and Biomechanics (MDRCBB) School of Dentistry, University of Minnesota. Before the transportation of teeth, the teeth were transferred to individual dry containers and defrosted at room temperature (about 24° C) for 14 hours. Wet paper towel was placed at the bottom of each container avoiding any contact with the carious surface and paper towel (Francescut et al., 2006). A moist cotton pellet was placed over the cavity to protect the carious lesions from desiccation. Each tooth was wrapped with a moist cotton swab and carefully placed in a small aluminium packet. Thirty packets were prepared and then placed in one aluminium bag which was air vacuumed and placed in a thermocol box which was sealed and couriered to reach MDRCBB School of Dentistry, University of Minnesota for micro-CT scan within four days. All teeth were unpacked at once when it reaches MDRCBB School of Dentistry, University of Minnesota and kept in moist and refrigerated conditions for one week during the scanning. Once the micro-CT scanning was completed, the thirty teeth were packed and couriered back to the Biomaterial laboratory, Faculty of Dentistry, University of Malaya (Figure 3.20).

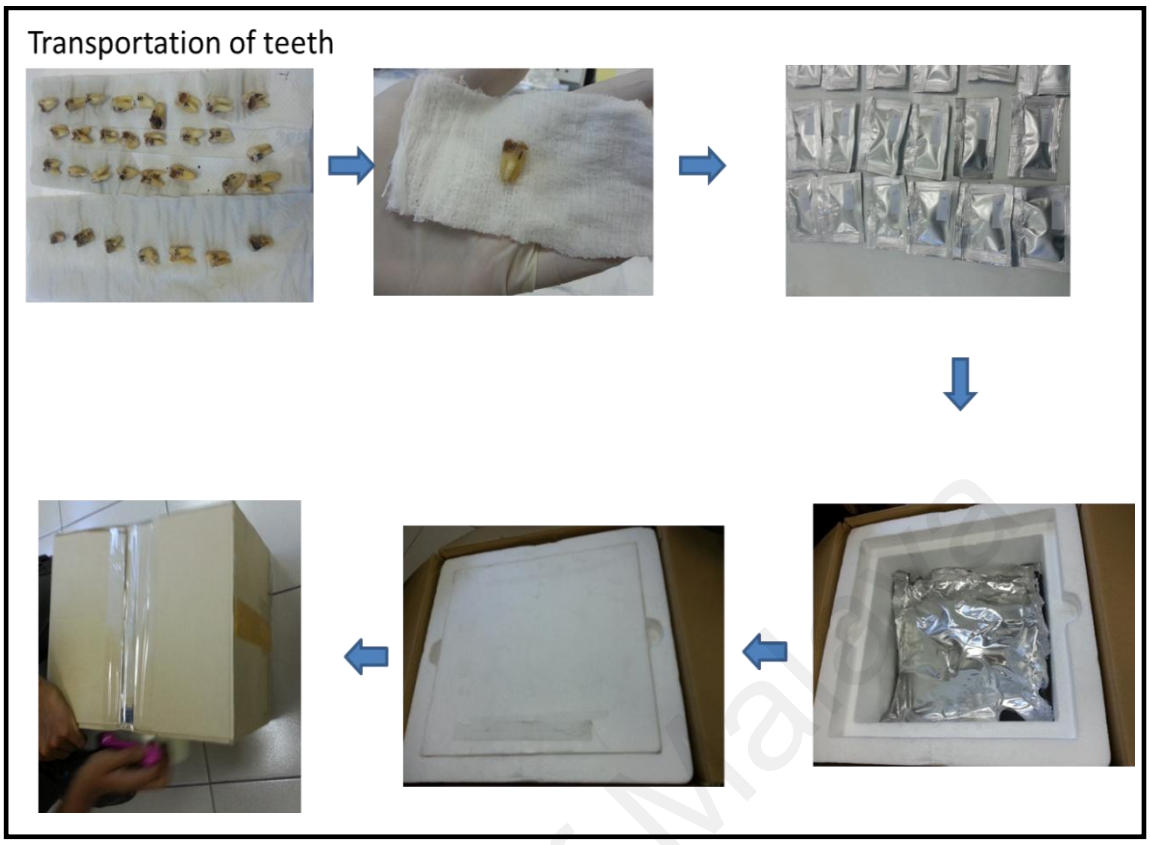

Figure 3.20 Packaging and transportation of teeth

3.4.3 Micro-CT scanning and image processing

The lower one-third of root of each tooth was embedded in resin block and placed vertically and scanned with the micro-CT system (Model XTH 255, X-tek system, Nikon Metrology, Brighton, MI, USA). Scanning was performed using tube voltage of 90 kV and tube current of 90 µA. A total of 720 projections with 4 frames per projection were taken at each scan. The micro-CT scan yielded images with approximately 2.12- 2.43 µm/ frame distance. Hydroxy apatite phantom disks with known mineral density (MD) were scanned before and during the scanning of teeth to ensure the calibration of the micro-CT system. The reconstruction of the volume data was achieved by using the CT Pro 3D software (Nikon, Metrology, Brighton, MI, USA). The reconstructed volume data was exported as a DICOM image stack and .VGL format for further image analysis. The reconstruction of the volume data can help

determining the distance between each frame. Eleven pre-constructed hydroxyapatite (HA) tablets with known MD ranging from 0.099 to 1.54 gm/cm^3 with standard dimension were used as phantoms for calibration purposes. The eleven HA tablets were vertically stacked using an acrylic holder and were positioned next to the scanned tooth each time.

3.4.4 Selection of cutting plane using cross-sectional micro-CT images

DICOM image format was used to reconstruct the micro-CT data into a 3D format by using VG Studio Max (Version 2.1.3, 64 but, Volume Graphics, Charlotte, NC, USA). Subsequently the 3D image stack or the volume data of each tooth were used for visualisation and quantitative measurements. Once the volume data were constructed in 3D, the surface determination was manually adjusted to determine the surface of the tooth. The surface determination histograms represented three bars in a form of histogram; each demonstrating the background, dentine and the enamel (Figure 3.21b) The iso-surface determination cut-off was set at the junction between the background and the outermost boarder of the carious dentine. The iso-surface setting assured that infected dentine was completely included as part of the 3D volume data for further exploration (Figure 3.21a).

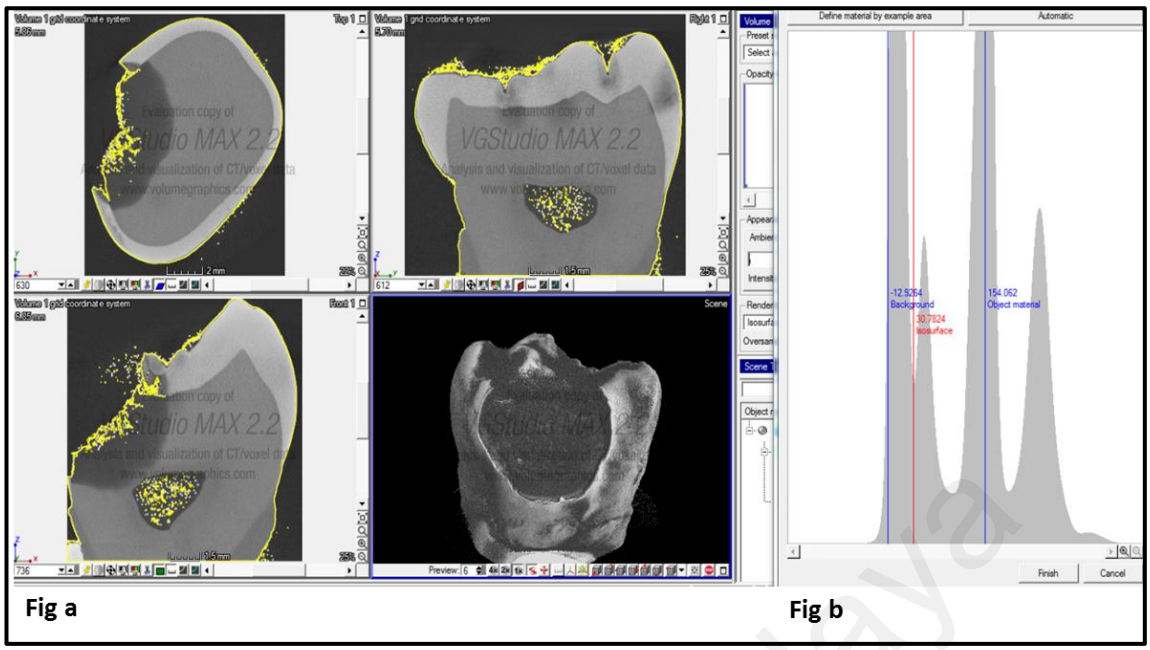

Figure 3.21 Surface determination of carious teeth

Figure 3.21 shows the coordinate position, 2-D slices of teeth in different angles and a histogram showing background and tooth materials. On the histogram image (Figure 3.21b), the blue line represents the centre of the material, while the red line determines the set iso-surface, and the yellow marked the regions on the respective views of the tooth surface. Figure 3.21a shows the live 2-D view of the tooth, with the remaining three images as front, top and right view.

Amongst the four viewing panes within the tripod coordinate system, the 3D preview window indicates the orientation of the currently chosen coordinate system (Figure 3.22a). Using this coordinate system icon bar, the tooth was positioned in a way that the 2D windows showed slices of the scanned mesio-distal direction (Figure 3.22b), along the z-axis or in depth occluso-pulpal (Figure 3.22c) and along the bucco-lingual directions (Figure 3.22d). Considering the view at the mesio-distal direction-axis which is perpendicular to the cross-sectional plane, the live 3D rendering preview window was locked. The slices in the z-axis were scrolled until the cross-section with the best visual segmentation of the infected, affected and healthy dentine volumes of detectable

intensity differences, which is dependent on the magnitude of intensity and change in the magnitude specific to a direction at a pixel, was selected.

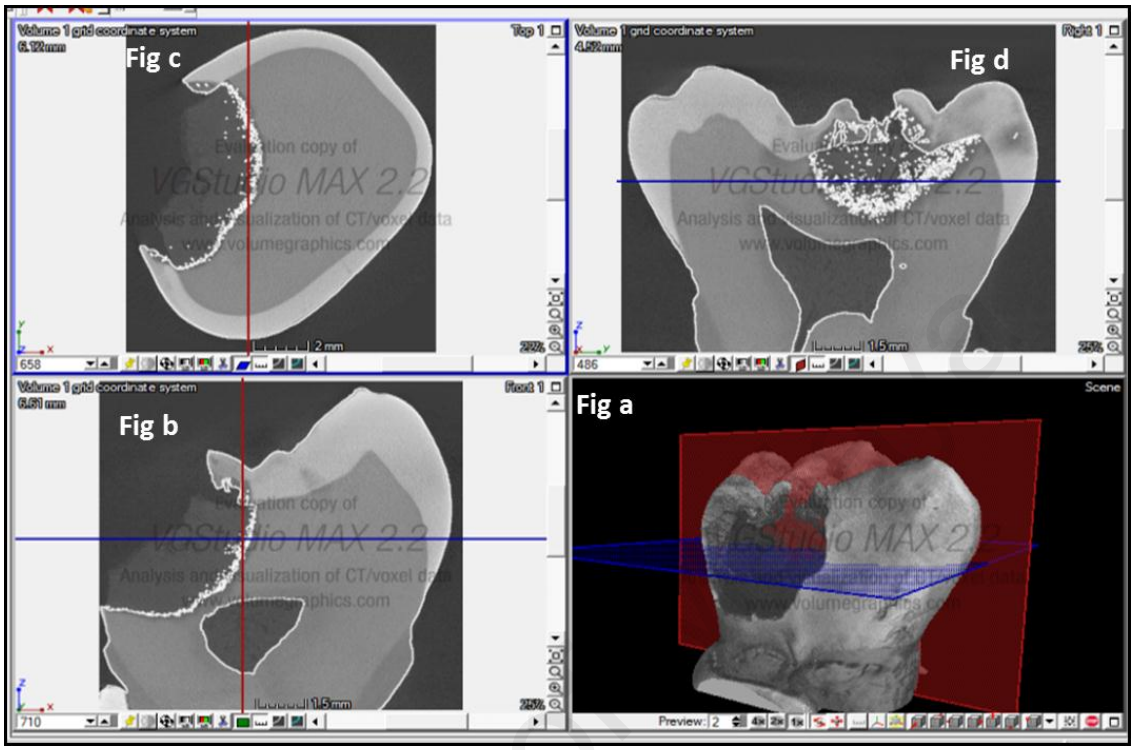

Figure 3.22 Selection of micro-CT slice

Figure 3.22 shows images of the tripod in the coordinate system. Figure 3.22a is a live 3-D view of a carious tooth. The lower right corner of the live 2-D view of the tooth shows the horizontal (blue) line as the position of the section and the vertical (red) line as only added information of the reference point. Figure 3.22c shows the slicing sectioning used to determine the choice of the cutting plane visual segmentation of infected, affected and healthy dentine of visually detectable intensity differences.

Opacity rendering option was used to adjust the intensity in samples where dentine caries layers were not clearly distinguishable. The carefully chosen slice along the x-axis window pane, showed the biggest bulk and the clearer demarcation amongst the three layers. Along with the visual classification using the intensity difference, a line plot at the chosen cross-sectional plane was drawn across the infected, affected and

healthy dentine and their respective line plots (Figure 3.23). The line graph demonstrates the change of attenuation values starting from the lower to the highest values from A-point (HD) crossing (AD) till B-point (ID). This step validated the chosen section had all three layers present and would be the best choice of plane to be selected for further investigation.

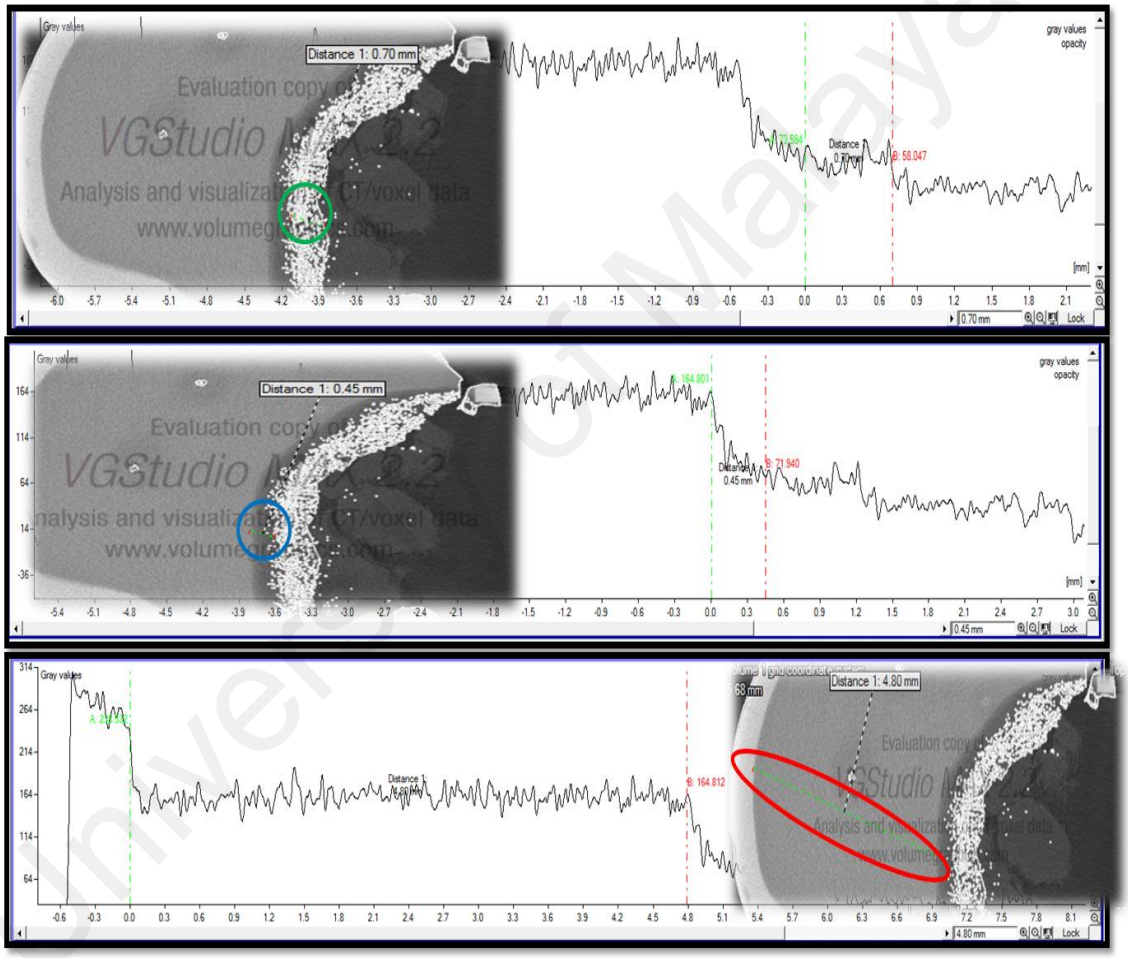

Figure 3.23 Approximating attenuation values of carious and healthy dentine

Figure 3.23 shows images with highlighted circular region in green, blue and red representing infected, affected and healthy dentine and their corresponding line graphs. In healthy dentine the figure with the red circular regions on the line graph shows a green dotted line (DEJ) point-A shows the highest attenuation value, while towards the

end of point –B is the affected region with the infected dentine showing the lowest attenuation intensity value (red dotted line).

3.4.5 Teeth sectioning and sample preparation

After the selection of the micro-CT slice, the teeth needed to be sectioned in the same cross-sectional plane. This cutting plane was determined by selecting several landmarks around the chosen cross-sectional surface in the VG studio Max (Version 2.1.3, 64 but, Volume Graphics, Charlotte, NC, USA). Three reference landmarks were selected; x1, x2 and y1 along the x and y coordinates. These coordinate points were then translated using a black Sharpie marker (Fiber tip, Sanford, Bellwood, IL) on the tooth surface and joined together with a reference line which would guide the sectioning of the tooth in a precise chosen plane (Figure 3.24). The accuracy of transferring these landmark points with a marker were marginally compromised, however later, with a slight adjustment of the planes using VG studio, perfect matching was obtained.

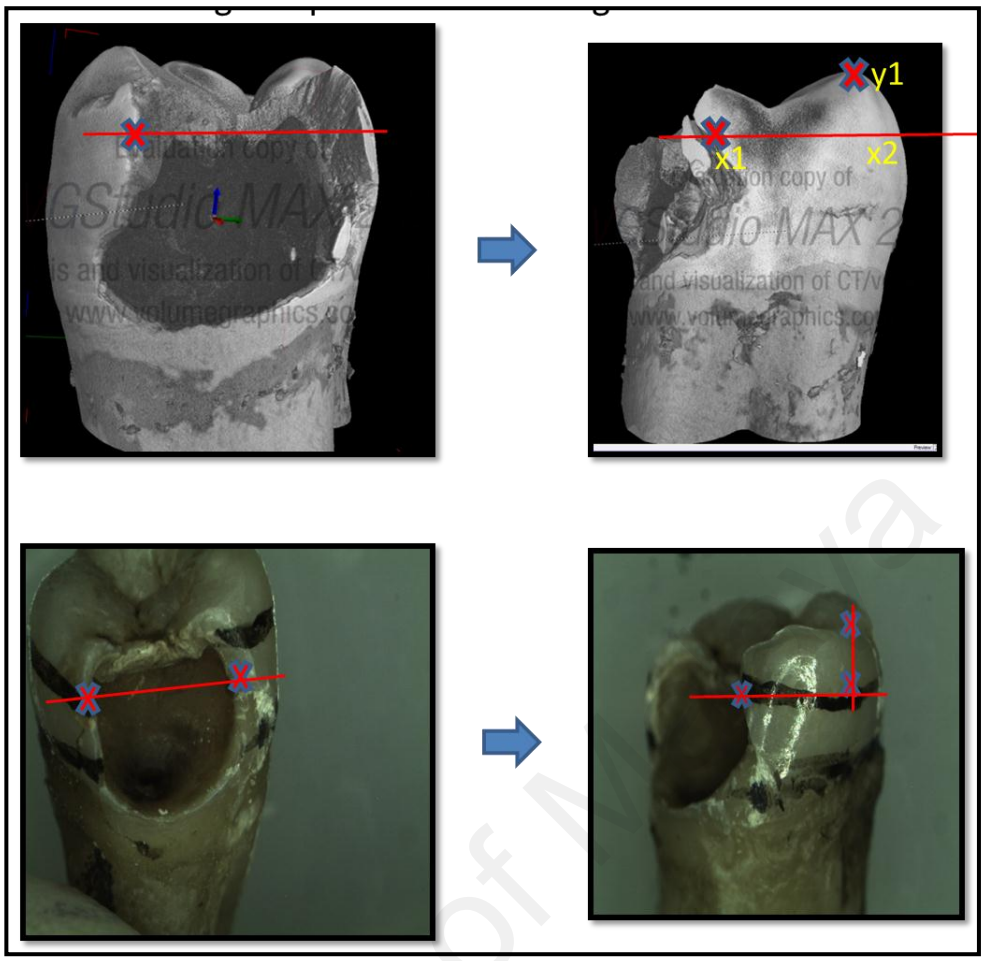

Figure 3.24 transfer of reference points from the chosen plane of section to tooth surface.

Roots were sectioned 1.5 mm below the cemento-enamel Junction (CEJ), ensuring the cut surface of the coronal part was completely flat. Each carious coronal part of the tooth was then glued upright inside separate plastic moulds (5x5x2 mm) using fixation adhesive (Technovit 7230 VLC, Exact), and resin was poured until the crown was fully submerged and was left to set for 24 hours. The set resin block with the crown completely embedded measuring 5x5x2 mm was obtained. The landmarks and reference lines over the embedded tooth surface were then translated over the resin block using a black Sharpie marker (Fiber tip, Sanford, Bellwood, IL) as a guide for sectioning. A water proof adhesive tape was placed on the reference line to ascertain proper

positioning of the resin block in the high-speed cutting machine during the sectioning procedure (Figure 3.25).

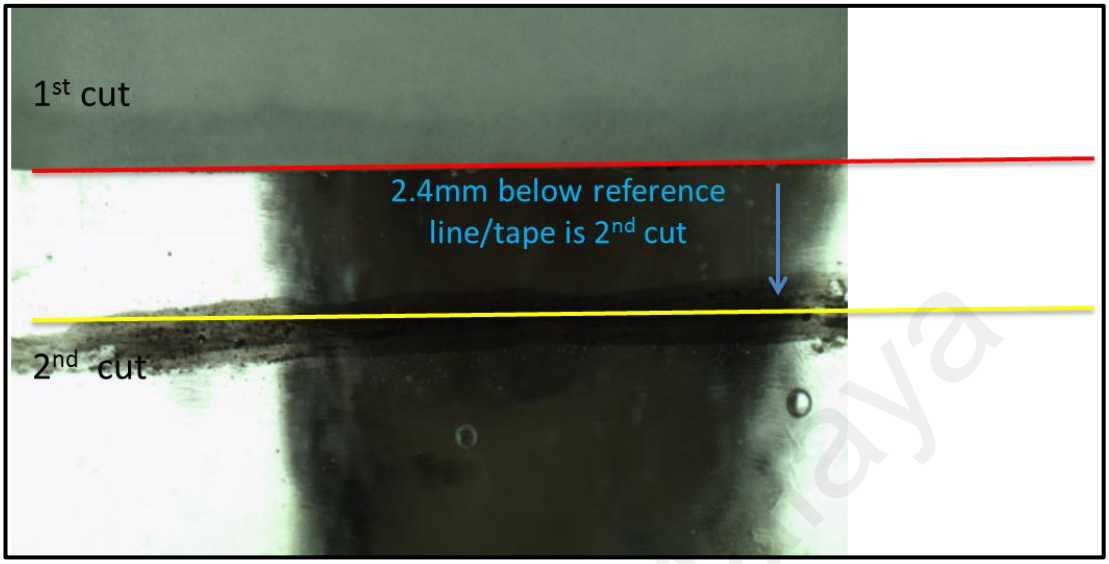

Figure 3.25 Sample preparation and sectioning plane

The red line in Figure 3.25 shows the first reference line translated from the tooth to the resin block. An adhesive tape was placed on the top of the reference line for precision positioning during cutting. The second reference line was drawn measuring 2.0mm-2.4mm away from the adhesive tape (yellow line).

The set resin block with the carious crown completely embedded were subsequently sectioned using a high speed microtome (Micracut 176, Metkon Ins., Ltd., Bursa, Turkey) with high speed cutting machine using 150 grit diamond cutting blade. The teeth embedded in the blocks were cut along the adhesive tape in straight lines (Figure 3.25). The dentine slabs were flat measuring approximately 2.0 to 2.5mm thick (Figure 3.26). Polishing and finishing was not carried out after sectioning to avoid affecting the friable infected layer. Samples were imaged at 1.8x magnification under a stereomicroscope. The dentine slabs were labelled and wrapped with moist cotton swab until further analysis can be carried out.

Figure 3.26 Approximating thickness of dentine slabs

3.4.6 Matching micro-CT and stereo-images of sectioned sample surfaces

The stereo microscope image of the sectioned dentine slab and the selected micro-CT slices were placed in Microsoft Office PowerPoint® 2010 adjacent to each other. Visual matching was done to ensure both the surfaces were matched and the area of investigation was similar. If the anatomical landmarks were different, minor adjustments were made in the micro-CT slices, using tripod coordinate system in VG studio Max (Version 2.1.3, 64 but, Volume Graphics, Charlotte, NC, USA) by tilting the mesial/distal or buccal/lingual direction of the tooth, until the surface landmarks and dentine caries layers completely matched the prepared dentine slabs. Out of thirty samples, 21 samples perfectly matched the selected surfaces (Figure 3.27), while the remaining 9 were excluded due to difficulty in matching the surfaces (Figure 3.28).

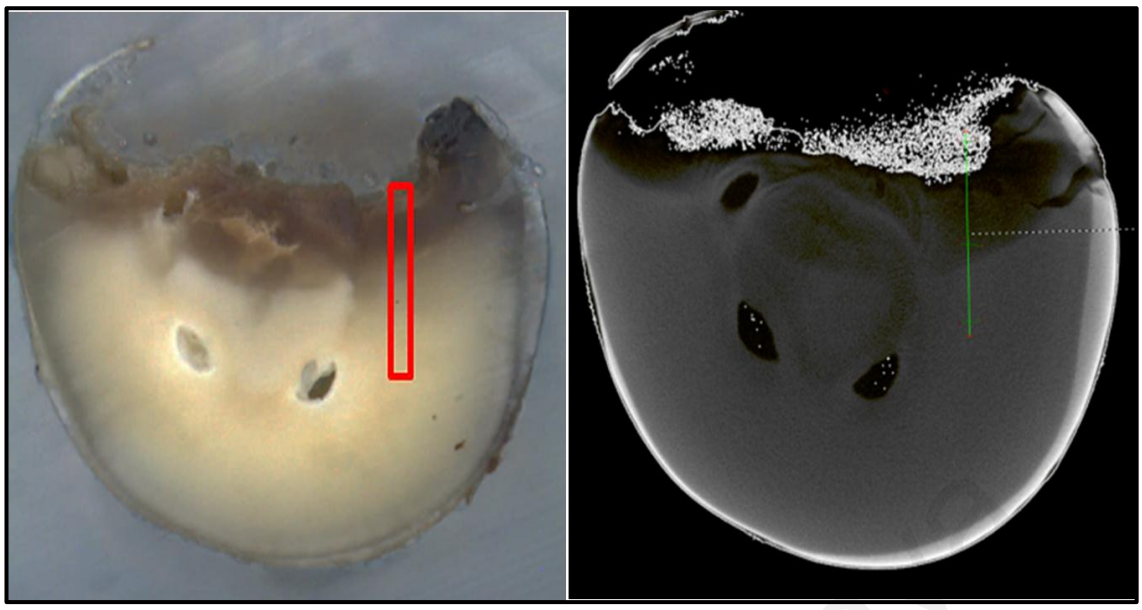

Figure 3.27 Perfectly matched samples of stereomicroscope and micro-CT image

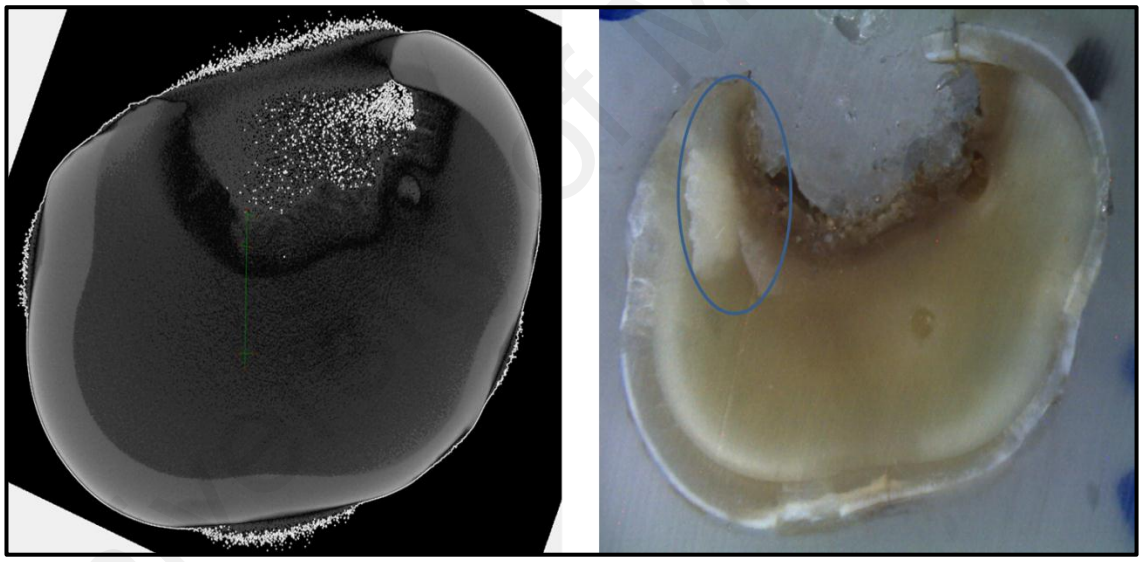

Figure 3.28 Exclusion of non-perfectly matched samples

3.4.7 Extracting attenuation coefficient using line plots and automated regions of interest

On the chosen x-axis of the micro-CT tomogram slice, a line plot measuring 3.05 mm using a distance measuring tool in VG studio Max (Version 2.1.3, 64, Volume Graphics, Charlotte, NC, USA) was drawn across the three layers within a selected area.

The attenuation points of the entire line plot against the total distance of the line plot were saved in excel sheets. The direction of the line plot was specific to the direction of the vector, with each line beginning from a visually higher intensity area (ID) to the lowest intensity area (HD). Each line plot showed a line graph, representing the distance measured on the x-axis and the attenuation values on the y-axis. The line graph having all three dentine layers showed two steps between ID and AD, and AD and HD, demarcating the three layers from each other. Using the measuring scale, each layer were measured separately using quantitative demarcation seen on a line graph and a visual intensity difference as the cut off points between these layers (Figure 3.29). An average voxel aspect ratio between two measurement points was 2.5 µm resolution. Three automated 2X2 shaped (approximately 651 voxels) ROI were drawn in the centre of each separately measured line for ID, AD and HD. The mean attenuation, minimum, maximum and number of voxels involved in the ROIs saved for every drawn automated ROI was saved in an excel sheets.

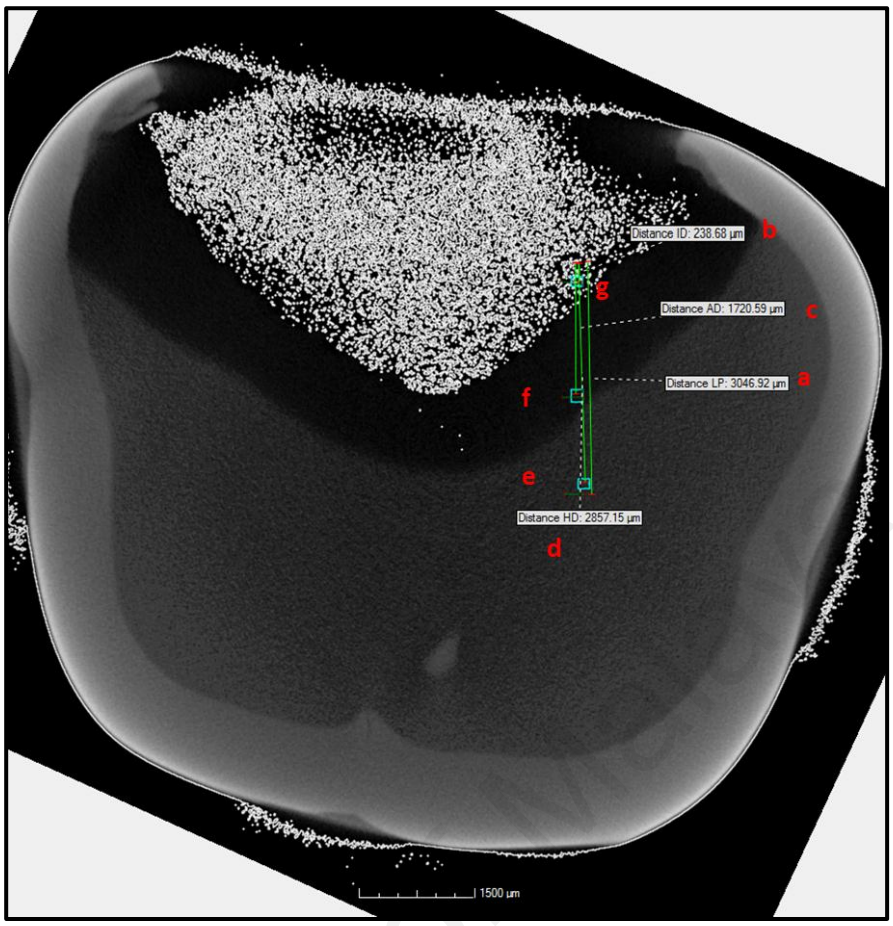

Figure 3.29 Extracting attenuation using line plots and ROIs from dentine layers

Figure 3.29 shows the cross-section of a micro-CT slice with line plots and ROIs. Figures 3.29a &g show that the measured length of the line plot is 3045µm with its respective ROI. In Figure 3.29b the distance of the ID layer measured at 268 µm along with its respective ROIs. In Figures 3.29 c & f the distance of the AD layer measured at 1720 µm, In Figures d & e the distance of the HD layer measured at 2857 µm along with its respective ROI. These measurements of line plots of each dentine layer were used against the standard graduated copper grid during OCT data extraction.

3.4.8 ROIs and measurements on sectioned samples surfaces

Figures 3.30a and 3.30b were used to translate the positioning of the copper grid on the dentine sample. A 3.05 mm-diameter copper grid (G200PB, Durasin Inc, PA) with 85 µm inter-bar distance and 45 µm-bar width was halved and placed next to the investigated areas as chosen in the micro-CT x-axis plane to aid localization (Figure 3.30c). The 3.05 mm copper grid would standardize and make the dentine layers comparable to the line plot measured on the micro-CT x-axis plane. Adhesive tape was used to maintain the position of the copper grid over the caries surface (Figure 3.30c). Another adhesive tape was placed leaving 2mm distance across the outer edge of the cut copper grid; this defined the area of interest for the OCT scan.

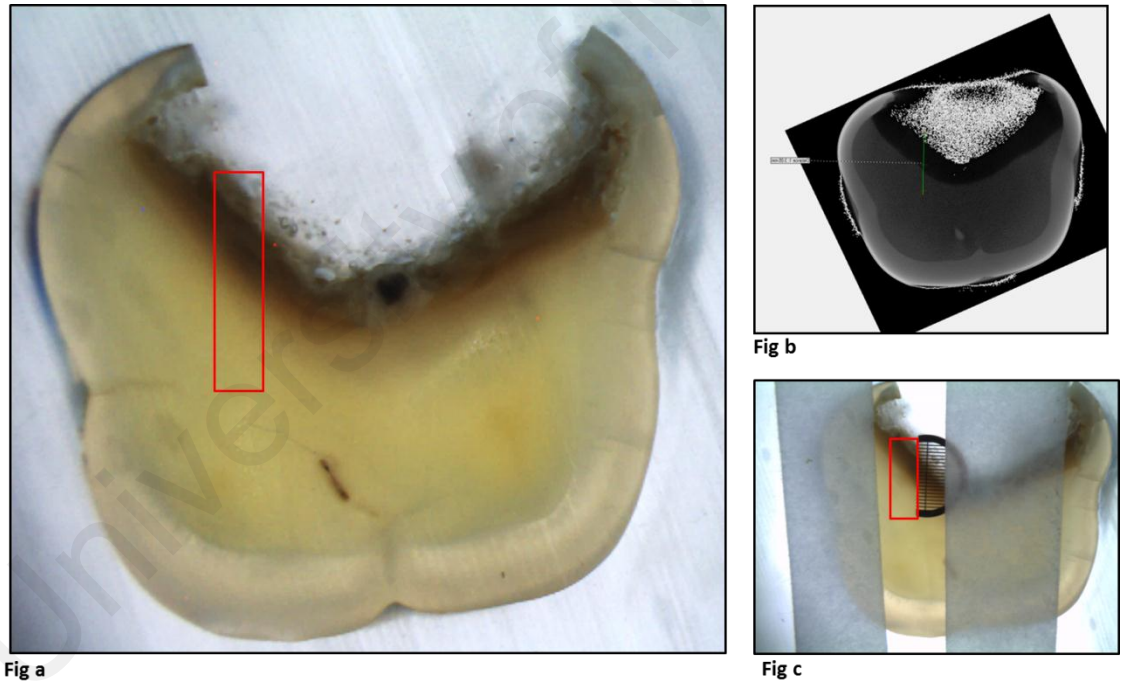

Figure 3.30 Matching the ROI between the line plot from the micro-CT slice using the copper grid for OCT scanning.

In Figure 3.30a the red highlighted box shows the entire ROI which will be OCT scanned, The green line in Figure 3.30b represents the line plot (3.05mm) extracted from the micro-CT slice which is positioned within the red box in Figure 3.30c,where t

the copper grid (3.05mm) with 85 µm inter-bar distance and 45 µm-bar width was halved and placed next to the identified investigation areas (red box), in order to divide the area into 20 quanta of 85 µm. These quanta were used to facilitate localisation of the layers of ID, AD and HD (as identified by micro-CT) in OCT scans.

3.4.9 OCT scanning and data processing

A Swept Source OCT imaging system (OCT 1300SS Thorlab Ltd., USA) with emission wavelength cantered at 1325 nm, lateral resolution of 11 µm and axial resolution of 9 µm in air was used in this study. Three-dimensional (3D) scans of 1024 x 1024 x 512 pixels in the x-y-z directions were obtained from each sample. This corresponded to a scanned surface of 3.0 mm X 3.5 mm (x-y) which fully encompassed the investigation area, and an optical depth of 3 mm in air or physical depth of 1.90 mm in the dentine when the refractive index of the dentine ($\eta = 1.54$) in the near-infrared spectrum was used (Meng et al., 2009). The dentine slabs were placed horizontal on a translation stage, perpendicular to the OCT laser probe. The translation stage was adjusted at the x – z axis between 10 - 20 degrees to reduce specular reflections. The distance of the sectioned surface to the top border of the displayed B-scan window on the Thorlab OCT software was set at 0.3 mm and the laser was positioned at the centre of the investigation area. Three hundred and one B-scans were generated with an approximately 3.41µm distance between each scan. The B-scans were captured in a logarithmic scale with a brightness and contrast configured to cover an intensity signal level range of -40 dB to -10 dB.

A bespoke Graphic unit interface (GUI) software version 2.0 was upgraded to version 3.0 in MATLAB (Mathworks, USA) for processing the OCT data. 3D OCT scans (.FRG) format were loaded in the GUI software. Surface determination settings were applied on the entire volume data (c-scan) which facilitated aligning the 3D scans and

generating enface OCT view of aligned surface with the option of depth resolution and selection of regions of interest within the investigated area (Figure 3.31a). The aligned surface view was used for drawing a line plot measuring 3.05 mm on the y-axis parallel to the copper grid across all three layers (Figure 3.31). The width of each line plot was an average of 20 pixel points along the x-axis. In addition, a cross-sectional view (B-scan) (Figure 3.31c) was used as an option to visualize the structural changes within a 100 pixel depth point Intensity gradient value in the logarithmic scale for up to 100 pixels or 351µm subsurface of the line plot drawn was selected from all samples and exported from the bespoke software to excel for further analysis.

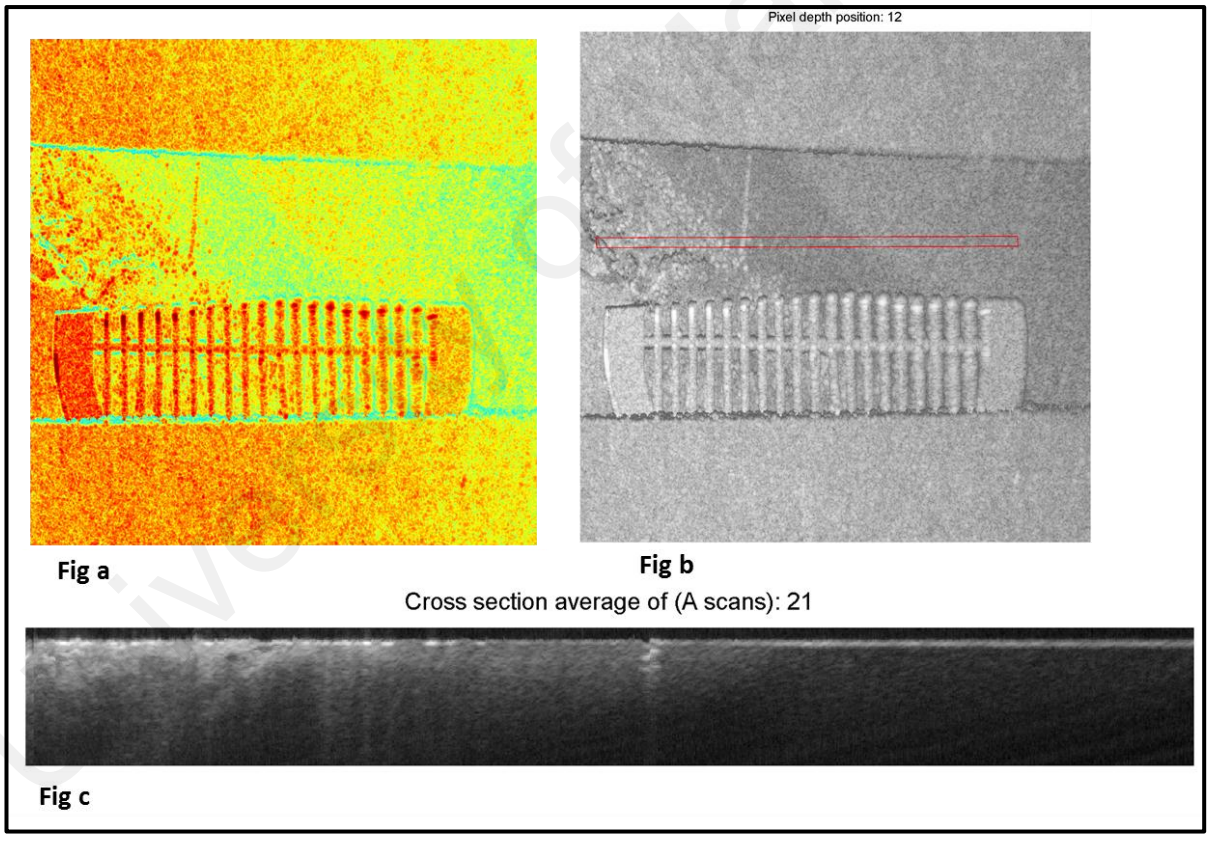

Figure 3.31 OCT aligned surface view, line plot and its B-scan

Figure 3.31 shows three images from the OCT bespoke software. Figure 3.31a shows a colour enhanced image of the same enface image showing the copper grid, adhesive tape and dentine layers. Figure 3.31b shows the grey value enface image of the scanned

dentine slab. The line plot measuring 3.05 mm is drawn on the enface image along the y-axis parallel to the copper grid across all three dentine layers. Figure 3.31c shows the cross-section (B-scan) to visualize the structural changes within the 100 pixel depth point below the tooth-air interface. A line plot was drawn at the 12^{th} pixel position below the tooth-air interface.

3.4.10 HA attenuation coefficient and its MD

Stacked DICOM images of hydroxyapatite (HA) tablets scanned with every batch of samples were uploaded in the imaging software ImageJ (Version 1.47d, National Institutes of Health (NIH), Bethesda, MD, USA). An area of a total of 2500 voxel measurements of the attenuation coefficient were extracted from each HA tablet and were averaged using the software ImageJ (Version 1.47d, National Institutes of Health (NIH), Bethesda, MD, USA). Scanning was performed using X-rays produced with a tube voltage of 90 kV and tube current of 90 µA To avoid possible beam hardening artifacts, the measurement of the attenuation coefficient was restricted to a middle area of 50×50 on the centre slice of each HA tablet (Figure 3.32). Therefore, the averaged attenuation coefficients were then plotted against the densities of the HA tablets using Microsoft Office Excel® 2010 to establish their relationship.

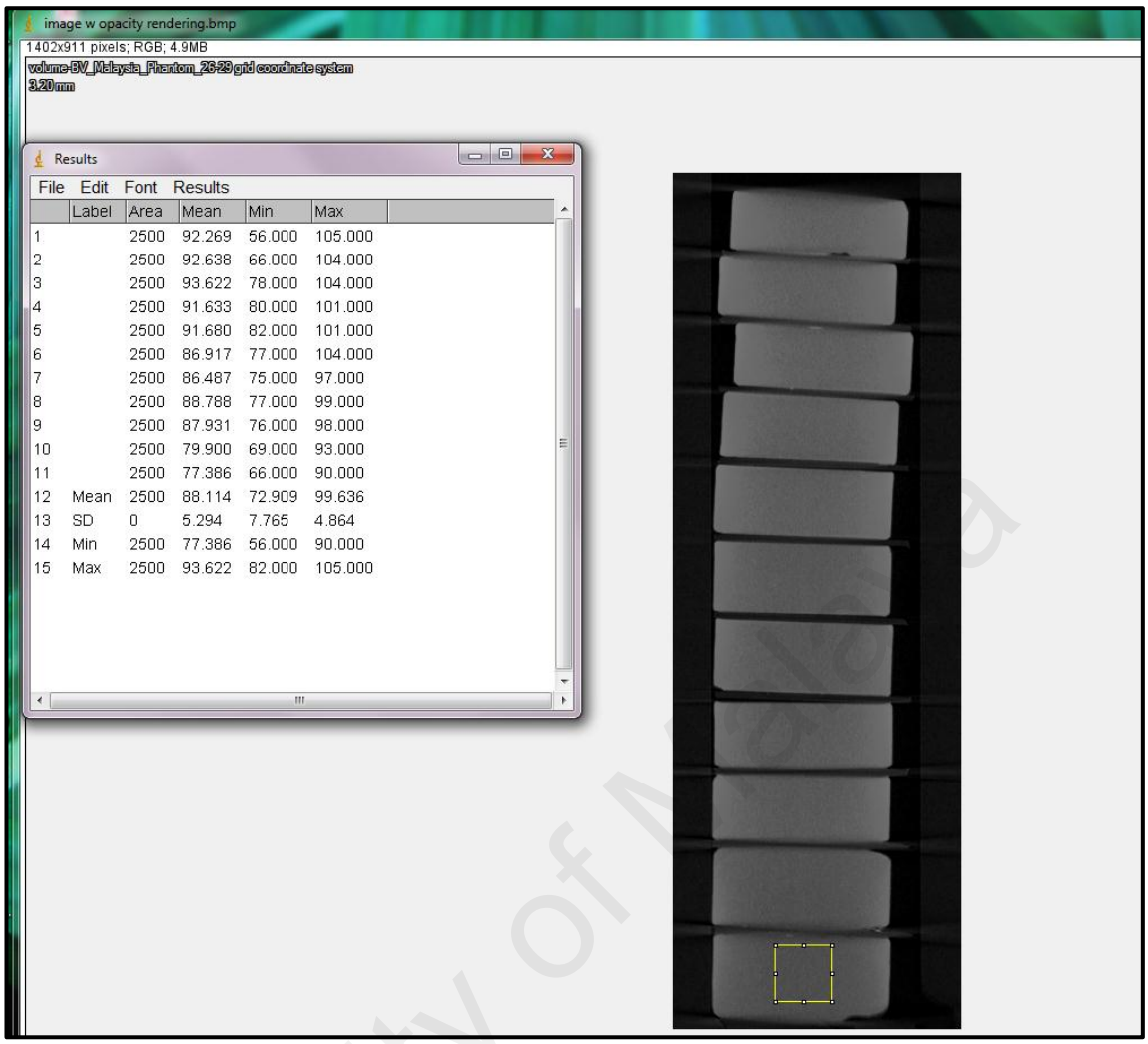

Figure 3.32 extracting attenuation coefficients from HD tablets

Figure 3.32 shows the stacked HD tablets, a ROI measuring 50×50 pixels on the middle area of the centre slice of each HA tablet was drawn to extract its attenuations. As shown in Table 3.1, the densities of the eleven intact HA tablets ranged from 0.99 to 1.48 g cm−3, and the corresponding attenuation coefficients ranged from 109.00 to 168.00 cm^{-1}. Within these ranges of attenuation coefficient values, the HA mineral density is linearly related at $R^2 = 0.99$, using the expression of following equation:

$$\mu = 116.08 \rho - 5.051$$

where μ is the linear attenuation coefficient (cm−1) and ρ is the density (g cm−3).

Table 3.3: Physical measurements of HA tablets used, along with its known mineral density and calculated attenuation coefficient values.

	Weight (mg)	Diameter (mm)	Thickness (mm)	Volume (mm3)	Density (g cm^{-3})	Attenuation coefficient *(cm^{-1})
1	25.0	4.01	2.01	25.372	0.985	109
2	26.2	4.03	1.95	24.861	1.054	119
3	25.4	4.00	1.84	23.110	1.099	122.00
4	25.3	4.01	1.51	19.061	1.327	145.00
5	25.3	4.02	1.50	19.029	1.33	149.00
6	26.4	4.03	1.67	21.291	1.24	140.00
7	25.7	4.03	1.61	20.526	1.252	141.00
8	25.7	4.03	1.57	20.016	1.384	155.00
9	26.5	4.02	1.48	18.775	1.411	156.00
10	25.6	4.02	1.39	17.633	1.452	167.00
11	27.0	4.02	1.44	18.268	1.478	168.00

*Scanning was performed using X-rays produced with a tube voltage of 90 kV and tube current of 90 μA.

3.4.11 Micro-CT and OCT data analysis

3.4.11.1 MD calculation using attenuation coefficient from ROI and line plots

The attenuation from the automated ROI was considered as the preliminary baseline value which was used to create cut off values for line plots. The mean, minimum and maximum attenuation values from automated ROI of ID, AD and HD were converted to MD using the equation derived from the known MD of HA phantoms equation stated in 3.4.10 The mean value of the maximum attenuation coefficients of ID (124.98) cm^{-1}

and AD (158.0) cm^{-1} layer was chosen as the cut-off value for between ID and AD, and AD and HD layers respectively. The converted MD values of the cut off values between ID and AD, and AD and HD was 1.10 g cm^{-3} and 1.38 g cm^{-3} respectively.

3.4.11.2 Matching line profiles of MD and OCT (*I*)

The measured distance of the respective ID, AD and HD layers were positioned against the MD and OCT intensity values. The pixel/distance ratio aspect for the OCT and the micro-CT were 3.41 µm and 2.43 µm respectively, due to the difference in the acquired resolution. The distance of the line plots between OCT and micro-CT was matched by truncating the micro-CT attenuation values. Since the micro-CT had higher resolutions compared to OCT, the attenuation values were reduced using the following equation:

Equation: *New truncated microCT value*= (**distance in pixel*distance in pixel of micro-CT line plots / distance in pixel of OCT line plots**) + **1**

The new truncated micro-CT line graphs were matched to the OCT line graphs (Figure 3.33c). The ID, AD and HD layers were segmented based on the selected cut-off values as stated in 3.4.11.1. These were applied on the line plot data to create a threshold and to distinguish each layer corresponding to the distance measured. The attenuation coefficients of the entire line plot were also converted to the corresponding MD using the equation stated in 3.4.10.

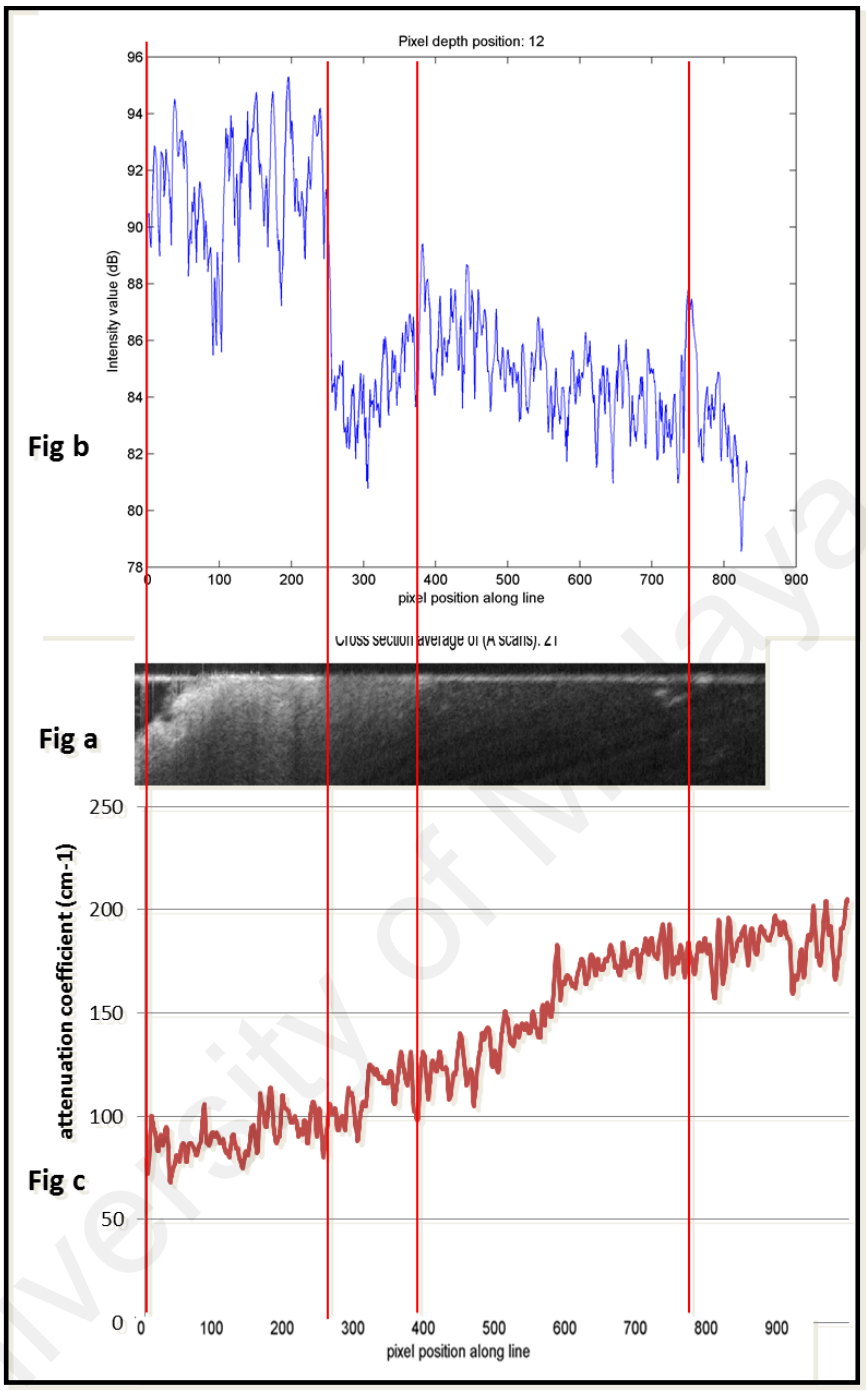

Figure 3.33 Matching line profile of attenuation coefficient *(*cm^{-1}*)* and OCT *I*

Figure 3.33 shows the truncated line plots of the micro-CT matched with the OCT line graphs of the same region. In Figure 3.33a the B-scans showing the depth profile of the three layer., The high intensity area represents the infected dentine between the first two red line, the region between the two middle red line is the region of moderate intensity, while the region between the last two red lines is with the lowest intensity representing

healthy dentine. In Figure 3.33b the OCT intensity line graph plotted over 800 pixel distance across three dentine layers, with the infected dentine region showing the highest backscattered intensity which slowly lowers when in the healthy region. Figure 3.33c shows the region with the infected dentine showing the lowest attenuation coefficient values (80-100 cm^{-1}), the affected region is between (100-125 cm^{-1}) and the healthy dentine showing higher attenuation coefficient values ranged between (140-170 cm^{-1}).The relationship of OCT *I* with attenuation coefficient (cm^{-1}) was studied using a scatter plot (Figure 3.34)

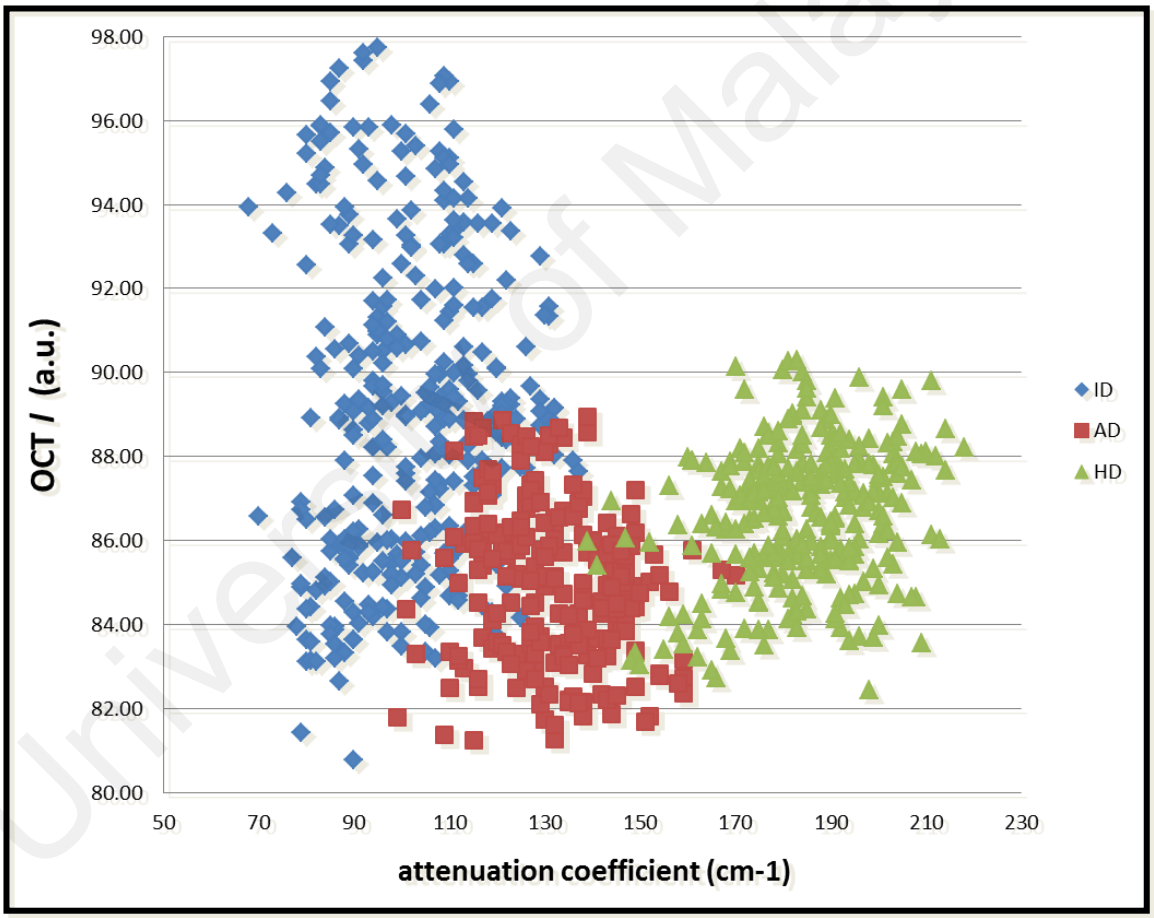

Figure 3.34 OCT *I* and attenuation coefficient (cm^{-1}) scatter plot

Observing the trends between OCT *I* and attenuation coefficient (cm^{-1}), a new OCT outcome measure was formed as represented by ΔI by calculating the difference

between the maximum and minimum OCT intensity for each layer (Figure 3.34). ΔI is represented by the function below:

$$\Delta I = \text{Max } I - \text{Min } I$$

Max I and Min I are the representative mean values of the maximum and minimum intensity. Calculations were made from the dentine layers of each sample (n=21), the overall mean value was calculated by average.

3.4.12 Statistical analysis

Statistical analysis were performed to detect the difference of MD within the three dentine layers. The data were analysed using the Shapiro-Wilk test to verify the assumption of normality. One-way ANOVA test was performed to assess the difference between mean MD of mean OCT I and ΔI. The Levens test as a test of homogeneity of variance suggested no significant difference between the groups and Tukeys HSD and Bonferroni as parametric test were used for further analyses. Significance and level of relationship between the MD and the OCT outcome measures were examined by the Pearson correlation test. The means and standard deviation were calculated for MD and OCT I, and MD and ΔI for each layer.

Receiver operating characteristic (ROC) curve analysis was performed to find the best cut-off point for the OCT outcome measure by determining the highest positive likelihood ratio (PLR) (sensitivity/[1_specificity]). The optimum cut off value was defined as the test result which is at the highest sensitivity and specificity indicating a perfect separation of the test value of the groups (Zweig & Campbell, 1993). The ROC graphic representation shows a line which is when closest to the left upper corner of the curve it is of value 1.0, while the theoretical area of 0.5 indicates no distributional difference between the ID and AD layers. These analyses were performed with a

statistical software (SPSS; Chicago, IL, USA) using nonparametric 95% confidence interval and compared to the area of 0.5 ($p < 0.05$) in establishing the diagnostic performance of OCT outcome measures in differentiating carious dentine layers.

CHAPTER 4: RESULTS

4.1 Dentine caries structure and OCT results

4.1.1 Comparison of OCT en-face scan (generated with Thorlabs OCT software) with stereomicroscope images.

Figure 4.1(b) shows the stereomicroscope image of a prepared dentine slab with the halved gilder grid placed adjacent to the chosen investigation site. Adhesive tape is seen to keep the gilder grid firmly in place and demarcate the boundary of investigation. The topmost border of the gilder grid is placed towards the outer border of the ID and resin. While its lowest most border is within the healthy dentine. Dentine tissues adjacent to line two to line five were irregular and rough and were identified as the ID layer. It was observed to be in a saucer shape with its lowest point adjacent to line 5 and it travels upwards below the grid and to the adjacent demarcating adhesive tape. Adjacent to lines 6 and 7 the tissues appear smooth and dark brown, demarcating it from the outer ID layer and inner HD layer. This layer could possibly be the AD layer but cannot be confirmed until validated histologically. From lines 11-20 white creamy blemish to light yellow colour is observed from the healthy dentine which appears smooth and flat.

Figure 4.1a shows the OCT en-face image of a prepared sample. The entire gilder grid and epoxy resin appears black due to lowest backscattered intensity. Whereas the remaining teeth tissues, including the adhesive tape showed a range of different colours suggesting these are high intensity backscattered areas. The Thorlabs OCT software produces a default grey scale en-face image to represent levels of intensity. However, the intermediate shades of grey levels are not distinguishable by the naked eye. In order to enhance the contrast of these intermediary grey scales, a colour scheme expressed in a range from -40 to 0 dB (Figure 4.1c) was chosen. The expressed colour range is dependent on the severity of backscattering from the sample tissues; the highest *I* appear

red (0 to -10), yellow to green (-10 to -20), blue (-20 to -35) and black (-35 to -40). Within the ID layer, red areas are clearly seen at the outermost boundary of ID with a few speckles adjacent to lines two and three. This suggests that the highest *I* is from the highly porous tissues of ID layer. Adjacent to lines two to five a moderate range of backscattering is seen showing shades of bright neon yellow and green codes as part of the ID layer. Adjacent to lines six to nine, the brightness and intensity of yellow and green appear to fade away with a hue of blue appearing in the background. The healthy tissues are within the range of -25 to -35 dB suggesting the lowest *I*.

The overall comparison of the enface images from two different methods showed that the difference in colour and texture from outer infected dentine to healthy dentine as seen in stereomicroscope images was comparable to the degree of backscattered intensity as expressed using the colour scheme. The outer irregular infected dentine from lines two to five shows greater signal intensity from 0 to -20 dB (notice red and bright yellow), suggesting that the ID layer is highly porous with more open space in the matrix, expressing the highest *I* out of all dentine layers (Figures 4.1a and b). The following layer, which is distinctly dark brown was difficult to identify on the OCT enface images, although it was observed that bright yellow (-10dB) was missing in this layer and light yellow and green (-20) with light blue (-10) started to appear in the background. The yellow healthy dentine appeared predominantly with dark blue background (-30) and light blue-green speckles on it.

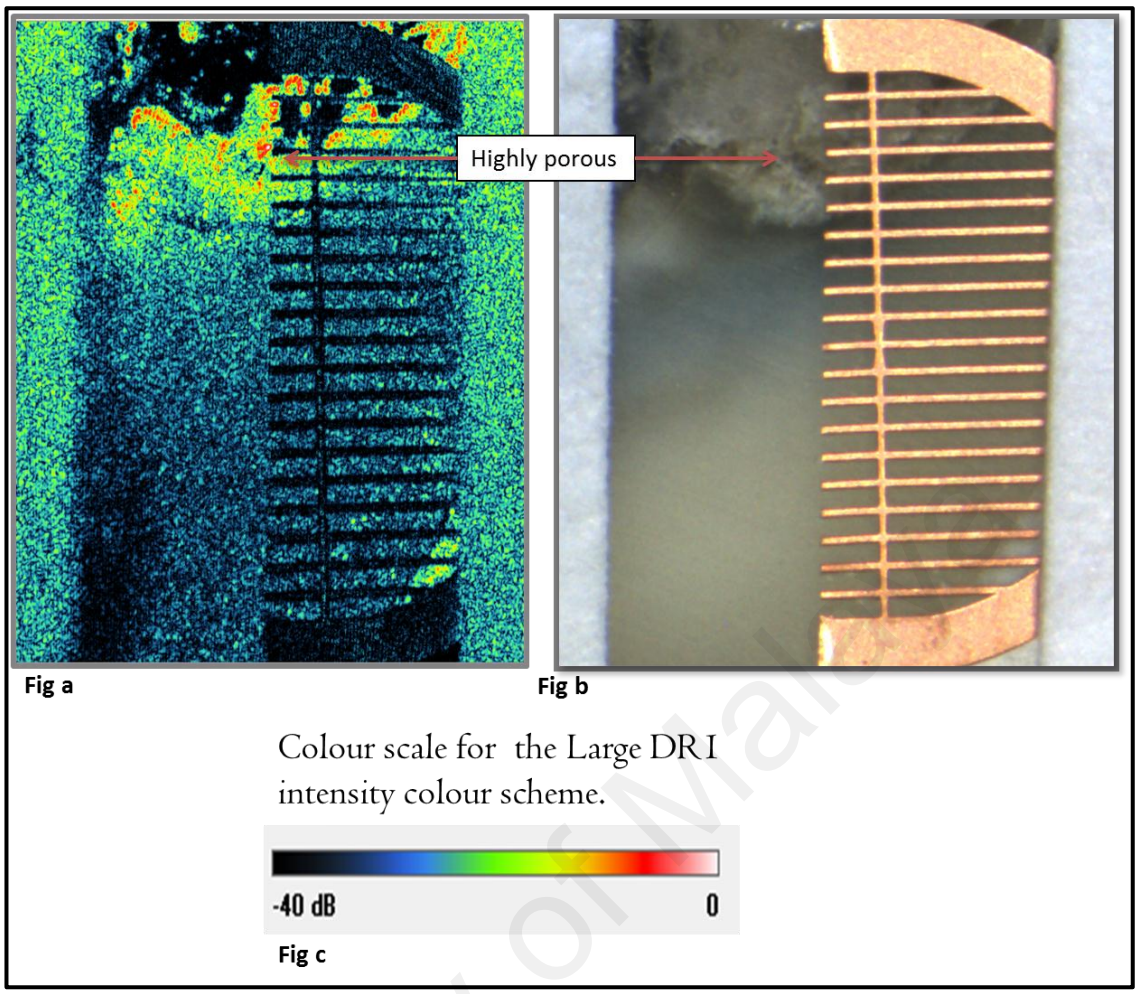

Figure 4.1 OCT enface and stereomicroscope image comparison

Figure 4.1a shows the OCT enface scans and Figure 4.1b shows the stereomicroscope images of carious and healthy dentine. Stereomicroscope images at 1.8 x magnification was captured to observe an overall appearance of dentine layers. Similarly, for the OCT enface images scan, an overall shape, intensity gradient and difference in colour schemes were taken into account to establish the difference between the layers.

4.1.2 SEM Scans

Figure 4.2(a) shows the long span surface view at 50x magnification, indicating continuous changes from the outer carious dentine through the inner affected dentine layers and to the healthy dentine. Although the dentine layers were continuous, it was challenging to identify the transition between the boundaries of the three dentine layers at this magnification.

The identification of the ID layer was rather uncomplicated as it is located at the outer most junction of the dentine sample, and there was complete absence of intertubular (ITD) and peritubular (PTD). It showed widespread denaturation and decomposed mass of dentine matrix and no apatite crystals were seen. There was also complete absence of intertubular and peritubular dentine structure (Figure4.2 b).

The junction between the inner most ID layer and the outer most AD layer, the usual structures of ITD and PTD as seen in HD dentine was not distinct. The ITD appeared uneven and not smooth, and the shape of the dentinal lumens was disorganized with complete absence of PTD (Figure 4.2 c). Identifying the start of the AD layer was a most challenging task due to the subtle structural changes occurring at the micrometre level. The AD layer was first established when the presence of intact and smooth ITD was seen. PTD dentine started appearing distinct and identifiable as the shape of it appeared undistorted yet the thickness of the PTD was not same as that of the healthy dentine, suggesting leaching out of minerals with intact dentine matrix. The PTD appeared in irregular patterns as the distribution of dentinal tubules in Figure 4.2d shows.

Healthy dentine showed a standard pattern of evenly distributed circular dentinal tubule lumen, between the periodic distributions of dentine tubules the ITD appeared as

smooth and flat. The PTD appeared thick and hypermineralised when compared to the ITD and evenly forms the wall of the dentinal tubule (Figure 4.2e). None of the images captured in this study were at ultra-high resolution to assess the changes at the crystal level and are therefore not used as descriptive features seen within these observations.

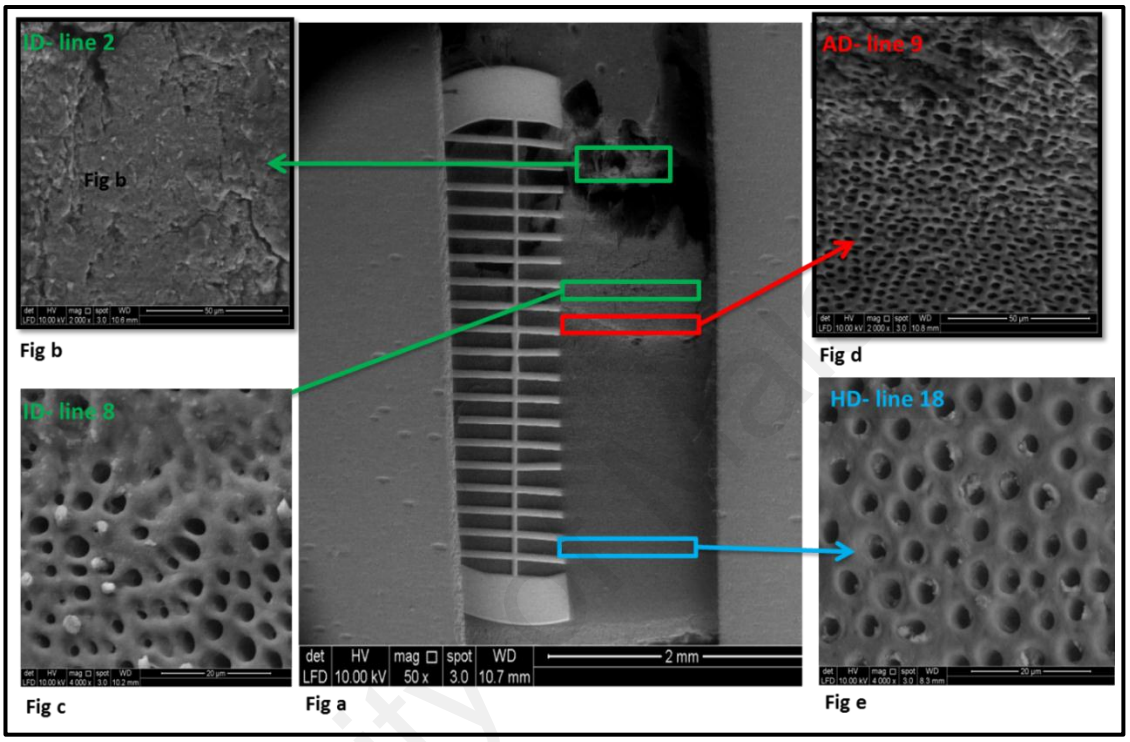

Figure 4.2: Identification of carious and healthy dentine using Pugach's classification

Figure 4.2a shows the SEM image at 50 x magnification with carious and healthy dentine layers, halved gilder grid and adhesive tape. Figure 4.2b shows the ID layer with denatured and decomposed mass of dentine matrix and complete absence of PTD. Figure 4.2c shows the ID layer just above the AD layer, showing distorted and non-elliptical PTD. Figure 4.2d shows that the PTD has gradually started to appear and is identifiable. The ITD and PTD both are distinguishable and the PTD is undistorted and is elliptical shape. HD in the lower right corner visibly shows tubule lumens lined by highly mineralized cuffs of PTD.

4.2 Comparison with OCT en-face scan with SEM scans

Figure 4.3 shows the microstructures observed under SEM was compared with OCT enface scans.

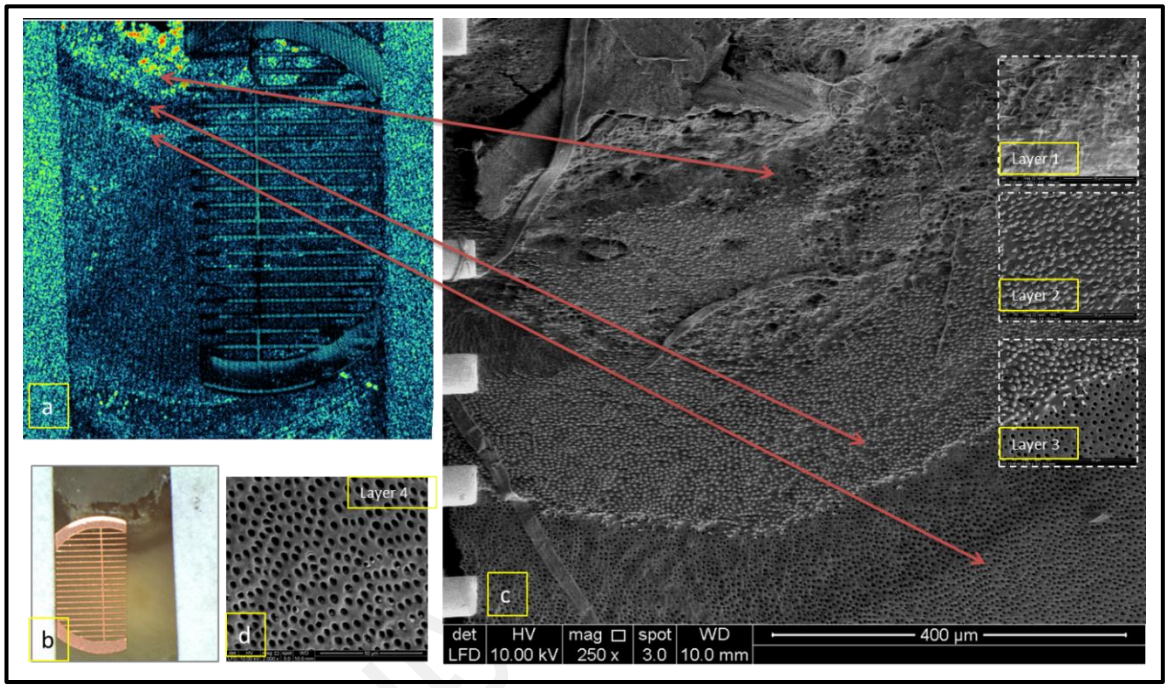

Figure 4.3: Comparison with OCT en-face scan with SEM scans

Figure 4.3a shows the OCT enface scans Figure 4.3b is the corresponding stereomicroscope image at 1.8x magnification and Figure 4.3c is a SEM image at 250 x magnification. In Figure 4.3c, layer 1, the ID layer is seen with a completely denatured and decomposed mass of dentine matrix and the absence of PTD. The corresponding OCT en-face scan shows the outer irregular infected dentine adjacent to lines 1 and 2 with a greater signal intensity (bright red and yellow, Figure 4.3a). In Figure 4.3c layer 2, it can be seen that the ITD and PTD both are visible but some intertubular deposition and occlusion are also seen. The corresponding structures of the OCT en-face scans show light yellow and green colour scheme with light blue in the background. The

healthy dentine visibly shows tubule lumens lined by highly mineralized cuffs of PTD (Figure d) with corresponding dark blue colour seen in OCT enface scans.

4.2.1 Attenuation characteristics of OCT backscattered intensity through ID, AD and HD

The preparation of samples, scanning process with OCT and processing of OCT data were described in Section 3.2.3, 3.2.4 and 3.2.8.1 respectively.

Figure 4.4 shows the MEAN depth-resolved intensity (*I*) profile (A-scan) of the first 100 μm of ID, AD and HD layers. At the beginning, the backscattered intensity, *I*, is observed to increase from the level of background noise until it reaches a maximum (I_{max}) and the distance of this occurrence is defined as the tooth-air interface. It is approximately 11.72 μm thick. The I_{max} for AD and HD were similar with the I_{max} of AD at 95.23 ± 2.37 a.u. (mean ± SD) and HD at 94.66 ± 2.90 a.u. while ID showed the lowest I_{max} at 91.28 ± 3.35 a.u.

Thereafter, *I* started to attenuate as it passes through the dentine. Two distinct rates of attenuation could be observed in all three ID, AD and HD. Initially, a fast exponential attenuation was observed, followed by a slower and more linear attenuation. The juncture between these two rates of attenuation were observed to be similar for all the three layers, which is approximately at 23.44 μm from the start of the tooth air interface. In phase I, HD exhibited the fastest rate of attenuation (- 0.56 a.u./μm), followed by AD (- 0.43 a.u./μm) and ID (- 0.38 a.u./μm). In Phase II, the rate of attenuation of HD and AD were very similar, - 0.06 and - 0.04 a.u./μm respectively, with AD maintaining a constant higher intensity than HD. Meanwhile, ID exhibited very little attenuation (- 0.01 a.u./μm) and appear to exhibit a third degree polynomial pattern where a second

peak approximately 54.3 µm below the tooth-air interface was observed. This characteristic was not observed in the AD and HD layers.

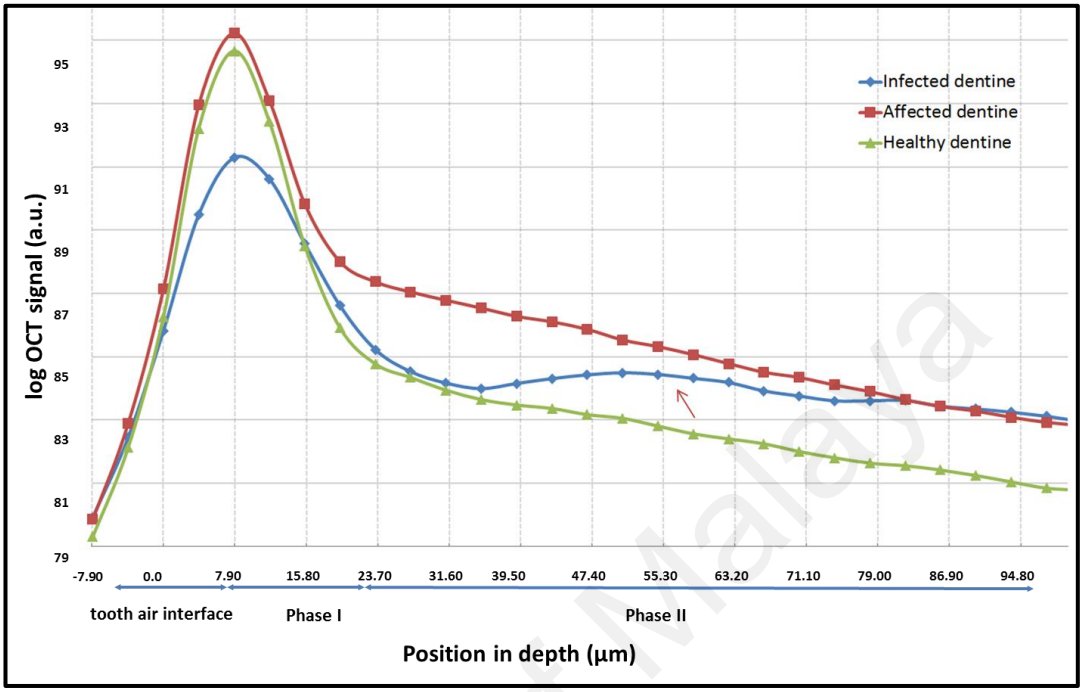

Figure 4.4: Mean depth-resolved intensity (*I*) profile (A-scan) of the first 100 µm of ID, AD and HD layers

Figure 4.4 shows the mean depth-resolved intensity profile (A-scans) of ID, AD and HD layers (n=25). The tooth-air interface starts from where the intensity increased from the level of background noise until it reaches a maximum, I_{max}. The faster Phase I attenuation and slower Phase II of attenuation is shown. Arrow shows the bimodal pattern of attenuation of ID.

4.2.2 Mathematical characterization of the attenuation of ID, AD and HD

The characteristics of the attenuation of the OCT intensity was further explored by determining the best line using exponential, polynomial and linear function. The best fitting of line within 101.56 µm depth of ID, AD and HD is seen in Figure 4.5. Shallower slope for the exponential fit was observed for ID in both the depths. The R^2

values of exponential curve were 0.582, 0.783, and 0.674 for ID, AD and HD layers respectively. The exponential curve equation showed better fitting for AD and HD compared to the R^2 value for ID. The R^2 value of the exponential curve for ID showed least reliability and needed further exploration. Best fit of equation for ID was polynomial fitting line, which yielded the R^2 value of 0.794. Linear fitting was explored for OCT intensity attenuation in Phase I, which confirmed the R^2 value of 0.977, 0.907 and 0.931 for ID, AD and HD (Figure 4.3). Similarly, linear fitting was explored in Phase II yielding best fit at 0.081, 0.998 and 0.994 for ID, AD and HD respectively (Figure 4.4). The comparison of R^2 value and best fit regression line for ID, AD and HD of total, phase I and II are tabulated in Table 4.1.

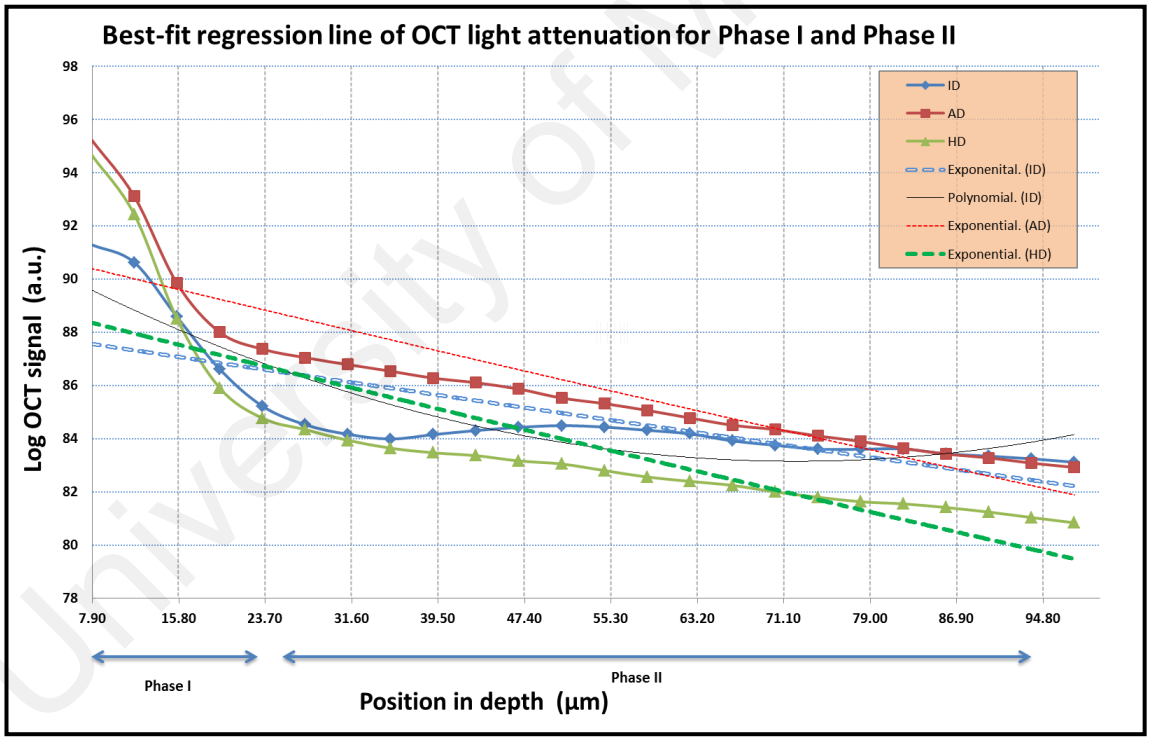

Figure 4.5: Best fit regression line of OCT light attenuation for Phase I and II

Figure 4.5 shows mean A scans of the ID, AD and HD from I_{max} onwards, showing Phase I and Phase II of OCT light attenuation. The best fitting of line within 100µm depth of ID, AD and HD is shown using exponential regression curve. The exponential

curve could be fit with an R^2 value of 0.58, 0.78 and 0.67 for ID, AD and HD respectively. The lower R^2 of ID using the exponential curve was replaced with a polygonal line fitting, showing increase in R^2 value upto 0.74.

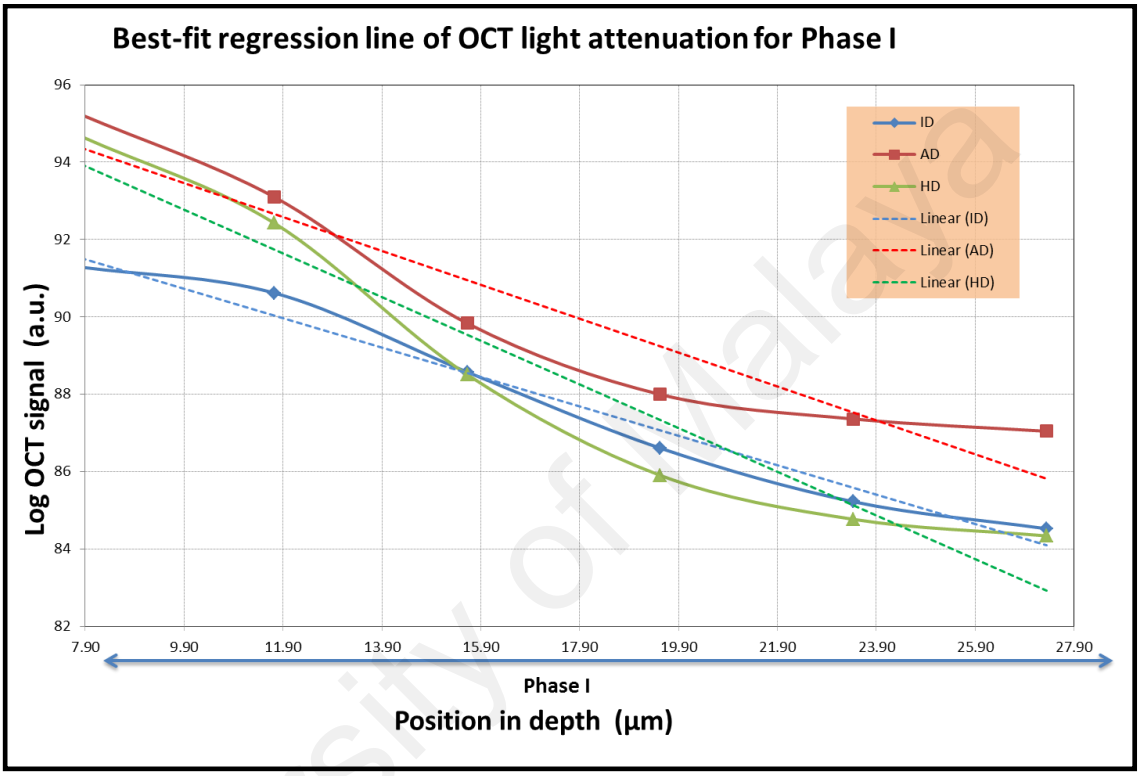

Figure 4.6: Best fit regression line of OCT light attenuation for Phase I

Figure 4.6 shows Phase I light attenuation. Linear function was used to assess trend line reliability for ID, AD and HD OCT light attenuation. The linear curve could be fit with an R^2 value of 0.97, 0.91 and 0.93 for ID, AD and HD respectively.

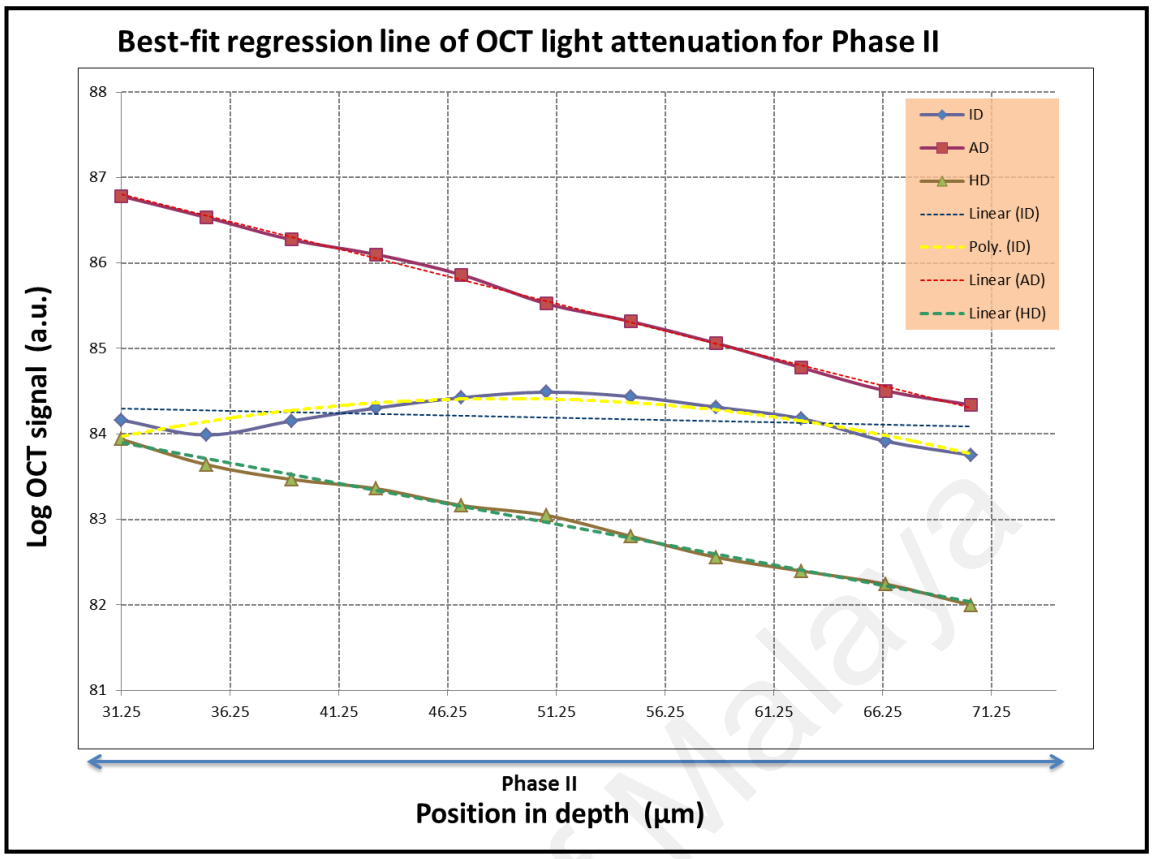

Figure 4.7: Best fit regression line of OCT light attenuation for Phase II

Figure 4.7 shows Phase II OCT light attenuation. Linear function was used to assess trend line reliability for ID, AD and HD OCT light attenuation. The linear curve could be fit with an R^2 value of 0.08, 0.99 and 0.99 for ID, AD and HD respectively. The lower R^2 of ID using the exponential curve was replaced with a polynomial line fitting, showing an increase in R^2 value up to 0.81.

Table 4.1: R^2 values of regression lines at total, phase I and II OCT light attenuations for ID, AD and HD layers

	Phase I	Phase II
ID	0.976 Linear reg	0.083 Linear reg
		0.819 Polynomial reg
AD	0.907 Linear reg	0.998 Linear reg
HD	0.931 Linear reg	0.994 Linear reg:

Table 4.1 shows R^2 values from different functions of fit line at total, phase I and II for ID, AD and HD layer. ID shows lower R^2 value in total and phase II when exponential and linear fitting was used, however the R^2 value increased when polynomial regression line was applied.

Mean and standard deviation for I_{max} and AUC combined and R in total, phase I and II is represented in Table 4.2 and Table 4.3 respectively.

4.2.3 Differentiation of ID, AD and HD with outcome measure derived from the depth-resolved intensity (I) profile (A-scan).

The outcome measures used were $I_{max,}$ R and AUC, as described in Section 3.2.8.2.

Due to the different attenuation rates and pattern observed during Phases I and II of attenuation, three phases of AUC were computed and they were:

i) AUC_T, i.e. Area under the curve from the start of the tooth-air interface up to 74.21 µm in depth

ii) AUC_I, i.e. Area under the curve from I_{max} up to the juncture between phase I and II which in this study is found to be at 23.44µm from the start of the tooth-air interface

iii) AUC_{II}, i.e. Area under the curve from the juncture between phase I and II up to 74.21 µm in depth.

Tables 4.2 shows the mean and standard deviation of I_{max} and AUC_T, AUC_I and AUC_{II} .

R was computed for each depth points after I_{max}.

Table 4.2: I_{max}, AUC_T, AUC_I, and AUC_{II} of ID, AD and HD.

	I_{max}	AUC_T	AUC_I	AUC_{II}
ID	91.29 (±3.35)	31510.94 (±741.17)	1714.58 (±51.21)	6549.35 (±274.67)
AD	95.23 (±2.36)	31506.71 (±523.61)	1755.60 (±41.32)	6613.46 (±135.81)
HD	94.66 (±2.89)	30949.18 (±442.04)	1723.09 (±44.36)	6427.38 (±126.88)

Tables 4.2 shows the mean and standard deviation of I_{max} and AUC_T, AUC_I and AUC_{II} .

The I_{max} intensity observed for ID was lowest and noticeably different than AD and HD.

Table 4.3: *R* for ID, AD and HD layers

R in Phase I				
ID	0.99 (±0.01)	0.97 (±0.02)	0.95 (±0.03)	0.93 (±0.04)
AD	0.98 (±0.01)	0.94 (±0.02)	0.92 (±0.03)	0.92 (±0.03)
HD	0.98 (±0.01)	0.94 (±0.02)	0.91 (±0.03)	0.90 (±0.03)

R in Phase II													
ID	0.93 (±0.05)	0.92 (±0.05)	0.92 (±0.05)	0.92 (±0.05)	0.92 (±0.05)	0.93 (±0.05)	0.93 (±0.05)	0.93 (±0.05)	0.92 (±0.05)	0.92 (±0.05)	0.92 (±0.05)	0.92 (±0.05)	0.92 (±0.05)
AD	0.19 (±0.03)	0.91 (±0.03)	0.91 (±0.03)	0.91 (±0.03)	0.90 (±0.03)	0.90 (±0.03)	0.90 (±0.03)	0.90 (±0.03)	0.89 (±0.03)	0.89 (±0.03)	0.89 (±0.03)	0.89 (±0.03)	0.88 (±0.03)
HD	0.89 (±0.03)	0.89 (±0.03)	0.88 (±0.03)	0.88 (±0.03)	0.88 (±0.03)	0.88 (±0.03)	0.88 (±0.03)	0.88 (±0.03)	0.87 (±0.03)	0.87 (±0.03)	0.87 (±0.03)	0.87 (±0.03)	0.86 (±0.03)

Tables 4.3 shows the mean and standard deviation of *R* of the three dentine layers at phase I and II. *R* for ID manifested larger standard deviation when compared to AD and HD.

4.2.3.1 Comparison of mean I_{max} between ID, AD and HD

The Shapiro-Wilk test was used to confirm the assumption of normality and it was found the data was normally distributed. Hence the One-way Analysis of Variance (ANOVA) test was performed to compare the mean value of I_{max} between ID, AD and HD

One-way ANOVA showed overall significant difference between three dentine layers ($p< 0.001$). Post hoc comparison using Tukey's HSD test showed that only I_{max} of AD and HD were not significantly different (Table 4.4).

Table 4.4: Results of post hoc test of mean I_{max} between ID, AD and HD

Comparison	P-value
ID vs AD	0.001
ID vs HD	0.001
AD vs HD	0.838 *

Table 4.4 shows the results of the post hoc Tukey's test, comparing I_{max} of ID, AD and HD. (*) highlights P value of more than 0.05.

4.2.3.2 Comparison of mean AUC_T, AUC_I, and AUC_{II} between ID, AD and HD.

To determine whether there was significant difference of mean values AUC_T, AUC_I, *and* AUC_{II} between ID, AD and HD, the two-way repeated measures ANOVA was used. Mauchly's Test was used to evaluate the sphericity assumption. The sphericity assumption is the assumption that the different values of paired repeated measures of outcome measures have equal variance. If sphericity was not met, the adjusted F-value of the Greenhouse-Geisser correction was considered. Results of Mauchly's Test showed that the sphericity assumption for the AUC mean was violated ($\chi 2$ =140.452 , $p<0.01$) therefore the adjusted F-value of the Greenhouse-Geisser correction was considered.

The results of repeated measure ANOVA on overall *AUC* showed that the interaction between dentine layers and three phases was statistically significant (F (7.880, 2.149) =1267130.8, $P<0.01$, $\eta_p^2=0.180$). Post hoc test (Bonferroni) was applied to compare the mean scores (Table 4.5).

Table 4.5 Two-way ANOVA for mean AUC and dentine layers

Source	SS	df	MS	F	P value	Partial Eta Squared
Mean AUC	37833053963	1.074	3521656436	219008.8	< 0.01	1.00
Dentine layer	2967956.60	2	1483978.30	7.216	< 0.01	0.167
Dentine layer* Mean AUC	2722550.16	2.149	1267130.8	7.880	< 0.01	0.180

Post hoc Bonferroni test was subsequently applied to compare the mean of AUC_T, AUC_I, and AUC_{II} between ID, AD and HD. The summary of the results is shown in Table 4.7.

4.2.3.3 Comparison of mean R between ID, AD and HD

Two way repeated measure ANOVA was used to compare *R* of different depth points between ID, AD and HD. Mauchly's Test was used to evaluate the sphericity assumption and the result showed that the sphericity assumption for mean *R* was violated ($\chi 2 = 2692.675$, $p<0.01$) and therefore the adjusted F-value of Greenhouse-Geisser correction was considered.

Results showed that the interaction between dentine layers and R at the various depth points was statistically significant ($P < 0.05$) (Table 4.6). Therefore to test the related hypothesis, post hoc test (Bonferroni) was applied to compare the mean scores,

Table 4.6: Two-way ANOVA mean R and dentine layers

Source	SS	df	MS	F	P value	Partial Eta Squared
Depth in *R*	0.680	2.127	0.319	255.156	< 0.01	0.780
Dentine layers	0.392	2	0.196	11.512	< 0.01	0.242
Dentine layer* depth in *R*	0.025	4.254	0.006	4.738	< 0.01	0.116

Post hoc Bonferroni test was subsequently applied to compare the mean of *R* at various depth points for ID, AD and HD. The result of Bonferroni test revealed that between ID and AD, *R* at 11 - 19 µm depth points (Phase I) and 50 - 74 µm depth points (Phase II) were statistically significant ($p < 0.05$). As for between AD and HD, *R* was only significantly different at one depth point, which is at 35 µm (Phase II). Between ID and HD, *R* was significantly different at depth points from 11µm - 74 µm ($p < 0.05$). The summary of significant differences in *R* for ID, AD and HD are presented in Table 4.7.

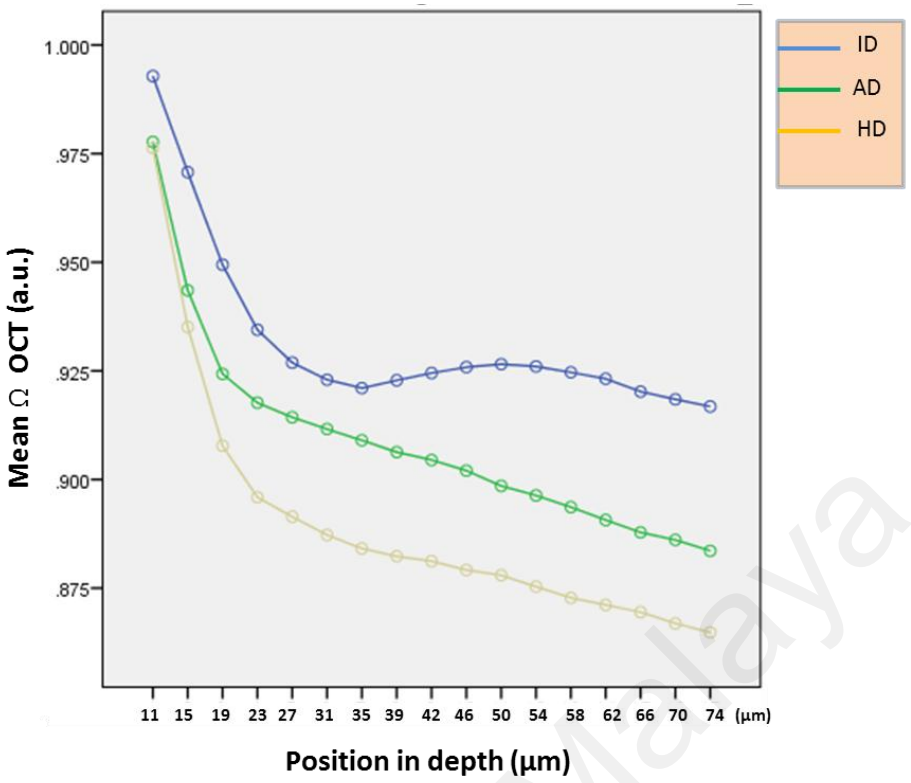

Figure 4.8: The mean plot of R at various depth points for ID, AD and HD

Table 4.7: Summary of outcome measures that are significantly different for ID, AD and HD

	I_{max}	AUC_T	AUC_I	AUC_{II}	R
ID vs AD	√		√		√ All depth points except between 20 – 49 µm
AD vs HD		√		√	√ Only at 35 µm depth point
ID vs HD	√	√			√ All depth points from 11 – 74 µm

Table 4.7 shows a summary of the outcome measures that are significantly different across the three layers with √ representing significant difference ($p > 0.05$).

4.2.4 Classification of dentine layers using Linear Discriminant Stepwise Regression Analysis (LDA) and Receiver Operating Characteristics (ROC)

A discriminant analysis was performed to develop a classification function (linear discriminant function—LDF) designed to identify the outcome measures which can classify ID, AD and HD layers with maximum accuracy. Stepwise LDA regression was used since multiple outcome variables were used as predictors in analysing the discrimination abilities for ID, AD and HD layers. Out of all significant outcome measures the standardized canonical discriminant coefficients were used to rank the importance of each outcome measure. LDF was used with two different combinations of data. First, all dentine layers were grouped together to identify the significant outcome measure with the highest discrimination abilities at the three phases. While in the second method, the data was split into three groups: Group 1= ID vs AD, Group 2= AD vs HD and Group 3= ID vs HD. LDF was performed to compare two dentine layers at a time to identify the significant outcome measure with the highest discrimination abilities at the three phases.

Discriminant analysis assumes covariance matrices are equivalent and this assumption was considered during the analysis to achieve the normality in data. The natural log of the determinants of each group's covariance matrix and the pooled within-group covariance were checked if they were almost equal to one another for the assumption of equality of covariance matrices. Stepwise regression included each outcome measure at a time, the parameter with the highest F statistics shows the contribution which minimizes the overall Wilks' Lambda value. If the Wilks' Lambda p-value was less than 0.05, it was concluded that the corresponding function explains the group membership well. The standardized canonical discriminant coefficients were used to

rank the importance of each OCT outcome measure. A high standardized discriminant function coefficient means that the groups significantly differ the most on that variable. The Classification for test Data was used to assess the accuracy of classification. Original accuracy and cross-validation accuracy were both reported. The cross-validation used in LDF was to assess the accuracy by treating each training data as the test data, while excluding it from the training data to judge which group it should be classified to, and then verifying whether the classification is correct or not.

The predicted group classification was generated in the data sheet. New dummy variables were prepared for the ID, AD and HD groups and was run against the original grouping of dentine layers to establish the sensitivity and accuracy of OCT outcome measure by using ROC curve analysis.

4.2.4.1 LDA and ROC with dentine layers grouped together

4.2.4.2 *R as a discriminant*

R was generated from multiple depth points within the depth of the tissue and was analysed separately for I_{max} and *AUC*. Multiple depth points of *R* was explored in relation to total, Fazes I and II included all dentine layers. *R* contributed significantly in discriminant function ($p < 0.001$), at total, Phases I and II. For total, 65.4%, 23.5% and 42.8% of the ID, AD and HD groups were correctly classified, with an overall cross-validated accuracy of 52.2%. For Phase I, 66.0%, 20.0% and 42.0% of the ID, AD and HD groups were correctly classified, with an overall cross-validated accuracy of 49.3%. For Phase II, 71.1%, 32.9% and 35.4% of the ID, AD and HD groups were correctly classified, with an overall cross-validated accuracy of 56.1% (Table 4.8). The ROC areas, optimal sensitivities and specificities levels from the new predicted group membership against original dentine layer groups are shown in Tables 4.9.

Table 4.8: R as a discriminant measure between three different phases when all dentine layers were grouped together

Phase	Sig	Original Accuracy	Cross-validated Accuracy
Total	.001	52.2%	52.2%
Phase I	.001	49.3%	49.3%
Phase II	.001	56.1%	56.1%

Table 4.8 shows *R* significantly contributed to discriminant function in all phases. However, in Phase II *R* shows higher cross-validation accuracy when compared with total and Phase I. The overall accuracy of *R* was considered low when the dentine layers were grouped together.

Table 4.9: ROC, sensitivity, and specificity of R for each dentine layers at total, phase I and II when dentine layers are grouped together

Phase	Dentine layer	Sn	SP	AUC on ROC
Total	ID	55.4%	81.0%	0.682
	AD	43.9%	69.0%	0.564
	HD	52.8%	81.2%	0.670
Phase I	ID	48.5%	79.3%	0.639
	AD	47.6%	69.0%	0.583
	HD	50.8%	78.7%	0.647
Phase II	ID	61.6%	84.3%	0.730
	AD	50.0%	71.4%	0.607
	HD	54.1%	80.3%	0.672

Table 4.9 shows overall Phase II with higher ROC values for ID, AD and HD dentine layers when compared with total and Phase I.

4.2.4.3 I_{max} and *AUC as a discriminant*

Stepwise LDA regression showed I_{max}, AUC_T and AUC_{II} contributed significantly in discriminant function (p> 0.001). 72.0%, 60.0% and 72.0% of the ID, AD and HD groups were correctly classified, with an overall accuracy of 70.7% (Table 4.10). Amongst all the significantly contributing outcome measures in discriminant function (p> 0.001), AUC_T mean was ranked the most significant contributing outcome measure showing the highest standardized discriminant function coefficient. The ROC areas, optimal sensitivities and specificities levels from the new predicted group membership against original dentine layer groups are shown in Tables 4.11.

Table 4.10: I_{max}, AUC_T, AUC_I and AUC_{II} as a discriminant measure when dentine layers are grouped together

Layers	Outcome measure	Sig	Std. Discriminant Function Coefficient	Original Accuracy	Cross-validated Accuracy
All layers	I_{max}	.001	1.034	70.7%	68.0%
	AUC_T	.001	-1.598		
	AUC_{II}	.001	1.109		

Table 4.10 shows I_{max} AUC total and Phase II significantly contributed to discriminant function. However, AUC mean total contributed highest at reaching the 70.7% original accuracy. The overall accuracy was considered good considering all the dentine layers were grouped together.

Table 4.11: ROC sensitivity, and specificity of I_{max} and AUC for each dentine layers at total, phase I and II when dentine layers are grouped together

Outcome measure	Dentine layer	Sn	SP	AUC on ROC
AUC_T	ID	70.4%	87.5%	0.789
	AD	68.2%	81.1%	0.747
	HD	73.1%	87.8%	0.804

Table 4.11 shows that the AUC_T mean measure has the highest AUC value for all dentine layers. The overall ROC value of outcome measure was considered high considering the dentine layers were grouped together.

4.2.4.4 LDA and ROC with dentine layers grouped separately

4.2.4.5 *R as a discriminant*

The data was grouped with two dentine layers at a time; 1= ID vs AD, Group 2= AD vs HD and Group 3= ID vs HD. First, LDA was performed to compare ID vs AD with *R*, which contributed significantly in discriminant function ($p > 0.001$) for total, Phases I and II. For total, 65.4% and 66.4% of the ID and AD groups were correctly classified, with an overall cross-validated accuracy of 65.9%. For Phase I, 66.0% and 62.0% of the ID and AD groups were correctly classified, with an overall cross-validated accuracy of 64.0%. And for Phase II, 71.0% and 68.3% of the ID and AD groups were correctly classified, with an overall cross-validated accuracy of 69.7%.

Next, LDF was performed comparing AD vs HD with *R*, which contributed significantly in discriminant function ($p > 0.001$) for total, Phases I and II. For total, 57.2% and 67.8% of the AD and HD groups were correctly classified, with an overall cross-validated accuracy of 62.5%. For Phase I, 58.0% and 62.0% of the ID and AD groups were correctly classified, with an overall cross-validated accuracy of 60.0%. And for Phase II, 64.6% and 64.3% of the ID and AD groups were correctly classified, with an overall cross-validated accuracy of 64.5%.

When comparing ID vs HD with *R*, which contributed significantly in discriminant function ($p < 0.001$) for total, Phases I and II. For total, 75.8% and 24.4% of the ID and HD groups were correctly classified, with an overall cross-validated accuracy of 75.4%. For Phase I, 70.0% and 66.0% of the ID and HD groups were correctly classified, with an overall cross-validated accuracy of 68.0%. And for Phase II, 78.8% and 80.9% of the ID and HD groups were correctly classified, with an overall cross-validated accuracy of 79.8% (Table 4.12). The ROC areas, optimal sensitivities and specificities levels from the new predicted group membership against original dentine layer groups are shown in Tables 4.13.

Table 4.12: R as a discriminant measure between two dentine layers at a time at Total, Phase I and II

Phase	Layers	Sig	Original Accuracy	Cross-validated Accuracy
ID vs AD	Total	.001	65.9%	65.9%
	Phase I	.001	64.0%	64.0%
	Phase II	.001	69.7%	69.7%
AD vs HD	Total	.001	62.5%	62.5%
	Phase I	.001	60.0%	60.0%
	Phase II	.001	64.5%	64.5%
ID vs HD	Total	.001	75.4%	75.4%
	Phase I	.001	68.0%	68.0%
	Phase II	.001	79.8%	79.8%

Table 4.12 shows ***R*** as a classifier to discriminate between two dentine layers at a time. Overall Phase II shows higher accuracy when discriminating any two layers at a time compared to total and Phase I.

Table 4.13: ROC sensitivity, and specificity of R between two dentine layers at a time

Group	Depth Phase	Dentine layer	Sn	SP	AUC on ROC
ID vs AD	Total	ID	66.0%	65.6%	0.659
		AD	65.7%	66.0%	
	Phase I	ID	63.5%	64.4%	0.640
		AD	64.6%	63.5%	
	Phase II	ID	69.2%	73.3%	0.697
		AD	73.3%	69.2%	
AD vs HD	Total	AD	63.9%	61.3%	0.626
		HD	61.3%	63.9%	
	Phase I	AD	60.4%	59.6%	0.600
		HD	59.6%	60.4%	
	Phase II	AD	64.4%	64.5%	0.645
		HD	64.5%	64.4%	
ID vs HD	Total	ID	75.2%	75.6%	0.754
		HD	75.6%	72.5%	
	Phase I	ID	67.3%	68.7%	0.680
		HD	68.7%	67.3%	
	Phase II	ID	80.5%	79.2%	0.799
		HD	79.2%	80.5%	

Table 4.12 shows ***R*** in Phase II obtained higher ROC values for the ID, AD and HD dentine layers when compared to total and Phase I.

4.2.4.6 I_{max} and *AUC as a discriminant*

LDF was performed comparing ID vs AD with I_{max}, $AUC_{T,}$ AUC_I and AUC_{II}. Only I_{max} contributed significantly in discriminant function ($p< 0.001$). Of the ID and AD groups, 64.0% and 80.0% were correctly classified, with an overall cross-validated accuracy of 72.0%.

Between AD vs HD the outcome measures used were I_{max} and $AUC_{T,}$ AUC_I and AUC_{II}. Only AUC_{II}. contributed significantly in discriminant function ($p< 0.001$). Of the ID and AD groups,80.0% and 84.0% were correctly classified, with an overall cross-validated accuracy of 82.0%.

Between ID vs HD the outcome measures used were I_{max} and $AUC_{T,}$ AUC_I and AUC_{II}. $I_{max,}$ $AUC_{T,}$ and AUC_{II} contributed significantly in discriminant function ($p< 0.001$). AUC_T ranked the most significant contributing outcome measure showing the highest standardized discriminant function coefficient. Of the ID and AD groups, 76.0% and 88.0% were correctly classified, with an overall cross-validated accuracy of 82.0%.

Overall, the best outcome measure to discriminate when dentine layers were grouped and separated is presented in Table 4.16.

Table 4.14: Mean I_{max} and mean AUC as a discriminant measure between dentine layers at a time at three different phases

Dentine layers	Phase	Outcome measures	Sig	Std. Canonical Dis Func Coef	Original Accuracy	Cross-validated Accuracy
ID vs AD	Total Phase I Phase II	I_{max}	.001	1.00	72.0%	72.0%
AD vs HD	Total Phase I Phase II	AUC_{II}	.001	1.00	82.0%	82.0%
ID vs HD	Total Phase I Phase II	AUC_{T*}	.001	-1.680	84.0%	82.0%

Table 4.14 shows I_{max} and mean $AUC_{T,}$ AUC_I and AUC_{II} contributed significantly in discriminant function. However, I_{max} contributed significantly at discriminating between ID and AD and ID and HD. While AUC_{II} contributed significantly at discriminating between AD and AD. ID can be discriminated against AD, while AD can be discriminated against HD with an overall accuracy of above 80% when using I_{max} and mean AUC for total, Phase I and Phase II.* the most significant contributing outcome measure.

Table 4.15: ROC, sensitivity, and specificity of I_{max} and AUC measures between two dentine layers at one time

Group	Depth Phase	Outcome measures	AUC on ROC	Dentine layer	Sn	SP
ID vs AD	Total Phase I Phase II	I_{max}	0.726	ID	76.2%	69.0%
				AD	69.0%	67.2%
AD vs HD	Total Phase I Phase II	AUC_{II}	0.821	AD	83.3%	80.8%
				HD	80.8%	83.3%
ID vs HD	Total Phase I Phase II	I_{max} ,$AUC_{T,}$ AUC_{II}	0.842	ID	87.0%	81.5%
				HD	81.5%	87.0%

Table 4.15 shows ROC values when discriminating any two dentine layers using I_{max} and mean $AUC_{T,}$ AUC_{I} and AUC_{II}. I_{max} and AUC showed high ROC values when discriminating between AD and HD and ID and HD.

Table 4.16: Overall best outcome measure to discriminate dentine layers using LDA accuracy, ROC values, sensitivity, and specificity

Group	Outcome measures &Phase	Accuracy	Cross-validated	ROC Value	Sn	SP
Dentine layers grouped together						
All dentine layers	$I_{max,}$ AUC_T *and* AUC_{II}	70.7%	68.0%	ID 0.789	70.4%	87.5%
				AD 0.747	68.2%	81.1%
				HD 0.804	73.1%	87.8%
Between two dentine layers						
ID vs AD	*R* Phase II	79.8%	79.8%	0.799	80.5%	79.2%
					79.2%	80.5%
AD vs HD	AUC_{II}	82.0%	82.0%	0.821	83.3%	80.8%
					80.8%	83.3%
ID vs HD	I_{max} $AUC_{T,}$ and AUC_{II}	84.0%	82.0%	0.842	87.0%	81.5%
					81.5%	87.0%

Table 4.16 shows ***R*** as the best overall outcome measure to discriminate when the dentine layers were grouped and separated.

4.2.5 Classification of dentine layers using Artificial Neural Network (ANN) and Receiver operating characteristics (ROC)

Similar to LDF, ANN was designed to identify and combine the best OCT outcome measures to differentiate the ID, AD and HD layers. ANN was used with two different combinations of data. First, all the dentine layers were grouped together to test the

significant and most effective OCT outcome measure between 3 different depth phases. While in the second method, the data was split into three separate groups: Group 1= ID vs AD, Group 2= AD vs HD and Group 3= ID vs HD. ANN was performed to compare two dentine layers at a time using its respective OCT outcome measure at three different depth phases. In ANN confusion matrix graphs, ID, AD and HD is represented as Class I, II and III. The cell in the lower right blue colour represents over all accuracy, true classified cases in green and misclassified cases in red.

4.2.5.1 ANN and ROC analysis with three dentine layers grouped together

R, AUC_T, AUC_I and AUC_{II} and I_{max} with dentine layers grouped together

ANN was run separately from R, while I_{max} and AUC_T, AUC_I and AUC_{II} were explored together for all dentine layers. All confusion matrixes for R at the various depth points within total, Phases I and II reported 55.2%, 53.7% and 60.1% as the overall accuracy of classification respectively. Similarly, for I_{max} and AUC_T, AUC_I and AUC_{II} combined, it was reported 80.0%, as overall accuracy of classification. The best outcome measure for group classification of the ID, AD and HD layers was I_{max} and AUC_T, AUC_I and AUC_{II} combined providing accuracy of 80.0% (Figure 4.7) and its related ROC curve (Figure 4.8).

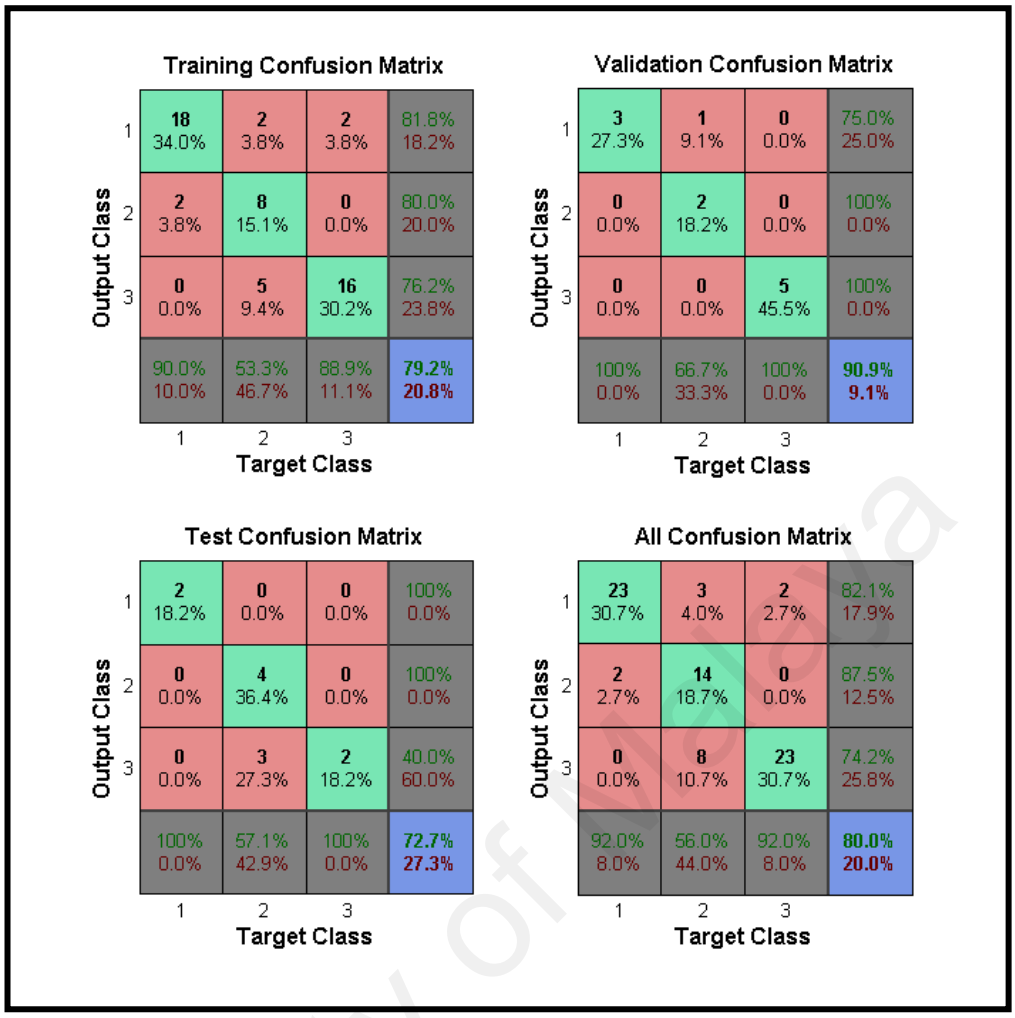

Figure 4.9: Confusion matrixes of I_{max} and *AUCT, AUCI and AUCII* combined for all phases and dentine layers

Figure 4.9 shows prediction of dentine layers at each stage of ANN method. All confusion matrix shows out of 25 representatives of each layers for ID and HD, 2 cases were diagnosed as false positives as AD layers and as ID layers respectively. However, for AD layers out 25 samples, 14 were diagnosed as true positives, while 3 and 8 cases were diagnosed as false positive as ID and HD layers. ID, AD and HD is represented as Class I, II and III.

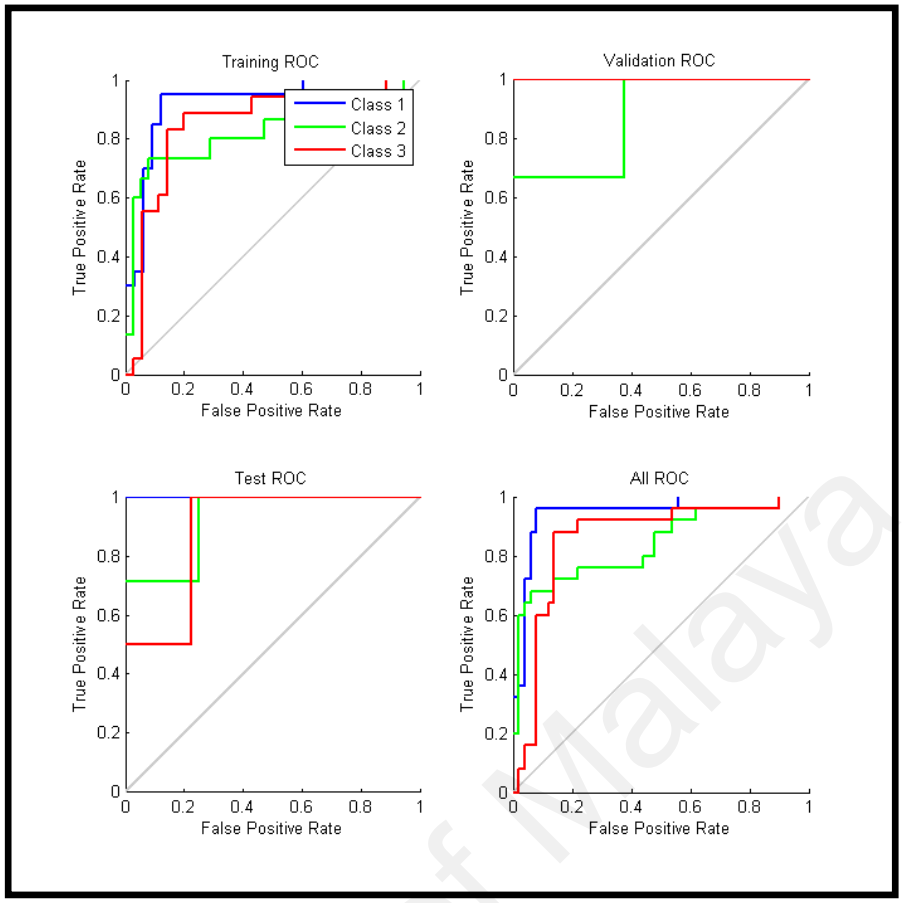

Figure 4.10: ROC curve of combined I_{max}, AUC_T, AUC_I and AUC_{II} and dentine layers

4.2.5.2 ANN and ROC analysis with dentine layers analysed separately

***R*, *AUC* and I_{max} for all phases between ID and AD**

ANN was run separately from *R*, while I_{max} and AUC_T, AUC_I and AUC_{II} were explored together between ID and AD. All confusion matrixes for *R* at total, Phases I and II reported 70.4%, 68.0% and 75.4% as the overall accuracy of classification respectively. Similarly, for I_{max} and AUC_T, AUC_I and AUC_{II}, 84.0%, was reported as overall accuracy of classification. The best outcome measure for group classification between the ID and AD layers was a combination of I_{max} and AUC_T, AUC_I and AUC_{II} providing an accuracy of 84.0% (Figure 4.9) with its related ROC curve (Figure 4.10).

Figure 4.11: Confusion matrixes of combined I_{max} AUC_T, AUC_I and AUC_{II} between ID and AD

Figure 4.9 shows the prediction of dentine layers at each stage of the ANN method. All confusion matrix shows that out of 25 representatives of each layer for ID and AD, 3 and 5 cases were diagnosed false positives as ID layers and AD layers respectively. The overall prediction accuracy was 84.0%.

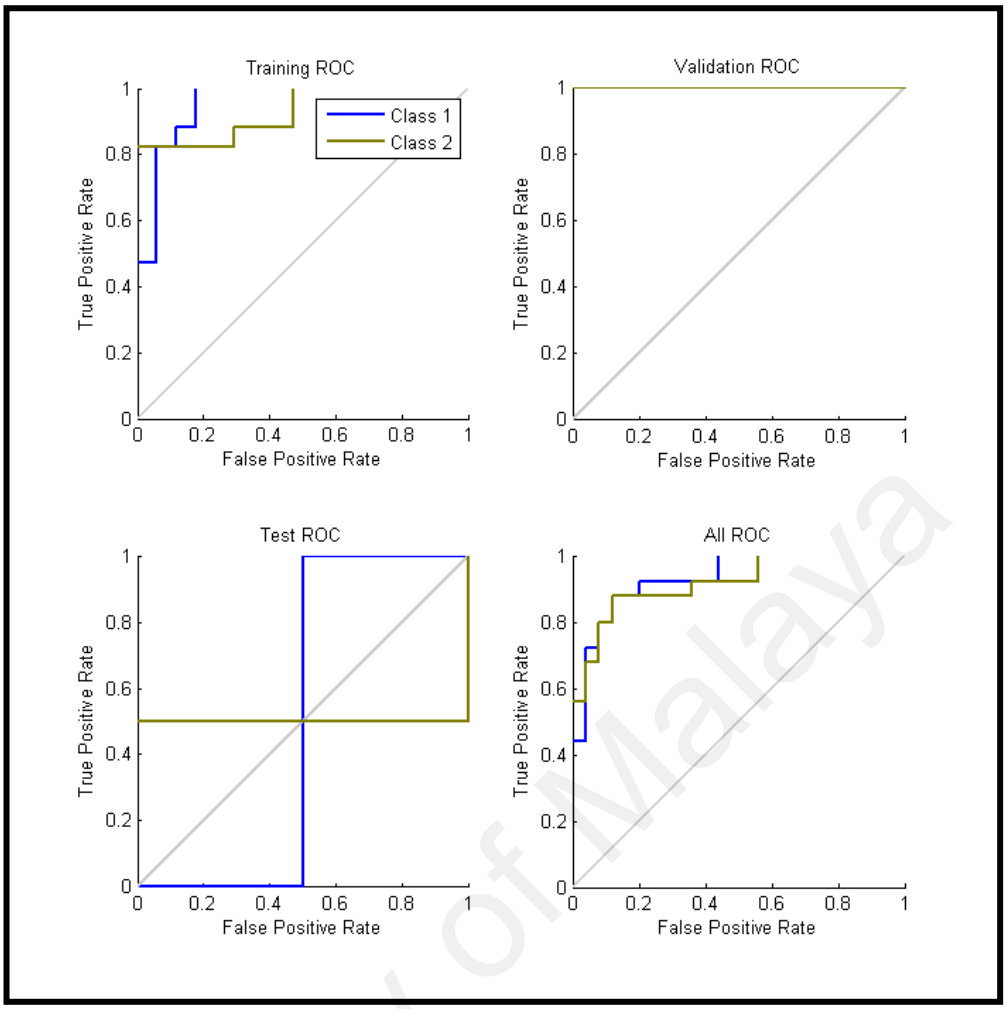

Figure 4.12: ROC curve of combined I_{max} AUC_T, AUC_I and AUC_{II} between ID and AD

R, AUC and I_{max} at total, phase I and II between AD and HD

ANN was run separately from *R*, while I_{max}, AUC_T, AUC_I and AUC_{II} were explored together between AD and HD. All confusion matrixes reported for *R* at various depth points within total, Phases I and II reported 65.4%, 65.0% and 68.0% as the overall accuracy of classification respectively. Similarly, for combined I_{max}, AUC_T, AUC_I and AUC_{II} 88.0% was reported as the overall accuracy of classification. The best outcome measure for group classification between AD and HD layer was I_{max} AUC_T, AUC_I and AUC_{II} with an accuracy of 88.0% (Figure 4.11) and its related ROC curve (Figure 4.12).

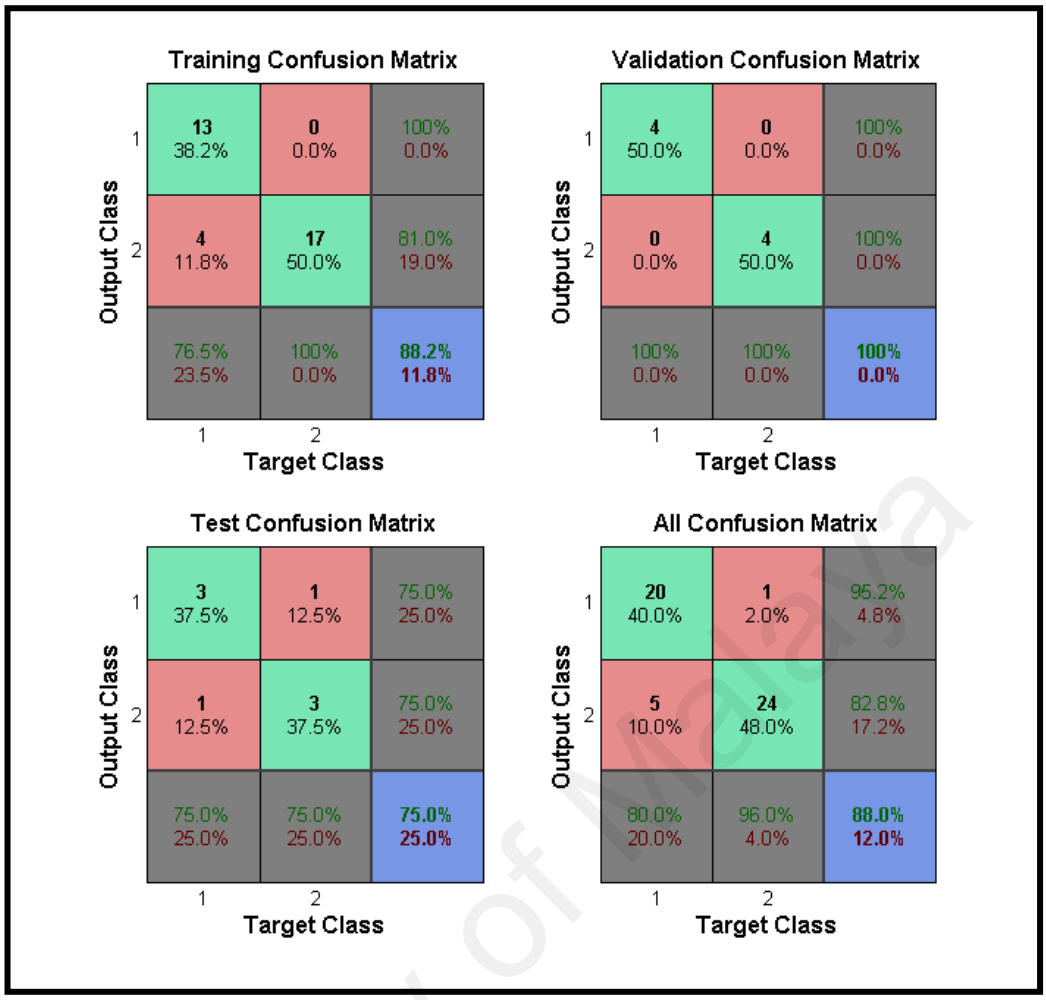

Figure 4.13: Confusion matrixes combined for I_{max} AUC_T, AUC_I and AUC_{II} between AD and HD

Figure 4.13 shows the prediction of dentine layers at each stage of the ANN method. All confusion matrix shows out of 25 representatives of each layer for AD and HD, 5 and 3 cases were diagnosed false positive as ID layers and AD layers respectively. The overall prediction accuracy was 88.0%.

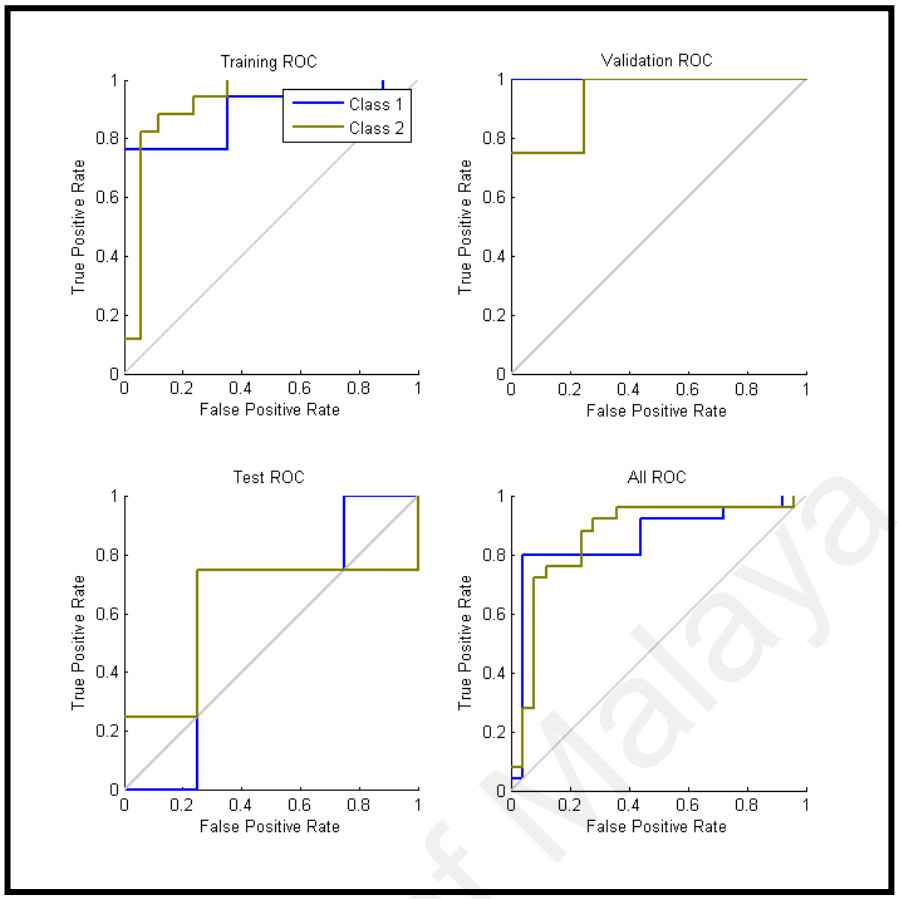

Figure 4.14: ROC curve of I_{max} and *AUC* between AD and HD

R, AUC and I_{max} at total, phase I and II between AD and HD

ANN was run separately from *R*, while combined I_{max} AUC_T, AUC_I and AUC_{II} was explored together between AD and HD. All confusion matrixes reported for *R* at various depth points within total, Phases I and II reported 76.9%, 75.5% and 81.8% as the overall accuracy of classification respectively. Similarly, for combined I_{max} AUC_T, AUC_I and AUC_{II} 94% was reported as overall accuracy of classification. The best outcome measure for group classification between the ID and HD layer was I_{max} and AUC with an accuracy of 94.0% (Figure 4.13) and its related ROC curve (Figure 4.14).

Figure 4.15: Confusion matrixes of I_{max} and *AUC* at total depth between ID and HD layers

Figure 4.15 shows prediction of dentine layers at each stage of the ANN method. All confusion matrix shows out of 25 representatives of each layer for ID and HD, 1 and 3 cases were diagnosed false positive as ID layers and HD layers respectively. The overall prediction accuracy was 94.0%.

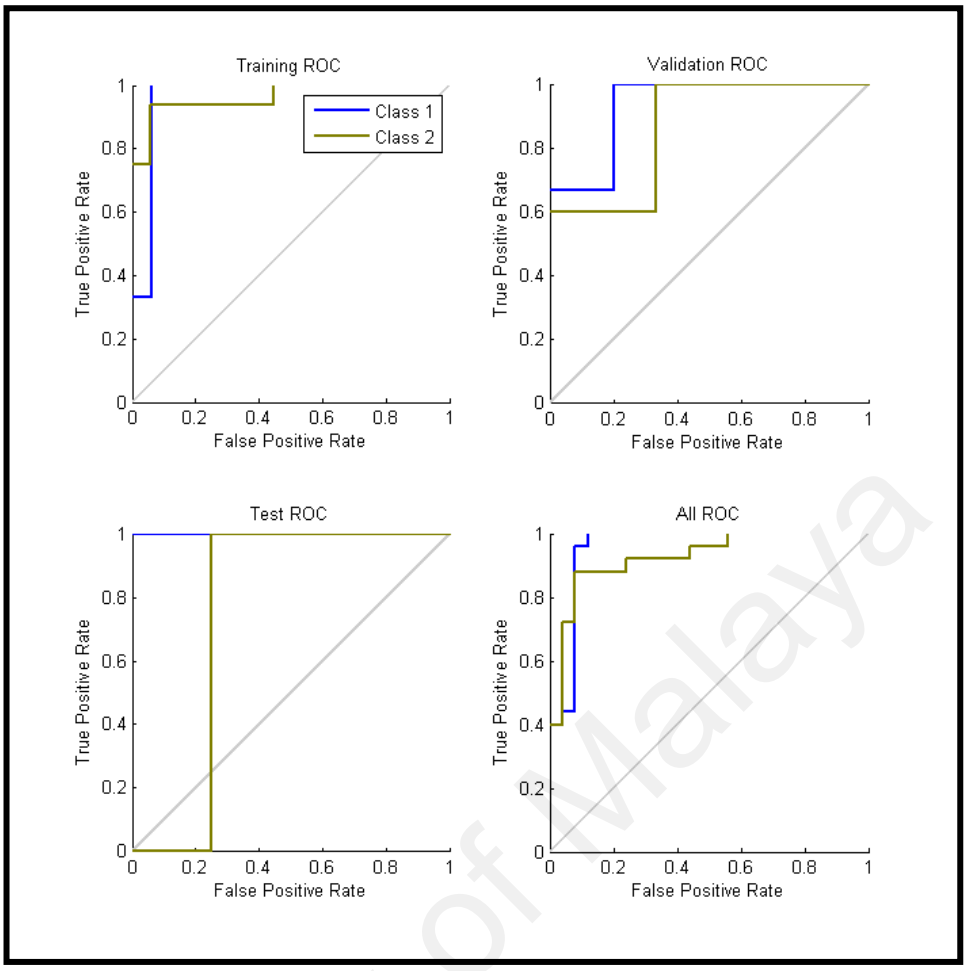

Figure 4.16: ROC curve of I_{max} and *AUC* between ID and HD

4.3 Bio-chemical composition of dentine caries and OCT results

EDX analysis for the identification of major elements in ID, AD and HD includes Calcium (Ca) and Phosphorous (P) weight percent (wt %), while other elements found in trace amounts when compared to Ca and P such as Mg, C, Cl and Zn are not represented because of their low contribution and wt %.

4.3.1 Mean Ca and P wt % and Ca:P ratios of three dentine layer

Mean wt % (± SD) of Ca and P in ID, AD and HD were reported as 6.52 (± 2.82), 12.03 (±3.97) and 19.67 (± 3.81) and 2.22 (±1.11), 5.75 (± 1.98) and 9.84 (± 1.61) for the respective elements and the dentine layers (Figure 4.13). While the mean calculated Ca:P ratio for ID, AD and HD were 3.28 (± 1.52), 2.11 (± 0.94) and 2.01 (± 0.30) respectively.

4.3.2 Comparison of major elements of dentine caries layers

Statistical test were performed to detect the difference in the Ca, P wt% and Ca:P ratio between three dentine layers. The data was analysed using the Levene statistics test to verify if the assumption of homogeneity of variance is met or not. The Leven test revealed asumposition of homogeneity of variance was only violated for Ca:P ratio ($p< 0.05$). Therefore, for the Ca and P wt%, one-way ANOVA followed by the Bonferroni test was used. For Ca:P ratios, Welch's ANOVA and Brown-Forsythe followed by Games-Howell test were applied due to their robustness towards homogeneity of variance. One-way ANOVA revealed there was significant difference in the Ca and P wt% at the ($p< 0.05$) among dentine layers [$F(2,72) = 85.52$, $p=0.001$] and [$F(2,72) = 140.26$, $p=0.001$] respectively. The Bonferroni test demonstrated that the Ca and P wt% was significantly different at the $p<0.05$ within all three dentine layers (Figure 4.15). Welche's ANOVA and Brown-Forsyth revealed that there was significant difference in

the Ca and P wt% at the (p< 0.05) among dentine layers [F(2,72) = 14.89, p = 0.001]. The Games-Howell test demonstrated that the Ca:P ratio was significantly different between ID and AD at and ID and HD at the (p< 0.05) while it was not significant between AD and HD layer (p= 0.460).

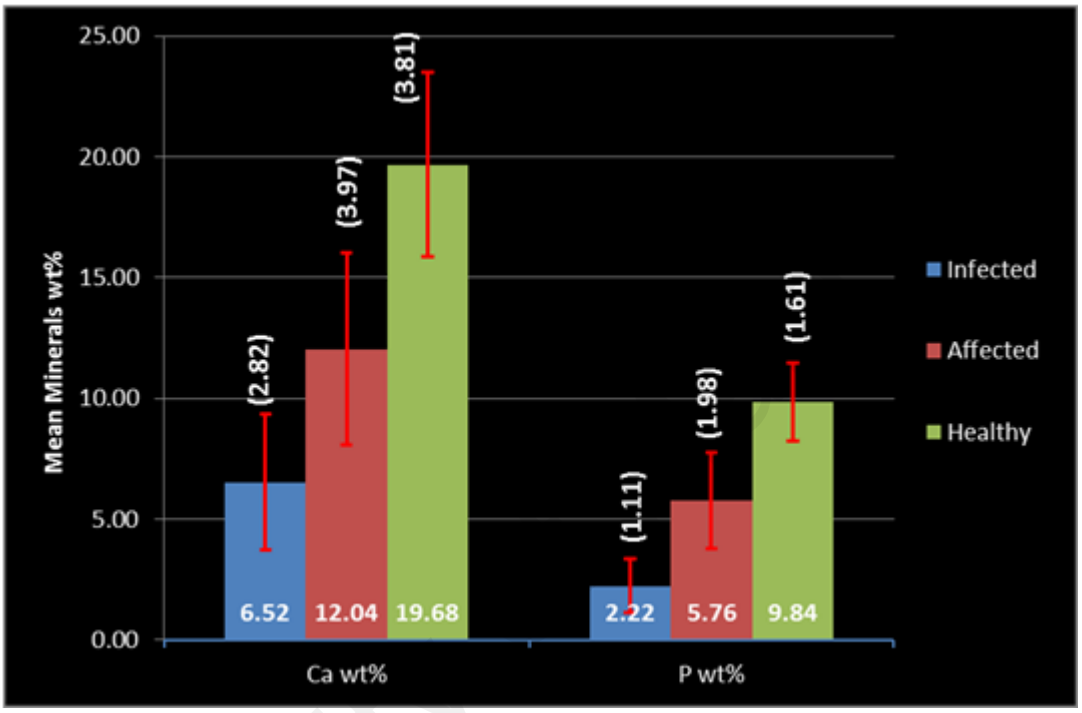

Figure 4.17: Comparison of major elements between ID, AD and HD

Figures 4.17 shows the mean values for Ca wt% and P wt % and its standard deviations for dentine layers. One-way ANOVA and Bonferroni test yielded significant differences amongst and between all three dentine layers (P < 0.05).

4.3.3 Relationship between the Ca, P wt% and Ca:P ratio and selected OCT outcome measure

Pearson correlation test was used to determine if there was a statistically significant relationship between Ca, P wt%, Ca:P ratio and I_{max}, R, AUC_T and AUC_{II} as significant outcome measure stated in Table 4.16. Only, I_{max} and R Phase II were significantly correlated to Ca, P and Ca:P ratios. I_{max} demonstrated moderate positive relationship

with Ca (*r*= 0.448) (Fig.4.18) and P (*r*= 0.479) (Fig.4.19), and moderate negative relationship with Ca:P ratios (*r*= -0.431) (Fig.4.20). *R* demonstrated significant but weak negative correlation with Ca (*r*= 0.315), P (*r*= 0.360), and with Ca:P ratios (*r*= -0.279). The overall difference and correlation between major elements and OCT outcome measures is stated in Table 4.17.

Table 4.17: Pearson's Correlation Coefficient of between major elements and OCT outcome measures

	Ca wt%	**P wt%**	**Ca:P**
I_{max}	0.448 0.001*	0.479 0.001*	-0.431 0.001*
R	-0.315 0.006*	-0.360 0.001*	-0.279 0.015
AUC_T	-0.223 0.054	-0.226 0.051	.011 0.927
AUC_{II}	-0.126 0.283	-0.150 0.199	0.052 0.656

Table 4.17 shows I_{max} and R were significantly correlated to Ca, P (wt%) and Ca:P ratios. I_{max} demonstrated moderate positive relationship with Ca and P, and moderate negative relationship with Ca:P ratios.

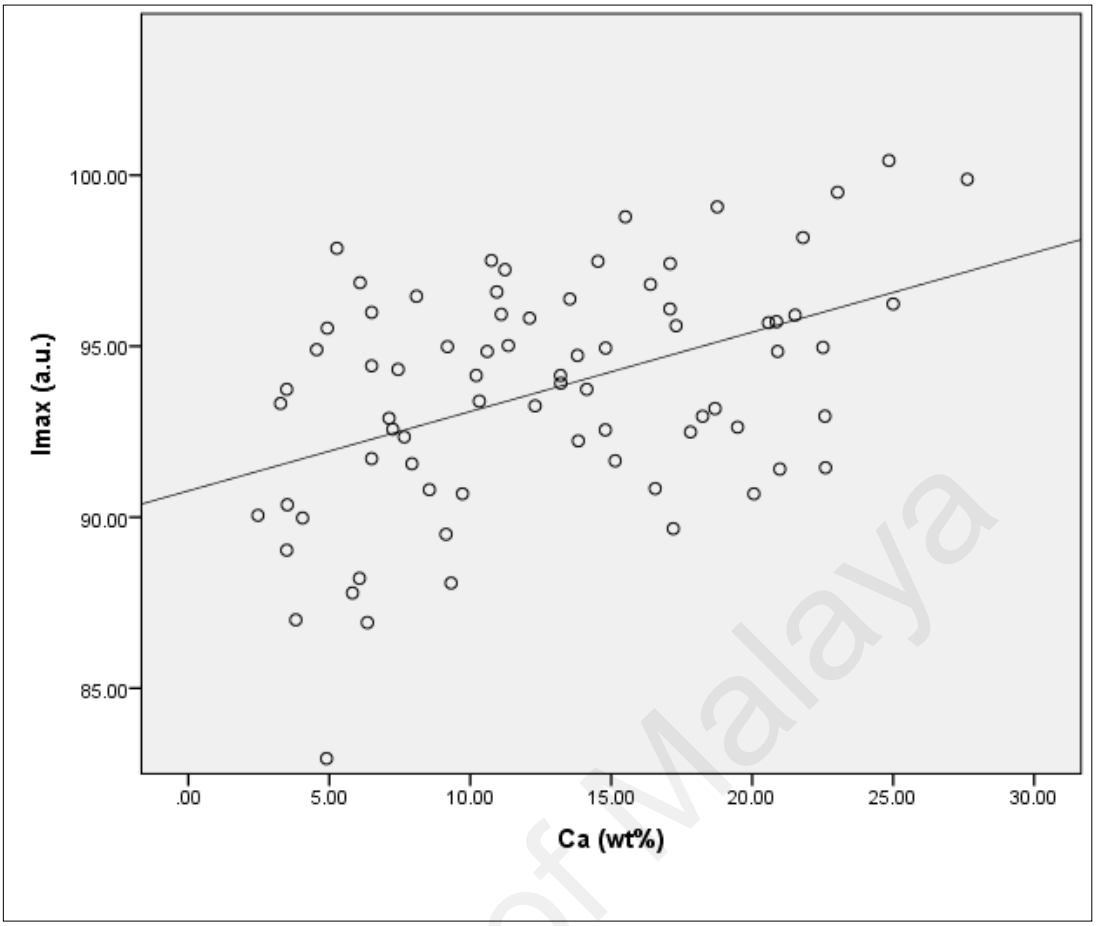

Figure 4.18: Relationship between Ca (wt%) and *Imax*

Figure 4.18 shows significant relationship between Ca wt% and I_{max} ($p < 0.001$). The Pearson correlation coefficient of r=0.448 indicated a moderate and positive correlation between the two variables.

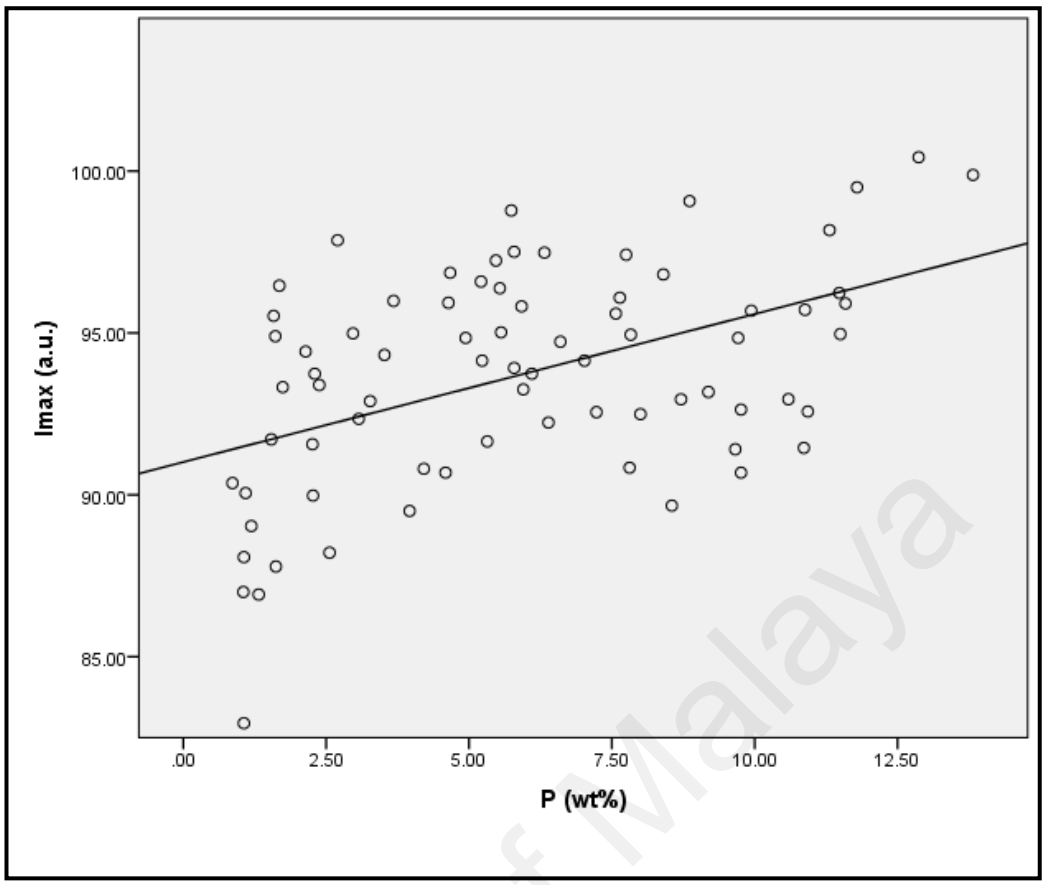

Figure 4.19: Relationship between P (wt%) and *Imax*

Figure 4.19 shows significant relationship between P (wt%) and I_{max} ($p < 0.001$). The Pearson correlation coefficient of r=-0.431 indicated a moderate and negative correlation between the two variables.

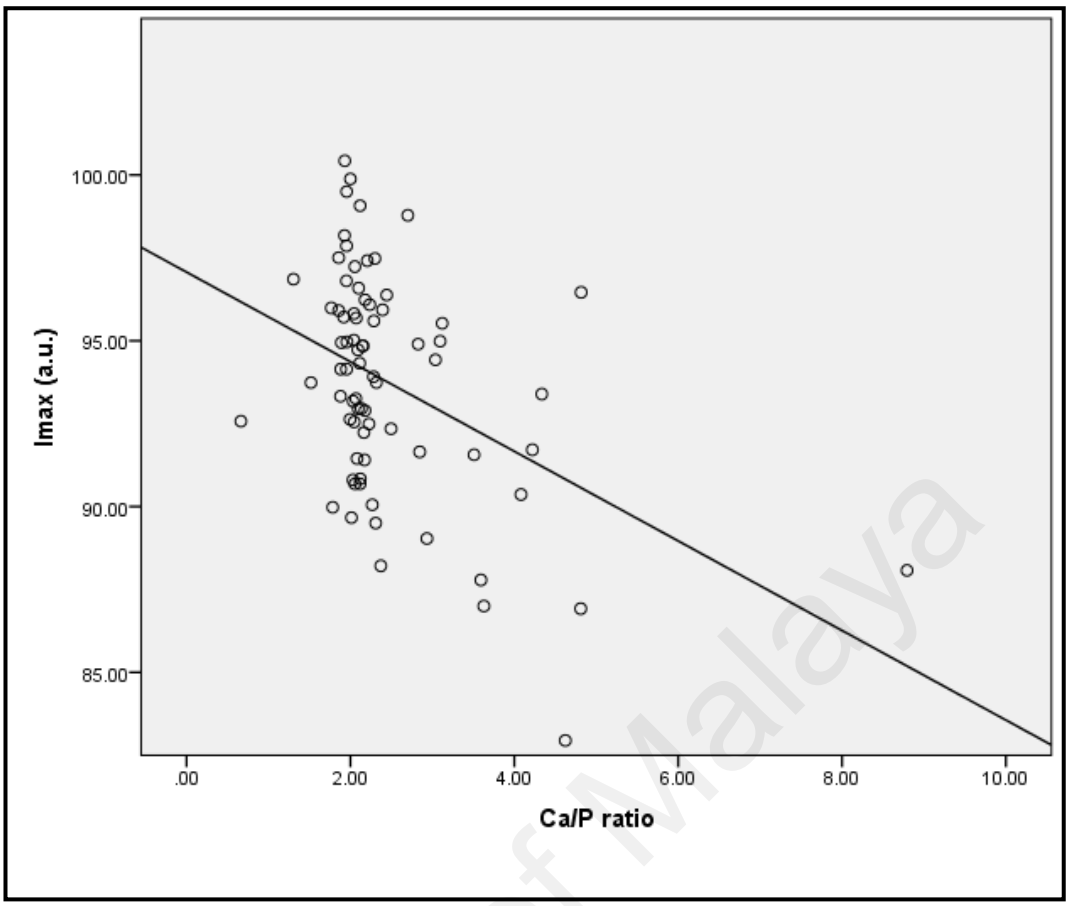

Figure 4.20: Relationship between Ca:P ratio and *Imax*

Figure 4.20 shows significant relationship between Ca:P ratios and mean I_{max} values ($p < 0.001$). The Pearson correlation coefficient of r=-0.479 indicated a moderate and negative correlation between the two variables.

4.4 Dentine caries mineral densities and OCT results

Results of this research objective are presented in following sections: 1) The attenuation coefficients and MD values of ID, AD and HD using automated ROIs as preliminary baseline values. 2) Mean MD values from line plots and its corresponding OCT outcome measure and its level of difference between three dentine layers. 3) The relationship between MD and OCT outcome measures. The last sections, determines the cut-off between ID and AD using OCT outcome measures.

4.4.1 Attenuation and MD values extracted from automated ROI of dentine layers (n=21)

Figure 4.21 is a micro-CT scan (cross-sectional plane) of carious tooth using VG Studio Max (Version 2.1.3, 64 bit, Volume Graphics, Charlotte, NC, USA). Preliminary mean, minimum and maximum attenuation values were converted to MD using the equation stated in Section 3.4.10. Table 4.18 represents the preliminary attenuation coefficient and MD for ID, AD and HD. The minimum MD values of dentine layers were not used for further analysis to ensure least overlap between the layers. The mean to maximum MD for ID, AD and HD ranged between: 0.82-1.10, 1.13-1.38, and 1.53-1.78 gm/cm-3.

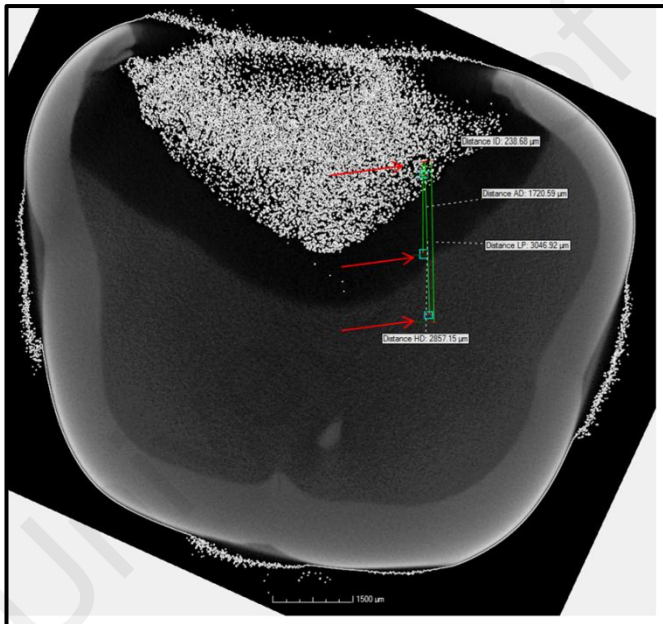

Fig a

	ID	AD	HD
Data range limit:	758.0	758.0	758
Volume [µm³]:	0.0	0.0	0.0
Minimum:	55.0	91.0	132.0
Maximum:	100.0	145.0	186.0
Amount of voxel:	213.0	281.0	228.0
Mean:	74.4	119.3	158.7
Deviation:	8.5	9.6	11.2
Bounding Box X [µm]:	6.2	5.6	5.2
Bounding Box Y [µm]:	10.7	10.9	11.0
Bounding Box Z [µm]:	3.2	4.5	5.5
Relative Volume [%]:	100.0	100.0	100.0

Fig b

Figure 4.21: Micro-CT scanned cross-sectional plane of carious tooth and the details from automated ROI

Figure 4.21a shows an image of a cross-sectional plane of a sample with three dentine layers. Three standardized ROIs in blue boxes (red arrows) are drawn for ID, AD and

HD layer. The mean, minimum and maximum attenuation values of each layer are presented in Figure 4.21b.

Table 4.18: Mean and maximum attenuation coefficient and MD values from automated ROIs of three dentine layers (n=25)

Dentine layers	Mean attenuation coefficient(cm^{-1})	Maximum attenuation coefficient(cm^{-1})	Mean MD ($g\ cm^{-3}$)	Maximum MD($g\ cm^{-3}$)
ID	92.02	124.98	0.82	1.10
AD	128.55	158.00	1.13	1.38
HD	175.98	205.49	1.53	1.78

Table 4.18 shows mean and maximum attenuation coefficient values and its converted corresponding mineral densities for ID, AD and HD layers.

4.4.2 MD and OCT outcome measures difference between three dentine layers (n=21)

Descriptive statistics for MD, *I* and *ΔI* are presented in Table 4.19 , mean MD ($g\ cm^{-3}$) of ID, AD and HD layer was 0.87, 1.16 and 1.52 respectively. While the OCT *I* (a.u.) for ID, AD and HD was 91.12, 89.21 and 88.97 respectively. The *ΔI* (a.u.) showed higher difference when compared to *I* amongst the three dentine layers; *ΔI* reported for ID, AD and HD was 13.70, 7.61 and 8.10 (Table 4.19).

Table 4.19 MD, *I and* Δ*I* for ID, AD and HD

	MD (g cm^{-3})			*I* (a.u.)			*ΔI*(a.u.)		
	Mean (± SD)	Min	Max	Mean (± SD)	Min	Max	Mean (± SD)	Min	Max
ID	0.87 (± 0.10)	0.66	1.05	91.12 (± 2.25)	86.53	95.90	13.79 (±2.65)	9.21	18.33
AD	1.16 (± 0.82)	0.99	1.28	89.21 (±3.19)	85.00	95.60	7.61 (±3.04)	3.45	15.29
HD	1.52 (± 0.13)	1.32	11.56	88.97 (± 2.49)	84.29	95.33	8.10 (± 1.97)	5.16	11.56

4.4.3 Detecting difference in MD, *I* and *ΔI* as outcome measures for three dentine layers (n=21)

One-way ANOVA and post-hoc-Tukey revealed that there was a significant difference in MD amongst all three dentine layers ($p < 0.05$) (Table 4.20). For outcome measure *I*, One-way ANOVA revealed significant difference between three dentine layers ($p < 0.05$) however, the post-hoc-Tukey indicated significant difference was only between ID and HD ($p=0.031$), while no significant difference were found between ID and AD ($p=0.062$), AD and HD ($p=0.953$) dentine layers (Table 4.20). For Δ*I*, One-way ANOVA revealed that there was a significant difference between the three dentine layers ($p < 0.05$). The post-hoc-Tukey indicated that there was a significant difference between ID and AD, and ID and HD ($p < 0.05$), while no significant difference was found between the AD and HD ($p=0.851$) layers (Table 4.20).

Table 4.20: Statistical difference of MD values in ID, AD and HD layers (n = 21)

Comparison	**MD (P-value)**	**OCT *I* (P-value)**	**OCT *ΔI* (P-value)**
ID vs AD	(0.001)	(0.062)*	(0.001)
AD vs HD	(0.001)	(0.953)*	(0.815)*
AD vs HD	(0.001)	(0.031)	(0.001)

Table 4.20 shows there is a statistical difference between MD, OCT outcome measures and three dentine layers. * mean with the same letter are not significantly different using the post-hoc-Tukey Kramer test ($p > 0.05$). *I* was not found to be significant in determining difference between ID and AD.

4.4.4 Relationships between MD and OCT outcome variables

Two OCT outcome measures were analysed for assessing the relationship between MD and OCT output measures. Initially, the OCT intensity (*I*) was placed as a variable in scatter plot against MD. The visual trends of scatter plot were assessed. There was distinct vertical spread observed for majority of the sample for ID and a few for AD, while more horizontal spread was observed for HD. ΔI was created as a second outcome measure as detailed in methods section 3.4.11.2. Significance and level of relationship between MD and OCT outcome measures were examined by Pearson correlation test. The mean and standard deviation were calculated for MD, *I* and ΔI for each layer. Pearson correlation test was performed to determine statistically significant relationship between MD and *I* and ΔI.

Relationship between MD and *I*

Based on the Pearson correlation coefficient test, there was significant relationship between MD and OCT *I* for all specimens ($p < 0.001$). However, Pearson correlation coefficient of r=-0.359 indicated a moderate and negative correlation between two variables (Table 4.21). A linear function was fitted to the variable relationship with a R^2 value of 0.129 (Fig 4.22).

Relationship between MD and *ΔI*

Based on the Pearson correlation coefficient test, there was a significant relationship between mineral density and OCT ΔI for all specimens ($p < 0.001$). However, Pearson correlation coefficient r=-0.531 indicated a strong and negative correlation between the two variables (Table4.19) A linear function was fitted to the variable relationship with a R^2 value of 0.282 (Fig 4.21)

Table 4.21: Relationship between MD and outcome measures

	Correlation coefficients	**P-value***
MD vs *I*	-0.359	<0.001*
MD vs *ΔI*	-0.531	<0.001*

Table 4.21 shows* Significant correlation existed between MD and both outcome measures. However *ΔI* showed strong correlation.

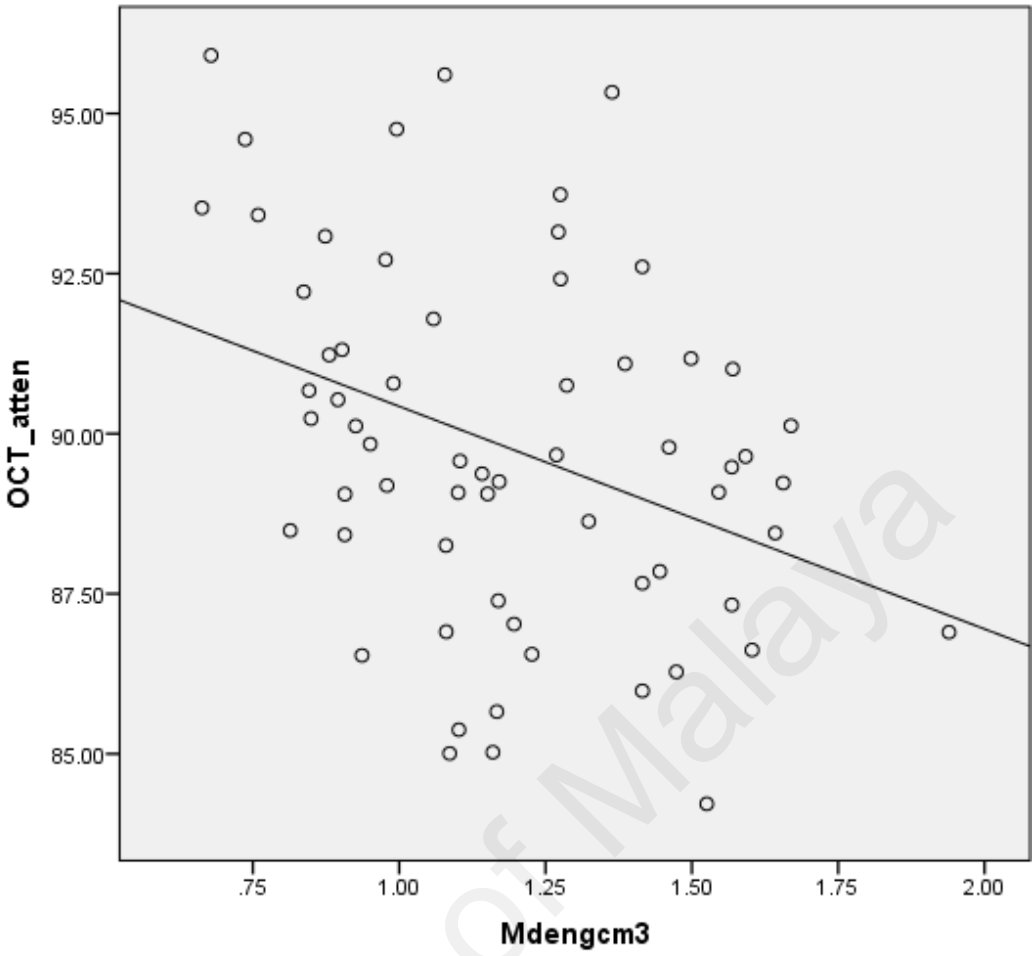

Figure 4.22: Relationship between MD and *I*.

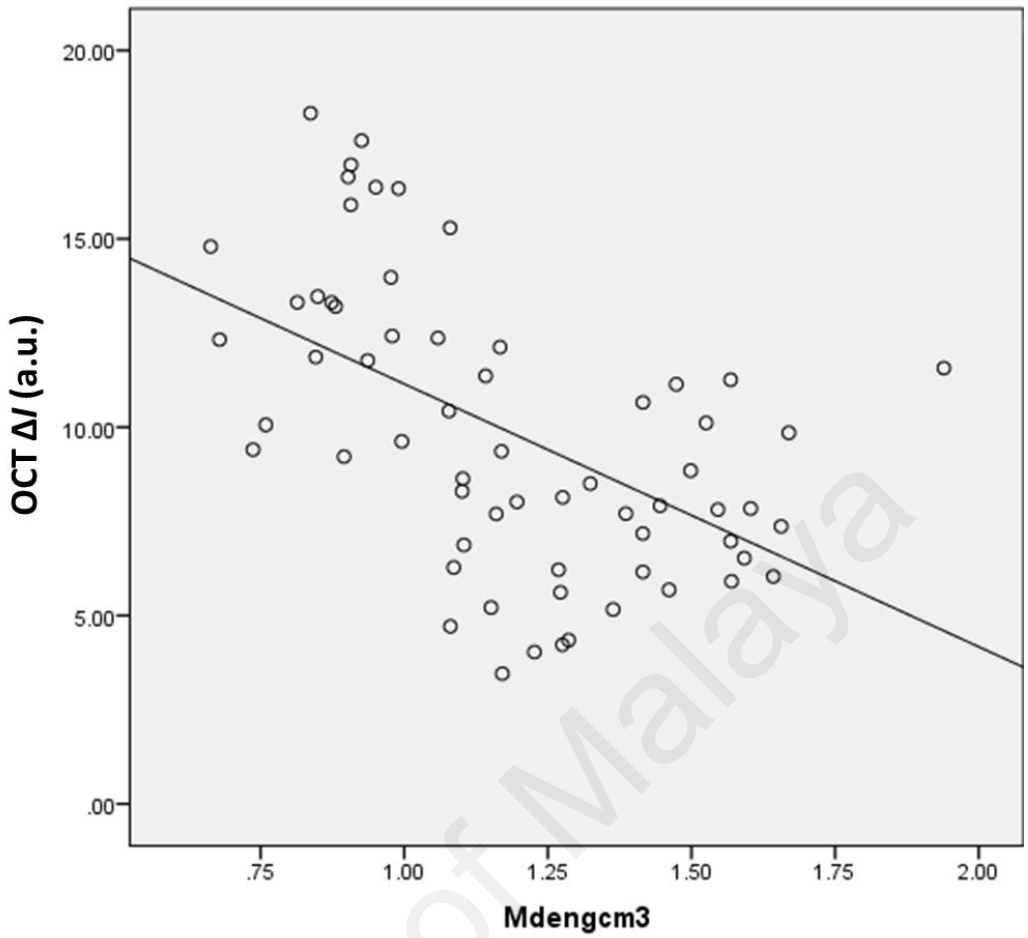

Figure 4.23: Relationship between MD and Δ*I*

4.4.5 Using *ΔI* threshold values to identify cut-off value between dentine layers

The results from Section 4.4.4 established Δ*I* as a better outcome measure to discriminate between ID and AD. Receiver operating characteristic (ROC) curve analysis was performed to find the best cut-off point for OCT ΔI by determining the highest positive likelihood ratio (PLR) (sensitivity/[1_specificity]). At a cut off value of 9.29 (a.u.), the Δ*I* value showed 95% sensitivity and 75.4% specificity in differentiating ID from AD layer. However, at 9.84 (a.u.) the Δ*I* value was limited to 90.5% sensitivity but higher specificity was achieved up to 81.0% in differentiating ID from AD dentine layer (Table 4.22). We evaluated that the optimum cut off value was defined as the test result which is a good trade off between sensitivity and specificity indicating a perfect

separation of the test value of the groups. Since it is important the affected layer must be detected at accurate point, higher specificity was preferred and the optimum cut off point between infected and affected dentine layer was a reliable trade off value observed at 9.84 (a.u.). A ROC curve was obtained by plotting ΔI points as shown in Figure 4.24. The AUC was reported (AUC =0.937) with SE = 0.038 and 95% confidence interval (CI) from 0.863 to 1.000.

Table 4.22 OCT ΔI values and its corresponding sensitivity and specificity values

Positive if Greater Than or Equal Two	Sensitivity	1 - Specificity	Specificity
2.45667166	1	1	0
3.74330847	1	0.952	4.8
4.12700588	1	0.905	9.5
4.28499009	1	0.857	14.3
4.52941526	1	0.81	19
4.96270866	1	0.762	23.8
5.41424632	1	0.714	28.6
5.91632464	1	0.667	33.3
6.24616903	1	0.619	38.1
6.57445428	1	0.571	42.9
7.28484242	1	0.524	47.6
7.85682189	1	0.476	52.4
8.07698973	1	0.429	57.1
8.21788825	1	0.381	61.9
8.46522895	1	0.333	66.7
8.92485642	1	0.286	71.4
9.28946277	0.952	0.286	71.4
9.38239666	0.952	0.238	76.2
9.51368838	0.905	0.238	76.2
9.84304181	**0.905**	**0.19**	**81.0**
10.2450072	0.857	0.19	81
10.8935011	0.857	0.143	85.7
11.565832	0.857	0.095	90.5
11.8165712	0.81	0.095	90.5
11.9922684	0.762	0.095	90.5
12.2241736	0.762	0.048	95.2
12.3464751	0.714	0.048	95.2
12.3939958	0.667	0.048	95.2
12.8124908	0.619	0.048	95.2
13.2582453	0.571	0.048	95.2
13.3119036	0.524	0.048	95.2
13.3894447	0.476	0.048	95.2
13.7212535	0.429	0.048	95.2
14.3851936	0.381	0.048	95.2
15.0428211	0.333	0.048	95.2
15.5956456	0.333	0	100
16.1176315	0.286	0	100
16.3525579	0.238	0	100
16.5050685	0.19	0	100
16.8032866	0.143	0	100
17.2865028	0.095	0	100
17.9702121	0.048	0	100
19.3339593	0	0	100

Table 4.22 shows ΔI at 9.84 a.u. with sensitivity at 90.5% and specificity at 81.0% to be considered as ideal threshold value to discriminate between ID and AD.

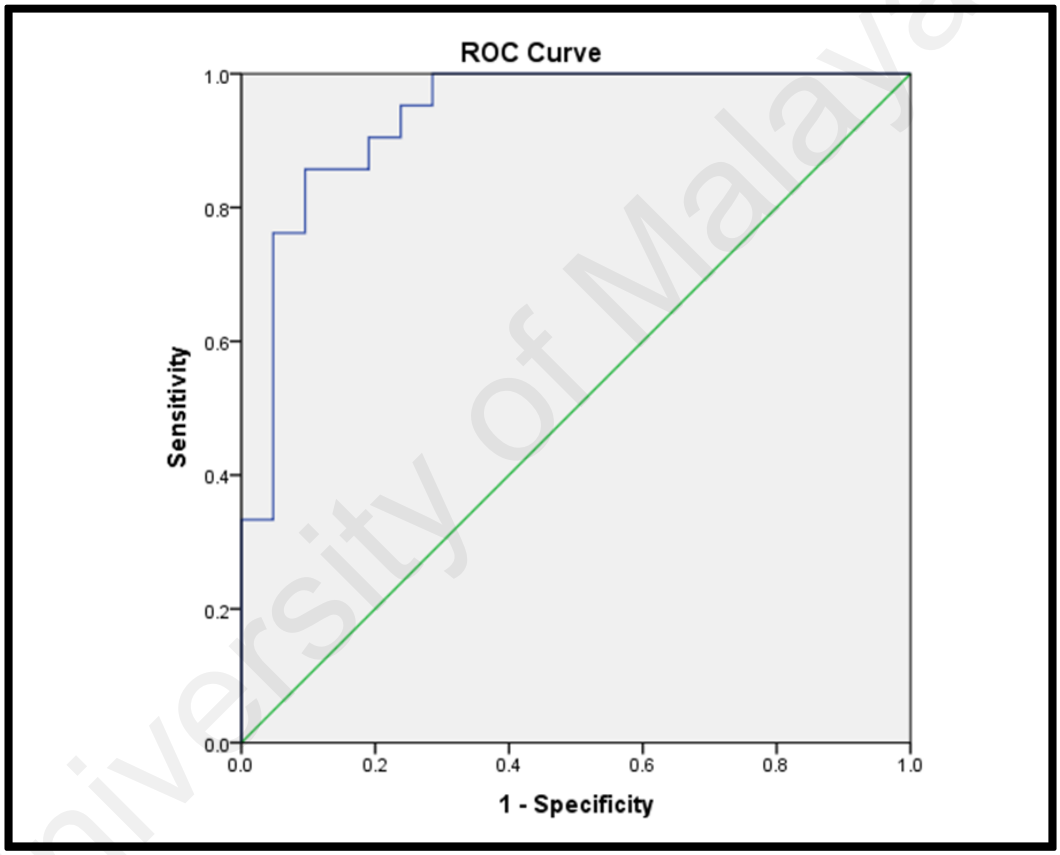

Figure 4.24: ROC plot of ΔI

Figure 4.24 shows the ROC plot of ΔI in discriminating between ID and AD at (AUC value on ROC = 0.937).

CHAPTER 5: DISCUSSION

This chapter discusses the rationale of methods used in the experiments and significant results observed from research objectives i, ii and iii. Each research objective explores the relationship between the OCT outcome measures with structural, bio-chemical and mineral densities of dentine layers. This approach was designed to assess the overall performance of using OCT signals in the characterization and differentiation of the three dentine layers. Key methodical stages involving sample selection and preparation, standardizations and OCT related scanning and analysis are also discussed in this section.

5.1 Microstructure and OCT of dentine layers

The aim of this in-vitro study is three fold: to characterise the ID, AD and HD layers using OCT signals, to explore OCT outcome measures in the differentiation of three dentine layers and to assess the accuracy of the prediction and classification of ID, AD and HD using OCT outcome measures. Before the results, methodological considerations, histological classification based on SEM images of dentine caries and OCT scanning methods are discussed.

5.1.1 Methodological consideration

In this study human teeth, with natural occurring coronal dentine caries were used. Histologically natural dentine caries involves ID, AD and HD layers which are established by the Fusayamas' group of researchers (Ogawa et al., 1983; Ogushi & Fusayama, 1975). Naturally occurring ID layer biologically involves bacterial lead collagen denaturation, while AD layer shows some ultrastructural changes within ITD and PTD and the formation of transparent dentine. However when dentine caries is artificially induced using microbiological or pH cyclic model, these micro-

characteristics are often missing. Specifically, it is difficult to emulate the ultrastructural changes occurring within biomenieralisable AD layer (Marquezan et al., 2009; Shellis, 1994). Similar limitation has been reported when using in situ-caries-inducing models (Moron et al., 2013).

In this study, the natural biological variations of the size and distribution of ID, AD and HD layers were managed by setting stringent inclusion criteria during sample selection, OCT scanning and data extraction. Considering the friable nature of the ID layer, pilot studies using multiple storage mediums demonstrated that freezing and thawing was the most suitable method to store and prepare the dentine caries slabs. ICDAS criteria with Code 5 and 6 were used to select the carious teeth, as the severity at this stage provides maximum bulk of ID layer. To further standardize the grouping of dentine lesions, visual-tactile methods were used to exclude carious teeth with low bulk of outer ID layer and carious surfaces which appeared shiny and hard. ID layer with soft and yellow to light brown coloured dentine were included in the study. Gentle probing was performed to establish that dentine lesion is in active stage (Braga, Mendes, & Ekstrand, 2010). Research shows active dentine caries that is under bacterial attack gives a biological reaction by depositing minerals and formation of hypermineralised translucent dentine, which is part of AD layer (Arnold, Konopka, & Gaengler, 2001; Daculsi et al., 1987). This consideration has helped to optimize the teeth sample selection.

To have sizable representation of OCT data from each dentine layer, 1024 single intensity points in x and y direction were considered, yielding ultrahigh resolution (2.9µm x 3.4 µm, transverse x longitudinal resolution, 3000µm x 3500 µm; 1024 x 1024 pixels) during OCT scanning. High resolution imaging increases the likelihood of accurate representative of each dentine layer under investigation. During OCT data

extraction, algorithmic construction of the ROIs drawn for each layer averaged those intensity points which resulted in a mean quantified value from each sample. The mean value at each depth point was calculated from all 25 samples for respective dentine layer and was represented as depth resolved mean A-scan. This was achieved by using bespoke Graphic unit interface (GUI) software developed in MATLAB (The Mathworks, USA) for the OCT caries research under HIR UM.C / 625 / 1 / HIR / MOHE /_Dent_/1.

5.1.1.1 Scanning Electron Microscope

Since the aim of this study was to histologically characterise the three dentine layer, several pilots were attempted at various stages of research to protect the carious surfaces from getting altered. The dentine slabs were not polished and smear layer was removed using sonication with weak chelating agent. These methods helped to maintain the ultrastructural topography before SEM analysis.

Using SEM images, the observation made were as following: ID layer appeared as decomposed mass of irregular structures, occasionally loose scattered collagen-like fibres with leaf-like crystals suspended to it was seen. Huge voids with asymmetrical hollow spaces were observed while PTD was completely absent within this dentine layer. These observations were similar to the histological cross sections of ID as described by Ogushi and Fusayama (1975). Masrshall et al demonstrated loss of PTD and destruction of collagen within the intertubular dentine matrix as advanced demineralization was considered infected dentine (Marshall, Chang, Gansky, & Marshall, 2001). After establishing the ID layer, every 125µm distance (width of bar + inter-bar distance of copper gird) partial or complete presence of first sighting of undistorted PTD was considered to identify AD layer. The first emergence of PTD was classified as the beginning of the AD layer, and along with this parameter, enlarged

dentine tubule lumens were seen, surrounded by the thin collagen meshwork of ITD, which was comparable to healthy dentine but had irregular roughness in the surface. Research has shown that emergence of PTD as a sign of bio-remineralizable dentine (G. W. Marshall, Jr. et al., 2001), while Kinney et al demonstrated a linear relationship between the kind and severity of the demineralization of ultrastructure of dentine (ITD and PTD) (Kinney et al., 1995). Healthy dentine was recognized as dense homogenous minerals cuff-like structure surrounding the dentinal tubules referred to as PTD, while the ITD was thick and evenly distributed. These findings matched those of the earliest research on visualizing the microscopic appearance of healthy dentine by Frank and Takuma et al (Frank, 1959; Takuma, 1960).

Considering the observations made from each dentine layer, Pugach et al criteria for classification of ID and AD, which was based on evidence similar to previous research. Pugach et al used the presence of PTD and tubule occlusion linked with level of demineralization of dentine; however PTD ratings were reported to be a better indicator of demineralization when compared to occlusion of tubules (Pugach et al., 2009). Another reason why the occlusion of tubule was not considered as a parameter in this study was due to the fact that occlusion of tubules associated with Mg-substituted b-TCP crystals (whitelockite) has not been consistently detected when observing the ultrastructure of carious dentine in the literature (Frank and Voegel, 1980; Zavgorodniy et al., 2008). However, the Pugach classification does not consider the obvious changes occurring with the collagen mesh work of Intertubular dentine matrix which is the biggest bulk of dentine and can be considered as limitation of this method. Consequently, two parameters which were used in this study were: First, observing the complete absence of PTD as indication of advanced demineralization as an affirmation of ID layer. Second, the appearance of undistorted PTD observed within the transition of layers will represent as AD layer. While HD was identified having smooth ITD and

PTD both with clear evenly distributed ring-like dentine tubules. These histological landmarks provided a defined demarcation between the three layers.

5.1.1.2 Optical Coherence Tomography

The I_{max} of OCT signal was seen at 7.81 µm; this position may also be referred to as dentine-air interface. At this interface, strong specular reflection often appearing as high intensity columnar artefacts could be reaching several order of magnitude (~20-30db). The speckle is created due to coherent addition of waves with a random phase distribution. The light propagating along altered paths on and within dentine layers acquire random phase shifts due to backscattering at the surface and the structural layout of the sample being scanned. This surface reflection can conceal the actual backscatter information arising from the deeper parts of the tissue (Fried et al., 2002). Even if high-resolution OCT system is used (axial resolution < 10-µm), the intensity decreases by 3db at 10 µm below the surface (Kang et al., 2012). Evidence shows the specular reflection is highest when the surface is smooth and shiny, while the intensity of specular reflection decreases with roughening of surface (Liu, Yamazaki, Zhou, & Matsumiya, 2002; Rakhmatullina et al., 2011). Dentine caries samples are porous and have voids filled with air and water/dentinal fluid when compared to enamel, therefore specular reflection created during OCT scanning was less attributed to surface reflection. It is important to note that in this study the scanned surfaces of dentine caries slabs were > 300µm thick and cut in cross-sectional plane, creating the dentine tubules perpendicular to the laser beam. Whereas, the ROIs selected for investigation was within superficial depth of 100µm. Evidence suggests that dentine with cross-cut tubules (n = 1.49) with small angle parallel to the direction of beam resulted significantly with lower refractive index when compared to long cut (n = 1.60) and oblique cut dentine (n = 1.56) (I. Hariri et al., 2012). In terms of the thickness of dentine

slabs used in this study, Fried et al demonstrated that light scattering when using Nd:YLP 1053nm laser for dentine sample > 300µm thick with tubules in a plane perpendicular to the laser beam observed no anisotropy and tubule orientation has insignificant effect (Fried et al., 1995). Therefore the bulk scattering arising from superficial depth can be attributed to the structural characteristics of the dentine layers and is not likely to get masked by surface scattering, internal reflections and multiple scattering.

In this study, the surface scattering was managed using a combination of methods aiming to avoid specular reflection during OCT scanning. Techniques such as digital image processing (Adler, Ko, & Fujimoto, 2004) and creating an angle up to 45° to the incidence of light (Rakhmatullina et al., 2011) and systematically excluding combination of depths when samples are more homogenously demineralized (Amaechi, Higham, Podoleanu, Rogers, & Jackson, 2001) are a few examples which are commonly used in OCT related research. During OCT scanning, the samples and the light source was kept constant, while an angulation of sample was titled within the range of 10-25° using a customized jig. Later, digital imaging processing was attempted using bespoke software which deconvolved tilted surface into aligning surface data using customized algorithm written in MATLAB software. It was found that when the samples were placed flat and perpendicular to the laser beam at 90° and a tilt of 10-25°, majority of the samples were significantly free of specular reflection.

5.1.2 Characterizing dentine layers

To characterise dentine layers, averaged depth-resolved mean A-scans up to 100µm was considered, at 74µm an overlap between ID and AD was seen indicating the probability of the dentine layers getting identical. Therefore the depth points chosen for further analysis was between 7.90 – 74.22µm. This method helped to confirm that the

respective chosen superficial dentine layer identified as ID, AD and HD was optimum for differentiation. Overall OCT light behaviour of infected dentine notably was different when compared with the AD and HD in assessing averaged mean A-scans. The difference was observed as the ID having lowest I_{max} and attenuation rates, larger standard deviations and the presence of bimodal effect. The probability of the ID layer having lowest I_{MAX} and attenuation rates is because, the dentinal tubules are considered the predominant cause of scattering in dentine (Ten Bosch & Zijp, 1987; Vaarkamp, ten Bosch, & Verdonschot, 1995). Whereas infected dentine is a form of liquefaction foci with no remnant of dentine tubules. After tubular invasion of bacteria it causes tubular sclerosis, leading to collapse and form a coalesce of tubules (E. A. Kidd & Fejerskov, 2004; Thylstrup & Qvist, 1987). Zijp and ten Bosch mathematically calculated the Mie scattering distribution in their experiment considering the mineral crystals, collagen fibrils and tubular structure as separate entities of healthy dentine. They found the lowest scattering coefficient (μ_s) was from mineral crystals (μ_s =1.7 x 10^{-5} mm^{-1}) followed by scattering by collagen fibrils (μ_s =19 mm^{-1}) and dentine tubules resulting highest scattering up to (μ_s =140 mm^{-1}) (Zijp & Bosch, 1993). The role of collagen fibrils in healthy dentine has shown positive contribution for scattering of light within dentine structures(A Kienle et al., 2006), however the role of scattering within decomposed remnants of collagen with bacterial presence in infected dentine is unknown. Walton et al and Kienle et al showed that the presence of air and intertubular fluid within collagen-hydroxyapatite matrix of healthy dentine together propagates the light leading to longer optical path length (A Kienle et al., 2006; Walton, Outhwaite, & Pashley, 1976). This fact may contribute significantly as caries-infected dentine predominantly consists of denatured collagen (healthy collagen, n=1.40) with scanty of amounts of minerals (n=1.62) and increased presence of low-n medium (air, n =1.0 or moisture n = 1.33) when compared with caries-affected and healthy dentine, would

affect the optical path length and lower rate of attenuation of light. According to Zavgorodniy et al the ultrastructure of carious lesions, showed histological images of infected dentine comprised of decomposed softened dentine followed by turbid demineralized dentine (Zavgorodniy et al., 2008). Both of these zones in infected dentine are extremely heterogeneous exposing deteriorated mass of collagen fibres with scattered and loosely attached mineral crystals (Ogushi & Fusayama, 1975; Sarnat, 1965a). Also the turbid zone when compared to softened demineralized zone contains irregular and various extent of dead tracts (Arnold et al., 2003) and needle like crystals which vary greatly in shapes and diameter (Zavgorodniy et al., 2008). The histology of these layers supports the presence of distinctive presence of bimodal effect emerging from deeper layers of ID as the light backscattered due to the varied heterogonous structures present within this layer. The larger standard deviations of OCT signals from infected dentine are also likely to occur because of the similar reasons explained above.

Mathematical models were used to assess the trends observed for overall, Phases I and II mean A-scans for dentine layers. Linear regression of finding the best-fitting straight line indicates the vertical lines from the OCT signal points to the regression line show minimum sum of the squared errors of prediction for model under test, the R^2 value was used to quantify goodness of fit at each model. Higher values of R^2 indicated that the curve of the model being applied comes closer to the data. Figure 4.1 shows the R^2 value for ID was much lower in magnitude at total (R^2 = 0.582) and Phase II (R^2 = 0.083) when compared to AD and HD using linear regression analysis. However, when polynomial regression model was used the R^2 for ID increased up to 0.794 and 0.819 in total and Phase II respectively. This signifies that when using OCT signals the ID behaves significantly different to AD and HD and has its own unique characteristics which aid in differentiation from AD and HD. This is a novel finding which has not been earlier reported in the literature.

Slight difference between AD and HD was noted at I_{MAX} and greater difference in attenuation rates. I_{max} at AD was slightly higher than HD, indicating increased backscatter from structures of AD than HD. Increased I_{max} and lower attenuation rates in Phase I for AD when compared to HD is possible due to the findings reported by Zijp and Ten Bosch, who indicated the change in light scattering properties of decalcified dentine is attributed to increased cross-section diameter of the dentinal tubules (Zijp & ten Bosch, 1991). They also suggested that this change of scattering property can be used to quantify dentine caries back in 1991, which this study has established using OCT as an optical source to discriminate the dentine layers.

Scattering coefficient of healthy dentine ranges using angularly resolved goniometer (index-matched) was between 250-280 cm^{-1} (Fried et al., 1995) while integrating sphere measurements (non-index matching) was 130-180 cm^{-1} (Zijp & Bosch, 1993). Increased scattering resulting from the anisotropy effect of healthy dentine is due to propagation of light scattering parallel and perpendicular to dentine tubules with collagen fibrils playing the least role creating birefringence (X. J. Wang et al., 1999). Another explanation for the increased scattering observed in healthy dentine is explained by Franhoufer diffraction patterns detailed in the Zijp experiments as showing decreases of intensity functioning as faster at smaller angles of dentine tubules when compared to larger angle (Zijp & Bosch, 1993). Histological images in this study shows AD to have increased in the size of dentine tubules, changes in PTD, rougher ITD and infrequent presence of Intertubular minerals causing increase in backscatter at $I_{max.}$ While HD showed the highest attenuation rate compared to AD. These findings were similar to Mandhurah et al which compared attenuation coefficients at 2mm depth of natural carious, healthy and attrited transparent dentine (Mandurah et al., 2015). The attenuation coefficient of transparent dentine was (0.61 a.u./μm) significantly different and slower compared to sound dentine (1.05 a.u./μm), where as in our experiment the

caries-affected dentine showed attenuation at (-0.43 a.u./μm) and healthy dentine at (-0.56 a.u./μm). Although the depths and samples used in both studies were not comparable but an overall relationship of attenuation between AD and HD was similar, this can be attributed to histological changes which occur in original dentine structure to form a modified caries-affected dentine substrate (Vasiliadis, Darling, & Levers, 1983). However Mandhurah et al reported carious dentine with highest attenuation (2.23 a.u./μm) compared to attenuation of ID layer from our experiment, which was (0.38 a.u./μm), possibly due to the difference of depth considered in both experiments. Qualitative observation of mean A-scans of infected dentine from both experiments within 100μm depth behaved in a very similar fashion; however no bimodal trend was observed in their study.

5.1.3 Comparing OCT outcome measures

One of the main objectives of this research was to identify an outcome measure which can significantly discriminate the three dentine layers from each other within their superficial depths. We started with exploring the common outcome measures used in OCT linked caries research, namely attenuations (Mandurah et al., 2013), integrated reflectivity (Kang et al., 2010; Manesh et al., 2009a), fractional differences (Chew, Zakian, Pretty, & Ellwood, 2014), area under the curve (Louie et al., 2010) and peak intensity (Bakhsh, Sadr, Shimada, Tagami, & Sumi, 2011) and spectral peak ratio analysis (Sowa et al., 2007). After initial exploration using logarithmic OCT signal data in depth, the outcome measures chosen for analysis were maximum intensity points (I_{max}), area under the curve and ratios on the basis that each of the measures were different in respect to its mathematical calculations. Each outcome measures were then grouped with total, Phases I and II depths respectively, creating new outcome variables using predetermined differences of attenuation rates observed in Phases I and II depths.

I_{max} being a representative of single intensity point was not grouped with any of the phases and was analysed separately.

One-way ANOVA for I_{MAX} showed that there was significant difference between caries-infected and caries-affected dentine layer (Table 4.4). Whereas Two-way ANOVA for *AUC* showed that there was significant difference between caries-infected and caries-affected at AUC_I (Table 4.5). While for *R* the difference was significant in both Phases I and II except at 20-49µm. AUC_I as an outcome measure to differentiate between caries-infected and caries-affected showed greatest effect size (Table. 4.6). Mean I_{max} is positioned at tooth-air interface whereas AUC_I is calculated from point of I_{max} to 27µm deep, both outcome measures are considered as significant measures to discriminate the two layers. However, there was insignificant difference between 20-49µm depth between Phases I and II for ratio and could not be suggested as a robust outcome measure. Caries-affected dentine had the highest I_{max} value when compared to infected and healthy dentine, behaving similar to highly mineralized enamel tissues in terms of optical transmittance when compared to infected dentine which was devoid of minerals and structure. Although dentine and enamel demonstrate different scattering potentials, Deyhle et al demonstrated, using spatially resolved small angle x-ray scattering, that caries-affected dentine appeared brighter, yielded stronger scattering signals than heathy enamel and dentine(Deyhle, Bunk, & Muller, 2011). Caries-affected dentine exhibiting the highest I_{max} and larger AUC_I can be attributed to the variation seen in mean crystallite size and changes in peri and inter-tubular dentine (Takuma, Tohda, Watanabe, & Yama, 1986). Whereas low I_{max} signals observed from caries-infected is similar to results reported when in-vitro root dentine caries model was used and decrease in reflectivity was observed with increase in demineralization (Amaechi et al., 2004; Freitas et al., 2009). Manesh et al which artificially induced caries on natural coronal dentine surface using laser, showed OCT signals to have low reflectivity when

lesion severity was high (Manesh et al., 2009a). One study which had OCT scanned naturally attired sclerotic dentine showed similar highest I_{MAX} when compared with carious and healthy dentine(Mandurah et al., 2015). In the same study comparing the mean A-scan of naturally sclerotic dentine with carious dentine an observation can be inferred that mean AUC of carious dentine was less than mean AUC of sclerotic dentine which is similar to the observations from our study. It is equitable to infer that the fast attenuation rate of caries-affected dentine seen in Phase I when compared with infected dentine, creates the significant difference in mean AUC_I.

Caries-infected dentine and healthy dentine were significantly different at mean I_{max} (table 4.4), AUC_T, and R at total, phase I and II (table 4.5) when using One-way ANOVA and Two-way ANOVA test respectively. This established that all OCT outcome measures except mean AUC_I and AUC_{II} can be used as significant indicators for differentiation. This can be attributed to atypical characteristics observed of caries-infected dentine as can be seen in Figure 4.,4. Considering the difference in attenuation rates in both phases, the presence of bio-modal effect and due to polynomial fit of data rather linear fit when exploring the regression models. The optical magnification property of healthy dentine has been studied extensively in respect to the sectioning plane of dentine (I. Hariri et al., 2012; A Kienle et al., 2006; Walton et al., 1976; Zijp & ten Bosch, 1991) and wavelengths of lasers used (Chan, Darling, Chan, & Fried, 2014; Fried et al., 1995; Zakian, Pretty, & Ellwood, 2009). The cross- sectional plane and lasers between 1300-1650nm used with healthy dentine has shown high scattering coefficient and actually increases the amount of light backscattered from deeper parts of the dentine (Chan et al., 2014). The literature suggests that light scattering in healthy dentine is caused by the tubules as the light is guided along the tubules due to the scattering by the tubules. Also, in addition to anisotropic optical property of dentine tubules, the presence of healthy collagen fibrils embedded in the mineral matrix

contributes to the forward scattering pattern of dentine tubules (A Kienle et al., 2006). Out of seven, five of OCT outcome parameters were significant in differentiating caries-infected dentine and healthy dentine which can be attributed to be due to the distinct histological and optical differences discussed.

Caries-affected dentine and healthy dentine were only significantly different at mean AUC_T and AUC_{II}, while ratios were only significantly different at 35µm of Phase I (Table 4.5) when using Two-way ANOVA test. Therefore AUC_T and AUC_{II}, both representing the largest depth included for analysis contains maximum characteristics belonging to both the dentine layers. Both the dentine layers are similar in terms of presence of the intertubular dentine matrix with some variations in the peritubular dentine which was the significant parameter used during histological differentiation. However, caries-affected dentine contains translucent zone due to partial intra-tubular mineralization of random tubules (Arnold et al., 2003) yet this may not possibly be affecting the mean AUC of extremely superficial depths. The histology of caries-affected dentine shows the emergence of undistorted peritubular dentine and other complex structures within which when the light travels it may cause an effect on the refractive index of the dentine (Hariri et al., 2013) Therefore, it is probable to state here that attenuation of light for caries-affected dentine in total and Phase II would mainly differ from healthy dentine due to the difference in the surface topography of both dentine layers. Qualitative observation seeing mean A-scans from Mandhurah et al shows the sclerotic affected dentine has larger AUC within 2mm depth when compared to sound dentine, which is similar to the mean A-scans in this study (Mandurah et al., 2015).

5.1.4 Predicting dentine layers using OCT outcome measures

After establishing that the OCT outcome measure can differentiate dentine layers, the following objective of this research was to assess the accuracy of prediction to classify each dentine layer using the outcome measures. The choice and rationale of prediction methods would be discussed in this section followed by the highlighting of the key results.

5.1.4.1 Statistical Considerations

Recently, there is increase in the demand to develop and validate models and prediction rules to improve the clinical decision making in the field of medicine (Froelicher, Shetler, & Ashley, 2002; Randolph, Guyatt, Calvin, Doig, & Richardson, 1998) and dentistry (Mago, Prasad, Bhatia, & Mago, 2008; Mendonca, 2004). The prediction rules involved in clinical situation to discriminate between diseased and healthy tissues can be achieved using various statistical techniques such as Linear discriminant analysis (LDA) and Logistic regression (LR) (Wasson, Sox, Neff, & Goldman, 1985). LDA and LR are commonly used in multivariate analysis when the outcome variables are in categorical form; both aiming to develop linear classification models. LR is the preferred choice when there is dichotomous outcome variable and the goal of prediction is to assess the effect of the predictor variable on the outcome or cause relationship between dependent and independent variables (Hosmer Jr & Lemeshow, 2004). However, LDA analysis is used to determine which independent variable can discriminate significantly between two or more dependent variables. Relying on the new observation, it derives a classification model for predicting group membership (Press & Wilson, 1978). In this study, a variant of LDA that is stepwise discriminant analysis and Canonical discriminant analysis were considered. The stepwise discriminant analysis included and eliminated each OCT outcome measure in the model to evaluate the

predictor which provides the next best discrimination. The *F*-value of stepwise discriminant analysis assessed the extent of contribution it makes towards the prediction of group membership. Whereas canonical discriminant values were used to determine the first rank out of all outcome measure, depending on the level of contribution made to the discrimination between groups. However, it is important to note that LDA is a sensitive technique and in order to increase its prediction ability certain assumptions need to be met. Therefore, the data was checked for its normal distribution and equal covariance matrix (Worth & Cronin, 2003). LDA has been commonly used in dental research where optical spectral properties of light were used for discrimination between diseased and healthy tissues (Madhuri et al., 2003; Sharwani et al., 2006; Swinson, Jerjes, El-Maaytah, Norris, & Hopper, 2006), genetic finger printing of cancer cells (Hwang et al., 2003), dental caries prediction (Bjorndal, Darvann, & Lussi, 1999; Tamaki et al., 2009) and its risk assessment (Ito, Hayashi, Hamasaki, & Ebisu, 2011; Leverett et al., 1993).

Due to the limitation of LDA, which are capable to discriminate linearly separable predictors, other techniques such as Artificial Neural Network are potential alternatives to be used for data which are complex and linearly non-separable (White, 1989). The advantage of using ANN as a discriminant method may benefit this work because clinically dentine caries is a continuum of heterogeneous dentine layers. It would be reasonable to accept an approach which would use multiple OCT outcome measure for the classification of dentine which is not linearly separable. ANN is capable to detect the maximum possible interaction between predictor variables using different training algorithm and requires less formal statistical training (Tu, 1996). ANN is considered one of the variants of machine learning and is part of knowledge, discovery and data mining, and is considered as part of modern computing tools in dentistry (Gansky, 2003). ANN uses pattern recognition by using the data to train, test and validate using a

generalized delta rule (Rumelhart, Hinton, & Williams, 1985). The training of data begins with input of data, and using the existing connection weights also known as hidden layers, it generates its output units. The first training generates the error values for each output unit by comparing the actual output with the desired output. These errors are then fed backwards through the network and when the system is re-tested it uses those errors in generating the newer desired outputs. By repeating this process a few times for each pattern, the training data set increases its accuracy of prediction. Utility of ANN in comparison to LDA has shown more powerful discriminating levels to classify medical diseases (French, Dawson, & Dobbs, 1997; Winterer et al., 1998). In recent years, ANN has been used in dentistry to classify oral lesions using laser induced autofluoresnce spectroscopic studies (Nayak et al., 2006; van Staveren et al., 2000) and dental caries prediction when using radiographs (Devito, de Souza Barbosa, & Felippe Filho, 2008) camera with intra-oral radiographs images (Kositbowornchai, Siriteptawee, Plermkamon, Bureerat, & Chetchotsak, 2006) and using biological variables (Gansky, 2003).

5.1.4.2 Accuracy of prediction

The analysis to determine the accuracy of prediction was explored using LDA and ANN methods for R, $I_{max,}$, $AUC_{T,}$ AUC_I and AUC_{II} applied on two sets of data for statistical analysis: i) all three dentine layers grouped together at a time and ii) only two dentine layers grouped at a time. I_{max} and $AUC_{T,}$ AUC_I and AUC_{II} R

When the dentine layers were grouped together, LDA statistical method showed an overall cross-validated accuracy up to only 68%, with an ROC value up to 0.78, 0.74 and 0.80 for ID, AD and HD. However, using ANN, the overall cross-validated accuracy was significantly increased up to 80%, with 92.0%, 56.0% and 92.0% for ID, AD and HD respectively. Although LDA reported lower prediction accuracy when

compared to ANN, it was able to detect the single most significant contributing predictor which was $AUC_{T.}$ ANN used all OCT outcome measures together except ratios to yield higher prediction accuracy. Overall, ANN was able to accurately classify dentine layers with an increase of 12% when compared to LDA. The results of ANN indicate that the likelihood of *AUC* and I_{max} as combined outcome measures has high accuracy when diagnosing ID and HD layers, however the AD layer showed to be more frequently misdiagnosed as HD layer.

Clinically, active occlusal dentine caries is arranged in order so that, the first and the outer most layer is often the ID layer, underneath it is the AD layer and the deepest part is healthy dentine. Therefore, visually it would not be possible to encounter all dentine layers simultaneously and only one dentine layer appear at a time during the excavation process. However, the reason to group all dentine layers together was only to put OCT outcome measure in extreme test conditions and identify lowest boarders of accuracy. Observing the attenuation rates from mean A-scans of AD and HD layers, it is probable to state that false positive would occur from I_{max} and $AUC_{I.}$ It would be interesting to observe ANN results if AUC total and Phase II is analysed separately to achieve higher discrimination between the two layers.

When ID and AD dentine layers were grouped together, LDA statistical method showed an overall cross-validated accuracy up to only 79.8%, with an ROC value of 0.799 for ID, and AD. However, the accuracy of ANN showed significant increase in the overall cross-validated accuracy up to 84.0%, with 88.0% and 80.0% for ID and AD layers respectively. Overall, ANN was able to accurately classify ID and AD layers with an increase of 4 % when compared to LDA. Clinically, the discrimination between these two layers is the most relevant as the outer infected layer structure are obliterated and the inner affected layer is dentine substrate that is unaltered and needs preservation (T.

Fusayama, 1993). To compare the level of accuracy of OCT outcome measure with previously known techniques which aids in identifying dentine caries layers would be difficult as to our knowledge there are no studies which has reported accuracy of detection for ID and AD layers separately. However, laser fluorescence based technologies such as LIFEDT and FACE relies on fluorophores produced by bacteria to identify dentine layers (Ganter et al., 2014; Panayotov et al., 2013) making them open to criticism. The identification of AD layer, based on its structure and composition is clinically essential for effective adhesion with restorative material (Marshall Jr et al., 1997). Several reports have shown that defining a boundary between ID and AD is considered as one of the most challenging clinical decisions and is often dependent on the clinician's subjective interpretation (Banerjee, Kidd, & Watson, 2000; Thompson et al., 2008). This discrepancy of inaccurate tissues removal end points (Rindal et al., 2014) often leads to compromised pulpal health (Murray et al., 2003), vitality of tooth (Wisithphrom et al., 2006), marginal gaps in adhesive restoration(Dennison & Sarrett, 2012), and weakening of tooth structure causing failure of future restorations (D. Ricketts et al., 2013). The preliminary results to use OCT outcome measure to discriminate ID and AD layers up to 84% makes it the most important and relevant finding, aiming to achieve better clinical outcomes when treating dentine caries.

When AD and HD dentine layers were grouped together, LDA statistical method showed an overall cross-validated accuracy up to only 82.0%, with an ROC value up to 0.821 for AD and HD. LDA reported AUC_{II} as the single most significant contributing predictor. However, the accuracy of ANN showed significant increase in the overall cross-validated accuracy up to 88.0%, with 80.0% and 96.0% for AD and HD layer respectively. Overall, ANN was able to accurately classify AD and HD layers with an increase of 4 % when compared to LDA. Mean A-scans shows significant difference in attenuation rates of AD layer to HD layer in AUC_{I} *and* $_{II}$. This optical difference in

depth resolved mean A-scan suggests micro-structural differences within these two layers. However, it is suggested that there is little mechanical changes (nano-hardness and elastic modulus) observed between these two layers, making it impossible to discriminate using the tactile method (G. W. Marshall et al., 2001).

Differentiation of AD from HD layers is clinically relevant, with extensive research conducted to determine the optical, mechanical and bio-chemical properties of AD (Azevedo et al., 2011; G. W. Marshall et al., 2001; Vidal et al., 2014). These properties of caries-affected dentine play an important role in forming effective bonds between dentine and resin-bonding adhesive material (Nakajima et al., 1995; Sattabanasuk, Burrow, Shimada, & Tagami, 2006; Van Meerbeek et al., 1993). Unfortunately, several studies which aimed to explore the resin- caries-affected dentine bond strengths have used caries detector dye (Banerjee et al., 2010) knowing it causes overstaining of sound dentine (Banerjee et al., 2003). While other researchers use simulated affected dentine, (Sattabanasuk et al., 2006; Van Meerbeek et al., 1993) which is dissimilar to clinical affected dentine. A recent systematic review which assessed the effectiveness of 3-step etch-and-resin adhesives to AD versus HD layers showed 60% with no difference in strength (Ekambaram, Yiu, & Matinlinna, 2015).

When ID and HD dentine layers were grouped together, LDA statistical method showed an overall cross-validated accuracy up to only 82.0%, with an ROC value up to 0.842 for ID, and HD. However, the accuracy of ANN showed significant increase in the overall cross-validated accuracy up to 94.0%, with 96.0% and 92.0% for ID and HD layer respectively. The most important clinically relevant finding was low false positive cases when discriminating between ID and HD layers. With only 25 samples and naturally variant dentine caries, 94% accuracy can be considered as a vital step for caries diagnostic research. However, ANN has been used first in the identification and

classification of dentine layers. Considering ANN classification is based on neural nets therefore it must be used with caution and it needs more validation for future use.

5.2 Bio-chemical composition and OCT of dentine layers

The aim of this in-vitro study is: to quantify and compare the major elements of ID, AD and HD layers and to explore the relationship between the major elements and OCT outcome measures of three dentine layers. Before presenting the results, methodological considerations will be discussed.

5.2.1 Methodological consideration

In dental research major elemental content of teeth has been evaluated using energy dispersive X-ray analysis (EDX) (Arnold et al., 2001; Daculsi et al., 1987), X-ray diffraction (Xue, Zavgorodniy, Kennedy, Swain, & Li, 2013), electrical impedance spectroscopy (EIS) (Eldarrat, Wood, Kale, & High, 2007), Fourier Transform Infrared Spectroscopy (FTIR), and X-ray Photoelectron Spectroscopy (XPS) (Zamudio-Ortega et al., 2014), Back scatter election microscope (Angker et al., 2004; Banerjee & Boyde, 1998). Meanwhile trace and minor elements are reported to use coupled plasma mass spectrometry (Brown et al., 2004) and EDX (Zaichick, Ovchjarenko, & Zaichick, 1999). Each of these methods has its specific purpose and certain advantages over other techniques. XRD, XRF, and FTIR spectrum analyses the samples in powder form to identify the crystallinity mineral phases and to determine the presence of elements depending on the strength of absorption of the respective elemental bands. However, XPS and EDS are surface techniques to quantify the element of the samples. EDX was found to be the most widely used method to quantify the elemental in weight and volume % during in-vitro analysis of healthy dentine (Arnold & Gaengler, 2007), root dentine (Arnold, Bietau, Renner, & Gaengler, 2007), carious dentine (Angker et al.,

2004; Arnold et al., 2001; Arnold et al., 2003; Magnus et al., 2013) and hyper-mineralized dentine (Daculsi et al., 1987; Khunkar et al., 2015).

Natural dentine is composed of almost 70% inorganic components, 20% organic and 10% water by weight and 45%, 33% and 22% by volume. Out of the 70% Ca and P are the major elements forming hydroxyapatite crystals [Ca5(PO4)3(OH)], while the remaining elements in trace amounts are Mg, Zn, C and O (Nanci, 2008). Therefore, evaluating only Ca and P as the major elements and comparing the difference between the three dentine layer provide sufficient understanding of bio-chemical composition, This trend has also been observed in other studies which compared the elements between sound and carious dentine (Angker et al., 2004; Arnold et al., 2001; Magnus et al., 2013). Magnesium (Mg) is found in higher levels in dentine at 2.12 wt% when compared to enamel at 1.11 wt % (LeGeros, 1990). However, they do not play a significant role in the overall composition of dentine structure and was therefore not included as part of the elemental analysis for this study. In addition, the Ca:P ratio of hydroxyapatite was calculated for this study, as it implies the basic overall composition of sound dentine which is around 1.67, subject to anatomical location, technique of assessment and type of crystal (Hennequin & Douillard, 1995; G. W. Marshall Jr, 1993).

EDX is a micro-analytical technique used in conjunction with SEM. The functioning of EDX is based on emission of the X-ray photons from external sources which strike with the atoms present on the surface of the investigation site, in return it generates a characteristic X-ray spectrum of that element. A resulting electron vacancy is occupied by an electron of higher shell, and an X-ray is emitted (characteristic X-rays) to equilibrate the energy variance between the two electrons. The X-ray detector processes the number of produced X-rays vs their energy. The energy of the X-ray is the unique

characteristic of the element from which the X-ray was emitted. A quantitative determination of the elements is attained and evaluated by using the band of the energy vs. the relative counts of the detected X-rays (Heslop-Harrison, 1990).

Within the limitation of this study, knowing EDX is a surface analysis and the spatial resolution is the function of the density of the material being scanned, the samples surfaces are required to be polished for better absorbance as they have limited beam spot size. However, these limitations were overcome by adopting some methods as discussed in the literature (Besinis, van Noort, & Martin, 2016). The samples were coated with standardized thickness of gold layer in vacuum evaporated carbon, using full frame scan mode instead of spot mode and maintaining the beam excitation voltage up to 20 kv increases the accuracy of the results. When analysing the elemental composition of demineralized dentine, the effect of dehydration is one of the major concerns (Nyvad, ten Cate, & Fejerskov, 1989; van Strijp, Buijs, & ten Cate, 1995). To overcome this, moist cotton was used throughout the experiments, although these measures were taken, specimen shrinkages and underestimation of elements may have occurred till the samples reach the stage of EDX analysis. Another limitation was the teeth samples were not standardized considering age, gender and other environmental factors, as it has been reported that concentration of Ca and P may vary due to these factors (Derise & Ritchey, 1974; Lakomaa & Rytomaa, 1977). Although all dentine slabs were prepared from coronal dentine caries, the elemental property of sound dentine differs from one anatomical site to another. Several studies have reported the quantitative difference of Calcium hydroxyl apatite mineral apatite [Ca10 (PO4)6 OH2] maturation ranges (59.30 - 41.82 wt%) between outermost EDJ to innermost circumpulpal dentine (Angker et al., 2004; Magne, Weiss, Bouler, Laboux, & Daculsi, 2001). Similar change in the distribution of mineral composition near mantel and circumpulpal dentine was observed when bovine teeth samples were used (Verdelis et

al., 2003; Verdelis et al., 2007). Magnesium replacing the Ca apatite crystals and formation of β-TCP whitelockite crystal deposition within translucent zone of AD layer is one of the classical and biochemical changes occurring in affected dentine (Daculsi et al., 1987). However during EDX analysis the aim was to measures the major elements and Ca:P ratios and its relationship with OCT outcome measures.

5.2.2 Difference of major elements between dentine layers

The Ca and P content detected in the ID layer of carious dentin was of significant lower amount when compared to quantities within AD and HD layers of remineralisable dentine. These overall results are consistent with other studies considering the difference observed between dentine caries zone (Angker et al., 2004; Arnold et al., 2007; Arnold et al., 2001; Arnold et al., 2003; Magnus et al., 2013) and size and depth between deep dentine cavities (Little, Dirksen, & Schlueter, 1965). The variations of Ca and P content observed in these three dentine layers are comparable to Arnold et al work which used natural coronal dentine caries lesion and EDX micro-surface analysis technique (Arnold et al., 2001; Arnold et al., 2003) while others used either simulated dentine caries (Daculsi et al., 1987), root dentine caries surfaces (Arnold et al., 2007), animal teeth (Tjaderhane, Hietala, & Larmas, 1995) and micro-radiography techniques (Angker et al., 2004; Tjaderhane et al., 1995). The Ca and P wt% observed of the ID, AD and HD layers in this study ranged between 6.52-19.67 and 2.22-9.84 respectively, whereas Arnold et al reported significant higher wt% of Ca and P content considering the variations seen within the three dentine layers (Arnold et al., 2003). The probable reason for this difference is due to the fact that dentine caries slab became desiccated and shirked rapidly during OCT and SEM scanning, losing the fluid, making it friable and the minerals quantities can drop low (van Strijp et al., 1995). The mean wt% of Ca and P when compared to another study, which used the dry weight technique sourced

from open cavities and the thick decay reported similar results, which was approximated at 6.37 and 3.61 respectively. A dentine slab with sound and demineralized areas exposed to air for 15 minutes can significantly reduce lesion depth up to 21% resulting in an underestimation of mineral loss up to 44% (van Strijp et al., 1995). Under the influence of microradiography this shrinkage resulting mineral loss is even estimated higher (Nyvad et al., 1989). The probable amount of shrinkage it may cause for the mineral loss take place under the influence of OCT broadband light at 1310nm is not known.

In this study, there was a significant difference of Ca and P wt% between three dentine layers, which is similar to the findings from previous studies (Arnold et al., 2001; Arnold et al., 2003). The Ca:P ratio which reflects the overall composition of hydroxyapatite crystal lattice was only present between the ID and AD layers and the ID and HD layers, which was also in accordance to previous findings by Arnold et al (Arnold et al., 2001; Arnold et al., 2003). In this study the Ca:P ratio of the ID, AD and HD layer was 3.28 (± 1.52), 2.11 (± 0.94) and 2.01 (± 0.30) respectively. Little et al reported Ca:P ratios from deeper layers infected of soft carious dentine ranged between 1:2.13, while harder carious dentine was approximately 1:2.23 and for sound dentine it was of 2.03 (Little et al., 1965). Another study reported the Ca:P ratio of healthy dentine as 1:2.04 (± 0.31)(Levine, 1973). The Ca:P ratios of AD and HD layers was similar to the previous research (Arnold et al., 2001; Arnold et al., 2003; Levine, 1973; Little et al., 1965). However, the large standard deviation of Ca:P ratio seen in ID layer was due to extremely low levels of P when compared to Ca in the ID layer. The probable reasons could be complete obliteration of the peritubular dentine in the ID layer which is mainly composed of calcium-proteolipid-phospholipid-phosphate complex (Gotliv & Veis, 2007) and during the demineralization process, phosphate and carbonate are rapidly dissolved, lowering the mineral-matrix ratio (LeGeros, 1990). Similar difference in the

phosphate and carbonate peaks was observed between caries-affected dentine and healthy dentine (Y. Wang et al., 2007). Arnold et al specifically observed Ca:P ratios of AD and HD layers in respect to intra and peritubular dentine and found that there was no difference, between HD layer and peritubular dentine, and the difference was present between the intratubular dentine of translucent and sound dentine. They also found that sound intertubular dentine and affected intertubular dentin does not differ (Arnold et al., 2001). Although Ca and P wt% values were lower and of significant different between AD and HD layers, the Ca:P ratio were of similar values. The results of this study suggest that Ca:P ratio, which represents an overall structure of the crystal lattice of the AD and HD layers is the same.

5.2.3 Relationship between major elements and OCT outcome measures of dentine layers

To establish the relationship between OCT outcome measures and elemental variables, four OCT outcome measures with the highest discrimination ability were included in this analysis (extracted from Table 4.16). I_{max}, R, AUC_T and AUC_{II} were the significant outcome measures when the dentine layers were analysed grouped and separately. Meanwhile for the element analysis, Ca, P wt% and Ca:P ratios were used.

I_{max} *and* R, were both significantly correlated with outcome measure, however, I_{max} *and* R, was moderately correlated respectively. The probable reason I_{max} was moderately correlated to Ca and P wt% and Ca:P ratio was because I_{max} appeared at air-surface interface at about 7.81 µm, which is approximately 11.72 µm thick considering the optical light started to increase from the background level (approximately at -3.91 µm). Similarly, in this study EDX was used as the surface elemental analysis technique with high penetration power and aiming for high accuracy. EDX analysis when performed at flat surfaces with beam voltage up to 20KV, following standard voltage range (10-20

KV), its accuracy can reach up to 90-95%(Zierold, 2002). However, within technical limitation such as the amount of radiation collected is limited up to 1% of the total emitted X-ray and increasing the voltage could have caused damage to dentine specimens.

Extensive research has been done on establishing the relationship between OCT integrated reflectivity and integrated mineral loss for dentine (Amaechi et al., 2004; Lee, Darling, et al., 2009; Manesh et al., 2009a; Manesh, Darling, & Fried, 2009b). To our best knowledge there has been no research done that evaluated the relationship between OCT light behaviour and the elemental analysis of dentine layers. A study reported significant amount of linear relationship between the element changes and mineral loss from demineralized dentine. The expected elemental change and mineral loss was linked to the difference occurring in small crystallites structures (Ten Cate, Nyvad, Van de Plassche-Simons, & Fejerskov, 1991). LeGeros assessed the crystallographic changes during dentinal caries process and have shown that change in crystal lattice parameters, crystal size / internal stain, crystal-chemical stability (LeGeros, 1990). The Ca substitution significantly expands in both a- and c-axis of lattice dimensions, whereas Mg incorporation during dentine caries process causes reduction in crystallinity and increase in crystal size (LeGeros, 1990). The behaviour of OCT broadband light is highly dependent on the ultra-structural morphology of dentine (I. Hariri et al., 2012; X. J. Wang et al., 1999). This behaviour of light has been extensively explained earlier considering the scattering distribution arising from variation of tissue orientation (Fried et al., 1995; Walton et al., 1976; Zijp & Bosch, 1993). In this study, significant positive correlation between backscattered intensity from OCT and amount of Ca and P observed in the ID, AD and HD layers could be explained considering the Ca and P was extensively leached out from the ID layer causing collapse of ITD and PTD leaving voids and scattered decomposed mass of

matrix. Extremely low amount of asymmetrical Ca and P mineral lattices mainly attached to the decomposed dentine matrix along with pockets of air and low intensity of backscattering from the ID layer is seen at I_{MAX} and can create change in the refractive index. The low-n medium can create change in the optical path length (Walton et al., 1976).

The mineral content and its distinct tubular arrangement; the tubules are cuffed around with highly mineralized layer termed as peritubular dentine, which is sharply demarcated from the intertubular dentine. The mineral content of these peritubular dentine is approximately 40% higher compared to intertubular dentine (Nanci, 2008). Dentine is considered highly evolved bio-mineralized neural crest derived mesenchymal structure, which functions with relaying sensitivity in and out of teeth, continuous reparative ability with aging and hypermineralised response to external stimuli like caries(Nanci, 2008) These self-regulated patho-morphological reactionary properties of dentine towards carious attack involves bio-chemical changes in the peritubular, intratubular dentine tubules (Arnold et al., 2001).

Some of the recent studies have established the change of mineral composition within sound and different layers of demineralizing dentine in natural occurring caries (Angker et al., 2004; Arnold et al., 2003) and to use this change of mineral composition in the detection of carious dentine (Banerjee & Boyde, 1998). Arnold et al, included natural occurring deep dentine caries and established the histological layers into outer demineralizing dentine (infected dentine), inner translucent dentine (affected dentine) and intact or sound dentine (healthy dentine). Using EDX, it was established that Ca and P wt% was lowest in the infected dentine (10.43 and 4.48 wt %), followed by affected dentine (28.40 and 14.14 wt%) and the highest amount was in healthy dentine 32.51 and 16.74 wt %). The Ca:P ratio of infected, affected and healthy dentine was

2.01, 1.98 and 1.92. The Ca wt% was highly significant in all three layers while the Ca:P ratio was only statistically different between infected and healthy dentine (Arnold et al., 2001). Ca:P ratio, representing the average apatite mineral composition in carious dentine shows the highest drop with the minimum value reported at less than 10 wt% compared to healthy dentine which ranges between 59-41 wt %, also considering 20 wt % is kept constant for organic content (Angker et al., 2004).

5.3 Mineral density and OCT of dentine layers

The aim of this study is: to quantify and compare the mineral density (MD) of the ID, AD and HD layers, to explore the relationship between the MD and OCT outcome measures of three dentine layers and to establish a cut-off point between ID and AD dentine layer using OCT outcome measures. Before presenting the results, methodological considerations, histological classification based on the MD of dentine layers and OCT data extraction methods will be discussed.

5.3.1 Methodological consideration

In this study thirty human teeth, with natural coronal dentine caries were used. Teeth transportation from extraction site, storage methods and selection of teeth were based on the same methods as the earlier objectives. To protect the outer dentine layer from drying during the transportation of teeth to University of Minnesota, a few protocols were adhered to. In-vitro studies with dentine samples under experiment use moist gauze to maintain the relative humidity which protects the samples from drying and undergoing dimensional changes (Charlton & Beatty, 1994; Grigoratos, Knowles, Ng, & Gulabivala, 2001). Carious teeth wrapped in moist gauze were air vacuumed in aluminium bags and sealed in thermocol box (Figure 3.20). In this study design the teeth were scanned using micro-CT X-ray imaging as gold standard method prior to preparing dentine slabs and OCT scanning. This approach aided in visualizing multiple

cross-sectional planes and in selecting the best sectioned plane with the biggest bulk of dentine layers using reconstructed volume data into high resolution 3D images of carious teeth. Also, keeping the tooth intact would pose lesser risk of the outer most infected dentine to desiccate. Within the limitation of this approach, acquiring a perfect section of dentine slab that matches the selected corresponding micro-CT slice was a challenging task. However, some steps were taken to minimize the mismatch: 1. roots were sectioned as flat as possible so it is placed perpendicular and straight at the base of the mould, 2. three reference points x1, x2 and y1 were marked on the tooth surface and translated to a resin block to achieve accurate reference for a cutting plane (Figure 3.24) and 3. the cutting blade was in straight line, matching the reference line over resin block (Figure 3.25). A second reference line was drawn next to the cutting line to create standardized thickness (2.0-2.4mm) of dentine slabs (Figure 3.25). Furthermore, nine samples were excluded to achieve perfect matching of planes by using surface landmark from micro-CT planes and stereomicroscope images of dentine slabs as references areas.

MD distribution patterns provide comprehensive information about changes occurring in healthy dentine as demineralization occurs during the carious process. Before calculating the MD, micro-CT imaging technique was used to reconstruct the volume data to select the best cross-sectional plane with sufficient spread of all three dentine layers and to calculate the respective attenuation coefficient of the ID, AD and HD layers. Micro-CT has an advantage over other conventional radiographic methods as it can create 3D volume data by acquiring high resolution spatial distribution of the attenuation coefficient. Studies in caries research has shown a difference in the grey values seen in reconstructed micro-CT slices that corresponds to the changes in X-ray attenuation coefficient which can be converted into MD values by using the appropriate calibration methods (Djomehri et al., 2015; Elliott, Wong, Anderson, Davis, & Dowker,

1998; Willmott, Wong, & Davis, 2007). A linear relationship between X-ray attenuation and the MD has been established which is extensively used in the demineralization and remineralization research of calcified tissues (Kinney et al., 1995; Kinney, Marshall, & Marshall, 1994; Zou, Hunter, & Swain, 2011). However, the determination of MD using attenuation coefficient requires some considerations as healthy and carious dentine limits the accuracy due to uneven specimen thickness and varying MD (Zou, Gao, Jones, Hunter, & Swain, 2009). Polychromatic X-rays compared to synchrotron radiation uses broad continuous spectrum in conventional benchtop micro-CT systems, which tends to shift towards higher energy (beam hardening) as the attenuation through samples rises, since low-energy photons are commonly more attenuated than high-energy photons (Chappard et al., 2006). The unwanted beam hardening which renders inaccuracies in measuring MD often appears as dark bands, cupping, flares or streak artifacts (Duerinckx & Macovski, 1978; Joseph & Spital, 1978). There are several techniques mentioned in the literature to correct the beam hardening effect by using beam filtration (Meganck, Kozloff, Thornton, Broski, & Goldstein, 2009), correction during reconstruction (Schuller et al., 2015) and MD calibration (Chen & Fok, 2014; T. T. Huang, Jones, He, Darendeliler, & Swain, 2007; Schweizer et al., 2007). In this study, after a few pilots, showed that with the beam voltage set at 90 kv, tube current 90 µA as the micro-CT scanning settings with a total of 720 projections with four frames per projection significantly minimized the shadows, artifacts and overlap of images. Managing the beam voltage and tube current follows the energy based beam hardening correction principle altering the polychromatic nature of X-ray into singular data (Van de Casteele, Van Dyck, Sijbers, & Raman, 2004) and averaging method was used to reduce the noise of each projection frame, enhancing the signal-to-noise ratio (Schwass, Swain, Purton, & Leichter, 2009).

To create standardized calibration systems for micro-CT, many researchers have used aluminium, copper or customized phantoms that relates to tissues under examination. Although, it is difficult to create phantoms which can mimic complex dentine structures, pure hydroxyapatite (HAP) sintered homogeneously with precise densities can commonly be used for calcified dental tissues (T. T. Huang et al., 2010; Schweizer et al., 2007). HAP customized phantoms has shown minimal polychromatic dishing effects when fabricated across a complete range of dimensions (Schwass et al., 2009). The preparation of HAP phantoms used in this study is detailed in Chen et al (Chen & Fok, 2014). Eleven phantoms discs with density ranged between 0.99 to 1.48 g cm^{-3}were used during every batch of micro-CT scanning of carious teeth for calibration standardization (Table 3.1). Considering the beam hardening artefact appears on the boarders of phantoms disks, measurement of the attenuation coefficient was restricted to the centre of the slice of each HAP tablet. MD values used for the phantoms in this study were within the established and known range of MD between carious to healthy dentine. Kinney et al showed that when synchrotron X-ray radiation was used sound and healthy dentine was 1.29 and 0.55 g cm^{-3} (Kinney et al., 1994). Willmott et al has reported the mineral concentration of healthy and carious dentine was 1.42 and 0.37 g cm^{-3} respectively, when quantifying the dentine layer in deciduous molars (Willmott et al., 2007). In another study which compared the MD of healthy dentine, translucent or hyper-mineralized and carious was between 1.48-1.59, 1.85-2.7 and 0.34-1.45 g cm^{-3} respectively (Djomehri et al., 2015). Considering all three studies, the MD values of eleven phantoms (Table 3.3) was well within the known MD values of dentine layers, except for the Djomehri et al study in which translucent dentine was above 1.85 g cm^{-3} and was not applicable in this study.

Natural dentine caries lesions is a continuum of biological layers, and to clinically and histologically identify boundaries between these layers is a challenging task (A.

Banerjee, E. A. Kidd, et al., 2000; Zheng et al., 2003). Similarly, there is lack of evidence in the literature which establishes the boundary between dentine layers using MD, and a precise delineation of dentine caries lesion is difficult to achieve (Wong, Willmott, & Davis, 2006). Considering this challenge the identification and extraction of MD for each layer was first done by visual segmentation via detectable difference of intensity, followed by drawing an approximately standardized automated ROI to extract the range from mean to maximum MD values of each layer (Figure 4.17). The mean to maximum MD value of ID and HD layers was 0.82 – 1.10 and 1.53 – 1.78 g cm^{-3} respectively; these values matched the MD values from previous studies (Djomehri et al., 2015; Kinney et al., 1994; Willmott et al., 2007), whereas the range of MD value for AD layer was 1.13 – 1.38 g cm^{-3} which matched the MD values reported by Wong et al as boundary of carious and healthy dentine (Wong et al., 2006). The mean extracted MD values from automated ROI provided a reference to identify the dentine layers and were further used to calculate the MD of the line plots which will be compared to OCT line plots.

Standardization of line plots to extract MD values and OCT backscatter were achieved by using 3.05mm as a standard length of copper grid and distance between two adhesive tape provided a reference in x-y direction and x-z direction respectively. A straight line ruler was used to draw a line plot (3.05mm) in VG studio Max which self-generated qualitative and quantities attenuation coefficient measurements and later converted to MD values. Whereas an added feature was customized within bespoke OCT software which averaged 20 A-scans to generate one single line plot with corresponding length of copper grid (3.05mm) and quantitative intensity in excel sheet were exported. To avoid the line plot from being confounded by specular reflection, another feature within the OCT bespoke software was visualization and selection of cross-section (b-scan) to draw the line plot and extract its corresponding light intensity. 12 pixels below tooth-air

interface was the chosen depth and place for drawing the line plot. Since the OCT and micro-CT scanning was done at different resolution and needed to be equated with a standard distance of 3.05mm, the truncation formula was developed to compensate the OCT and micro-CT pixel distance aspect ratio of 3.41 µm and 2.43 µm respectively.

5.3.2 Difference of MD, I and ΔI between dentine layers

MD of healthy and carious dentine has been studied by various researchers using micro-radiography technique (Arends et al., 1989; Chen & Fok, 2014; Djomehri et al., 2015; Joves et al., 2013; Kinney et al., 1995; Kinney et al., 1994; Neves A, Coutinho, Vivan Cardoso, Jaecques, & Van Meerbeek, 2010; Schwass et al., 2009; Willmott et al., 2007; Wong et al., 2006; Zou et al., 2011). Low MD values of the ID layer are a combination of the bacterial zone and the inner soft dentine caries. The volume percentage of the bacterial zone is contributed by 7% of inorganic, 25% organic and 68% water or air occupying the pore spaces. While the partially demineralized dentine loses 25% of the inorganic content and retains up to 30% of organic portion. The hard portion of caries-affected dentine only loses 1/6 of inorganic and 1/12 of organic portion when compared to sound dentine (Manly & Deakins, 1940).

In order to calculate the MD values of dentine layers, it was essential to determine the boundaries between ID and AD and AD and HD layers. To established the cut-off point between ID and AD preference was given to use the average of maximum MD value (1.10 gm cm-^{3}) rather than average of mean MD values (0.82 gm cm-^{3}) of ID layer as reference point and was applied on a line plot to segment the ID from the AD layer. Willmott et al aimed to delineate carious from healthy dentine using mineral density and used the upper and lower limits of MD to establish a similar approach to attain a cut-off point, the boundary between these two layers is considered clinically extremely relevant as it aids in determining caries removal endpoint (Willmott et al., 2007). The average of

maximum MD from the ID layer was considered higher compared to other studies which reported mean MD of carious dentine (Djomehri et al., 2015; Willmott et al., 2007), Therefore in this study considering the upper limit of the MD values will not compromise or a line plot was 0.87 g cm^{-3} (± 0.10), which is well within the range of the MD values of carious dentine reported in previous research (Djomehri et al., 2015).

Preliminary attenuation coefficient converted to the MD values for the AD and HD layers between the mean and maximum was 1.13-1.38 and 1.53-1.78 g cm^{-3}. The cut-off point between AD and HD was established by using the average of the maximum MD value of the AD (1.38 gm g cm^{-3}) applied on the line plot to segment the AD from the HD layer. The extracted MD value of the AD layer from the line plot was 1.16 g cm^{-3} (± 0.10), which was approximately near to MD values 1.20 g cm^{-3}used in a research by Wong et al to outline between carious and sound dentine. However it was not clearly stated in their research if AD layer was included as part of carious dentine (Wong et al., 2006). Joves et al reported naturally occurring AD layer entails significant morphological differences due to biological variations and the mean MD at 0 to 50 µm depth can range from 7.91 (± 3.64) to 27.75 (± 9.27) volume % (Joves et al., 2013).

The structural composition of healthy dentine can be assessed by volumetric density of HAP and its distribution within the highly mineralized peritubular dentine and intertubular dentine (Nanci, 2008). Neves et al used micro tomography to quantify mineral density for sound enamel and dentine as 2.89 and 1.74 g cm^{-3}respectively (Neves A et al., 2010). In this study the MD of healthy dentine was ranged between 1.32 – 1.86 g cm^{-3}with 1.52 g cm^{-3}as mean value, these values are similar with previously reported MD values of sound dentine. The MD calculated for healthy dentine in this study was of molar teeth and mostly the line plot was towards the periphery dentine of teeth or near to the enamel. The densities of molars are estimated around 1.62 g

cm^{-3}and for incisors approximately 1.46 g/cm3(Davis & Wong, 1996; Manly & Deakins, 1940), with the MD at peripheral dentine reported at 1.56 g cm^{-3}and circumpulpal dentine at 1.34 g cm^{-3}(Kinney et al., 1994).

OCT *I* measure showed significant difference only between the ID and HD layers. It seemed that wide-ranged standard deviation of the AD layer compared to the ID and HD was too heterogeneous and extracting backscattered intensity from this layer may overlap with adjacent dentine layers. The mean OCT *I* measure of the AD (89.21) was much closer to that of the HD (88.97), while that of the ID (91.12) was significantly increased and different from both layers (a.u.). Meanwhile, ΔI showed significant difference between all layers except between AD and HD. This outcome measure was calculated based on the relationship and trends of the data points using a scatter plot between the MD and the OCT *I* measure. This seemed to be a probable reason for a significant difference being observed between the ID and AD layers. An increased vertical spread suggested a wider range of optical intensity and was a unique characteristic of the ID layer and indicative of heterogeneous dentine layer producing inconsistent backscattered intensity.

5.3.3 Relationship between MD and OCT outcome measures of dentine layers

Several studies has shown a linear relationship between the magnitude of OCT measures and mineral loss when experimenting with artificial enamel caries (Amaechi et al., 2003; R. S. Jones, C. L. Darling, J. D. Featherstone, & D. Fried, 2006; Ngaotheppitak, Darling, & Fried, 2005), simulated dentine caries model (Amaechi et al., 2004; Lee, Darling, et al., 2009; Manesh et al., 2009a, 2009b), and natural dentine caries (Manesh et al., 2008). The Pearson correlation between the OCT data and the mineral density from simulated smooth surface enamel caries is reported as r = 1.00 (Amaechi et al., 2004), natural occlusal carious lesion as r= 0.75 (Douglas, Fried, &

Darling, 2010) and natural white spot lesion as *r*=0.68 (Ngaotheppitak et al., 2005). However, common outcome measures used in these studies was integrated reflectivity (loss of OCT intensity) with depth as a function to assess the lesion severity which was matched with the integrated mineral loss by matching the profiles. Since the aim is to assess the lesion severity within depth, the incident linearly polarized light and the reflectivity in the orthogonal state to the incident polarization can be directly integrated to assess the lesion severity(Douglas et al., 2010; D. Fried et al., 2002). Also, many of these studies used transverse microradiography (TMR) and digital microradiography (DM). Although TMR can permit measurement at micro scale, this method requires the samples to be physically cut into very thin sections, risking loss of material and creating a superimposition effect due to the variation in anatomy (Damen, Exterkate, & ten Cate, 1997). Whereas, with recent development in radiographic techniques, Micro-CT has an edge over TMR as it does not require specimen preparation and enables 3D construction of the samples at ultrahigh micrometres resolution (Neves A et al., 2010; Swain & Xue, 2009; Zaslansky et al., 2010; Zou et al., 2011).

In this study, the aim was not to assess the lesion severity, therefore the integrated reflectivity in the perpendicular axis (B-scans) of OCT scans was not used as an outcome, preference was given to average the means of the line profiles from en-face direction of each dentine layer and compare this with the corresponding line profile of the dentine layer and its respective mean density. It is known that the integrated reflectivity in the orthogonal axis of natural lesion correlate well with the integrated mineral loss (D. Fried et al., 2002; Ngaotheppitak et al., 2005). However, when analysing the surface OCT intensity, there are strong reflections, which can interfere with the measurement; these high intensity surface reflections were avoided by selecting the enface plane approximately 12 pixels or 40-50μm below the tooth air-interface. During the selection of enface plane within 12 pixel depth, the high intensity reflections

were not included, also the outcome measures are not linked to depth resolved intensity and to fix the depth values (200µm) between the integrated values and the levels of demineralization may not be applicable in this study as suggested by Fried

(D. Fried et al., 2002).

OCT *I* based on the optical reflectivity and OCT *ΔI* calculated based on the optical characteristics of the dentine layer, both outcome measures showed significant correlation with the MD of corresponding dentine structures. Yet, the correlation between mean OCT *I* and MD was 0.367 and was considered low. The correlation between mean OCT *ΔI* and MD was 0.531 and considered a moderate relationship. Manesh et al showed, although the integrated reflectivity increased with the increase in demineralization as seen in our study, the correlation between the integrated reflectivity and the MD using PS-OCT and TMR was as low as r=0.419 when scanning natural root dentine caries (Manesh et al., 2008). However, when simulated root dentine lesion on bovine and human tissues was induced, the correlation significantly increased up to r= 0.68 when using SS-OCT (Natsume et al., 2011) and r= 0.77 when using PS-OCT (Manesh et al., 2008). Both the studies had used TMR to measure the mineral loss and suggested the low correlation was due to the fracture of the friable carious dentine during sample preparation (Manesh et al., 2008). Natsume et al, reported difficulty in locating the MD investigation site to plot the OCT depth profile on the same corresponding location and subjective demarcation of sound and healthy dentine relying on black-white contrast (Natsume et al., 2011). These factors were considered in this study, by using micro-CT as a non-destructive technique, using copper mesh for standardization and measurement and detailed matching of stereo-microscope images of dentine slabs and micro-CT slices. It seemed the probable reason for low correlation between MD and OCT outcome measure was due to inherent nature of heterogeneous

natural caries lesion, which may overlap between ID and AD layers; and AD and HD layers. Also, the line plot used for extracting OCT intensity was at the average of 20 a-scans which may not be sufficient to measure the average enface intensity of each dentine layer.

5.3.4 OCT cut-off point between ID and AD layer

ΔI measure showed significant difference between ID and AD and AD and HD. Also, it was statistically significant with moderate correlation with MD. This outcome measure can be considered as a significant finding clinically, the differentiation between ID and AD can enhance the optimization of cavity preparation by identifying the AD layer before entering the sound dentine. This early identification and differentiation of dentine layer will help establish accurate caries excavation endpoint and reduce risks of pulpal exposure. The emphasis on methods help aid dentists in finding accurate depth point, and enhance clinical decision in clinical decision making (Rindal et al., 2014)

Receiver operating characteristic (ROC) curve analysis showed a cut off value at 9.29 (a.u.), the ΔI value showed 95% sensitivity and 75.4% specificity in differentiating ID from AD layer with ROC value of 0.937. In OCT research, cut-off points have been used to demarcate between sound and demineralized tissues in function of lesion depth (Espigares et al., 2015; Le, Darling, & Fried, 2010). However, it is complicated to use exponential decay of light as parameter to demarcate the tissues, 1/e2 decrease in intensity can be chosen as an approach but this is not effective as a standard method (Can, Darling, Ho, & Fried, 2008). In this study, we have adapted a novel method of assessing the trend of ID layers and compared with AD layer using the scatter plot which suggested that ID layers is higher on vertical spread while AD is on horizontal spread. However, it should be noted that these trends are observed within the limitation

of this current study and it is recommended to apply these results on larger sample sizes to extrapolate the findings.

CHAPTER 6: CONCLUSION

Emphasis is made in the literature to develop an accurate method to delineate the boundary between caries-infected and caries-affected dentine clinically. This is considered as one of the fundamental research question in caries management (A. Banerjee, E. A. Kidd, et al., 2000; Neves, Coutinho, Cardoso, et al., 2011; D. Ricketts, 2001; Schwendicke et al., 2016; Secilmis et al., 2013). Preservation of caries-affected dentine during caries removal will reduce risk of pulp exposure and enhance structural integrity and maintain tooth function. To address this unmet need, the potential of OCT was explored.

Within the limitations of this study, it can be concluded that the attenuation characteristics of OCT backscattered intensity, the derived outcome measure can significantly differentiate and predict the dentine layers with high accuracy. This conclusion was based on the following:

i. The OCT software colour scheme expressed in dB correspond significantly to the microstructural changes observed in the SEM images of all three dentine layers.
ii. Difference in rate of light attenuation between the ID, AD and HD layers observed in two phases signifies unique optical characteristic of each layer.
iii. ID showed polynomial pattern ($R^2 = 0.794$) as goodness of fit model which was different to exponential attenuation seen in AD and HD ($R^2 = 0.783$ and 0.998).
iv. I_{max}, and AUC_T are two common OCT outcome measures that significantly differentiated any two dentine layers.
v. ANN showed 84% and 88% accuracy in delineating ID and AD, and AD and HD respectively.

vi. Significant differences was found between Ca and P wt % and Ca:P ratio between all three dentine layers, however, there was no significant difference between the AD and HD layers.

vii. Significant positive relationship was found between Ca and P wt% and I_{max} as OCT outcome measure; it showed moderate correlation.

viii. Significant negative relationship was found between Ca:P ratio and I_{max} as OCT outcome measure; it showed moderate correlation.

ix. Significant differences of MD was found between all three dentine layers

x. ΔI showed significant difference between all dentine layers except AD and HD

xi. Significant negative correlation was found between MD and ΔI as OCT outcome measure, it showed moderate correlation.

xii. ΔI was able to discriminate ID and AD layer with 90.5% sensitivity and 81.0% specificity

6.1 Study limitations

To our knowledge, this is the first study which optically characterised dentine layers with an aim to develop outcome measures to aid in high accuracy of prediction of dentine layers, making comparison with available literature challenging. The limitations of the study are as follows:

i. natural occurring dentine caries from extracted teeth are exposed to different variables in oral environment and may affect the lesion accordingly

ii. Age and gender of patients who consented to give his/her extracted tooth was not recorded, structural and compositional may vary- especially in the caries-affected and healthy dentine layer.

iii. Natural dentine caries tends to desiccate quickly, some variation may have occurred in outer dentine layers during specimen scanning and exposure to radiation.

iv. The organic content of dentine layers was not considered to estimate its relationship with OCT intensity and its measures.

Developing the OCT outcome measures and testing its accuracy shows the capability of this system to identify and discriminate dentine layers. Although this study has shown significant moderate correlation with composition and mineral density, it may not completely reveal these relationships as due to structural variations which may co-exist with certain elemental composition and density of investigated dentine layers.

6.2 Clinical significance

International Caries Consensus Collaboration (ICCC) on managing deep carious lesions have recently agreed that currently used criterion such as hardness, colour, moisture, metabolic product and visual characteristics are weak indicators to be used by dentists during removal of dentine caries lesions. Considering these uncertainties, challenges and strong recommendations, there is growing evidence which demonstrates less invasive strategies are effective for managing dental caries, while dentists are encouraged to provide risk-based excavation strategies (F. S. Schwendicke, E J., 2016). The results of this study showed that OCT could be a potentially accurate diagnostic tool to assist dentists with decision-making during caries removal. Optical characterization will aid in discriminating these layers during excavation and gain familiarity with the properties of substrate dentine for successful restorations.

6.3 Future studies

Suggestions for future studies are as following:

i. Using significant OCT outcome measures to colour map dentine layers and assess its detection accuracy on a new set of data.
ii. Validate the OCT outcome measure in function of depth for dentine caries that has direction of progression in occlusal pulpal direction.
iii. Validate the OCT outcome measures to study other characteristic properties of the residual dentine for use of adhesion.
iv. Validate the use of OCT outcome measures by real time excavation of the ID layer in an in-vitro set up.

REFERENCES

Aamdal-Scheie, A., Luan, W. M., Dahlen, G., & Fejerskov, O. (1996). Plaque pH and microflora of dental plaque on sound and carious root surfaces. *Journal of Dental Research, 75*(11), 1901-1908.

Adler, D. C., Ko, T. H., & Fujimoto, J. G. (2004). Speckle reduction in optical coherence tomography images by use of a spatially adaptive wavelet filter. *Opt Lett, 29*(24), 2878-2880.

Al-Khateeb, S., Exterkate, R., De Josselin de Jong, E., Angmar-Månsson, B., & Ten Cate, J. (2002). Light-induced fluorescence studies on dehydration of incipient enamel lesions. *Caries Research, 36*(1), 25-30.

Alfano, R., & Yao, S. (1981). Human teeth with and without dental caries studied by visible luminescent spectroscopy. *Journal of Dental Research, 60*(2), 120-122.

Alves, L. S., Fontanella, V., Damo, A. C., Ferreira de Oliveira, E., & Maltz, M. (2010). Qualitative and quantitative radiographic assessment of sealed carious dentin: a 10-year prospective study. *Oral Surgery, Oral Medicine, Oral Pathology, Oral Radiology and Endodontics, 109*(1), 135-141. doi: 10.1016/j.tripleo.2009.08.021

Amaechi, B. T., Higham, S. M., Podoleanu, A. G., Rogers, J. A., & Jackson, D. A. (2001). Use of optical coherence tomography for assessment of dental caries: quantitative procedure. *Journal of Oral Rehabilitation, 28*(12), 1092-1093.

Amaechi, B. T., Podoleanu, A. G., Komarov, G., Higham, S. M., & Jackson, D. A. (2004). Quantification of root caries using optical coherence tomography and microradiography: a correlational study. *Oral Health Prev Dent, 2*(4), 377-382.

Amaechi, B. T., Podoleanu, A. G., Kornarov, G. N., Rogers, J. A., Higham, S. M., & Jacksow, D. A. (2003). Application of optical coherence tomography for imaging and assessment of early dental caries lesions. *Laser Physics, 13*(5), 703-710.

Angker, L., Nockolds, C., Swain, M. V., & Kilpatrick, N. (2004). Quantitative analysis of the mineral content of sound and carious primary dentine using BSE imaging. *Archives of Oral Biology, 49*(2), 99-107.

Arends, J., Ruben, J., & Jongebloed, W. L. (1989). Dentine caries in vivo. Combined scanning electron microscopic and microradiographic investigation. *Caries Research, 23*(1), 36-41.

Arnold, W., Bietau, V., Renner, P. O., & Gaengler, P. (2007). Micromorphological and micronanalytical characterization of stagnating and progressing root caries lesions. *Archives of Oral Biology, 52*(6), 591-597.

Arnold, W., & Gaengler, P. (2007). Quantitative analysis of the calcium and phosphorus content of developing and permanent human teeth. *Ann Anat, 189*(2), 183-190.

Arnold, W., Gaengler, P., & Saeuberlich, E. (2000). Distribution and volumetric assessment of initial approximal caries lesions in human premolars and permanent molars using computer-aided three-dimensional reconstruction. *Archives of Oral Biology, 45*(12), 1065-1071.

Arnold, W., Konopka, S., & Gaengler, P. (2001). Qualitative and quantitative assessment of intratubular dentin formation in human natural carious lesions. *Calcified Tissue International, 69*(5), 268-273.

Arnold, W., Konopka, S., Kriwalsky, M., & Gaengler, P. (2003). Morphological analysis and chemical content of natural dentin carious lesion zones. *Ann Anat, 185*(5), 419-424.

Astvaldsdottir, A., Ahlund, K., Holbrook, W. P., de Verdier, B., & Tranaeus, S. (2012). Approximal Caries Detection by DIFOTI: In Vitro Comparison of Diagnostic Accuracy/Efficacy with Film and Digital Radiography. *Int J Dent, 2012*, 326401.

Ayna, B., Celenk, S., Atakul, F., Sezgin, B., & Ozekinci, T. (2003). Evaluation of clinical and microbiological features of deep carious lesions in primary molars. *Journal of Dentistry for Children, 70*(1), 15-18.

Ayo-Yusuf, O. A., Driessen, C. H., & Botha, A. J. (2005). SEM-EDX study of prepared human dentine surfaces exposed to gingival retraction fluids. *Journal of Dentistry, 33*(9), 731-739.

Azevedo, C. S., Trung, L. C., Simionato, M. R., Freitas, A. Z., & Matos, A. B. (2011). Evaluation of caries-affected dentin with optical coherence tomography. *Braz Oral Res, 25*(5), 407-413.

Bader, J. D., & Shugars, D. A. (1997). What do we know about how dentists make caries related treatment decisions? *Community dent and oral epidemiol, 25*(1), 97-103.

Bader, J. D., & Shugars, D. A. (2006). The evidence supporting alternative management strategies for early occlusal caries and suspected occlusal dentinal caries. *Journal of Evidence-Based Dental Practice, 6*(1), 91-100.

Bader, J. D., Shugars, D. A., & Bonito, A. J. (2001). Systematic reviews of selected dental caries diagnostic and management methods. *Journal of Dental Education, 65*(10), 960-968.

Bader, J. D., Shugars, D. A., & Bonito, A. J. (2002). A systematic review of the performance of methods for identifying carious lesions. *Journal of Public Health Dentistry, 62*(4), 201-213.

Baelum, V. (2008). Caries management: technical solutions to biological problems or evidence-based care? *Journal of Oral Rehabilitation, 35*(2), 135-151.

Baelum, V., Heidmann, J., & Nyvad, B. (2006). Dental caries paradigms in diagnosis and diagnostic research. *European Journal of Oral Sciences, 114*(4), 263-277.

Bakhsh, T. A., Sadr, A., Shimada, Y., Tagami, J., & Sumi, Y. (2011). Non-invasive quantification of resin–dentin interfacial gaps using optical coherence tomography: validation against confocal microscopy. *Dental Materials, 27*(9), 915-925.

Banerjee, A. (2013). Minimal intervention dentistry: part 7. Minimally invasive operative caries management: rationale and techniques. *British Dental Journal, 214*(3), 107-111.

Banerjee, A., & Boyde, A. (1998). Autofluorescence and mineral content of carious dentine: scanning optical and backscattered electron microscopic studies. *Caries Research, 32*(3), 219-226.

Banerjee, A., Gilmour, A., Kidd, E., & Watson, T. (2004). Relationship between S. mutans and the autofluorescence of carious dentin. *American Journal of Dentistry, 17*(4), 233-236.

Banerjee, A., Kellow, S., Mannocci, F., Cook, R. J., & Watson, T. F. (2010). An in vitro evaluation of microtensile bond strengths of two adhesive bonding agents to residual dentine after caries removal using three excavation techniques. *Journal of Dentistry, 38*(6), 480-489.

Banerjee, A., Kidd, E. A., & Watson, T. F. (2000). In vitro evaluation of five alternative methods of carious dentine excavation. *Caries Research, 34*(2), 144-150.

Banerjee, A., Kidd, E. A., & Watson, T. F. (2003). In vitro validation of carious dentin removed using different excavation criteria. *American Journal of Dentistry, 16*(4), 228-230.

Banerjee, A., Watson, T., & Kidd, E. (2000). Conservative dentistry: dentine caries excavation: a review of current clinical techniques. *British Dental Journal, 188*(9), 476-482.

Banerjee, A., Watson, T. F., & Kidd, E. A. (2000a). Dentine caries excavation: a review of current clinical techniques. *British Dental Journal, 188*(9), 476-482.

Banerjee, A., Watson, T. F., & Kidd, E. A. (2000b). Dentine caries: take it or leave it? *Dental Update, 27*(6), 272-276.

Banerjee, A., Yasseri, M., & Munson, M. (2002). A method for the detection and quantification of bacteria in human carious dentine using fluorescent in situ hybridisation. *Journal of Dentistry, 30*(7-8), 359-363.

Beighton, D. (2005). The complex oral microflora of high-risk individuals and groups and its role in the caries process. *Community Dentistry and Oral Epidemiology, 33*(4), 248-255.

Belda-Ferre, P., Alcaraz, L. D., Cabrera-Rubio, R., Romero, H., Simon-Soro, A., Pignatelli, M., & Mira, A. (2012). The oral metagenome in health and disease. *ISME J, 6*(1), 46-56.

Bergenholtz, G., & Spangberg, L. (2004). Controversies in Endodontics. *Critical Reviews in Oral Biology and Medicine, 15*(2), 99-114.

Bertassoni, L. E., Habelitz, S., Marshall, S. J., & Marshall, G. W. (2011). Mechanical recovery of dentin following remineralization in vitro—an indentation study. *Journal of Biomechanics, 44*(1), 176-181.

Besinis, A., van Noort, R., & Martin, N. (2016). The use of acetone to enhance the infiltration of HA nanoparticles into a demineralized dentin collagen matrix. *Dental Materials, 32*(3), 385-393.

Bin-Shuwaish, M., Yaman, P., Dennison, J., & Neiva, G. (2008). The correlation of DIFOTI to clinical and radiographic images in Class II carious lesions. *Journal of the American Dental Association, 139*(10), 1374-1381.

Bjorndal, L. (2002). Dentin and pulp reactions to caries and operative treatment: biological variables affecting treatment outcome. *Endodontic Topics, 2*(1), 10-23.

Bjorndal, L. (2008). The caries process and its effect on the pulp: the science is changing and so is our understanding. *Pediatric Dentistry, 30*(3), 192-196.

Bjorndal, L., Darvann, T., & Lussi, A. (1999). A computerized analysis of the relation between the occlusal enamel caries lesion and the demineralized dentin. *European Journal of Oral Sciences, 107*(3), 176-182.

Bjorndal, L., & Larsen, T. (2000). Changes in the cultivable flora in deep carious lesions following a stepwise excavation procedure. *Caries Research, 34*(6), 502-508. doi: 16631

Bjorndal, L., Larsen, T., & Thylstrup, A. (1997). A clinical and microbiological study of deep carious lesions during stepwise excavation using long treatment intervals. *Caries Research, 31*(6), 411-417.

Bjørndal, L., & Thylstrup, A. (1995). A structural analysis of approximal enamel caries lesions and subjacent dentin reactions. *European Journal of Oral Sciences, 103*(1), 25-31.

Black, G. V. (1908). *Cavity preparation: The technical procedures in filling teeth. In A Work on Operative Dentistry in Two Voumes* (Vol. 2): Chicago: Medico-dental publishing Co.

Bönecker, M., Toi, C., & Cleaton-Jones, P. (2003). Mutans streptococci and lactobacilli in carious dentine before and after Atraumatic Restorative Treatment. *Journal of Dentistry, 31*(6), 423-428.

Boston, D. W., & Liao, J. (2004). Staining of non-carious human coronal dentin by caries dyes. *Operative Dentistry, 29*(3), 280-286.

Botello-Harbaum, M. T., Matthews, A. G., Collie, D., Vena, D. A., Craig, R. G., Curro, F. A.,. Network, P. (2012). Level of oral health impacts among patients

participating in PEARL: a dental practice-based research network. *Community Dentistry and Oral Epidemiology, 40*(4), 332-342.

Braga, M. M., Mendes, F. M., & Ekstrand, K. R. (2010). Detection activity assessment and diagnosis of dental caries lesions. *Dental Clinics of North America, 54*(3), 479-493.

Braun, A., Graefen, O., Nolden, R., & Frentzen, M. (2000). Comparative study of conventional caries diagnosis versus laser fluorescence measurement. *Deutsche Zahnarztliche Zeitschrift, 55*(4), 248-251.

Bretz, W. A., Corby, P. M., Hart, T. C., Costa, S., Coelho, M. Q., Weyant, R. J., . . . Schork, N. J. (2005). Dental caries and microbial acid production in twins. *Caries Research, 39*(3), 168-172.

Brezinski, M. E. (2006). *Optical coherence tomography: principles and applications*: Access Online via Elsevier.

Brodbelt, R., O'brien, W., Fan, P., Frazer-Dib, J., & Yu, R. (1981). Translucency of human dental enamel. *Journal of Dental Research, 60*(10), 1749-1753.

Brown, C. J., Chenery, S. R., Smith, B., Mason, C., Tomkins, A., Roberts, G. J., . . . Tiberindwa, J. V. (2004). Environmental influences on the trace element content of teeth--implications for disease and nutritional status. *Archives of Oral Biology, 49*(9), 705-717.

Burt, B. A., & Pai, S. (2001). Sugar consumption and caries risk: a systematic review. *Journal of Dental Education, 65*(10), 1017-1023.

Can, A. M., Darling, C. L., Ho, C., & Fried, D. (2008). Non-destructive assessment of inhibition of demineralization in dental enamel irradiated by a lambda=9.3-microm CO2 laser at ablative irradiation intensities with PS-OCT. *Lasers in Surgery and Medicine, 40*(5), 342-349.

Ccahuana-Vasquez, R. A., Tabchoury, C. P., Tenuta, L. M., Del Bel Cury, A. A., Vale, G. C., & Cury, J. A. (2007). Effect of frequency of sucrose exposure on dental biofilm composition and enamel demineralization in the presence of fluoride. *Caries Research, 41*(1), 9-15.

Cevc, G., Schara, M., & Skaleric, U. (1980). The caries resistance of human teeth is determined by the spatial arrangement of hydroxyapatite microcrystals in the enamel. *Nature, 286*(5771), 425-426.

Chan, A. C., Darling, C. L., Chan, K. H., & Fried, D. (2014). Attenuation of near-IR light through dentin at wavelengths from 1300-1650-nm. *Proc Soc Photo Opt Instrum Eng, 8929*, 89290m.

Chappard, C., Basillais, A., Benhamou, L., Bonassie, A., Brunet-Imbault, B., Bonnet, N., & Peyrin, F. (2006). Comparison of synchrotron radiation and conventional x-ray microcomputed tomography for assessing trabecular bone microarchitecture of human femoral heads. *Medical Physics, 33*(9), 3568-3577.

Charlton, D. G., & Beatty, M. W. (1994). The effect of dentin surface moisture on bond strength to dentin bonding agents. *Operative Dentistry, 19*(4), 154-158.

Chen, Y., & Fok, A. (2014). Stress distributions in human teeth modeled with a natural graded material distribution. *Dental Materials, 30*(12), e337-348.

Chen, Y., Otis, L., Piao, D., & Zhu, Q. (2005). Characterization of dentin, enamel, and carious lesions by a polarization-sensitive optical coherence tomography system. *Appl Opt, 44*(11), 2041-2048.

Chew, H. P., Zakian, C. M., Pretty, I. A., & Ellwood, R. P. (2014). Measuring initial enamel erosion with quantitative light-induced fluorescence and optical coherence tomography: an in vitro validation study. *Caries Research, 48*(3), 254-262.

Chhour, K. L., Nadkarni, M. A., Byun, R., Martin, F. E., Jacques, N. A., & Hunter, N. (2005). Molecular analysis of microbial diversity in advanced caries. *Journal of Clinical Microbiology, 43*(2), 843-849.

Chong, M. J., Seow, W. K., Purdie, D. M., Cheng, E., & Wan, V. (2003). Visual-tactile examination compared with conventional radiography, digital radiography, and Diagnodent in the diagnosis of occlusal occult caries in extracted premolars. *Pediatric Dentistry, 25*(4), 341-349.

Cortes, D., Ellwood, R., & Ekstrand, K. (2003). An in vitro comparison of a combined FOTI/visual examination of occlusal caries with other caries diagnostic methods and the effect of stain on their diagnostic performance. *Caries Research, 37*(1), 8-16.

Crespo, K. E., Torres, J. E., & Recio, M. E. (2004). Reasoning process characteristics in the diagnostic skills of beginner, competent, and expert dentists. *Journal of Dental Education, 68*(12), 1235-1244.

Daculsi, G., LeGeros, R. Z., Jean, A., & Kerebel, B. (1987). Possible physico-chemical processes in human dentin caries. *Journal of Dental Research, 66*(8), 1356-1359.

Damen, J. J., Exterkate, R. A., & ten Cate, J. M. (1997). Reproducibility of TMR for the determination of longitudinal mineral changes in dental hard tissues. *Advances in Dental Research, 11*(4), 415-419.

Darling, C. L., Huynh, G. D., & Fried, D. (2006). Light scattering properties of natural and artificially demineralized dental enamel at 1310nm. *J biomed opt, 11*(3), 034011-034023.

Davis, G. R., & Wong, F. S. (1996). X-ray microtomography of bones and teeth. *Physiological Measurement, 17*(3), 121-146.

de Almeida Neves, A., Coutinho, E., Cardoso, M. V., Lambrechts, P., & Van Meerbeek, B. (2011). Current concepts and techniques for caries excavation and adhesion to residual dentin. *J Adhes Dent, 13*(1), 7-22.

de Oliveira Mota, C. C., Gueiros, L. A., Maia, A. M., Santos-Silva, A. R., Gomes, A. S., Alves Fde, A., . . . Lopes, M. A. (2013). Optical coherence tomography as an auxiliary tool for the screening of radiation-related caries. *Photomedicine and Laser Surgery, 31*(7), 301-306.

Dennison, J. B., & Sarrett, D. C. (2012). Prediction and diagnosis of clinical outcomes affecting restoration margins. *Journal of Oral Rehabilitation, 39*(4), 301-318.

Derise, N. L., & Ritchey, S. J. (1974). Mineral composition of normal human enamel and dentin and the relation of composition to dental caries. II. Microminerals. *J Dent Res, 53*(4), 853-858.

Devito, K. L., de Souza Barbosa, F., & Felippe Filho, W. N. (2008). An artificial multilayer perceptron neural network for diagnosis of proximal dental caries. *Oral Surgery, Oral Medicine, Oral Pathology, Oral Radiology and Endodontics, 106*(6), 879-884.

Deyhle, H., Bunk, O., & Muller, B. (2011). Nanostructure of healthy and caries-affected human teeth. *Nanomedicine: Nanotechnology, Biology, and Medicine, 7*(6), 694-701.

Diniz, M. B., Rodrigues, J. A., Hug, I., Cordeiro Rde, C., & Lussi, A. (2009). Reproducibility and accuracy of the ICDAS-II for occlusal caries detection. *Community Dentistry and Oral Epidemiology, 37*(5), 399-404.

Djomehri, S. I., Candell, S., Case, T., Browning, A., Marshall, G. W., Yun, W., . . . Ho, S. P. (2015). Mineral density volume gradients in normal and diseased human tissues. *PloS One, 10*(4), e0121611. doi: 10.1371/journal.pone.0121611

Douglas, S. M., Fried, D., & Darling, C. L. (2010). Imaging Natural Occlusal Caries Lesions with Optical Coherence Tomography. *Proc Soc Photo Opt Instrum Eng, 7549*, 75490N.

Duangthip, D., Jiang, M., Chu, C. H., & Lo, E. C. (2015). Non-surgical treatment of dentin caries in preschool children--systematic review. *BMC Oral Health, 15*, 44.

Duerinckx, A. J., & Macovski, A. (1978). Polychromatic streak artifacts in computed tomography images. *Journal of Computer Assisted Tomography, 2*(4), 481-487.

Eberhard, J., Bode, K., Hedderich, J., & Jepsen, S. (2008). Cavity size difference after caries removal by a fluorescence-controlled Er:YAG laser and by conventional bur treatment. *Clinical Oral Investigations, 12*(4), 311-318.

Ekambaram, M., Yiu, C. K. Y., & Matinlinna, J. P. (2015). Bonding of resin adhesives to caries-affected dentin–A systematic review. *Int J Adhesion and Adhesives, 61*, 23-34.

Ekstrand, K. (2004). Improving clinical visual detection—potential for caries clinical trials. *Journal of Dental Research, 83*(suppl 1), C67-C71.

Ekstrand, K., Kuzmina, I., Bjorndal, L., & Thylstrup, A. (1995). Relationship between external and histologic features of progressive stages of caries in the occlusal fossa. *Caries Research, 29*(4), 243-250.

Eldarrat, A. H., Wood, D. J., Kale, G. M., & High, A. S. (2007). Age-related changes in ac-impedance spectroscopy studies of normal human dentine. *Journal of Materials Science: Materials in Medicine, 18*(6), 1203-1210.

Elliott, J. C., Wong, F. S., Anderson, P., Davis, G. R., & Dowker, S. E. (1998). Determination of mineral concentration in dental enamel from X-ray attenuation measurements. *Connective Tissue Research, 38*(1-4), 61-72; discussion 73-69.

Ericson, D., Kidd, E., McComb, D., Mjor, I., & Noack, M. J. (2003). Minimally Invasive Dentistry--concepts and techniques in cariology. *Oral Health Prev Dent, 1*(1), 59-72.

Espigares, J., Sadr, A., Hamba, H., Shimada, Y., Otsuki, M., Tagami, J., & Sumi, Y. (2015). Assessment of natural enamel lesions with optical coherence tomography in comparison with microfocus x-ray computed tomography. *J Med Imaging (Bellingham), 2*(1), 014001.

Featherstone, J. D. (2004). The continuum of dental caries--evidence for a dynamic disease process. *Journal of Dental Research, 83 Spec No C*, C39-42.

Featherstone, J. D. (2006). Caries prevention and reversal based on the caries balance. *Pediatric Dentistry, 28*(2), 128-132; discussion 192-128.

Fejerskov, O. (2004). Changing paradigms in concepts on dental caries: consequences for oral health care. *Caries Research, 38*(3), 182-191.

Fejerskov, O., & Kidd, E. (2008). *Dental caries: the disease and its clinical management*: John Wiley & Sons.

Fejerskov, O., & Nyvad, B. (2003). Is dental caries an infectious disease? Diagnostic and treatment consequences for the practitioner. *Nordic dentistry*, 141-151.

Fejerskov, O., Scheie, A. A., & Manji, F. (1992). The effect of sucrose on plaque pH in the primary and permanent dentition of caries-inactive and-active Kenyan children. *Journal of Dental Research, 71*(1), 25-31.

Feuchter., T. (2015). Supercontinuum Sources Enhance UHR-OCT Methods. *Bio Photonics*.

Francescut, P., Zimmerli, B., & Lussi, A. (2006). Influence of different storage methods on laser fluorescence values: a two-year study. *Caries Research, 40*(3), 181-185.

Frank, R. M. (1959). Electron microscopy of undecalcified sections of human adult dentine. *Archives of Oral Biology, 1*, 29-32.

Frank, R. M. (1990). Structural events in the caries process in enamel, cementum, and dentin. *Journal of Dental Research, 69 Spec No*(2 suppl), 559-566; discussion 634-556.

Freitas, A. Z., Zezell, D. M., Mayer, M. P. A., Ribeiro, A. C., Gomes, A. S. L., & Vieira, N. D. (2009). Determination of dental decay rates with optical coherence tomography. *Laser Physics Letters, 6*(12), 896-900.

French, B. M., Dawson, M. R., & Dobbs, A. R. (1997). Classification and staging of dementia of the Alzheimer type: a comparison between neural networks and linear discriminant analysis. *Archives of Neurology, 54*(8), 1001-1009.

Frencken, J. E., Peters, M. C., Manton, D. J., Leal, S. C., Gordan, V. V., & Eden, E. (2012). Minimal intervention dentistry for managing dental caries - a review: report of a FDI task group. *International Dental Journal, 62*(5), 223-243.

Fried, D., Glena, R. E., Featherstone, J. D., & Seka, W. (1995). Nature of light scattering in dental enamel and dentin at visible and near-infrared wavelengths. *Appl Opt, 34*(7), 1278-1285.

Fried, D., Xie, J., Shafi, S., Featherstone, J. D., Breunig, T. M., & Le, C. (2002). Imaging caries lesions and lesion progression with polarization sensitive optical coherence tomography. *J Biomed Opt, 7*(4), 618-627.

Fried, D., Xie, J., Shafi, S., Featherstone, J. D., Breunig, T. M., & Le, C. (2002). Imaging caries lesions and lesion progression with polarization sensitive optical coherence tomography. *Journal of Biomedical Optics, 7*(4), 618-627.

Froelicher, V., Shetler, K., & Ashley, E. (2002). Better decisions through science: exercise testing scores. *Prog in cardio diseases, 44*(5), 395-414.

Fusayama, T. (1991). Intratubular crystal deposition and remineralization of carious dentin. *Journal de Biologie Buccale, 19*(3), 255-262.

Fusayama, T. (1993). A Simple Pain-Free Adhesive Restorative System by Minimal Reduction and Total Etching. *Ishiyaku Euro-America Inc. St Louis, Missouri.*

Fusayama, T., & Kurosaki, N. (1972). Structure and removal of carious dentin. *International Dental Journal, 22*(3), 401-411.

Fusayama, T., Okuse, K., & Hosoda, H. (1966). Relationship between hardness, discoloration, and microbial invasion in carious dentin. *J Dental Res, 45*(4), 1033-1046.

Fusayama, T., & Terashima, S. (1972). Differentiation of two layers of carious dentin by staining. *The Bulletin of Tokyo Medical and Dental University, 19*(1), 83.

Gage, J. P. (1984). Electrophoretic characterization of peptides from normal mature human dentine. *Archives of Oral Biology, 29*(8), 575-580.

Gansky, S. A. (2003). Dental data mining: potential pitfalls and practical issues. *Advances in Dental Research, 17*, 109-114.

Ganter, P., Al-Ahmad, A., Wrbas, K. T., Hellwig, E., & Altenburger, M. J. (2014). The use of computer-assisted FACE for minimal-invasive caries excavation. *Clinical Oral Investigations, 18*(3), 745-751.

Gotliv, B. A., & Veis, A. (2007). Peritubular dentin, a vertebrate apatitic mineralized tissue without collagen: role of a phospholipid-proteolipid complex. *Calcified Tissue International, 81*(3), 191-205.

Grieve, A. R., Alani, A., & Saunders, W. P. (1991). The effects on the dental pulp of a composite resin and two dentine bonding agents and associated bacterial microleakage. *International Endodontic Journal, 24*(3), 108-118.

Grigoratos, D., Knowles, J., Ng, Y. L., & Gulabivala, K. (2001). Effect of exposing dentine to sodium hypochlorite and calcium hydroxide on its flexural strength and elastic modulus. *International Endodontic Journal, 34*(2), 113-119.

Grindefjord, M., Dahllof, G., Nilsson, B., & Modeer, T. (1996). Stepwise prediction of dental caries in children up to 3.5 years of age. *Caries Research, 30*(4), 256-266.

Gross, E. L., Beall, C. J., Kutsch, S. R., Firestone, N. D., Leys, E. J., & Griffen, A. L. (2012). Beyond Streptococcus mutans: dental caries onset linked to multiple species by 16S rRNA community analysis.

Gugnani, N., Pandit, I., Srivastava, N., Gupta, M., & Gugnani, S. (2011). Light induced fluorescence evaluation: A novel concept for caries diagnosis and excavation. *J Conserv Dent, 14*(4), 418-422.

Gustafsson, B. E., Quensel, C. E., Lanke, L. S., Lundqvist, C., Grahnen, H., Bonow, B. E., & Krasse, B. (1954). The Vipeholm dental caries study; the effect of different levels of carbohydrate intake on caries activity in 436 individuals observed for five years. *Acta Odontologica Scandinavica, 11*(3-4), 232-264.

Haikel, Y., Frank, R. M., & Voegel, J. C. (1983). Scanning electron microscopy of the human enamel surface layer of incipient carious lesions. *Caries Research, 17*(1), 1-13.

Hamama, H., Yiu, C., Burrow, M. F., & King, N. M. (2015). Systematic Review and Meta-Analysis of Randomized Clinical Trials on Chemomechanical Caries Removal. *Operative Dentistry, 40*(4), E167-178.

Hamilton, J. C., Gregory, W. A., & Valentine, J. B. (2006). Diagnodent measurements and correlation with the depth and volume of minimally invasive cavity preparations. *Operative Dentistry, 31*(3), 291-296.

Handelman, S. L. (1991). Therapeutic use of sealants for incipient or early carious lesions in children and young adults. *Proceedings of the Finnish Dental Society, 87*(4), 463-475.

Hariri, I., Sadr, A., Nakashima, S., Shimada, Y., Tagami, J., & Sumi, Y. (2013). Estimation of the enamel and dentin mineral content from the refractive index. *Caries Research, 47*(1), 18-26.

Hariri, I., Sadr, A., Shimada, Y., Tagami, J., & Sumi, Y. (2012). Effects of structural orientation of enamel and dentine on light attenuation and local refractive index: an optical coherence tomography study. *Journal of Dentistry, 40*(5), 387-396.

Hariri, I., Sadr, A., Shimada, Y., Tagami, J., & Sumi, Y. (2012). Effects of structural orientation of enamel and dentine on light attenuation and local refractive index: an optical coherence tomography study. *J Dent, 40*(5), 387-396.

Hayashi, M., Fujitani, M., Yamaki, C., & Momoi, Y. (2011). Ways of enhancing pulp preservation by stepwise excavation--a systematic review. *Journal of Dentistry, 39*(2), 95-107.

Heino, J., Arridge, S., Sikora, J., & Somersalo, E. (2003). Anisotropic effects in highly scattering media. *Physical Review. E: Statistical, Nonlinear, and Soft Matter Physics, 68*(3 Pt 1), 031908.

Heinrich-Weltzien, R., Weerheijm, K. L., Kuhnisch, J., Oehme, T., & Stosser, L. (2002). Clinical evaluation of visual, radiographic, and laser fluorescence methods for detection of occlusal caries. *ASDC Journal of Dentistry for Children, 69*(2), 127-132, 123.

Hennequin, M., & Douillard, Y. (1995). Effects of citric acid treatment on the Ca, P and Mg contents of human dental roots. *Journal of Clinical Periodontology, 22*(7), 550-557.

Heslop-Harrison, J. S. (1990). Energy dispersive X-ray analysis *Phys M Plant Sci* (pp. 244-277): Springer.

Hevinga, M. A., Opdam, N. J., Frencken, J. E., Truin, G. J., & Huysmans, M. C. (2010). Does incomplete caries removal reduce strength of restored teeth? *Journal of Dental Research, 89*(11), 1270-1275.

Higgs, J. (2008). *Clinical reasoning in the health professions*: Elsevier Health Sciences.

Hiraishi, N., Kitasako, Y., Nikaido, T., Foxton, R. M., Tagami, J., & Nomura, S. (2003). Evaluation of active and arrested carious dentin using a pH-imaging microscope and an X-ray analytical microscope. *Operative Dentistry, 28*(5), 598-604.

Holmen, L., Thylstrup, A., Ogaard, B., & Kragh, F. (1985). A scanning electron microscopic study of progressive stages of enamel caries in vivo. *Caries Research, 19*(4), 355-367.

Hosmer Jr, D. W., & Lemeshow, S. (2004). *Applied logistic regression*: John Wiley & Sons.

Hosoya, Y., Taguchi, T., & Tay, F. R. (2007). Evaluation of a new caries detecting dye for primary and permanent carious dentin. *Journal of Dentistry, 35*(2), 137-143.

Huang, D., Swanson, E. A., Lin, C. P., Schuman, J. S., Stinson, W. G., Chang, W., et al. (1991). Optical coherence tomography. *Science, 254*(5035), 1178-1181.

Huang, T. T., He, L. H., Darendeliler, M. A., & Swain, M. V. (2010). Nano-indentation characterisation of natural carious white spot lesions. *Caries Research, 44*(2), 101-107.

Huang, T. T., Jones, A. S., He, L. H., Darendeliler, M. A., & Swain, M. V. (2007). Characterisation of enamel white spot lesions using X-ray micro-tomography. *Journal of Dentistry, 35*(9), 737-743.

Huber, R., Wojtkowski, M., Taira, K., Fujimoto, J., & Hsu, K. (2005). Amplified, frequency swept lasers for frequency domain reflectometry and OCT imaging: design and scaling principles. *Optics Express, 13*(9), 3513-3528.

Hwang, D., Alevizos, I., Schmitt, W. A., Misra, J., Ohyama, H., Todd, R., . . . Stephanopoulos, G. (2003). Genomic dissection for characterization of cancerous oral epithelium tissues using transcription profiling. *Oral Oncology, 39*(3), 259-268.

Ie, Y. L., & Verdonschot, E. H. (1994). Performance of diagnostic systems in occlusal caries detection compared. *Community Dentistry and Oral Epidemiology, 22*(3), 187-191.

Ismail, A. I., Sohn, W., Tellez, M., Amaya, A., Sen, A., Hasson, H., & Pitts, N. B. (2007). The International Caries Detection and Assessment System (ICDAS): an integrated system for measuring dental caries. *Community Dentistry and Oral Epidemiology, 35*(3), 170-178.

Ito, A., Hayashi, M., Hamasaki, T., & Ebisu, S. (2011). Risk assessment of dental caries by using Classification and Regression Trees. *Journal of Dentistry, 39*(6), 457-463.

Iwami, Y., Hayashi, N., Yamamoto, H., Hayashi, M., Takeshige, F., & Ebisu, S. (2007). Evaluating the objectivity of caries removal with a caries detector dye using color evaluation and PCR. *Journal of Dentistry, 35*(9), 749-754.

Iwami, Y., Shimizu, A., Hayashi, M., Takeshige, F., & Ebisu, S. (2006). Relationship between colors of carious dentin and laser fluorescence evaluations in caries diagnosis. *Dental Materials Journal, 25*(3), 584-590.

Iwami, Y., Shimizu, A., Narimatsu, M., Kinomoto, Y., & Ebisu, S. (2005). The relationship between the color of carious dentin stained with a caries detector dye and bacterial infection. *Operative Dentistry, 30*(1), 83.

Izatt, J. A., & Choma, M. A. (2008). Theory of optical coherence tomography *Optical coherence tomography* (pp. 47-72): Springer.

Jablonski-Momeni, A., Stucke, J., Steinberg, T., & Heinzel-Gutenbrunner, M. (2012). Use of ICDAS-II, Fluorescence-Based Methods, and Radiography in Detection and Treatment Decision of Occlusal Caries Lesions: An In Vitro Study. *Int J Dent, 2012*, 371595.

Johnson, M. W., Taylor, B. R., & Berman, D. S. (1969). The response of deciduous dentine to caries studied by correlated light and electron microscopy. *Caries Research, 3*(4), 348-368.

Jones, R., Darling, C., Featherstone, J., & Fried, D. (2006). Imaging artificial caries on the occlusal surfaces with polarization-sensitive optical coherence tomography. *Caries Research, 40*(2), 81-89.

Jones, R. S., Darling, C. L., Featherstone, J. D., & Fried, D. (2006). Imaging artificial caries on the occlusal surfaces with polarization-sensitive optical coherence tomography. *Caries Research, 40*(2), 81-89.

Jones, R. S., Darling, C. L., Featherstone, J. D., & Fried, D. (2006). Remineralization of in vitro dental caries assessed with polarization-sensitive optical coherence tomography. *Journal of Biomedical Optics, 11*(1), 014016-014019.

Joseph, P. M., & Spital, R. D. (1978). A method for correcting bone induced artifacts in computed tomography scanners. *J Comput Assist Tomogr, 2*(1), 100-108.

Joves, G. J., Inoue, G., Nakashima, S., Sadr, A., Nikaido, T., & Tagami, J. (2013). Mineral density, morphology and bond strength of natural versus artificial caries-affected dentin. *Dental Materials Journal, 32*(1), 138-143.

Kagayama, M., Sasano, Y., Sato, H., Kamakura, S., Motegi, K., & Mizoguchi, I. (1999). Confocal microscopy of dentinal tubules in human tooth stained with alizarin red. *Anatomy and Embryology, 199*(3), 233-238.

Kaidonis, J., & Townsend, G. (2015). The 'sialo–microbial–dental complex'in oral health and disease. *Annals of Anatomy-Anatomischer Anzeiger*.

Kang, H., Jiao, J. J., Lee, C., Le, M. H., Darling, C. L., & Fried, D. (2010). Nondestructive Assessment of Early Tooth Demineralization Using Cross-Polarization Optical Coherence Tomography. *IEEE J Sel Top Quantum Electron, 16*(4), 870-876.

Karjalainen, S., Soderling, E., Pelliniemi, L., & Foidart, J. M. (1986). Immunohistochemical localization of types I and III collagen and fibronectin in the dentine of carious human teeth. *Archives of Oral Biology, 31*(12), 801-806.

Kassirer, J. P. (1976). The principles of clinical decision making: an introduction to decision analysis. *Yale Journal of Biology and Medicine, 49*(2), 149-164.

Kay, E. J., Nuttall, N. M., & Knill-Jones, R. (1992). Restorative treatment thresholds and agreement in treatment decision-making. *Community Dentistry and Oral Epidemiology, 20*(5), 265-268.

Khunkar, S. J., Utaka, S., Hariri, I., Sadr, A., Ikeda, M., Nakashima, S., . . . Tagami, J. (2015). Formation and characterization of hypermineralized zone beneath dentine lesion body induced by topical fluoride in-vitro. *Archives of Oral Biology, 60*(4), 574-581.

Kidd, E. (2004). How 'clean'must a cavity be before restoration? *Caries Research, 38*(3), 305-313.

Kidd, E. (2005). *Essentials of Dental Caries: The Disease and Its Management: The disease and its management*: Oxford University Press.

Kidd, E., Joyston-Bechal, S., Smith, M., Allan, R., Howe, L., & Smith, S. (1989). The use of a caries detector dye in cavity preparation. *British Dental Journal, 167*(4), 132-134.

Kidd, E. A. (2004). How 'clean' must a cavity be before restoration? *Caries Research, 38*(3), 305-313.

Kidd, E. A., & Fejerskov, O. (2004). What constitutes dental caries? Histopathology of carious enamel and dentin related to the action of cariogenic biofilms. *Journal of Dental Research, 83 Spec No C*, C35-38.

Kidd, E. A., Joyston-Bechal, S., & Beighton, D. (1993). Microbiological validation of assessments of caries activity during cavity preparation. *Caries Research, 27*(5), 402-408.

Kidd, E. A., Ricketts, D. N., & Pitts, N. B. (1993). Occlusal caries diagnosis: a changing challenge for clinicians and epidemiologists. *Journal of Dentistry, 21*(6), 323-331.

Kidd, E. A., Smith, N., & Pickard, M. (1998). *Pickard's Manual of Operative Dentistry* (7th Edition ed.): Oxford University Press.

Kienle, A., Forster, F. K., Diebolder, R., & Hibst, R. (2003). Light propagation in dentin: influence of microstructure on anisotropy. *Physics in Medicine and Biology, 48*(2), N7.

Kienle, A., Michels, R., & Hibst, R. (2006). Magnification—A new look at a long-known optical property of dentin. *Journal of Dental Research, 85*(10), 955-959.

Kinney, J. H., Balooch, M., Haupt, D. L., Jr., Marshall, S. J., & Marshall, G. W., Jr. (1995). Mineral distribution and dimensional changes in human dentin during demineralization. *Journal of Dental Research, 74*(5), 1179-1184.

Kinney, J. H., Marshall, G. W., Jr., & Marshall, S. J. (1994). Three-dimensional mapping of mineral densities in carious dentin: theory and method. *Scanning Microscopy, 8*(2), 197-204; discussion 204-195.

Kinoshita, J., Shinomiya, H., Itoh, K., & Matsumoto, K. (2007). Light intensity evaluation of laser-induced fluorescence after caries removal using an experimental caries staining agent. *Dental Materials Journal, 26*(3), 307-311.

Kirkham, J., Brookes, S. J., Shore, R. C., Bonass, W. A., Smith, D. A., Wallwork, M. L., & Robinson, C. (1998). Atomic force microscopy studies of crystal surface topology during enamel development. *Connective Tissue Research, 38*(1-4), 91-100; discussion 139-145.

Kleter, G. A. (1998). Discoloration of dental carious lesions (a review). *Archives of Oral Biology, 43*(8), 629-632.

Ko, C., Tantbirojn, D., Wang, T., & Douglas, W. (2000). Optical scattering power for characterization of mineral loss. *Journal of Dental Research, 79*(8), 1584-1589.

Koenig, K., & Schneckenburger, H. (1994). Laser-induced autofluorescence for medical diagnosis. *J Fluoresc, 4*(1), 17-40.

Konig, K., Flemming, G., & Hibst, R. (1998). Laser-induced autofluorescence spectroscopy of dental caries. *Cellular and Molecular Biology (Noisy-Le-Grand, France), 44*(8), 1293-1300.

Kositbowornchai, S., Siriteptawee, S., Plermkamon, S., Bureerat, S., & Chetchotsak, D. (2006). An artificial neural network for detection of simulated dental caries. *Int J Comput Assist Radiol Surg, 1*(2), 91-96.

Koutsi, V., Noonan, R. G., Horner, J. A., Simpson, M. D., Matthews, W. G., & Pashley, D. H. (1994). The effect of dentin depth on the permeability and ultrastructure of primary molars. *Pediatric Dentistry, 16*(1), 29-35.

Krause, F., Braun, A., Eberhard, J., & Jepsen, S. (2007). Laser fluorescence measurements compared to electrical resistance of residual dentine in excavated cavities in vivo. *Caries Research, 41*(2), 135-140.

Kuboki, Y., Liu, C. F., & Fusayama, T. (1983). Mechanism of differential staining in carious dentin. *Journal of Dental Research, 62*(6), 713-714.

Lachapelle-Harvey, D., & Sevigny, J. (1985). Multiple regression analysis of dental status and related food behaviour of French Canadian adolescents. *Community Dentistry and Oral Epidemiology, 13*(4), 226-229.

Lakomaa, E. L., & Rytomaa, I. (1977). Mineral composition of enamel and dentin of primary and permanent teeth in Finland. *Scandinavian Journal of Dental Research, 85*(2), 89-95.

Larmas, M. (1972). Enzymes in Carious Human Dentine a Histochemical Akd Biochemical Study. *Acta Odontologica, 30*(5-6), 555-573.

Le, M. H., Darling, C. L., & Fried, D. (2010). Automated analysis of lesion depth and integrated reflectivity in PS-OCT scans of tooth demineralization. *Lasers in Surgery and Medicine, 42*(1), 62-68.

Lee, C., Darling, C. L., & Fried, D. (2009). Polarization-sensitive optical coherence tomographic imaging of artificial demineralization on exposed surfaces of tooth roots. *Dental Materials, 25*(6), 721-728.

Lee, C., Hsu, D. J., Le, M. H., Darling, C. L., & Fried, D. (2009). Non-destructive measurement of demineralization & remineralization in the occlusal pits and fissures of extracted 3 molars with PS-OCT. *Proc Soc Photo Opt Instrum Eng, 7162*(1).

LeGeros, R. Z. (1990). Chemical and crystallographic events in the caries process. *Journal of Dental Research, 69 Spec No*(2 suppl), 567-574; discussion 634-566.

Lehmann, M., Veitz-Keenan, A., Matthews, A. G., Vena, D., Grill, A., Craig, R. G.,. Thompson, V. P. (2012). Dentin caries activity in early occlusal lesions selected to receive operative treatment: findings from the Practitioners Engaged in

Applied Research and Learning (PEARL) Network. *Journal of the American Dental Association, 143*(4), 377-385.

Lennon, A. M. (2003). Fluorescence-aided caries excavation (FACE) compared to conventional method. *Operative Dentistry, 28*(4), 341-345.

Lennon, A. M., Attin, T., & Buchalla, W. (2007). Quantity of remaining bacteria and cavity size after excavation with FACE, caries detector dye and conventional excavation in vitro. *Operative Dentistry, 32*(3), 236-241.

Lennon, A. M., Buchalla, W., Rassner, B., Becker, K., & Attin, T. (2006). Efficiency of 4 caries excavation methods compared. *Operative Dentistry, 31*(5), 551-555.

Lennon, A. M., Buchalla, W., Switalski, L. M., & Stookey, G. K. (2002). Residual caries detection using visible fluorescence. *Caries Research, 36*(5), 315-319.

Leverett, D. H., Proskin, H. M., Featherstone, J. D., Adair, S. M., Eisenberg, A. D., Mundorff-Shrestha, S. A., . . . Billings, R. J. (1993). Caries risk assessment in a longitudinal discrimination study. *Journal of Dental Research, 72*(2), 538-543.

Levine, R. (1973). The differential inorganic composition of dentine within active and arrested carious lesions. *Caries Research, 7*(3), 245-260.

Li, J., Bowman, C., Fazel-Rezai, R., & Hewko, M. (2009). *Speckle reduction and lesion segmentation of OCT tooth images for early caries detection.* Paper presented at the Engineering in Medicine and Biology Society, 2009. EMBC 2009. Annual International Conference of the IEEE.

Little, M. F., Dirksen, T. R., & Schlueter, G. (1965). The CA, P, NA, and ash content at different depth in caries *Journal of Dental Research, 44*, 362-365.

Liu, J., Yamazaki, K., Zhou, Y., & Matsumiya, S. (2002). A reflective fiber optic sensor for surface roughness in-process measurement. *Journal of manufacturing science and engineering, 124*(3), 515-522.

Louie, T., Lee, C., Hsu, D., Hirasuna, K., Manesh, S., Staninec, M., . . . Fried, D. (2010). Clinical Assessment of Early Tooth Demineralization Using Polarization Sensitive Optical Coherence Tomography. *Lasers in Surgery and Medicine, 42*(10), 738-745. doi:

Lussi, A., Hibst, R., & Paulus, R. (2004). DIAGNOdent: an optical method for caries detection. *Journal of Dental Research, 83 Spec No C*(suppl 1), C80-83.

Lussi, A., Megert, B., Longbottom, C., Reich, E., & Francescut, P. (2001). Clinical performance of a laser fluorescence device for detection of occlusal caries lesions. *European Journal of Oral Sciences, 109*(1), 14-19.

Macho, G. A., Jiang, Y., & Spears, I. R. (2003). Enamel microstructure—a truly three-dimensional structure. *J Hum Evol, 45*(1), 81-90.

Madhuri, S., Vengadesan, N., Aruna, P., Koteeswaran, D., Venkatesan, P., & Ganesan, S. (2003). Native fluorescence spectroscopy of blood plasma in the

characterization of oral malignancy. *Photochemistry and Photobiology, 78*(2), 197-204.

Magne, D., Weiss, P., Bouler, J. M., Laboux, O., & Daculsi, G. (2001). Study of the maturation of the organic (type I collagen) and mineral (nonstoichiometric apatite) constituents of a calcified tissue (dentin) as a function of location: a Fourier transform infrared microspectroscopic investigation. *Journal of Bone and Mineral Research, 16*(4), 750-757.

Magnus, L., Maltz, M., Bavaresco, C., Bastos, L. F., & Hashizume, L. N. (2013). Biochemical composition of carious dentin and different layers of sound dentin. *Journal of Oral Science, 55*(2), 133-137.

Magnusson, B. O., & Sundell, S. O. (1977). Stepwise excavation of deep carious lesions in primary molars. *Journal of the International Association of Dentistry for Children, 8*(2), 36-40.

Mago, V. K., Prasad, B., Bhatia, A., & Mago, A. (2008). A decision making system for the treatment of dental caries. *Soft computing applications in business*, 231-242.

Makhija, S. K., Gilbert, G. H., Funkhouser, E., Bader, J. D., Gordan, V. V., Rindal, D. B., . . . National Dental, P. C. G. (2014). Characteristics, detection methods and treatment of questionable occlusal carious lesions: findings from the national dental practice-based research network. *Caries Research, 48*(3), 200-207.

Maltz, M., de Oliveira, E. F., Fontanella, V., & Bianchi, R. (2002). A clinical, microbiologic, and radiographic study of deep caries lesions after incomplete caries removal. *Quintessence International, 33*(2), 151-159.

Maltz, M., Oliveira, E., Fontanella, V., & Carminatti, G. (2007). Deep caries lesions after incomplete dentine caries removal: 40-month follow-up study. *Caries Research, 41*(6), 493-496.

Mandurah, M. M., Sadr, A., Bakhsh, T. A., Shimada, Y., Sumi, Y., & Tagami, J. (2015). Characterization of transparent dentin in attrited teeth using optical coherence tomography. *Lasers in Medical Science, 30*(4), 1189-1196.

Mandurah, M. M., Sadr, A., Shimada, Y., Kitasako, Y., Nakashima, S., Bakhsh, T. A., . . . Sumi, Y. (2013). Monitoring remineralization of enamel subsurface lesions by optical coherence tomography. *J Biomed Opt, 18*(4), 046006.

Manesh, S. K., Darling, C. L., & Fried, D. (2008). Imaging natural and artificial demineralization on dentin surfaces with polarization sensitive optical coherence tomography. *Proc Soc Photo Opt Instrum Eng, 6843*.

Manesh, S. K., Darling, C. L., & Fried, D. (2009a). Nondestructive assessment of dentin demineralization using polarization-sensitive optical coherence tomography after exposure to fluoride and laser irradiation. *J Biomed Mater Res B Appl Biomater, 90*(2), 802-812.

Manesh, S. K., Darling, C. L., & Fried, D. (2009b). Polarization-sensitive optical coherence tomography for the nondestructive assessment of the remineralization of dentin. *J Biomed Opt, 14*(4), 044002.

Manly, R. S., & Deakins, M. L. (1940). Changes in the volume per cent. of moisture, organic and inorganic material in dental caries. *Journal of Dental Research, 19*, 165-170.

Marcenes, W., Kassebaum, N. J., Bernabe, E., Flaxman, A., Naghavi, M., Lopez, A., & Murray, C. J. (2013). Global burden of oral conditions in 1990-2010: a systematic analysis. *Journal of Dental Research, 92*(7), 592-597.

Marquezan, M., Correa, F. N., Sanabe, M. E., Rodrigues Filho, L. E., Hebling, J., Guedes-Pinto, A. C., & Mendes, F. M. (2009). Artificial methods of dentine caries induction: A hardness and morphological comparative study. *Archives of Oral Biology, 54*(12), 1111-1117.

Marshall, G. W., Habelitz, S., Gallagher, R., Balooch, M., Balooch, G., & Marshall, S. J. (2001). Nanomechanical properties of hydrated carious human dentin. *Journal of Dental Research, 80*(8), 1768-1771.

Marshall, G. W., Jr., Chang, Y. J., Gansky, S. A., & Marshall, S. J. (2001). Demineralization of caries-affected transparent dentin by citric acid: an atomic force microscopy study. *Dental Materials, 17*(1), 45-52.

Marshall, G. W., Jr., Inai, N., Wu-Magidi, I. C., Balooch, M., Kinney, J. H., Tagami, J., & Marshall, S. J. (1997). Dentin demineralization: effects of dentin depth, pH and different acids. *Dental Materials, 13*(6), 338-343.

Marshall Jr, G. W. (1993). Dentin: Microstructure and characterization. *Quintessence International, 24*(9), 606-617.

Marshall Jr, G. W. (1993). Dentin: Microstructure and characterization. *Quintessence international (Berlin, Germany: 1985), 24*(9), 606-617.

Marshall Jr, G. W., Marshall, S. J., Kinney, J. H., & Balooch, M. (1997). The dentin substrate: structure and properties related to bonding. *Journal of Dentistry, 25*(6), 441-458.

Marthaler, T. M. (2004). Changes in dental caries 1953-2003. *Caries Research, 38*(3), 173-181. doi: 10.1159/000077752

Massara, M. L., Alves, J. B., & Brandao, P. R. (2002). Atraumatic restorative treatment: clinical, ultrastructural and chemical analysis. *Caries Research, 36*(6), 430-436. doi: 66534

Massler, M. (1967). Pulpal reactions to dental caries. *International Dental Journal, 17*(2), 441-460.

Matsumoto, K., Wang, X., Zhang, C., & Kinoshita, J. (2007). Effect of a novel Er:YAG laser in caries removal and cavity preparation: a clinical observation. *Photomedicine and Laser Surgery, 25*(1), 8-13.

Maupome, G., Schrader, S., Mannan, S., Garetto, L., & Eggertsson, H. (2010). Diagnostic thinking and information used in clinical decision-making: a qualitative study of expert and student dental clinicians. *BMC Oral Health, 10*, 11.

McComb, D. (2000). Caries-detector dyes--how accurate and useful are they? *Journal of the Canadian Dental Association. Journal de L'Association Dentaire Canadienne, 66*(4), 195-198.

Meganck, J. A., Kozloff, K. M., Thornton, M. M., Broski, S. M., & Goldstein, S. A. (2009). Beam hardening artifacts in micro-computed tomography scanning can be reduced by X-ray beam filtration and the resulting images can be used to accurately measure BMD. *Bone, 45*(6), 1104-1116.

Mejare, I., Stenlund, H., & Zelezny-Holmlund, C. (2004). Caries incidence and lesion progression from adolescence to young adulthood: a prospective 15-year cohort study in Sweden. *Caries Research, 38*(2), 130-141.

Mendonca, E. A. (2004). Clinical decision support systems: perspectives in dentistry. *Journal of Dental Education, 68*(6), 589-597.

Meng, Z., Yao, X. S., Yao, H., Liang, Y., Liu, T., Li, Y., . . . Lan, S. (2009). Measurement of the refractive index of human teeth by optical coherence tomography. *J Biomed Opt, 14*(3), 034010.

Mertz-Fairhurst, E. J., Curtis, J. W., Jr., Ergle, J. W., Rueggeberg, F. A., & Adair, S. M. (1998). Ultraconservative and cariostatic sealed restorations: results at year 10. *Journal of the American Dental Association, 129*(1), 55-66.

Moreno, E. C., Kresak, M., & Zahradnik, R. T. (1974). Fluoridated hydroxyapatite solubility and caries formation. *Nature, 247*(5435), 64-65.

Moron, B. M., Comar, L. P., Wiegand, A., Buchalla, W., Yu, H., Buzalaf, M. A., & Magalhaes, A. C. (2013). Different protocols to produce artificial dentine carious lesions in vitro and in situ: hardness and mineral content correlation. *Caries Research, 47*(2), 162-170.

Mount, G. J. (2007). A new paradigm for operative dentistry. *Australian Dental Journal, 52*(4), 264-270; quiz 342.

Mount, G. J., & Ngo, H. (2000). Minimal intervention: a new concept for operative dentistry. *Quintessence International, 31*(8), 527-533.

Mourant, J. R., Johnson, T. M., Carpenter, S., Guerra, A., Aida, T., & Freyer, J. P. (2002). Polarized angular dependent spectroscopy of epithelial cells and epithelial cell nuclei to determine the size scale of scattering structures. *J Biomed Opt, 7*(3), 378-387.

Moynihan, P., & Petersen, P. E. (2004). Diet, nutrition and the prevention of dental diseases. *Public Health Nutrition, 7*(1A), 201-226.

Munson, M. A., Banerjee, A., Watson, T. F., & Wade, W. G. (2004). Molecular analysis of the microflora associated with dental caries. *Journal of Clinical Microbiology, 42*(7), 3023-3029.

Murray, P. E., Smith, A. J., Windsor, L. J., & Mjor, I. A. (2003). Remaining dentine thickness and human pulp responses. *International Endodontic Journal, 36*(1), 33-43.

Nakajima, M., Sano, H., Burrow, M. F., Tagami, J., Yoshiyama, M., Ebisu, S., . . . Pashley, D. H. (1995). Tensile bond strength and SEM evaluation of caries-affected dentin using dentin adhesives. *Journal of Dental Research, 74*(10), 1679-1688.

Nanci, A. (2008). *Ten Cate's Oral Histology: Development, Structure, and Function* (8th edn ed.). Canada: Mosby Elsevier.

Natsume, Y., Nakashima, S., Sadr, A., Shimada, Y., Tagami, J., & Sumi, Y. (2011). Estimation of lesion progress in artificial root caries by swept source optical coherence tomography in comparison to transverse microradiography. *J Biomed Opt, 16*(7), 071408.

Nayak, G. S., Kamath, S., Pai, K. M., Sarkar, A., Ray, S., Kurien, J., . . . Mahato, K. K. (2006). Principal component analysis and artificial neural network analysis of oral tissue fluorescence spectra: classification of normal premalignant and malignant pathological conditions. *Biopolymers, 82*(2), 152-166.

Nelson, D. G. (1981). The influence of carbonate on the atomic structure and reactivity of hydroxyapatite. *Journal of Dental Research, 60 Spec No C*(3 suppl), 1621-1629.

Neves A, A., Coutinho, E., Vivan Cardoso, M., Jaecques, S. V., & Van Meerbeek, B. (2010). Micro-CT based quantitative evaluation of caries excavation. *Dental Materials, 26*(6), 579-588.

Neves, A. A., Coutinho, E., Cardoso, M. V., Lambrechts, P., & Van Meerbeek, B. (2011). Current concepts and techniques for caries excavation and adhesion to residual dentin. *Journal of Adhesive Dentistry, 13*(1), 7-22.

Neves, A. A., Coutinho, E., De Munck, J., Lambrechts, P., & Van Meerbeek, B. (2011). Does Diagnodent provide a reliable caries-removal endpoint? *Journal of Dentistry, 39*(5), 351-360.

Ngaotheppitak, P., Darling, C. L., & Fried, D. (2005). Measurement of the severity of natural smooth surface (interproximal) caries lesions with polarization sensitive optical coherence tomography. *Lasers in Surgery and Medicine, 37*(1), 78-88.

Nor, J. E., Feigal, R. J., Dennison, J. B., & Edwards, C. A. (1997). Dentin bonding: SEM comparison of the dentin surface in primary and permanent teeth. *Pediatric Dentistry, 19*(4), 246-252.

Nyvad, B. (2004). Diagnosis versus detection of caries. *Caries Research, 38*(3), 192-198.

Nyvad, B., Crielaard, W., Mira, A., Takahashi, N., & Beighton, D. (2013). Dental caries from a molecular microbiological perspective. *Caries Research, 47*(2), 89-102.

Nyvad, B., ten Cate, J. M., & Fejerskov, O. (1989). Microradiography of experimental root surface caries in man. *Caries Research, 23*(4), 218-224.

Ogawa, K., Yamashita, Y., Ichijo, T., & Fusayama, T. (1983). The ultrastructure and hardness of the transparent layer of human carious dentin. *Journal of Dental Research, 62*(1), 7-10.

Ogushi, K., & Fusayama, T. (1975). Electron microscopic structure of the two layers of carious dentin. *Journal of Dental Research, 54*(5), 1019-1026.

Opal, S., Garg, S., Dhindsa, A., & Taluja, T. (2014). Minimally invasive clinical approach in indirect pulp therapy and healing of deep carious lesions. *Journal of Clinical Pediatric Dentistry, 38*(3), 185-192.

Orhan, A. I., Oz, F. T., Ozcelik, B., & Orhan, K. (2008). A clinical and microbiological comparative study of deep carious lesion treatment in deciduous and young permanent molars. *Clinical Oral Investigations, 12*(4), 369-378.

Otis, L. L., Everett, M. J., Sathyam, U. S., & Colston, B. W., Jr. (2000). Optical coherence tomography: a new imaging technology for dentistry. *Journal of the American Dental Association, 131*(4), 511-514.

Palamara, J., Phakey, P. P., Rachinger, W. A., & Orams, H. J. (1986). Ultrastructure of the intact surface zone of white spot and brown spot carious lesions in human enamel. *Journal of Oral Pathology, 15*(1), 28-35.

Panayotov, I., Terrer, E., Salehi, H., Tassery, H., Yachouh, J., Cuisinier, F., & Levallois, B. (2013). In vitro investigation of fluorescence of carious dentin observed with a Soprolife® camera. *Clinical Oral Investigations, 17* (3), 757-763.

Pashley, D. H. (1985). Dentin-predentin complex and its permeability: physiologic overview. *Journal of Dental Research, 64 Spec No*, 613-620.

Pashley, D. H. (1996). Dynamics of the pulpo-dentin complex. *Critical Reviews in Oral Biology and Medicine, 7*(2), 104-133.

Perdigao, J. (2010). Dentin bonding—Variables related to the clinical situation and the substrate treatment. *Dental Materials, 26*(2), e24-e37.

Perelman, L. T., Backman, V., Wallace, M., Zonios, G., Manoharan, R., Nusrat, A., . . . Feld, M. S. (1998). Observation of periodic fine structure in reflectance from biological tissue: A new technique for measuring nuclear size distribution. *Physical Review Letters, 80*(3), 627-630.

Pitts, N. B. (2004). "ICDAS"--an international system for caries detection and assessment being developed to facilitate caries epidemiology, research and appropriate clinical management. *Community Dental Health, 21*(3), 193-198.

Pitts, N. B. (2004). Modern concepts of caries measurement. *Journal of Dental Research, 83 Spec No C*(suppl 1), C43-47.

Porter, A. E., Nalla, R. K., Minor, A., Jinschek, J. R., Kisielowski, C., Radmilovic, V., . . . Ritchie, R. O. (2005). A transmission electron microscopy study of mineralization in age-induced transparent dentin. *Biomaterials, 26*(36), 7650-7660.

Press, S. J., & Wilson, S. (1978). Choosing between logistic regression and discriminant analysis. *JASA, 73*(364), 699-705.

Pretty, I. A. (2006). Caries detection and diagnosis: novel technologies. *Journal of Dentistry, 34*(10), 727-739.

Pugach, M. K., Strother, J., Darling, C. L., Fried, D., Gansky, S. A., Marshall, S. J., & Marshall, G. W. (2009). Dentin caries zones: mineral, structure, and properties. *Journal of Dental Research, 88*(1), 71-76.

Raggio, D. P., Sonego, F. G., Camargo, L. B., Marquezan, M., & Imparato, J. C. (2010). Efficiency of different polyacrylic acid concentrations on the smear layer, after ART technique, by Scanning Electron Microscopy (SEM). *European Archives of Paediatric Dentistry, 11*(5), 232-235.

Rakhmatullina, E., Bossen, A., Hoschele, C., Wang, X., Beyeler, B., Meier, C., & Lussi, A. (2011). Application of the specular and diffuse reflection analysis for in vitro diagnostics of dental erosion: correlation with enamel softening, roughness, and calcium release. *J Biomed Opt, 16*(10), 107002.

Randolph, A. G., Guyatt, G. H., Calvin, J. E., Doig, G., & Richardson, W. S. (1998). Understanding articles describing clinical prediction tools. Evidence Based Medicine in Critical Care Group. *Critical Care Medicine, 26*(9), 1603-1612.

Rechmann, P., Charland, D., Rechmann, B. M., & Featherstone, J. D. (2012). Performance of laser fluorescence devices and visual examination for the detection of occlusal caries in permanent molars. *J Biomed Opt, 17*(3), 036006.

Ribeiro, C. C., Baratieri, L. N., Perdigao, J., Baratieri, N. M., & Ritter, A. V. (1999). A clinical, radiographic, and scanning electron microscopic evaluation of adhesive restorations on carious dentin in primary teeth. *Quintessence International, 30*(9), 591-599.

Ricketts, D. (2001). Management of the deep carious lesion and the vital pulp dentine complex. *British Dental Journal, 191*(11), 606-610.

Ricketts, D., Lamont, T., Innes, N. P., Kidd, E., & Clarkson, J. E. (2013). Operative caries management in adults and children. *Cochrane Database Syst Rev, 3*, CD003808.

Ricketts, D. N., Kidd, E. A., & Beighton, D. (1995). Operative and microbiological validation of visual, radiographic and electronic diagnosis of occlusal caries in non-cavitated teeth judged to be in need of operative care. *British Dental Journal, 179*(6), 214-220.

Ricketts, D. N., Kidd, E. A., Innes, N., & Clarkson, J. (2006a). Complete or ultraconservative removal of decayed tissue in unfilled teeth. *Cochrane Database Syst Rev*(3), CD003808.

Ricketts, D. N., Kidd, E. A., Innes, N., & Clarkson, J. (2006b). Complete or ultraconservative removal of decayed tissue in unfilled teeth. *Cochrane Database Syst Rev, 3*(3), CD003808.

Rindal, D. B., Gordan, V. V., Fellows, J. L., Spurlock, N. L., Bauer, M. R., Litaker, M. S., & Gilbert, G. H. (2014). Differences between reported and actual restored caries lesion depths: results from The Dental PBRN. *Texas Dental Journal, 131*(7), 520-528.

Robinson, C., Connell, S., Kirkham, J., Brookes, S. J., Shore, R. C., & Smith, A. M. (2004). The effect of fluoride on the developing tooth. *Caries Research, 38*(3), 268-276.

Rodrigues, J. A., Hug, I., Diniz, M. B., & Lussi, A. (2008). Performance of fluorescence methods, radiographic examination and ICDAS II on occlusal surfaces in vitro. *Caries Research, 42*(4), 297-304.

Rugg-Gunn, A. J., & Hackett, A. F. (1993). *Nutrition and dental health*: Oxford University Press, USA.

Rumelhart, D. E., Hinton, G. E., & Williams, R. J. (1985). Learning internal representations by error propagation. science (Ed.): DTIC Document.

Sarnat, H., Massler, M. . (1965a). Microstructure of active and arrested dentinal caries. *Journal of Dental Research, 44*(6), 1389-1410.

Sarnat, H., Massler, M. . (1965b). Microstructure of active and arrested dentinal caries. *Journal dental Research 44*, 1389-1401.

Sato, Y., & Fusayama, T. (1976). Removal of dentin by fuchsin staining. *Journal of Dental Research, 55*(4), 678-683.

Sattabanasuk, V., Burrow, M. F., Shimada, Y., & Tagami, J. (2006). Resin adhesion to caries-affected dentine after different removal methods. *Australian Dental Journal, 51*(2), 162-169.

Schuller, S., Sawall, S., Stannigel, K., Hulsbusch, M., Ulrici, J., Hell, E., & Kachelriess, M. (2015). Segmentation-free empirical beam hardening correction for CT. *Medical Physics, 42*(2), 794-803.

Schwass, D. R., Swain, M. V., Purton, D. G., & Leichter, J. W. (2009). A system of calibrating microtomography for use in caries research. *Caries Research, 43*(4), 314-321.

Schweizer, S., Hattendorf, B., Schneider, P., Aeschlimann, B., Gauckler, L., Muller, R., & Gunther, D. (2007). Preparation and characterization of calibration standards for bone density determination by micro-computed tomography. *Analyst, 132*(10), 1040-1045.

Schwendicke, F. (2016). Modern Concepts for Caries Tissue Removal. *J Esthet Restor Dent*.

Schwendicke, F., Dorfer, C. E., & Paris, S. (2013). Incomplete caries removal: a systematic review and meta-analysis. *Journal of Dental Research, 92*(4), 306-314.

Schwendicke, F., Frencken, J. E., Bjorndal, L., Maltz, M., Manton, D. J., Ricketts, D., . . . Innes, N. P. (2016). Managing Carious Lesions: Consensus Recommendations on Carious Tissue Removal. *Advances in Dental Research, 28*(2), 58-67.

Schwendicke, F., Tzschoppe, M., & Paris, S. (2015). Radiographic caries detection: A systematic review and meta-analysis. *Journal of Dentistry, 43*(8), 924-933.

Schwendicke, F. S., E J. (2016). Modern Concepts for Caries Tissue Removal. *J Esthet Restor Dent*.

Secilmis, A., Dilber, E., Ozturk, N., & Yilmaz, F. G. (2013). The Effect of Storage Solutions on Mineral Content of Enamel. *Materials Sciences and Applications, 4*(07), 439.

Selwitz, R. H., Ismail, A. I., & Pitts, N. B. (2007). Dental caries. *Lancet, 369*(9555), 51-59.

Serper, A., & Calt, S. (2002). The demineralizing effects of EDTA at different concentrations and pH. *Journal of Endodontics, 28*(7), 501-502.

Sharwani, A., Jerjes, W., Salih, V., Swinson, B., Bigio, I. J., El-Maaytah, M., & Hopper, C. (2006). Assessment of oral premalignancy using elastic scattering spectroscopy. *Oral Oncology, 42*(4), 343-349.

Sheiham, A., & James, W. P. (2015). Diet and Dental Caries: The Pivotal Role of Free Sugars Reemphasized. *Journal of Dental Research*, 0022034515590377.

Shellis, R. P. (1994). Effects of a supersaturated pulpal fluid on the formation of caries-like lesions on the roots of human teeth. *Caries Research, 28*(1), 14-20.

Shovelton, D. S. (1968). A study of deep carious dentine. *International Dental Journal, 18*(2), 392-405.

Silverstone, L., Johnson, N., Hardie, J., & Williams, R. (1981). The caries process in dentine: the response of dentine and pulp *Dental Caries* (pp. 162-186): Springer.

Simon-Soro, A., Belda-Ferre, P., Cabrera-Rubio, R., Alcaraz, L. D., & Mira, A. (2013). A tissue-dependent hypothesis of dental caries. *Caries Research, 47*(6), 591-600.

Slayton, R. L., Cooper, M. E., & Marazita, M. L. (2005). Tuftelin, mutans streptococci, and dental caries susceptibility. *Journal of Dental Research, 84*(8), 711-714.

Slootweg, P. J. (2007). *Dental pathology; Alterations Acquired After Tooth Eruption: Caries*: Springer.

Sohn, W., Burt, B. A., & Sowers, M. R. (2006). Carbonated soft drinks and dental caries in the primary dentition. *Journal of Dental Research, 85*(3), 262-266.

Soni, H. K., Sharma, A., & Sood, P. B. (2015). A comparative clinical study of various methods of caries removal in children. *European Archives of Paediatric Dentistry, 16*(1), 19-26.

Sowa, M. G., Popescu, D. P., Werner, J., Hewko, M., Ko, A. C., Payette, J., . . . Choo-Smith, L. P. (2007). Precision of Raman depolarization and optical attenuation measurements of sound tooth enamel. *Analytical and Bioanalytical Chemistry, 387*(5), 1613-1619.

Sultana, S., Toru, N., Asafujjoha, M., & Junji, T. (2006). Storage media to preserve dentin and their effects on surface properties. *Int Chin J Dent 6*, 123-129.

Swain, M. V., & Xue, J. (2009). State of the art of Micro-CT applications in dental research. *Int J Oral Sci, 1*(4), 177-188.

Swinson, B., Jerjes, W., El-Maaytah, M., Norris, P., & Hopper, C. (2006). Optical techniques in diagnosis of head and neck malignancy. *Oral Oncology, 42*(3), 221-228.

Takahashi, N., & Nyvad, B. (2011). The role of bacteria in the caries process: ecological perspectives. *Journal of Dental Research, 90*(3), 294-303.

Takuma, S. (1960). Electron microscopy of the structure around the dentinal tubule. *Journal of Dental Research, 39*, 973-981.

Takuma, S., Tohda, H., Watanabe, K., & Yama, S. (1986). Size increase of dentin crystals in the intertubular matrix due to caries. *Journal of Electron Microscopy, 35*(1), 60-65.

Tamaki, Y., Nomura, Y., Katsumura, S., Okada, A., Yamada, H., Tsuge, S., . . . Hanada, N. (2009). Construction of a dental caries prediction model by data mining. *Journal of Oral Science, 51*(1), 61-68.

Tay, F. R., Carvalho, R., Sano, H., & Pashley, D. H. (2000). Effect of smear layers on the bonding of a self-etching primer to dentin. *Journal of Adhesive Dentistry, 2*(2), 99-116.

Ten Bosch, J. J., & Angmar-Mansson, B. (2000). Characterization and validation of diagnostic methods: Assessment of Oral Health, Diagnostic Techniques and Validation Criteria. *Monogr Oral Sci. Karger, 17*, 174-189

Ten Bosch, J. J., & Zijp, J. R. (1987). *Optical properties of dentin. In Dentine and Dentine Reactions in the Oral Cavity* UK: IRL Press Ltd., Oxford.

ten Cate, J. M., Damen, J. J., & Buijs, M. J. (1998). Inhibition of dentin demineralization by fluoride in vitro. *Caries Research, 32*(2), 141-147.

Ten Cate, J. M., Nyvad, B., Van de Plassche-Simons, Y. M., & Fejerskov, O. (1991). A quantitative analysis of mineral loss and shrinkage of in vitro demineralized human root surfaces. *Journal of Dental Research, 70*(10), 1371-1374.

Terrer, E., Raskin, A., Koubi, S., Dionne, A., Weisrock, G., Sarraquigne, C., . . . Tassery, H. (2010). A new concept in restorative dentistry: LIFEDT-light-induced fluorescence evaluator for diagnosis and treatment: part 2 - treatment of dentinal caries. *Journal of Contemporary Dental Practice, 11*(1), E095-102.

Thompson, V., Craig, R. G., Curro, F. A., Green, W. S., & Ship, J. A. (2008). Treatment of deep carious lesions by complete excavation or partial removal: a critical review. *Journal of the American Dental Association, 139*(6), 705-712.

Thylstrup, A., & Qvist, V. (1987). *Principal enamel and dentine reactions during caries progression. In: Dentine and dentine reactions in the oral cavity.* (Oxford: IRL Press ed. Vol.). UK: Oxford: IRL.

Tjäderhane, L., Carrilho, M. R., Breschi, L., Tay, F. R., & Pashley, D. H. (2009). Dentin basic structure and composition—an overview. *Endodontic Topics, 20*(1), 3-29.

Tjaderhane, L., Hietala, E. L., & Larmas, M. (1995). Mineral element analysis of carious and sound rat dentin by electron probe microanalyzer combined with back-scattered electron image. *Journal of Dental Research, 74*(11), 1770-1774.

Trowbridge, H. O. (1981). Pathogenesis of pulpitis resulting from dental caries. *Journal of Endodontics, 7*(2), 52-60.

Tu, J. V. (1996). Advantages and disadvantages of using artificial neural networks versus logistic regression for predicting medical outcomes. *Journal of Clinical Epidemiology, 49*(11), 1225-1231.

Vaarkamp, J., ten Bosch, J. J., & Verdonschot, E. H. (1995). Propagation of light through human dental enamel and dentine. *Caries Research, 29*(1), 8-13.

Van de Casteele, E., Van Dyck, D., Sijbers, J., & Raman, E. (2004). A model-based correction method for beam hardening artefacts in X-ray microtomography. *J X-ray Sci Technol, 12*(1), 43-57.

van Houte, J. (1994). Role of micro-organisms in caries etiology. *Journal of Dental Research, 73*(3), 672-681.

Van Meerbeek, B., Dhem, A., Goret-Nicaise, M., Braem, M., Lambrechts, P., & VanHerle, G. (1993). Comparative SEM and TEM examination of the ultrastructure of the resin-dentin interdiffusion zone. *Journal of Dental Research, 72*(2), 495-501.

van Staveren, H. J., van Veen, R. L., Speelman, O. C., Witjes, M. J., Star, W. M., & Roodenburg, J. L. (2000). Classification of clinical autofluorescence spectra of oral leukoplakia using an artificial neural network: a pilot study. *Oral Oncology, 36*(3), 286-293.

van Strijp, A. J., Buijs, M. J., & ten Cate, J. M. (1995). Contact microradiography of dentine under wet conditions to prevent lesion shrinkage. *Caries Research, 29*(2), 107-110.

Vasiliadis, L., Darling, A. I., & Levers, B. G. (1983). The histology of sclerotic human root dentine. *Archives of Oral Biology, 28*(8), 693-700.

Verdelis, K., Crenshaw, M. A., Paschalis, E. P., Doty, S., Atti, E., & Boskey, A. L. (2003). Spectroscopic imaging of mineral maturation in bovine dentin. *Journal of Dental Research, 82*(9), 697-702.

Verdelis, K., Lukashova, L., Wright, J. T., Mendelsohn, R., Peterson, M. G., Doty, S., & Boskey, A. L. (2007). Maturational changes in dentin mineral properties. *Bone, 40*(5), 1399-1407.

Vidal, C. M., Tjaderhane, L., Scaffa, P. M., Tersariol, I. L., Pashley, D., Nader, H. B., . . . Carrilho, M. R. (2014). Abundance of MMPs and cysteine cathepsins in caries-affected dentin. *Journal of Dental Research, 93*(3), 269-274.

Vos, T., Barber, R.M., Bell, B., Bertozzi-Villa, A., Biryukov, S., Bolliger, I., Charlson, F., Davis, A., Degenhardt, L., Dicker, D. and Duan, L.,. (2015). Global, regional, and national incidence, prevalence, and years lived with disability for 301 acute and chronic diseases and injuries in 188 countries, 1990-2013: a systematic analysis for the Global Burden of Disease Study 2013. *Lancet, 386*(9995), 743-800.

Walsh, L. J., & Brostek, A. M. (2013). Minimum intervention dentistry principles and objectives. *Australian Dental Journal, 58 Suppl 1*, 3-16.

Walton, R. E., Outhwaite, W. C., & Pashley, D. F. (1976). Magnification--an interesting optical property of dentin. *Journal of Dental Research, 55*(4), 639-642.

Wang, X. J., Milner, T. E., de Boer, J. F., Zhang, Y., Pashley, D. H., & Nelson, J. S. (1999). Characterization of dentin and enamel by use of optical coherence tomography. *Appl Opt, 38*(10), 2092-2096.

Wang, Y., Spencer, P., & Walker, M. P. (2007). Chemical profile of adhesive/caries-affected dentin interfaces using Raman microspectroscopy. *J Biomed Mater Res A, 81*(2), 279-286.

Wasson, J. H., Sox, H. C., Neff, R. K., & Goldman, L. (1985). Clinical prediction rules. Applications and methodological standards. *New England Journal of Medicine, 313*(13), 793-799.

Weerheijm, K. L., Kreulen, C. M., de Soet, J. J., Groen, H. J., & van Amerongen, W. E. (1999). Bacterial counts in carious dentine under restorations: 2-year in vivo effects. *Caries Research, 33*(2), 130-134.

Wendell, S., Wang, X., Brown, M., Cooper, M. E., DeSensi, R. S., Weyant, R. J., . . . Marazita, M. L. (2010). Taste genes associated with dental caries. *Journal of Dental Research, 89*(11), 1198-1202.

White, H. (1989). Learning in artificial neural networks: A statistical perspective. *Neural Computation, 1*(4), 425-464.

WHO. (2008). *Harvard Initiative for Global Health, Institute for Health Metrics and Evaluation at the University of Washington, Johns Hopkins University, University of Queensland, World Health Organization. 2008. The global burden of diseases, injuries, and risk factors study*. Retrieved from http://www.healthdata.org/GBD

WHO. (2015). Guideline: sugars intake for adults and children. Geneva (Switzerland) *[accessed 2015 Aug 15]*. *http://who.int/nutrition/publications/guidelines/sugars_intake/en*.

Willmott, N. S., Wong, F. S., & Davis, G. R. (2007). An X-ray microtomography study on the mineral concentration of carious dentine removed during cavity preparation in deciduous molars. *Caries Research, 41*(2), 129-134.

Winterer, G., Ziller, M., Kloppel, B., Heinz, A., Schmidt, L. G., & Herrmann, W. M. (1998). Analysis of quantitative EEG with artificial neural networks and discriminant analysis--a methodological comparison. *Neuropsychobiology, 37*(1), 41-48.

Wisithphrom, K., Murray, P. E., About, I., & Windsor, L. J. (2006). Interactions between cavity preparation and restoration events and their effects on pulp vitality. *International Journal of Periodontics and Restorative Dentistry, 26*(6), 596-605.

Wong, F. S., Willmott, N. S., & Davis, G. R. (2006). Dentinal carious lesion in three dimensions. *International Journal of Paediatric Dentistry, 16*(6), 419-423.

Woodward, M., & Walker, A. R. (1994). Sugar consumption and dental caries: evidence from 90 countries. *British Dental Journal, 176*(8), 297-302.

Worth, A. P., & Cronin, M. T. (2003). The use of discriminant analysis, logistic regression and classification tree analysis in the development of classification models for human health effects. *Journal of Molecular Structure: THEOCHEM, 622*(1), 97-111.

Wright, J. T. (2010). Defining the contribution of genetics in the etiology of dental caries. *Journal of Dental Research, 89*(11), 1173-1174.

Xue, J., Zavgorodniy, A. V., Kennedy, B. J., Swain, M. V., & Li, W. (2013). X-ray microdiffraction, TEM characterization and texture analysis of human dentin and enamel. *Journal of Microscopy, 251*(2), 144-153.

Yip, H., Stevenson, A., & Beeley, J. (1994). The specificity of caries detector dyes in cavity preparation. *British dental journal, 176*(11), 417-421.

Yonemoto, K., Eguro, T., Maeda, T., & Tanaka, H. (2006). Application of Diagnodent as a guide for removing carious dentin with Er: YAG laser. *Journal of Dentistry, 34*(4), 269-276.

Young, D. A., & Featherstone, J. D. (2005). Digital imaging fiber-optic trans-illumination, F-speed radiographic film and depth of approximal lesions. *Journal of the American Dental Association, 136*(12), 1682-1687.

Youngquist, R. C., Carr, S., & Davies, D. E. (1987). Optical coherence-domain reflectometry: a new optical evaluation technique. *Opt Lett, 12*(3), 158-160.

Zaichick, V., Ovchjarenko, N., & Zaichick, S. (1999). In vivo energy dispersive X-ray fluorescence for measuring the content of essential and toxic trace elements in teeth. *Applied Radiation and Isotopes, 50*(2), 283-293.

Zakian, C., Pretty, I., & Ellwood, R. (2009). Near-infrared hyperspectral imaging of teeth for dental caries detection. *J Biomed Opt, 14*(6), 064047. doi: 10.1117/1.3275480

Zamudio-Ortega, C. M., Contreras-Bulnes, R., Scougall-Vilchis, R. J., Morales-Luckie, R. A., Olea-Mejia, O. F., & Rodriguez-Vilchis, L. E. (2014). Morphological, chemical and structural characterisation of deciduous enamel: SEM, EDS, XRD, FTIR and XPS analysis. *European Journal of Paediatric Dentistry, 15*(3), 275-280.

Zaslansky, P., Zabler, S., & Fratzl, P. (2010). 3D variations in human crown dentin tubule orientation: a phase-contrast microtomography study. *Dental Materials, 26*(1), e1-10.

Zavgorodniy, A. V., Rohanizadeh, R., & Swain, M. V. (2008). Ultrastructure of dentine carious lesions. *Archives of Oral Biology, 53*(2), 124-132.

Zero, D. T., van Houte, J., & Russo, J. (1986). The intra-oral effect on enamel demineralization of extracellular matrix material synthesized from sucrose by Streptococcus mutans. *Journal of Dental Research, 65*(6), 918-923.

Zheng, L., Hilton, J. F., Habelitz, S., Marshall, S. J., & Marshall, G. W. (2003). Dentin caries activity status related to hardness and elasticity. *European Journal of Oral Sciences, 111*(3), 243-252.

Zierold, K. (2002). Limitations and prospects of biological electron probe X-ray microanalysis. *J. Trace microprobe tech, 20*(2), 181-196.

Zijp, J. R., & Bosch, J. J. (1993). Theoretical model for the scattering of light by dentin and comparison with measurements. *Appl Opt, 32*(4), 411-415.

Zijp, J. R., & ten Bosch, J. J. (1991). Angular dependence of HeNe-laser light scattering by bovine and human dentine. *Archives of Oral Biology, 36*(4), 283-289.

Zou, W., Gao, J., Jones, A. S., Hunter, N., & Swain, M. V. (2009). Characterization of a novel calibration method for mineral density determination of dentine by X-ray micro-tomography. *Analyst, 134*(1), 72-79.

Zou, W., Hunter, N., & Swain, M. V. (2011). Application of polychromatic microCT for mineral density determination. *Journal of Dental Research, 90*(1), 18-30.

Zweig, M. H., & Campbell, G. (1993). Receiver-operating characteristic (ROC) plots: a fundamental evaluation tool in clinical medicine. *Clinical Chemistry, 39*(4), 561-577.

LIST OF PUBLICATIONS AND PRESENTED PAPERS

Presented papers

28-Jun-14	92nd General Session & Exhibition of the IADR. Cape Town, South Africa	Poster Presentation	Characterizing Dentine Caries: Optical Coherence Tomography-Scanning Electron Microscope
14-Aug-14	27th Annual Scientific meeting. IADR Southeast Asian Division (SEAADE). Kuching, Sarawak, Malaysia	Poster Presentation	Microbiome of Dentinal Caries and Plaque using Next-Generation-Sequencing
18-Apr-15	14thAnnual Scientific Meeting & 16th Annual General Meeting. Malaysian Section IADR	Poster Presentation Best Presentation and Student Travel Award	Differentiating Layers of Dentine Caries Using Optical Coherence Tomography and Energy Dispersion Spectrometric Microanalysis
1-June-15	62nd ORCA Congress. Brussels, Belgium.	Poster and Oral (Presented by Dr.Chew)	Identifying Naturally Occurring Infected, Affected and Healthy Dentine Using Optical Coherence Tomography (OCT)

Publications

May-14	Unusual Multiple Production of N-Acylhomoserine Lactones a by Burkholderia sp. Strain C10B Isolated from Dentine Caries	Sensors	Share Yuan Goh , Wen-Si Tan , Saad Ahmed Khan , Hooi Pin Chew, Noor Hayaty Abu Kasim , Wai-Fong Yin and Kok-Gan Chan
Feb-16	Quorum sensing activity of Citrobacter amalonaticus L8A, a bacterium isolated dental plaque	Scientific Reports	Share-Yuan Goh, Saad Ahmed Khan, Kok Keng Teh, Noor Hayaty Abu Kasim, Wai-Fong Yin & Kok-Gan Chan1